UNIVERSIDADE DE LISBOA

INSTITUTO SUPERIOR TÉCNICO

Development of Human Pluripotent Stem Cell-derived Cardiovascular Microtissues for Cardiotoxicity Screening

Mariana da Mota Veiga de Araújo Branco

Supervisor: Doctor Maria Margarida Fonseca Rodrigues Diogo

Co-supervisors: Doctor Perpétua Pinto-do-Ó

Thesis approved in public session to obtain the PhD Degree in

Bioengineering

Jury final classification: **Pass with Distinction**

2021

UNIVERSIDADE DE LISBOA
INSTITUTO SUPERIOR TÉCNICO

Development of Human Pluripotent Stem Cell-derived Cardiovascular Microtissues for Cardiotoxicity Screening

Mariana da Mota Veiga de Araújo Branco

Supervisor: Doctor Maria Margarida Fonseca Rodrigues Diogo
Co-supervisors: Doctor Perpétua Pinto-do-Ó

Thesis approved in public session to obtain the PhD Degree in
Bioengineering

Jury final classification: **Pass with Distinction**

Jury:

Chairperson: Doctor Joaquim Manuel Sampaio Cabral, Instituto Superior Técnico, Universidade de Lisboa

Members of the Committee:

Doctor Joaquim Manuel Sampaio Cabral, Instituto Superior Técnico, Universidade de Lisboa;
Doctor Lino da Silva Ferreira, Faculdade de Medicina, Universidade de Coimbra;
Doctor José António Henriques de Conde Belo, Faculdade de Ciências Médicas | Nova Medical School, Universidade Nova de Lisboa;
Doctor Maria Margarida Fonseca Rodrigues Diogo, Instituto Superior Técnico, Universidade de Lisboa;
Doctor Tiago Paulo Gonçalves Fernandes, Instituto Superior Técnico, Universidade de Lisboa.

2021

ABSTRACT

Human pluripotent stem cells (hPSCs) represent a unique source of any type of human cells and for that reason hPSC-derivatives have been highly explored in different *in vitro* applications, such as in disease modelling and drug screening settings, but also in regenerative medicine applications. Particularly in the cardiac field, considerable improvements have been made not only regarding the *in vitro* generation of the different cells that compose the human heart, but also in developing advanced cardiac models, which have been already proved to be a promising tool to study cardiac disorders *in vitro* and to be used in pre-clinical settings to assess the cardiotoxicity of new developed drugs.

The main objective of this thesis is to contribute to this effort with the development of an improved and physiologically more relevant multicellular tri-dimensional (3D) cardiac model that better mimics the *in vivo* microenvironment of the human heart than previous models. To attain this purpose, it was first developed a 3D cardiomyocyte (CM) differentiation platform that was further used as the starting point to establish a more complex cardiac model. We took advantage of a forced aggregation platform and the modulation of the Wnt signaling pathway to generate hPSC-CMs aggregates. Through a factorial design approach, it was possible to find the optimal concentration of the small molecule used for Wnt signaling activation during the first step of CM differentiation and hPSC-aggregate size at the beginning of differentiation, culminating in a robust and highly efficient (>85% $cTNT^+$ cells) 3D CM differentiation platform. Importantly, throughout the differentiation process, a side-by-side transcriptomic analysis was performed between the 3D cardiac differentiation platform and a parallel and equivalent 2D CM differentiation system. This analysis revealed that the 3D environment promotes a faster progression of the CM differentiation process, resulting in the generation of CMs with an improved maturation.

Moving on to the development of a more complex cardiac model, it was decided to explore the use of proepicardial cells (PECs), which have a crucial role during embryonic heart development and whose role is still poorly explored in the literature. Firstly, we developed for the first time a 3D PEC differentiation protocol from hPSCs by adapting the previously established 3D CM differentiation model, which generates ±80% $WT1^+$ hPSC-PECs after 11 days of differentiation. In addition, we have also contributed with novel insights on the main signaling cues that are involved in the generation of those cells *in vitro* from mesoderm progenitor cells. Moreover, it was found that our 3D protocol of hPSC commitment into cardiac mesoderm, generates a progenitor cell population composed of lateral plate mesoderm and definitive endoderm progenitors, which, in the case of PECs differentiation protocol, was responsible for the generation of a small population of $CDX2^+$ gut-like epithelial structures in PECs aggregates. Aiming the elimination of this population, different strategies were outlined, resulting in the observation that, through soluble factor manipulation during the first days of

hPSC commitment, it is possible to modulate the generation of endoderm progenitors, which can be further explored to minimize the generation of gut tube-like cells in PEC aggregates.

After the establishment of the hPSC-PEC differentiation protocol, we moved on to the development of a co-culture platform between CMs and PECs. The idea behind this strategy was to explore a more *in-vivo* like strategy to establish a multicellular and structurally organized 3D cardiac model. Through optimization of different parameters, specifically the time of PECs and CMs differentiation stage and fusion, the ratio of each cell population to be combined, and the addition of exogenous stimuli to promote interaction between both cell types, we succeeded in developing 3D co-cultured aggregates (CCA), which comply with the definition of a cardiac organoid. Specifically, we were able to generate 3D cardiac organoids that self-organized in a complex and well-defined structure, which (1) present a continuous $WT1^{+}$ epicardial-like layer surrounding a CM core, (2) shows a CM core with two distinct layers, an outer layer, contiguous to the epicardial layer, which is more compact and contains CMs more aligned and proliferative, and an inner area where CMs present a loose organization, (3) show an enriched staining for the gap junction Cx43 within the CM core, particularly enhanced near the epicardial layer, (4) show an enrichment in fibroblast/ECM proteins surrounding the organoids and within the CM core, (5) show an improved network of vascular cells, and (6) present evidences of improved functional maturation.

Although further studies are still needed to analyze the full impact of this new model in cardiac tissue functional and structural maturation, the preliminary results point to an improved/more realistic response to known drugs, which could be a relevant achievement when considering the use of this model for *in vitro* applications.

Keywords: human induced pluripotent stem cell differentiation, cardiomyocytes, epicardial cells, 3D multicellular cardiac model, 3D cardiac organoids

RESUMO

As células estaminais pluripotentes humanas representam uma fonte única de diferentes tipos de células com enorme potencial para aplicação *in vitro* e *in vivo*. Em particular, estas células, bem como os vários tipos de células derivadas, têm sido usadas em diversos estudos relacionados com o desenvolvimento embrionário humano, com a modulação de doenças, com o teste de novos fármacos, e em medicina regenerativa. Especificamente na área cardíaca, os avanços têm sido consideráveis, não só no que diz respeito ao desenvolvimento de protocolos que permitem gerar as diferentes células que compõe o coração humano adulto, como também no desenvolvimento de modelos cardíacos mais complexos e que tentam recapitular a estrutura e função observada no coração humano. Com estes modelos já se mostrou ser possível recapitular e estudar diferentes doenças cardíacas, bem como a possível utilização destes modelos durante a fase pré-clínica para avaliar a cardio-toxicidade de novas drogas.

O principal objectivo desta tese é contribuir para o desenvolvimento de um modelo cardíaco multicelular e tri-dimensional (3D) que seja mais fisiológico e que mimetize de forma o mais fiel possível o microambiente do coração humano, em termos funcionais e estruturais, para que possa vir a ser utilizado *in vitro* nas aplicações previamente mencionadas. Para alcançar este objectivo, começámos por desenvolver uma plataforma 3D para a diferenciação de cardiomiócitos (CMs) a partir de células pluripotentes humanas. Através da utilização de uma plataforma que permite fazer agregação forçada e utilizando um protocolo simples baseado na modulação da via de sinalização Wnt, foi possível gerar agregados de CMs ao fim de 15 dias de diferenciação. Através da optimização da concentração da molécula usada no primeiro passo da diferenciação para activar a via Wnt, e do tamanho dos agregados de células pluripotentes no início da diferenciação, foi possível desenvolver uma plataforma robusta que permite gerar agregados de CMs com uma eficiência igual ou superior a 85% (≥85% células $cTNT^{+}$). Com o objectivo de estudar o impacto associado à realização da em CMs em 3D, comparativamente com o sistema de diferenciação em monocamada (2D), realizou-se uma análise de transcriptómica usando pontos sucessivos ao longo da diferenciação para ambas as condições. Esta análise permitiu concluir que o processo de diferenciação em 3D induz uma predisposição das células pluripotentes a diferenciarem na linhagem de mesendoderme, o que culmina na progressão mais rápida do processo de diferenciação em 3D comparativamente com o que se observa em 2D, traduzindo-se no desenvolvimento de CM mais maduros no final do processo de diferenciação.

Progredindo para o desenvolvimento de um modelo 3D cardíaco mais complexo, decidiu-se explorar as células do pro-epicárdio (CPE), tendo em conta a sua importância no desenvolvimento, maturação e função do coração. O primeiro passo foi desenvolver uma plataforma 3D para obter estas células a partir de células pluripotentes humanas. Adaptando o protocolo previamente estabelecido para diferenciar CM em 3D foi possível chegar a uma plataforma que permite gerar ao

fim de 11 dias de diferenciação CPE com uma eficiência de aproximadamente 80% (±80% de células $WT1^+$). Em adição ao desenvolvimento da plataforma, foram também obtidas novas informações sobre as principais vias de sinalização envolvidas na especificação destas células a partir de progenitores de mesoderme. Através de uma análise mais pormenorizada da composição dos agregados de CPE, foi possível detectar a presença de estruturas epiteliais, que foram identificadas como células de intestino (±16% $CDX2^+$). Esta observação permitiu-nos perceber que na plataforma base que estabelecemos para o desenvolvimento de diferenciação cardíaca em 3D, é gerada uma população de progenitores composta não só por células da mesoderme como também por células da endoderme, a partir das quais são geradas as células de intestino presentes nos agregados de CPE. Com o objectivo de tentar eliminar esta população de células de intestino, diferentes estratégias foram delineadas, concluindo-se que através de pequenas mudanças na manipulação da via Wnt nos primeiros dias da diferenciação cardíaca, é possível eliminar os progenitores de endoderme e, eventualmente, permitir minimizar o aparecimento de células do intestino nos agregados de CPE.

Depois de estabelecida a plataforma para gerar as CPE, o próximo passo foi o desenvolvimento de uma modelo de co-cultura entre estas células e os CMs. Através da optimização de diferentes paramentos, como o momento da diferenciação de ambas as células que é mais apropriado para proceder à junção, o rácio em que ambas as células devem ser combinadas, bem como se seria ou não necessário activar exogenamente alguma via de sinalização para promover a integração e interacção entre os dois tipos celulares, foi possível desenvolver um modelo 3D cardíaca que obedece à definição de organóide. Em particular, gerou-se um modelo cardíaco que se organiza de forma autónoma numa estrutura complexa que (1) apresenta uma camada contínua de células do epicárdio que cobrem um núcleo de CM, (2) apresenta um núcleo de CMs onde é possível distinguir duas zonas diferentes, uma camada mais exterior e em contacto directo com as células do epicárdio, que é mais compacta e os CMs apresentam-se mais alinhados e com actividade proliferativa; e uma camada mais interna onde os CMs apresentação uma menor organização e encontram-se menos compactos, (3) apresenta uma maior expressão da “gap junction” CX43, que é extremamente importante na comunicação entre CMs e no estabelecimento de um tecido coeso e funcional, em toda a zona do núcleo de CM, mas com expressão mais evidente junto à camada externa de células do epicárdio, (4) apresenta uma maior quantidade de deposição de proteínas de matriz,, não só no nucelo de CMs, como também à volta do organóide, o que é indicativo de uma maior presença de fibroblastos, (5) apresenta uma rede de vascularização mais densa, e (6) apresenta indícios de uma maior maturação funcional, revelada através da resposta a diferentes fármacos, tudo estes pontos em comparação com agregados composto apenas por CM e com o mesmo tempo de cultura.

Apesar de ainda ser preciso analisar de forma mais robusta o impacto que este novo modelo 3D cardíaco tem ao nível de maturação estrutural e funcional dos CMs, estes resultados preliminares apontam para o desenvolvimento de um modelo mais realístico, que permite recapitular alguns princípios estruturais e funcionais observados nos estadios de desenvolvimento embrionário do coração humano.

Palavras-Chave: diferenciação de células estaminais pluripotentes induzidas humanas, cardiomiócitos, células do epicárdio, modelo 3D cardíaco multicelular, organóides cardíacos

ACKNOWLEDGEMENTS

4 anos. 4 anos que terminam agora. Durante estes últimos anos muitas foram as pessoas que fizeram parte desta aventura que foi o meu doutoramento e que sem elas nunca teria conseguido atingir os resultados apresentados nesta tese. É a cada uma dessas pessoas que agora agradeço.

Em primeiro lugar, agradeço ao Professor Joaquim Cabral por me ter dado a oportunidade de integrar o seu grupo de investigação, ainda antes do início do meu doutoramento, e por se ter sempre mostrado disponível para me ajudar. Agradeço de seguida às minhas orientadoras, Professora Margarida Diogo e Professora Perpétua Pinto-do-Ó. À Professora Margarida agradeço todas as conquistas que tive nestes últimos anos de trabalho. Obrigada Professora por ter sempre confiado em mim, na minha capacidade de trabalho, e por me ter dado a liberdade de explorar todas as ideias que fui tendo. Obrigada por me ter ajudado a reflectir de forma crítica sobre os resultados que fui tendo e por me ter ajudado a construir novos caminhos de investigação. Agradeço por me ter animado e dado forças para continuar nos momentos em que os obstáculos surgiram, e por ter festejado, tão ou mais que eu, nos momentos de conquista. Em termos pessoais, agradeço ter-me ajudado a pensar e a reflectir de forma mais calma e ponderada, e a aprender a controlar o meu instituto, por vezes impulsivo, de resolver os problemas. Obrigada por ter sido a melhor orientadora que podia ter tido! À Professora Perpétua agradeço primeiro que tudo ter aceite fazer parte da "equipa" do meu doutoramento! Agradeço a disponibilidade para discutir os resultados que fui tendo e o input valioso que permitiu abrir e seguir diferentes linhas de investigação.

Agradeço ao Tiago Fernandes, por todo o suporte desde os primeiros passos do meu doutoramento. Obrigada Tiago por teres tido paciência para me ensinar como trabalhar num laboratório, por me teres introduzido o mundo da investigação, por me teres ajudado a pensar ciência e a crescer enquanto cientista e pessoa, por teres sempre uma visão positiva de tudo, o que às vezes nestes fazes de maior stress, é o mais valioso. Obrigada por teres estado sempre lá quando precisei. Agradeço ao Carlos Rodrigues por todo o apoio que me deu ao longo destes anos. Ainda me lembro do primeiro dia que cheguei ao Tagus e lá estavas tu ao pé das escadas à minha espera para me mostrares o sítio onde iria passar os próximos anos! Obrigada por me teres integrado no grupo e por teres estado disponível para me ajudar e apoiar sempre que foi preciso.

Agradeço ao Tiago Dias. Sem dúvida alguma um dos grandes pilares desta jornada e da minha vida. Obrigada Tiago por me teres introduzido o mundo dos "mini corações produzidos em laboratório" e por me teres feito apaixonar por esse mundo. Aprendi tanto contigo que é difícil explicar por palavras. Obrigada por me ensinares a pensar de forma clara e assertiva, por me teres orientado, ajudando-me a planear experiências (longas e duras horas de "sofrimento" para ti, I know eheh), a olhar para os resultados de outra perspectiva, a reflectir de forma pragmática sobre os obstáculos

que fui tendo (que depois de falar contigo deixavam de parecer tão dramáticos), e fazendo-me aprender a saborear e valorizar mais as pequenas conquistas. Obrigada por teres estado sempre presente, mesmo em alturas que eu sei que não estavas tão bem. Obrigada por me ajudares a viver esta fase de forma mais calma e ponderada através das tuas palavras de apoio e compreensão. Foste e és a minha inspiração!

Agradeço ao Gonçalo Rodrigues que foi sem dúvida outra grande inspiração para mim. Apesar de teres abandonado o nosso gabinete logo no início do meu doutoramento, foi mesmo bom conhecer-te e aprender contigo! Foste tu que me inspiraste a ambicionar sempre mais e que me ensinaste que com trabalho tudo se consegue. A tua vontade de querer saber sempre mais e aprender coisas novas motivou-me a ser a investigadora que sou hoje!

Agradeço à Teresa e à Ana Rita, as minhas princesas! Obrigada por terem sido uma grande inspiração para mim. Teresa, sabes o quanto te agradeço tudo o que me ensinaste e o suporte que me deste mesmo antes do início do meu doutoramento. Obrigada por me apoiares incondicionalmente e teres estado presente sempre que precisei. Ana Rita, obrigada por seres uma grande amiga que tive a sorte de conhecer quando entrei para o Tagus! Obrigada por todas as risadas e parvoíces que foram tão ou mais importantes do que tudo o resto numa fase tao stressante como é um doutoramento. Mas obrigada também por teres estado sempre presente quando precisei de ajuda no trabalho, mas também a nível pessoal! Agradeço às duas terem sido o meu suporte, o meu apoio emocional para superar os piores momentos, mas também por partilharem e viverem comigo as conquistas que fui tendo.

Carina Maranga e João Cotovio, mores do meu coração, tanta coisa que tenho para vos agradecer!! Carinuxa por onde começar? Sem dúvida outro grande pilar destes últimos anos. Não imagino mesmo como teria sido possível passar por eles sem te ter na minha vida. Obrigada por aturares as minhas paranóias e por teres estado sempre lá para me ajudar em tudo, trabalho e a nível pessoal. Sempre que me fui abaixo estiveste sempre lá para me animar e puxar para cima. Obrigada por animares as minhas manhãs no laboratório, ao meu lado a “cantar”, “dançar” ou simplesmente a fazer umas flexões nos tempos mortos ahah; nas corridas frenéticas até à centrifuga quando ela teimava em “andar” (Shiuuu!!); ou mesmo quando estavas com a má do monte e mantinhas-te no silêncio a pipetar eheh. Por teres partilhado o gabinete e os lanches comigo onde as tuas bananuxas sempre quase podres se tornaram míticas. Obrigada por me motivares todos os dias a ser melhor pessoa e por me ensinares a relaxar e viver a vida com mais tranquilidade (missão difiiicil, eu sei, mas acho que consegui dar alguns passos nesse sentido!!). Fazemos uma boa dupla eheh. Cotovio, o que dizer sobre ti... Mais uma pessoa a quem tenho de agradecer por ter tornado os dias mais fácies, animados e positivos! Cada vez que pensava em escrever este paragrafo só me apetecia rir porque me lembro de todas as peripécias que só aconteceram contigo e que fizeram o meu dia tantas vezes xD. Acima de tudo obrigada pela tua amizade, és uma pessoa incrível e nunca,

mas nunca te vais livrar de mim! Obrigada por teres sido o meu braço direito em várias fases do meu trabalho e por teres estado sempre disponível para me ouvir falar sobre os meus resultados e me ajudares a pensar. Obrigada aos dois pelas risadas, jantaradas (pré-covid…), lanches, idas à praia,…Obrigada por terem estado ao meu lado! Uma das melhores coisas que levo deste doutoramento é sem dúvida as amizades que criei e as pessoas incríveis que agora fazem parte da minha vida, e vocês são duas delas.

Agradeço também a todos os membros do SCERG, em especial, à Claúdia Miranda por ter estado sempre disponível para me ajudar em tudo; à Geni por todo o conhecimento que me transmitiu e preocupação que demostrou comigo sempre, mesmo a nível pessoal, muito obrigada; ao Diogo Nogueira e João Carreira por ter tido paciência para partilhar o gabinete comigo eheh e por terem estado sempre disponíveis para me ajudar em tudo!; ao André Rodrigues, meu quase companheiro de RPI ahah obrigada pela tua amizade.

Por último, mas não menos importante, tenho muito a agradecer à minha família. Mãe, Pai e irmã mais fofa, obrigada por todo o apoio incondicional que me deram, não só nesta fase, mas sempre. Obrigada por mostrarem interesse e orgulho no meu trabalho e em mim, e por terem tido paciência para me ouvir falar sobre as minhas coisas, partilhando o meu entusiasmo, mesmo sabendo que por vezes era difícil de acompanhar! Obrigada por terem vibrado e festejado comigo as minhas conquistas, mas também por me ajudarem a ultrapassar os momentos de fraqueza, dando-me força para continuar e acreditando que era capaz de os ultrapassar. Foi uma fase desafiante para mim, mas sem dúvida também para vocês. Perceberam o quão importante o trabalho é para mim, e agradeço terem sempre tentado compreender e apoiar as minhas opções. Sei que nestes últimos anos se calhar nem sempre estive tão presente como deveria ou gostaria, mas a vida é uma aprendizagem, e hoje peço desculpa por isso. Gosto muito de vocês!! Agradeço também ao meu cunhadinho Carlos Filipe! Obrigada por teres aturado as minhas fúrias momentâneas quando alguma coisa não correu bem, pela competição saudável para ver quem trabalhava mais ou acordava mais cedo, e por teres mostrado interesse pelos meus “bichos”! Ah e quase me esquecia do incentivo nesta fase final que foi extremamente importante! “Já estas a escrever a tese?? Já está? O quê?! Vais escrever em Word??” eheh. Agradeço à minha Titi e aos meus primos, João e Francisco, por serem os meus maiores fãs, pelo orgulho demonstrado pelas minhas conquistas, e por terem sempre mostrado interesse, apoio e preocupação com o meu trabalho!! Agradeço também às minhas primas Cristina e Raquel por terem sido, tantas vezes, as pessoas que me ajudaram a voltar ao “mundo real”, a desligar do trabalho e que me animaram. Obrigada por fazerem parte da minha vida!

Dedico esta tese a duas pessoas muito especiais para mim, às minhas duas avós que infelizmente já não estão aqui comigo mas, onde quer que estejam, estão de certeza muito orgulhosas de mim ★★ .

TABLE OF CONTENTS

LIST OF FIGURES

LIST OF TABLES

LIST OF ABBREVIATIONS

#

2D – Two Dimensional

3D – Three Dimensional

A

AVN – Atrioventricular Node

AVC – Atrioventricular Canal

AP – Action Potential

APS – Anterior PS

aSHF – Anterior Second Heart Field

ACM – Arrhythmogenic Cardiomyopathy

B

BSA – Bovine Serum Albumin

C

CMs - Cardiomyocytes

cTNT – Cardiac Troponin T

CM – Cardiomyocyte

CFs – Cardiac Fibroblasts

CE – Coronary Endothelium

CCA – Co-Cultured Aggregates

E

ESC – Embryonic Stem Cell

EDTA – Ethylene Diamine Tetra Acetic

EB – Embryoid Body

ECs – Endothelial Cells

ECM – Extracellular Matrix

EPDCs – Epicardium Derived-Cells

EPO – Erythropoetin

EPCs – Endothelial Progenitor Cells

EMT – Epithelial-Mesenchymal Transition

EHT – Engineered Heart Tissues

EndoMT - Endothelial-to-Mesenchymal Transition

F

FBS – Fetal Bovine Serum

FHF – First Heart Field

G

GO – Gene Ontology

H

hiPSCs – Human Induced Pluripotent Stem Cells

hPSCs – Human Pluripotent Stem Cells

hESCs – Human Embryonic Stem cells

HTS – High-Throughput Screening

L

LV – Left Ventricle

LAT – Left Atrium

LPM – Lateral Plate Mesoderm

M

MYH7 – β-Myosin Heavy Chain

MYH6 – α-Myosin Heavy Chain

MT – Microtissue

MEA - Multielectrode Arrays Technology

MI – Myocardium Infarction

N

NGS – Normal Goat Serum

O

OFT – Outflow Tract

P

PS – Primitive Streak

PECs – Proepicardial Cells

PEO – Proepicardium Organ

pSHF – Posterior Second Heart Field

PSCs – Pluripotent Stem Cells

POSTN – Periostin

PFA - Paraformaldehyde

PE – Pro-Epicardium

PCA – Principal Component Analysis

Q

R

RV – Right Ventricle

RA – Retinoic Acid

RAT – Right Atrium

RYR - Ryanodine Receptor

RMP – Resting Membrane Potential

RT – Room Temperature

S

SAN – Sinoatrial Node

SR – Sarcoplasmic Reticulum

SHF – Second Heart Field

SV – Venous inflow tract

ST – Septum Transversum

SF – Serum Free

SMCs – Smooth Muscle Cells

T

TNNI1 – Slow Skeletal Troponin I

TNNI3 – Cardiac Troponin I

T-tubules – Transverse Tubules

TFs – Transcription Factors

AIM OF THE STUDY AND THESIS OUTLINE

Human Pluripotent Stem Cells (hPSCs) have a huge potential to be used in different applications. Particularly in the cardiac field, these cells have been used to study cardiogenesis *in vitro* and also as a cell source to generate the different cardiac cells that compose the human heart. These hPSC-derived cardiac cells are now being used to generate 3D cardiac models that try to recapitulate the multicellular, structural and functional complexity of the human heart. Although major improvements have been achieved in that particular field, and the promising applicability of those models in disease modelling and cardiotoxicity screening have been proved, it is still not described in the literature a model that resemble, at the different mentioned levels, the human heart. An extensive literature revision focused on (1) the knowledge regarding human heart development, and how that served as inspiration for the development of the current methods described in the literature to generate the different cardiac cells present in human heart from hPSCs, as well as, (2) the already described 3D cardiac models and the main achievements regarding *in vitro* applications with those models, is described in **Chapter I.**

The main objective of this thesis is to contribute to the effort of developing an improved and physiologically more relevant multicellular tri-dimensional (3D) cardiac model that better mimics the *in vivo* microenvironment of the heart, and that could be eventually integrated in a drug screening setting to assess cardiotoxicity of new developed drugs. To attain this purpose, in **Chapter II**, it was first established a simple, robust and efficient 3D cardiomyocyte (CM) differentiation process, based on a forced aggregation platform and on the simple Wnt signaling modulation protocol. In this chapter was also assessed the impact of performing the CM differentiation process in a 3D environment compared with 2D monolayer culture system, using for that a bulk transcriptomic analysis of sequential stages of both differentiations.

Moving towards the development of a more complex 3D cardiac model, pro-epicardial cells (PECs) were considerable a valuable cell source, still poorly explored in the literature, that could bring the structural and multicellular complexity to a 3D cardiac model. With that in mind, in **Chapter III**, it was established a platform for PECs generation from hPSCs in a 3D environment and additional studies were performed to elucidate the main signaling pathways involved in PECs specification from mesoderm progenitor cells and how it is possible to modulate the generation of those progenitors from hPSCs. In **Chapter IV**, it was explored the establishment of a 3D co-culture model between CM and PECs through combination of both cell types at a specific cell ratio. The final 3D cardiac model was analyzed regarding the multicellular composition, structural organization and functional maturation compared with age matched 3D CM aggregates.

I. INTRODUCTION

The content of this chapter was adapted from the publication:

Branco, M.A.; Cabral, J.M.S.; Diogo, M.M. From Human Pluripotent Stem Cells to 3D Cardiac Microtissues: Progress, Applications and Challenges. *Bioengineering* **2020**, *7*, 92, doi:10.3390/bioengineering703009

I.1 Human Heart Development

I.1.1 Adult Human Heart

The adult heart is a four-chamber organ, comprising the left and right atria, and the left and right ventricles, that is delimited by a heart wall composed of three different cell layers, the myocardium, the epicardium and the endocardium. The endocardium is the inner endothelial layer of the heart and the epicardium is the outer epithelial layer that covers the myocardium. The main function of the heart is pumping blood to the entire body. Heart contraction is controlled by the cardiac conduction system, which is responsible for the generation and propagation of the electrical stimuli to the working myocardium. The cardiac conduction system of the heart consists of (1) sinoatrial node (SAN) cardiomyocytes (CMs), also known as the pacemaker cells, which are responsible for the generation of the electric impulse, (2) atrioventricular node (AVN) CMs, and (3) the impulse-propagating His-Purkinje system, which is responsible for the conduction of the electric stimuli towards the working myocardium (Figure I-1).

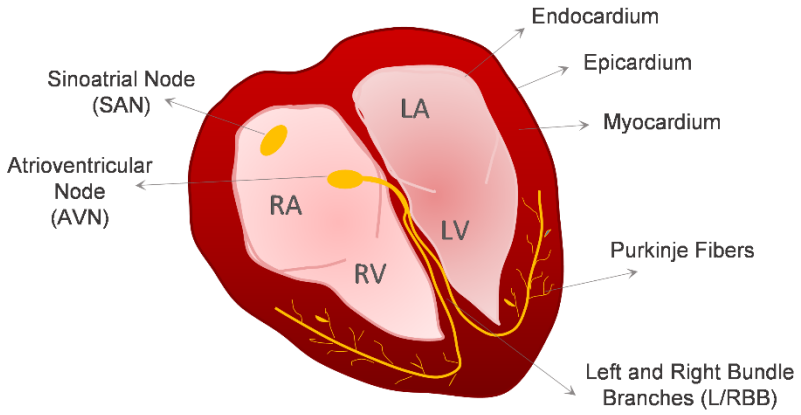

Figure I-1: Schematic representation of the human adult heart. Highlighted is the cardiac condition system composed by sinoatrial node (SAN), atrioventricular node (AVN), Left and Right Bundle Branches (LBB and RBB); and heart wall, composed of three different cell layers, the myocardium, the epicardium and the endocardium.

A recent study performed by Cui and co-workers, assessed the composition of human heart during the different stages of embryonic development, namely, (1) from 5 to 7 weeks of gestation, defined as early stage, (2) from 9 to 17 weeks, defined as mid-stage, and (3) from 20 to 25 weeks, defined as late stage (Cui et al., 2019). They observed that the CM composition of the developing heart starts at around 60% at early stages of development, and drastically decreases over time until

reaching a value of around 38%. This process occurs simultaneously with an increase of the non-CM cell population (Figure I-2A), suggesting the progressive relevance of these additional cells during fetal heart development. In the adult heart, CMs comprise the majority of the cardiac tissue volume, around 75%, but they account for only around 30% in atrial myocardium, and 50% in ventricle myocardium, of the total number of cells present in the adult heart (Figure I-2B) (Brutsaert, 2003; Camelliti et al., 2005; Pinto et al., 2016)(Litviňuková et al., 2020). The majority of the remaining cells are non-myocytes, predominantly cardiac fibroblasts (CFs), vascular endothelial cells (ECs) and immune cells (Pinto et al., 2016)(Litviňuková et al., 2020).

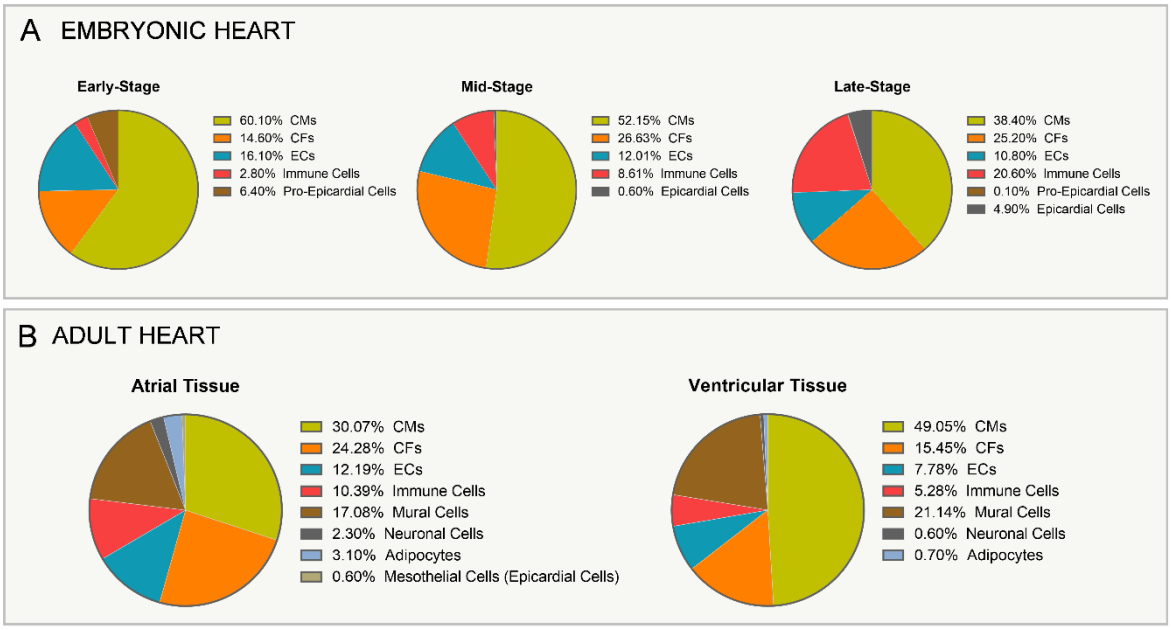

Figure I-2: Human heart cellular composition. Percentage of cell types that composed the human heart at different stages (early, middle and late) of human embryonic heart development (A) and in the adult heart (B). Data obtained and adapted from (Cui et al., 2019)(Litviňuková et al., 2020).

Regarding specifically the presence of different subtypes of CMs in the human heart, at early stages of development, the emergence of two different types of myocardium, the compact and the trabecular one, dictates the first segmentation within the CM population. Trabecular myocardium faces endocardium and compact myocardium, which has a high mitotic activity, faces the epicardium. Then, after chambers specification, CMs can be further partitioned into atrial and ventricular, and segmented into left and right regions. Each one of these CM subtypes present a region-specific expression signature in which regards to (1) ion channels and gap junction signature, which conditions the automaticity of contraction and propagation of the electric signal and consequently the action potential (AP) profile, and (2) sarcomere structure (Cui et al., 2019)(Litviňuková et al., 2020).

Concerning the vasculature of the heart, vascular cells include ECs and supporting mural cells, also referred as pericytes and vascular smooth muscle cells (SMCs), which stabilize vessels and have contractile function to regulate blood flow. Although sharing some common molecular markers, pericytes are located in small blood vessels, whereas SMCs cover larger caliber arteries and veins (Chen et al., 2016) (Litviňuková et al., 2020)(Zhang et al., 2018a). Cardiac ECs are present at different levels in human heart, specifically in (1) endocardium (endocardial cells), (2) coronary vasculature, (3) big blood vessels, including veins and arteries, and (4) valves (valvar cells). Each one of these subpopulations of ECs present different expression marker signatures and arise at different stages of development (Cui et al., 2019). In addition to vascular cells, CFs, through extracellular matrix (ECM) production, play also a vital role in embryonic heart development since they provide structural support for cardiac cells. CFs start as a highly proliferative cell population that gradually become more mature and exhibit an increased expression of many ECM proteins (Cui et al., 2019). In the adult heart, CFs are present within the myocardium (intrinsic fibroblasts) or at perivascular area, and arise from different sources, namely, epicardium, which is described as the major source of CFs present in myocardium (approximately 80%), endocardium, (perivascular fibroblasts), and neural crest lineages, which represent a small fraction. Each of these subtypes of CFs have a different expression profile signature and distinct functional properties (Litviňuková et al., 2020). Additionally, macrophages have also been identified as an intrinsic part to the working myocardium, accounting for approximately 7% of the non-myocyte cell population (Pinto et al., 2016). Although the requirement of macrophages for cardiac healing after injury is well reported, the specific function of cardiac macrophages in normal conditions is still not fully understood. However, it has been suggested that these cells may contribute for the normal conduction system of the heart (Hulsmans et al., 2017).

I.1.2 Early Steps of Embryonic Heart Development

I.1.2.1 Primitive Heart Tube Formation - Myocardium and Endocardium Specification

Heart is the first organ to be formed and to function in the embryo and it is, almost in total, a mesoderm-derived organ, with the exception of the cushions of the outflow tract, which have an ectoderm-derived neural crest origin.

Mesoderm and endoderm layers emerge from a common transient structure known as primitive streak (PS). Depending on the position within the developing embryo, PS is divided into three different regions, posterior, mid and anterior, which, due to different signaling stimuli, show different gene expression profiles and differentiation potential. Nodal and BMP signaling gradients along the PS are the main stimuli responsible for distinguishing the different progenitor populations specified at this time point of development. Anterior PS is exposed to high concentrations of Nodal, from where definitive endoderm progenitors are specified, whereas lower levels of Nodal in combination with BMP

and Wnt signaling activity are critical for mesoderm precursor specification. Three different subtypes of mesoderm derivatives can be specified including (1) the paraxial mesoderm, (2) the intermediate mesoderm and (3) the lateral mesoderm. This last is divided into two different layers, the somatic layer, which faces ectoderm, and the splanchnic layer, that faces endoderm. It is from this last-mentioned layer, localized in the mid PS, that cardiac precursors of the heart arise.

The mesodermal precursors cells in the PS are characterized by the expression of T-box factor Brachyury (T) and MIXL1 transcription factors. The primary cardiac mesoderm progenitor population that migrates from PS is marked by the expression of MESP1. A subpopulation of $MESP1^{+}$ cells migrates towards the anterior part of lateral plate mesoderm that will then split into two different progenitor pools known as first and second heart fields, FHF and SHF, respectively (Lescroart et al., 2014)(Devine et al., 2014). FHF progenitors migrate towards the anterior part of the embryo, forming the ventral part of the cardiac crescent, which is the first cardiac compartment that is morphologically identifiable during development and is formed by the fusion of the two symmetric lateral mesoderm parts after folding of the embryo. The SHF progenitors are located posteriorly and medially to the FHF pool, in the cardiac crescent. Due to the different location within the cardiac crescent, these two pools of progenitor cells are exposed to different signals that will condition the fate of those cells. The FHF progenitors are exclusively committed to a cardiogenic cell fate and develop into the primitive heart tube that starts to contract in order to pump blood throughout the entire developing embryo. The SHF progenitors are a proliferative cell population with delayed differentiation in comparison to FHF progenitors (Hutson et al., 2010)(Tirosh-Finkel et al., 2010)(Tzahor, 2007)(Dyer and Kirby, 2009). SHF progenitors migrate towards the primitive and looping heart tube, being responsible for its elongation at the inflow and outflow poles of the heart structure. Contrarily to FHF progenitors, SHF progenitor cells are multipotent cells that differentiate not only into CMs, but also into cardiovascular cells (Hutson et al., 2010). Both of these populations are characterized by a specific pattern of gene expression profiles, and give rise to distinct compartments of the adult heart. FHF was described as the cardiac progenitor population that gives rise to most of the left ventricle (LV) CMs as well as parts of atrial chamber, whereas SHF gives rise to the outflow tract (OFT), right ventricle (RV) CMs and the majority (two-third) of atrial myocardium (Cai et al., 2003).

Apart from the myocardium, primitive heart tube is also characterized by an inner layer of specialized ECs, the endocardium. Although much attention has been paid to the origin and molecular cues involved in myocardium development, endocardium specification is still not completely defined. However, different studies have addressed the hypothesis that myocardium and endocardium share a common cardiac progenitor cell population which is only segmented after lateral plate mesoderm establishment, and that endocardium lies between myocardial cells and the anterior visceral endoderm layer (Nakano et al., 2016) (Zhang et al., 2018a). Endocardium plays a crucial role in the induction of the first functional layer of CMs, the trabecular myocardium (Mikryukov et al., 2021), and it is an essential source of important cells that compose the heart (Nakano et al., 2016) (Zhang et al., 2018a). Endocardium has been described as the major source of intramyocardial coronary

endothelium during development and also to contribute to the majority of the mesenchymal cells that are present in mature valves, through a process known as endothelial-to-mesenchymal transition (EndoMT), which is a unique feature of the endocardial cells. The contribution of endocardial cells to the population of mural cells present in the heart has also been recently reported in the literature (Zhang et al., 2018a).

I.1.2.2 Pro-Epicardial Organ – Epicardium Origin and Establishment

The epicardium is the epithelial layer that covers the outer surface of the heart and plays an essential role in normal heart development. Contrarily to the myocardium and the endocardium layers, the epicardium originates outside the primitive heart tube in a transient structure, known as pro-epicardial organ (PEO), which develops from lateral plate mesoderm, at the base of the venous inflow tract of the heart tube, and in close proximity with the septum transversum (ST).

Following heart tube looping phase, pro-epicardial cells (PECs) migrate, attach and spread along the outer surface of the developing myocardium, ultimately giving rise to an epithelial sheet, the epicardium. Upon epicardium establishment, epicardial cells produce a layer of ECM between epicardium and myocardium, commonly called the sub-epicardium space, which is mainly composed by fibronectin, collagens I, IV, V and VI, laminin and vitronectin. Subsequently, a subset of epicardial cells invade the myocardium, undergo epithelial-to-mesenchymal (EMT) transition, originating the so-called epicardium derived-cells (EPDCs), which have a crucial role during embryonic heart development.

Although knowledge regarding the epicardium origin, establishment and role played during embryonic heart development have improved in the past years, a lot of information still remains to be collected.

I.1.2.2.1 Proposed Mechanisms and Signals Involved in Recruitment and Migration of PE Cells into the Developing Heart Tube

The first studies that focused on understanding the dynamics involved in PECs translocation into the developing myocardium pointed out to a combination of different mechanisms, specifically (1) the establishment of contact between the PEO and the myocardium through the development of cellular projections, and (2) through the release of PEC clusters of cells into the pericardial cavity that eventually reach the myocardium (Plavicki et al., 2014)(Nahirney et al., 2003)(Rodgers et al., 2008).

More recently, a study performed in mice revealed that PECs translocation to the myocardium is divided into two stages (Li et al., 2017a). An early stage, where both villous protrusions and free-floating cysts contribute to the translocation of PECs towards myocardium, and a later stage in which PEO directly contacts the myocardium (Figure I-3). In the first stage, it is also reported a third

mechanism in which PECs migrate directly along the surface of the inflow tract and onto the atrial surface, which is independent of the formation of cysts and villous protrusions (Hirose et al., 2006).

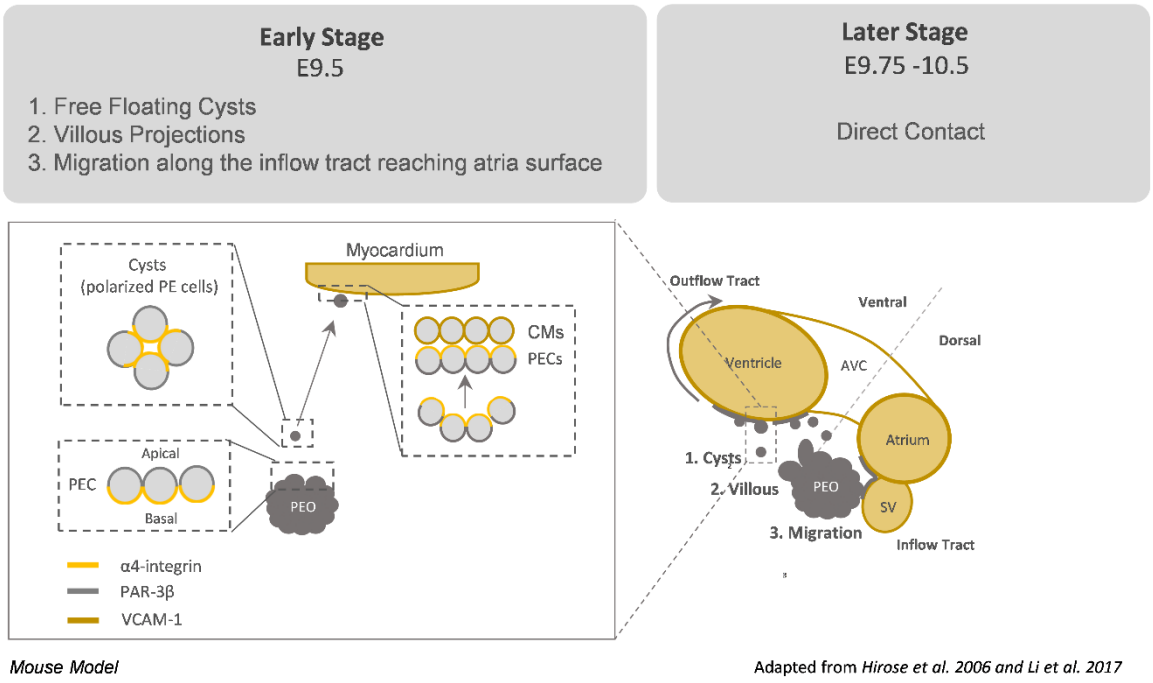

Figure I-3 PECs translocation and epicardium formation. Schematic representation of the proposed mechanisms involved in PEC translocation to the developing myocardium during heart development in a mouse model.

Several studies have tried to identify signals and cell adhesion molecules involved in the translocation of PECs to the heart. BMP signaling has been identified has a regulator of PECs translocation into the myocardium in chick embryos (Ishii et al., 2010). It was identified that BMP, which act as a paracrine factor and is expressed in the atrioventricular channel (AVC) of the developing heart tube, forces the attachment of PECs specifically at the AV junction. In addition, FGF2 was also described to promote PECs proliferation and translocation to myocardium in mice (Li et al., 2017a).

Genetic studies performed in mice suggested the importance of cell adhesion molecules in PECs attachment to the myocardium. This interaction has been described to be controlled by the α4-integrin in epicardial cells that binds to VCAM-1 ligand present in myocardium. The observation that α4- and V-CAM1-deficient mouse embryos lack epicardium covering the developing myocardium (Kwee et al., 1995; Yang et al., 1995) in addition to the observation that α4-integrins are expressed in the epicardial layer (Sengbusch et al., 2002) and that V-CAM1 is expressed by the cells of the underlying myocardial layer (Kwee et al., 1995), reinforce the idea that α4-integrin/VCAM-1 interaction plays a critical role in epicardium establishment. Additionally, it has been also stated that in α4-integrin null mice, not only the attachment of PECs to myocardium became compromised but the migration of PE

was also affected (Sengbusch et al., 2002). Other integrins, in addition to α4-integrin, have also been described to be involved in PECs attachment and migration into the myocardium (Pae et al., 2008). However, those integrins, although being important mediators, cannot support adhesion of PECs in the absence of α4-integrin, reinforcing the idea that α4 can potentially modulate the function of other integrins expressed in PECs. Additionally, the cell surface ligands, EphrinsB1 and EphrinsB2, and EphB receptors, specifically EphB1, EphB2, and EphB3, were detected in PECs and in the developing myocardium, respectively, and suggested to be also involved in PECs translocation to the developing myocardium but not in cell adhesion (Wengerhoff et al., 2010). Other important factor whose lack has been described to compromise PECs translocation to myocardium, specifically in cyst-mediated process, is the PAR3 (Figure I-3), a key polarity protein that is critical for the apical-cortical organization of PECs in cysts formation (Hirose et al., 2006). Although, in PAR3-deficient mice, some PECs were detected in embryos and the cells proliferate normally, cell cyst formation was compromised, which suggested that the epicardium development is selectively affected in PAR3-deficient embryos. In fact, the expression of VCAM-1 and α4-integrin were not affected in PAR3-deficient mice which justifies that PECs that reach the myocardium can attach and migrate.

Interestingly, heart beat and heart beat-derived fluid flow force were observed as an important stimuli to promote PECs migration and expansion on myocardium surface (Plavicki et al., 2014)(Peralta et al., 2013). Although inhibition of heart beat did not affect the specification of PECs or the development of PECs clusters, it prevented epicardium establishment (Plavicki et al., 2014).

I.1.2.2.2 Role of Epicardium and EPDCs in Heart Development

After epicardium establishment at the outer surface of the myocardium, a subset of epicardial cells undergo EMT, which is described to be dependent on the orientation of the epicardial cells in the basement membrane. It was demonstrated in mouse embryos (Wu et al., 2010) that epicardial cells that have a parallel orientation, divide, and both daughter cells remain in the epicardium whereas epicardial cells that have a perpendicular orientation, divide, and one of the daughter cells remains in the epicardium and the other migrates towards the myocardium.

I.1.2.2.2.1 Cell Fate Potential of Epicardial Cells

The identification of the main cardiac cells that derive from epicardium has been challenging, and contradictory results are described in literature. This is mainly due to the fact that the cell composition of PEO and respective cell marker-signature are still not completely disclosed, resulting in conflicting results and conclusions.

The most common markers used to identify PECs are *WT1, TCF21, TBX18, SCX and SEMA3D* (Cano et al., 2016; Katz et al., 2012; Lupu et al., 2020a). However, none of these markers are specific for PECs, which has been described as a possible reason for the contradictory results observed in

lineage tracing experiments to assess cell fate potential of PECs. The contribution of these cells to CFs and vascular smooth muscle cells (SMCs) has been largely reported in the literature and is well accepted (Carmona et al., 2002) (Guadix et al., 2006) (Dettman et al., 1998) (Vrancken Peeters et al., 1999) (Wessels et al., 2012) (Cai et al., 2008) (Zhou et al., 2009)(Acharya et al., 2012) (Volz et al., 2015). Regarding coronary endothelium (CE), although it is well accepted that the majority of CE arises from the endocardium (ventricular and sinuous venous inflow tract (SV)) (Wu et al., 2012)(Red-Horse et al., 2010), the contribution of PECs to CE is still controversial. In fact, the majority of the studies that used the epicardial cell promotors *TBX18, WT1* or *TCF21* for lineage tracing assays, observed a small or no contribution of PECs to the CE. However, a study performed by Kartz and colleagues, suggested that PEO comprise different subpopulations of cells, each one of them with different cell fate potential and marker signatures. They stated that *SCX* and *SEMA3D* positive cells, which they mentioned to have a largely distinct expression domain from those of TBX18- and WT1-expressing cells within the PEO, contribute for CE (Katz et al., 2012). Reinforcing also this idea, Cano and colleagues reported that, although CE has mainly a ventricular endocardium origin, a subpopulation of the ST/PEO ($GATA4^{+}$), contributes also to around 20% of the CE (Cano et al., 2016). They also demonstrated that the PE-derived ECs incorporate preferentially the intramyocardial coronary blood vessels. Additionally, a different study reported for the first time the expression of CCBE1, a extracellular matrix protein, in mouse epicardium and SV myocardium, and that this protein is necessary for the proper development of coronary vasculature of the heart, which may also suggest a link between PECs and CE establishment (Bonet et al., 2018)

A more recent work challenged the idea of the existence of subpopulations within the PEO with already pre-committed cell fates (Lupu et al., 2020a). Using *in situ* hybridization technology, Lu and co-workers showed that PECs that are translocated to the myocardium co-express the markers *WT1, TBX18, TCF21, SCX* and *SEMA3D* and contribute only to CFs and mural cells (Figure I-4). They additionally stated that the differences observed compared with other studies that used lineage tracing approaches were attributed to the fact that the Cre-driver genes used for cell tracing experiments may be expressed also in other non-pro-epicardial structures, namely the ST, that does not have a clear boundary with PEO. They opened the possibility that precursors of endothelial cells expressing markers such as SCX and SEMA3D may exist in ST contributing to the vasculature of the heart but via a non-epicardial route.

I.1.2.2.2.2 Relevance of Epicardium During Embryonic Heart Development

Epicardium has been also described to be involved in myocardium development and maturation. Particularly, it has been identified to play a crucial role in the development of the compact myocardium, since epicardium-deficient hearts showed thinning of the myocardial layer (Gittenberger-de Groot et al., 2000; Kastner et al., 1994; Kwee et al., 1995; Sucov et al., 1994; Yang et al., 1995). Although it is not completely clear yet which paracrine signals are secreted by epicardial

cells and the regulation behind the secretion of those factors, it is already proved that the epicardium releases mitogenic signal(s) that are required for myocardium growth. Erythropoetin (EPO) and retinoic acid (RA) seem to play a role in controlling the secretion of mitogens by the epicardium.

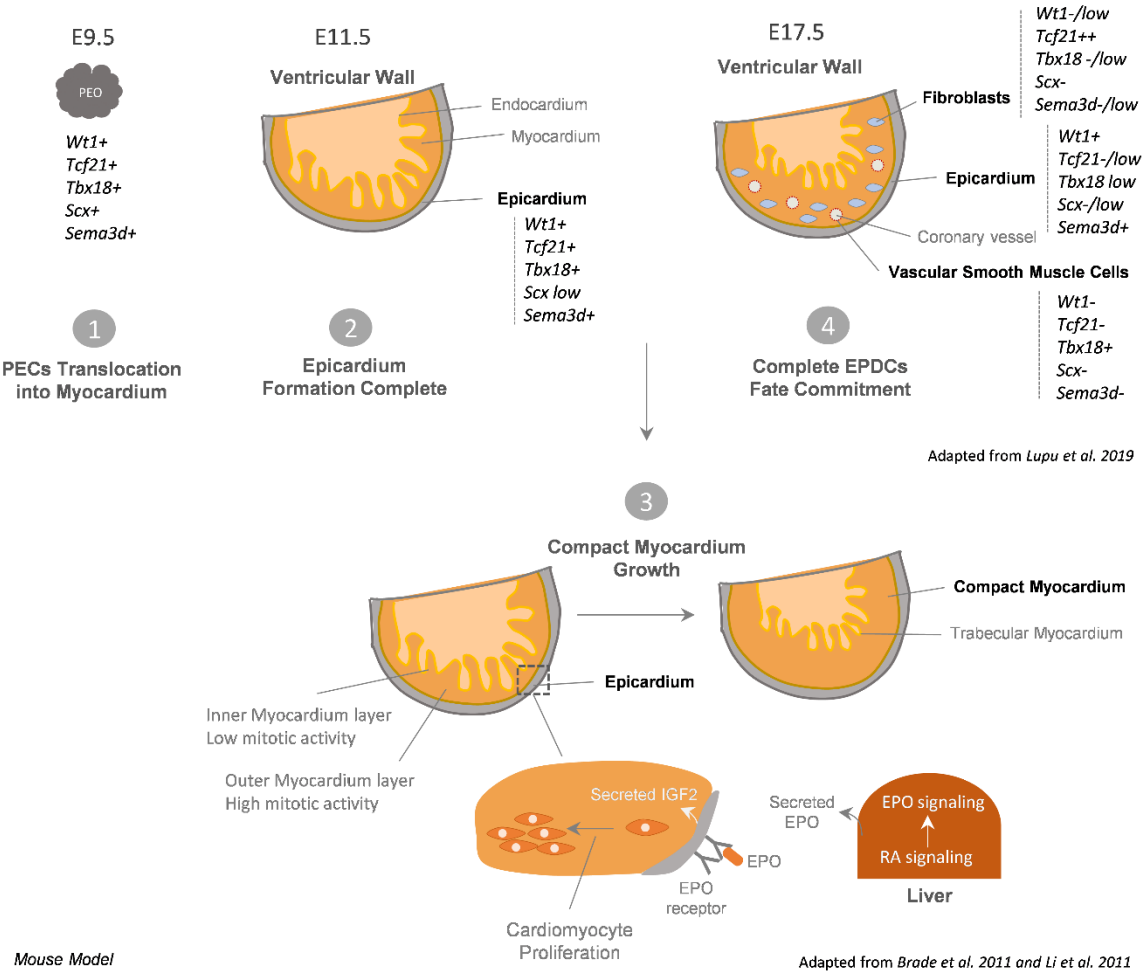

Figure I-4 Schematic representation of the different steps involved in epicardium establishment and respective contribution of EPDCs and epicardium to the developing myocardium. Information adapted from Lupu et al. 2019; Brade et al. 2011 and Li et al. 2011.

RA has been described to be involved in myocardium compact zone formation, since mouse embryos lacking retinoic acid receptor gene *Rxrα* (Sucov et al., 1994)(Kastner et al., 1994) suffer from an inability to proper form the compact zone. Additionally, EPO has been also implicated in ventricular compact zone growth, as *Epo*$^{-/-}$ and *Epor*$^{-/-}$ embryos exhibit ventricular myocardial thinning (Wu et al., 1999). Additionally, it has been also described that RA and EPO signals act in myocardial expansion in an indirect way, being responsible for controlling the secretion of mitogenic factors by the epicardium (Stuckmann et al., 2003). The origin of the RA and EPO, which are, specifically, the mitogenic factors that are released from the epicardium, is still an area of debate.

Although previous studies have suggested that RA signaling, specifically generated in the epicardium, was the one responsible for controlling the process of myocardium thickening (Chen et al., 2002)(Merki et al., 2005), more recent studies (Brade et al., 2011) challenged that idea and suggested that the RA signal event that control this process has an hepatic origin. They proposed a mechanism in which RA signaling generated by hepatic RALDH2 and RXRα positive cells, induces hepatic *Epo* expression, which resulted in EPO signaling activation in epicardium, being consequently responsible for the initiation of the mitogenic response in myocardium (Figure I-4). Interestingly, there were already evidences that expression of EPO in hepatic tissues is regulated by RA (Merki et al., 2005).

The mitogenic factors that are secreted by epicardium, PDGFs (Kang et al., 2008), FGFs (Merki et al., 2005)(Pennisi et al., 2003) (Lavine et al., 2005) and WNTs (Merki et al., 2005), have been identified by different studies as important mediators of myocardium growth. However, more recent studies identified IGF2 as the major mitogenic factor involved in myocardium compaction (Brade et al., 2011) (Li et al., 2011) and that EPO signaling activation in epicardium was described to be responsible for the induction of IGF2 secretion (Brade et al., 2011) (Figure I-4). Li and co-workers also added that the dependency of IGF signaling on supporting the formation of the compact zone in myocardium is restricted to a certain period of embryonic development (E10.5-14.5 period) and afterword's they suggested that other proliferative factors brought to the myocardium via the coronary vasculature are responsible for influencing myocardium proliferation (Li et al., 2011).

I.2 Human Pluripotent Stem Cells

Since a long time ago, stem cells have been defined as undifferentiated cells capable of self-renewal and production of specialized cells through differentiation. According to their differentiation potential, stem cells can be categorized in different subclasses. Totipotency is a characteristic attributed to stem cells that have the potential to originate an entire organism, including the capacity to originate all embryonic and extra-embryonic cell types, which means that only zygote and early blastomeres are included in this category. Pluripotent stem cells (PSCs) are capable of differentiating into all the cells present in adult organisms that come from the three-germ layers, ectoderm, mesoderm and endoderm, and into the germ cell lineage. Moving towards a decreased differentiation potential, multipotent stem cells are restricted to the capacity to generate the mature cell types of its tissue of origin and unipotent stem cells display limited developmental potential, giving rise to only a single cell type.

I.2.1 Human Embryonic Stem Cells

PSCs have a great potential for *in vitro* applications since they theoretically have the potential to be indefinitely expanded, while maintaining an undifferentiated state under the appropriate culture

conditions, and have the capability to differentiate into all cells present in the adult organism. PSCs can be isolated from the blastocyst, particularly from the inner cell mass (ICM) (Evans and Kaufman, 1981)(Martin, 1981). When cultured *in vitro* under conditions that allow indefinite self-renewal and pluripotent state maintenance, these cells are called embryonic stem cells (ESCs).

Only in 1998, the first human ESC (hESC) line was derived from a human blastocyst (Thomson, 1998). These cells are characterized by a network of gene regulatory transcription factors that are essential to maintain pluripotency, which includes the pluripotency transcription factors encoding genes octamer-binding transcription factor 4 (OCT4), SRY-box 2 (SOX2) and NANOG. The expression of these markers is normally used to assess pluripotency *in vitro*. In addition to the molecular signature, different functional assays are normally used to confirm the pluripotency of these cells, including the capacity for differentiation into the three-germ layers *in vitro* and teratoma formation *in vivo*, which is one of the most important features of pluripotent stem cells.

I.2.2 Human Induced Pluripotent Stem Cells

Although hESCs represented and still represent a valuable tool to perform developmental biology studies *in vitro* and are still the main cell source used to obtain progenitor/terminally differentiated cells that are being applied in on-going clinical trials, these cells have associated to them ethical concerns related with the destruction and manipulation of human embryos.

In 2006, a new age in the area of PSCs started. Takahashi and Yamanaka demonstrated for the first time that a somatic cell could be reprogramed to an early stage of development (Takahashi and Yamanaka, 2006). Using a cocktail of four transcription factors, Oct4, Sox2, Klf4 and c-Myc, they induced mouse fibroblasts into pluripotent stem cells. These reprogrammed cells received the name of induced pluripotent stem cells (iPSCs). One year later, the same group used the same methodology to reprogram human somatic cells into PSCs (Takahashi et al., 2007). In the same year, a different group demonstrated the generation hiPSCs using the same technology but using a different cocktail of factors (Oct4, Sox2, Nanog and Lin28), in which the oncogene c-MYC was replaced by the post-transcriptional regulator LIN28 (Yu et al., 2007). The hiPSCs share the same properties of hESCs, in terms of cell morphology, proliferation and transcriptional features (Yu et al., 2007) (Takahashi et al., 2007). However, despite the similarities, iPSCs can keep some epigenetic memory associated with the somatic cell of origin, which in some cases can be responsible to the fact that some iPSC lines are more prone to differentiate into a specific lineage (Kim et al., 2011).

I.3 Cardiovascular Lineages Specification from hPSCs – Lessons From *in vivo* Heart Development

The identification of the main steps that occur during the process of embryonic heart development and the knowledge of how the different cell populations are specified, have provided

the basis for the establishment of directed differentiation protocols to generate the entire repertoire of cardiac cells from hPSCs. Through the step-wise indirect or direct manipulation of different signaling pathways, it has been possible to guide the process of differentiation of hPSCs towards the different cardiac cell fates *in vitro*. Below, are summarized some of the main lessons learned from the *in vivo* heart development process that made possible and have been applied to develop *in vitro* cardiac differentiation protocols from hPSCs.

I.3.1 Generation of Cardiomyocytes from hPSC

I.3.1.1 2D Cardiomyocyte Differentiation Platforms

Knowing the main signaling pathways that are involved in mesoderm induction and cardiac specification *in vivo*, namely Wnt, BMP, Nodal/Activin A and FGF pathways, and in a step forward towards the development of more robust CM differentiation protocols from hPSCs *in vitro*, directed differentiation methods, using specific growth factors and small molecules in 2D monolayer culture systems, were firstly developed. One of the first methodologies for directed CM differentiation under 2D conditions was described by Laflamme and co-workers. Through manipulation of Activin and BMP signals, they achieved a yield of more than 30% CMs (β-myosin heavy chain – β-MHC^{+}), which were then enriched using a Percoll density gradient centrifugation (Laflamme et al., 2007). In 2010, Paige and colleagues (Paige et al., 2010) demonstrated the relevance of Wnt/β-catenin signaling in cardiac differentiation *in vitro*. They showed that, not only the inhibition of Wnt signaling at later stages of differentiation is critical to induce cardiac fate, but also the canonical Wnt signaling activation during the first stages of mesoderm commitment had a positive impact on CM differentiation, reinforcing the idea that Wnt signaling has a dual stage effect on CM specification as has been observed in *in vivo* models. They suggested that the combined manipulation of Wnt / Activin / BMP pathways should be explored to improve cardiac differentiation. The combination of mesoderm commitment using Activin A and BMP4, followed by canonical Wnt signaling inhibition, was further explored to improve CMs differentiation outcome in different reported monolayer protocols (Hudson et al., 2012)(Uosaki et al., 2011), however the efficiencies were still low and lacked reproducibility. In 2012, Lian and co-workers (Lian et al., 2012a) reported an efficient growth factor-free monolayer protocol, which relied solely on the temporal modulation of the Wnt signalling pathway by firstly activating that pathway for mesendoderm induction, using the GSK3B inhibitor CHIR, followed by a step of Wnt inhibition for cardiac lineage specification, using the small molecules IWP-2 or IWP-4. This protocol can generate an almost pure population of cardiomyocytes (up to 98% of cardiac troponin T (cTNT) positive cells). Since the establishment of this Wnt signalling-based protocol, several adaptations were reported in the literature. Interestingly, and having in mind the development of a chemically-defined CM differentiation method, that could be easily translated for clinical applications, Burridge and colleagues (Burridge et al., 2014a) took advantage of this protocol and adapted the culture medium

formulation to a chemically-defined version. In the Lian and colleague's version of Wnt signalling manipulation protocol, the basal medium used consisted in RPMI supplemented with B27. By titration of each one of the 27 compounds, Burridge and co-workers concluded that the basal medium RPMI supplemented only with ascorbic acid and BSA was sufficient to effectively induce CM differentiation. Additionally, in an attempt to adapt the protocol to a xeno-free environment, they also showed the possibility of replacing BSA with recombinant human albumin. Later on, Lian and co-workers, reported a new variation of the Wnt signaling protocol in which cardiac differentiation could be performed in RPMI basal medium supplemented with only three components, sodium selenite, progesterone and putrescine (Lian et al., 2015). In this way, a differentiation protocol free of albumin was developed. In fact, they observed that through a reduction of CHIR concentration, the BSA could be removed from the basal medium formulation without interfering with CM differentiation efficiency.

I.3.1.2 3D Cardiomyocyte Differentiation from hPSCs

The first attempts to perform CM differentiation from hPSCs in a 3D environment were based on the embryoid body's (EB) differentiation method. In this differentiation methodology, hPSCs are cultured as small clumps in suspension culture, allowing them to grow and to enter into spontaneous differentiation in basal medium containing serum (normally 20% of FBS) (Xu et al., 2002)(Zhang et al., 2009)(Zwi et al., 2009)(Kehat et al., 2001)(Huber et al., 2007)(He et al., 2003). This approach, due to the lack of defined cues to induce the cardiac differentiation, generates low percentages of CMs, which are normally assessed by the percentage of contracting EBs (from 1% to 22% of contracting EBs), in a non-reproducible way. However, this system allowed the acquisition of valuable biological information that later on was taken into consideration for the development of more robust and efficient 3D-based directed differentiation protocols.

I.3.1.2.1 Impact of hPSC-3D Aggregation on Cardiac Differentiation Potential

Taking advantage of micropatterned and forced aggregation platforms to generate size-controlled 3D aggregates of hPSCs, different studies have been performed to evaluate the impact of culturing hPSCs in a 3D environment in comparison with 2D culture. Several reports have shown that EB differentiation was influenced by hPSC aggregate size at the beginning of the process (Bauwens et al., 2008; Burridge et al., 2007; Mohr et al., 2010; Niebruegge et al., 2009). hPSC aggregate diameters ranging 250–350 μm were described as the optimal size to maximize cardiac gene expression and thus cardiac differentiation efficiency. Additionally, it was also stated that this controlled method for aggregate generation increased hPSC aggregate homogeneity at the beginning of differentiation, which resulted in a higher reproducibility and less variability between runs, compared to standard enzymatic methods to form EBs (Mohr et al., 2010).

Although the size of hPSCs aggregates had been shown to influence the differentiation outcome to different lineages, the molecular factors behind that effect were not clear at the beginning. To achieve a deeper understanding of these effects, different studies were performed (Azarin et al., 2012; Bauwens et al., 2011; Hsiao et al., 2014; Hwang et al., 2009). Using the EBs differentiation protocol, Azarin and co-workers (Azarin et al., 2012) suggested that cell-to-cell interactions experienced by the hPSCs in the undifferentiated state in 3D environment, trough, for example, E-cadherin interactions, could be responsible for the modulation of different signaling pathways that could later impact the differentiation outcome. Particularly, they observed that upon EB differentiation, hPSCs that had been previously cultured in micropatterned platforms (300x300µm) showed an upregulation of the canonical Wnt signaling pathway during the first days of differentiation, when compared with 2D cultured hPSCs, which resulted in a higher expression of genes associated with primitive streak, mesoderm and cardiac lineage commitment. In another study from the same group (Hsiao et al., 2014), it was suggested that hPSCs cultured in microwells showed an upregulation of BMP signaling and less transcriptional activity of genes involved in Activin/Nodal pathway, which they proposed to result in a priming of hPSCs towards differentiation, and consequently influenced the exit from pluripotency and germ lineage specification upon the beginning of differentiation. Through the analysis of important genes involved in cardiac differentiation, they observed that EB differentiation using microwell cultured hPSCs showed a strong peak of expression of Brachyury, a transcription factor that controls PS induction, which was not observed in EB differentiation performed with 2D cultured hPSCs. Similarly, mesendoderm lineage and early cardiogenesis genes, such as *ISL1* and *NKX2.5*, were upregulated in EB differentiation using microwell cultured hPSCs. Moreover, upregulation of the genes responsive to Wnt signaling, such as *WNT3A*, *WNT8A* and *LEF1*, Notch pathway genes such as *NOTCH1* and *DELTA1*, and representative genes from the TGFβ superfamily, such as *BMP2*, *BMP7*, *NOGGIN* and *NODAL*, were also upregulated in EBs obtained from microwell cultured hPSCs.

The effect of 3D aggregate size towards CM differentiation from hPSCs was later on confirmed by Bauwens and colleagues under serum-free conditions and using a directed CM differentiation protocol based on the manipulation of BMP4, Activin A and FGF for mesoderm induction and a second stage of DKK1 and VEGF media supplementation for cardiac mesoderm and CMs specification (Bauwens et al., 2011). As the cellular mechanism, they suggested that the aggregate size influences the extension of an endoderm layer during differentiation, being that the main reason behind the impact of aggregate size on cardiac induction and differentiation efficiency (endoderm-secreted factors). They additionally stated that the control of aggregate size at the beginning of differentiation allows the achievement of consistent and efficient cardiac induction runs.

More recently, other groups have demonstrated the impact of hPSC-aggregate size on CMs differentiation when using solely the temporal modulation of Wnt signaling by using a forced aggregation platform (Branco et al., 2019; Dahlmann et al., 2013) or a dynamic system (Chen et al., 2015a) for generation of hPSCs aggregates. In a recent study, a possible impact, at the transcriptional

level, of forced aggregation of hPSCs when compared to 2D cultured hPSCs was revealed (Branco et al., 2019). It was demonstrated that by culturing hPSCs under 3D conditions, in the presence of hPSC expansion medium, for 3 days, in a microwell platform (approx. 300 µm of diameter), these cells exhibited a priming for mesendoderm commitment, which further resulted in a faster exit from the pluripotency stage and primitive streak commitment upon cardiac differentiation induction, culminating in a faster CM differentiation progression and maturation when compared with 2D monolayer. It was suggested that these differences could be related not only with the higher degree of cell-to-cell interactions observed in 3D aggregates, but also with the oxygen gradients inside the spheroids, which, all together, culminated in a stabilization of TGF-β/Nodal pathway, upregulation of MAPK/JNK/ERK pathway and increased glycolysis metabolism, when compared with 2D-cultured hPSCs.

I.3.1.2.2 3D Cardiomyocyte Differentiation Platforms

Different 3D culture platforms have been described to successfully generate CMs from hPSCs. Depending on the purpose, the generation of the 3D aggregates of hPSCs for cardiac differentiation may rely on the use of dynamic systems, including different bioreactor configurations (Chen et al., 2015a; Fonoudi et al., 2015a; Halloin et al., 2019; Hemmi et al., 2014; Kempf et al., 2014a; Ting et al., 2014), or static conditions, where forced aggregation platforms, including microwell plates (Branco et al., 2019; Dahlmann et al., 2013), U- and V- 96-well plates (Burridge et al., 2011a; Zhang et al., 2015) and micropatterned surfaces (Ma et al., 2015) were used. Since the pre-differentiation stage and the early differentiation phase have a substantial impact on CM differentiation outcomes, as discussed before, the control of the initial population of 3D-hPSC aggregates in terms of aggregate size and homogeneity synergistically combined with optimized concentrations of growth factors and/or small molecules to induce the first commitment of hPSCs, are crucial for the success of the differentiation process. The use of microwell plates allows the generation of size controlled and homogenous populations of aggregates only through cell seeding density manipulation (number of cells/aggregates) (Branco et al., 2019; Dahlmann et al., 2013). In the case of dynamic systems, the size of aggregates and, depending on the platform, aggregates homogeneity, can be also controlled by controlling the cell seeding density, agitation rate and time in culture (Chen et al., 2015a). However, the variability in the size of the aggregates is generally higher in this type of dynamic systems when compared with forced aggregation platforms, which can comprise the reproducibility between biological runs. Both dynamic and microwell systems have been proven to generate highly pure populations of CMs (> 80% of CMs) within 10/16 days of differentiation (Table I-1). Although the aforementioned parameters (pre-differentiation period and concentration of small molecules and/or growth factors), highlighted in Table I-1, are critical for the success of the CM differentiation in the 3D environment, they should be synergistically optimized for the specific platform that is being used. A different hPSC-aggregate size at day 0 of differentiation or a different concentration of factors in

different culture platforms may result in identical efficiencies. Since there are already robust and efficient systems to generate CMs in 3D environment, the selection of the best protocol will depend on the final aim. Dynamic systems should be preferred for large scale production of CMs for example for regenerative medicine applications. On the other hand, to produce CMs or 3D cardiac MTs for *in vitro* applications, protocols that rely on microwell plates may be advantageous, since these are simpler and do not require sophisticated equipment nor specific expertise in bioprocessing and may allow an easier integration with medium- to high- throughput screening platforms.

I.3.2 Universal Cardiomyocyte Differentiation Protocol – a possibility or an Illusion?

Although the specification of CMs from hPSCs *in vitro* has been achieved with different methods, as it was described above, a common issue of the hPSC-derived CM differentiation protocols is related with high inconsistencies in differentiation efficiencies across various hESCs and hiPSCs lines (Tewary et al., 2018)(Kattman et al., 2011a)(Burridge et al., 2011b), which compromised the development of an universal method for CM differentiation. This variability is likely related to genetic and epigenetic differences between hPSC lines that directly impact their cardiac differentiation capacity. In an attempt to have a deeper understanding of the complex process of cardiac commitment, specifically regarding the first stages that include PS and mesoderm subtypes specification, and to develop more controlled differentiation processes, different studies focused on understanding the complex network of signals involved in cardiac commitment and to understand how those signals could be controlled *in vitro*.

BMP4 and Activin A signaling are the main regulators of anterior-posterior patterning of PS, in which BMP4 activation in the first stage of hPSCs commitment has a posteriorizing effect, whereas Activin A was identified as an anteriorizing agent (Loh et al., 2014a) (Loh et al., 2016a). The most anterior part of the PS is responsible for the generation of the definitive endoderm, whereas the mid/posterior PS progenitor cell population originates the cardiac mesoderm progenitors.

Table I-1. **Summary of studies reporting CM differentiation from hPSCs under 3D conditions.** The table highlights 3D-CM differentiation platforms using dynamic systems (bioreactors and spinner flasks) and static conditions (microwell plates and ULA attachment plates). Ø, diameter; ULA, Ultra Low Attachment Plate.

	Pre-Differentiation				Differentiation								
	Platform	**Time**	**Media**	**Aggregate Ø at D0**	**Platform**	**Media**		**Molecules**			**Duration**	**Efficiency**
Halloin et al. 2019	Stirred Bioreactor	2 Days	E8	± 125 µm	Stirred Bioreactor (500 mL)	CDM3*[1]		CHIR	D0 – D1	5 µM	10 Days	±1x10[6] CMs/mL
								IWP2	D1 – D3	5 µM		93 ± 5 % CMs
Chen et al. 2015	Spinner Flask	2 Days	StemPro hESC SFM + FGF2	200 ± 20 µm	Spinner Flask (125 mL – 1L)	RPMI+B27-INS	D0 – D4	CHIR	D0 – D1	6/12 µM*[2]	16 Days	±1×10[6] CMs/mL (1L) ± 2 × 10[6] CMs/mL (500 mL)
						RPMI+B27	D4 – D16	IWP4	D2 – D4	5 µM		> 90 % CMs
Fonoudi et. 2015	Stirred Bioreactor	5 Days	DMEM/F12+ FGF2	175 ± 25 µm	Stirred Bioreactor (100 mL)	RPMI + B27	D0 – D15	CHIR	D0 – D1	12 µM	15 Days	0.8 x 10[6] CMs/mL
								SB+Pur+IWP2	D2 – D4	5 µM each		> 80 % CMs
Branco et al. 2019	Aggrewell[TM]800	3 Days	mTeSR1	± 300 µm	Aggrewell[TM]800	D0 – D7	RPMI+B27-INS D0 – D7	CHIR	D0 – D1	11 µM	12 Days	± 20 x 10[6] CMs/plate
					ULA 6 well plate	D0 – D12	RPMI+ B27 D7 – D12	IWP4	D3 – D5	5 µM		> 85 % CMs
Burridge et al. 2011		-		*[6]	96-V ULA plate	D0 – D4	RPMI D0 – D10	*[5]			10 Days	± 0.4 x 10[6] CMs/plate
					96-U ULA plate	D4 – D10						> 80 % CMs
Dahlmann et al. 2013	Agarose Microwell plate	1 Day	FCM*[3]	400-500 µm*[4] (± 220 µm (D-3))	ULA 6 well plate	RPMI + B27-INS	D0 – D7	CHIR	D0 – D1	8 µM	10 Days	*[6]
	ULA 6 well plate	3 Days				RPMI + B27	D7 – D10	IWR1	D3 – D5	4 µM		Up to 65 % CMs

*[1] RPMI 1640 (+2 mM Glutamine) + 495 µg/mL Recombinant Human Albumin + 213 µg/mL Ascorbic Acid; *[2] Depending on the cell line; *[3] DMEM/F12 + GlutaMAX + 20% (v/v) Knockout serum replacement + 1% (v/v) non-essential amino acids + 0.1 mM β mercaptoethanol + 10 ng/mL FGF-2; *[4] Determined by bright field image analysis; *[5] D0-D2: BMP4 (25 ng/mL); FGF2 (5 ng/mL); PVA (4 mg/mL); h-Insulin (10 µg/mL); D2-D4: HAS (5 mg/mL); 280 µM L-ascorbic acid; D4 - forward: h-Insulin (10 µg/mL); *[6] Not specified*

Although Wnt and FGF signaling were not considered key elements for the anterior-posterior patterning of PS, the endogenous activity of both pathways was observed to be mandatory for PS formation (Loh et al., 2014a) (Loh et al., 2016a). This information is consistent with different protocols for cardiac differentiation that rely mainly on BMP4 manipulation alone, in the first step of cardiac commitment, or combined with low levels of Activin A. Although high levels of Nodal pathway activation during the first days of hPSCs commitment contribute to anterior PS specification, a low/basal activity of this signaling pathway is also important for the success of cardiac mesoderm induction (Rao et al., 2016). In fact, a study demonstrated that the basal level of Nodal signaling in hPSCs can condition the predisposition of those cells to undergo PS specification (higher levels of endogenous Nodal signaling) rather than neural commitment (lower level of endogenous Nodal signaling)(Tewary et al., 2018). This information may justify the observation that some reported CM differentiation protocols rely on the addition of Activin A for just one day as the first stimuli for hPSCs commitment, possibly as a priming step. Although Wnt signaling has been described not to be critical for anterior-posterior patterning of PS, this pathway is critical for the commitment of mid/posterior PS into anterior mesoderm from which cardiac progenitors arise. This is also in agreement with several protocols that exogenously activate Wnt signalling, alone or in combination, with BMP4 to induce lateral mesoderm differentiation.

Although it is now clear the main signals that should be modulated for cardiac commitment from hPSCs, protocols relying solely on the temporal modulation of Wnt signalling have been deeply studied. One of the first observations made is the increased variability of this process across biological runs and hPSC lines (Laco et al., 2018). This has been attributed to the fact that the success of these type of differentiation is deeply dependent on (1) the endogenous/basal activity of important signaling pathways in the pluripotency stage of each hPSC line, such as BMP4 and Nodal signalling, and (2) how Wnt signaling manipulation can interfere with the level of those signaling pathways throughout the differentiation process. This last factor is deeply dependent not only on the level of Wnt signaling activation, controlled by the concentration of the small molecules used, but also depends on other parameters such as cell confluence, which condition the concentration of paracrine signals released to the culture medium (Burridge et al., 2014a)(Zhao et al., 2019a) (Halloin et al., 2019) (Kempf et al., 2016a)(Burridge et al., 2011a). In fact, Kempf and co-workers (Kempf et al., 2016a) proved that, when lacking extrinsic BMP4 activation, BMP4 pathway activity is indirectly ensured by Wnt signaling activation, and the level of BMP4 signaling activity can be manipulated *in vitro* through small molecule CHIR concentration but also cell density. Additionally, canonical Wnt signalling activation has been also described to induce Nodal expression (Funa et al., 2015a), which, as described before, is an important signaling pathway that should be active during the first stages of cardiac differentiation. The importance of Wnt signaling activation duration and the timing for Wnt signaling inhibition was also stated in different reports as important parameters that control the success of this type of CM differentiation (Burridge et al., 2014a) (Halloin et al., 2019) (Zhao et al., 2019a) (Kempf et al., 2016a). This complex network of stimuli that are slightly controlled with Wnt signaling

manipulation, justifies that an optimized protocol can result in different outcomes depending on the hPSC line.

Altogether, these studies proved that BMP and Wnt signaling converge in controlling cardiac mesoderm specification, whereas FGF and Activin A signaling are additional important pathways that should be active by exogenous stimulation or indirectly through Wnt and BMP4 modulation. Additionally, these studies also reinforced the idea that the development of a simple and universal platform to generate CMs is very challenging. Particularly in the case of protocols that rely only on Wnt signaling manipulation, the process is more prone to variability since they deeply rely on several parameters that condition the endogenous activity of other signaling pathways. An interesting improvement to this kind of protocols may be the conditioning of the initial state of the different hPSCs cell lines to a mesendoderm primed level, which could be an important tool to overcome part of this problem.

I.3.3 Differentiation of hPSCs into Different Subtypes of Cardiomyocytes

Upon producing of CMs using the protocols mentioned in sections I.3.1.1 and I.3.1.2, two main limitations have been identified, namely the fact that hPSC-CMs are often (1) relatively immature compared with adult CMs, which will be further discussed in this chapter and (2) a mixed population of different subtypes of CMs, although most of the times they showed ventricular-like signature after prolonged time in culture (Burridge et al., 2014a; Lian et al., 2012a). Envisaging the future applicability of these hPSC-derived CMs in clinical applications as well as in disease modelling or drug screening studies, new protocols have emerged to specifically generate different subtypes of CMs and also to identify cell surface markers that could help on the selection and purification of those cells.

I.3.3.1 Atrial- versus Ventricular-like Cardiomyocytes

Cell lineage tracing experiments in animal models complemented with *in vitro* cardiogenic differentiation studies using mouse and human PSCs have been valuable tools for the identification of the developmental origin of the different subtypes of CMs present in the human heart (Figure I-5).

As mentioned in section I.1.2.1, FHF and SHF represent two distinct cardiac progenitor populations that contribute to different subtypes of cardiac cells *in vivo*, in which FHF progenitor cells differentiate early and have only cardiogenic potential, whereas SHF progeny have a period of proliferation before differentiation and are multipotent cells, being able to differentiate not only into CMs but also into vascular cells (Galdos et al., 2017).

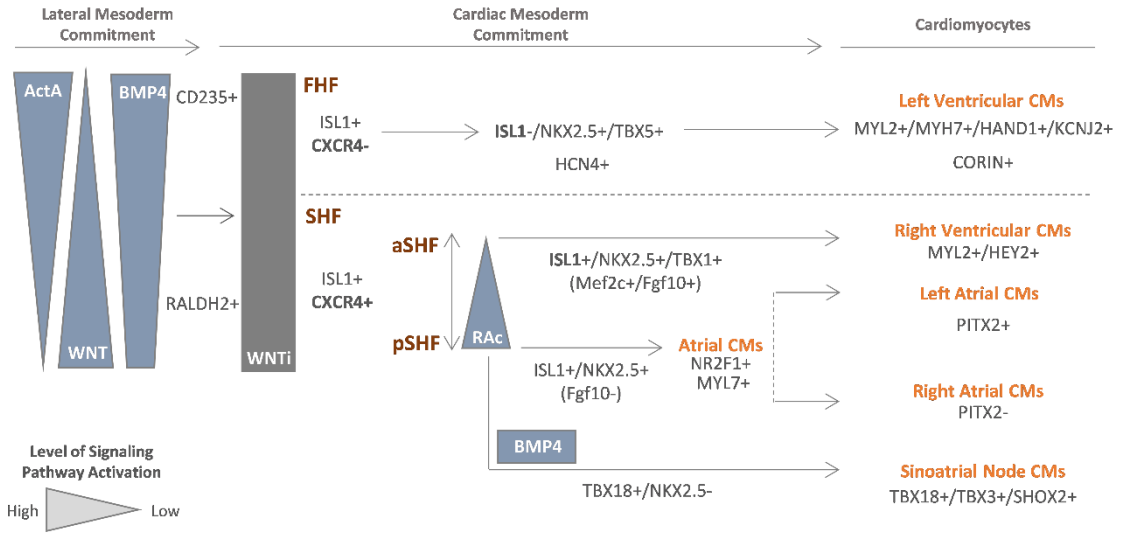

Figure I-5 *In vitro* modulation of hPSCs differentiation towards the different subtypes of CMs. FHF, First Heart Field; SHF, Second Heart Field; ActA, Activin A signaling; WNT, Wnt signaling; WNTi, Wnt signaling inhibition; RAc, retinoic acid signaling; aSHF, anterior SFH; pSHF, posterior SHF. Information collected from in vitro hPSCs cardiac differentiation studies ((Andersen et al., 2018; Cui et al., 2019; Lee et al., 2017b; Protze et al., 2017; Zhang et al., 2019b)). The markers in lowercase were taken from mice model studies.

Lineage tracing studies in mice embryos identified *Hcn4* and *Isl1* as two important markers that allow the distinction between FHF/SHF progenitors. Später and colleagues (Später et al., 2013), reported a predominant FHF localization of *Hcn4* in the early mouse embryo, being further on detected within the left ventricle, and downregulated thereafter. The expression of *Hcn4* in FHF cell population overlaps with *Tbx5* expression, which has been also identified to be predominantly expressed in the cardiac crescent (Bruneau et al., 1999). In the same study, the authors confirmed these findings using differentiation of hPSCs into the cardiac lineage, observing the presence of SHF and FHF progenitor cells after 6/7 days of differentiation. Through the isolation of hPSC-derived HCN4^{+}/FHF cells, they showed their preferential differentiation potential towards a cardiomyogenic cell fate.

Isl1 was firstly identified as a marker preferentially expressed in SHF cardiac progenitor cells (Cai et al., 2003). In a different study performed in mouse embryos, *Isl1* was described as a precardiac mesoderm marker that starts to be expressed prior to the FHF/SHF partitioning (Meilhac et al., 2004), and it is then transiently expressed in FHF progenitor cells while having a more prolonged expression in SHF. More recently, Andersen and colleagues, through *Isl1* tracing using a Isl1^{Cre} mice model (Andersen et al., 2018), suggested also that Isl1 is a pan-cardiac mesoderm marker. However, they also demonstrated, by using HCN4^{GFP} (FHF) and TBX1^{Cre} (SHF)(Huynh et al., 2007) mouse embryos, that *Isl1* expression is downregulated at embryonic day 8.5 (E8.5) in GFP^{+} cells, suggesting that Isl1 is transiently expressed in the FHF. Interestingly, in the same study the authors identified *CXCR4* as a cell surface marker that allowed to distinguish between FHF and SHF progenitor populations *in vivo* and at early stages of cardiac

differentiation from mESCs and hPSCs *in vitro*, at which time point both CXCR4$^+$ and CXCR4$^-$ populations express *ISL1*. Additionally, they showed that CXCR4$^+$ progenitor cells were more proliferative and multipotent, compared with the CXCR4$^-$ population, which mainly exhibited CM differentiation potential. The same authors suggested that higher levels of BMP4 activation during the mesoderm induction stage favors CXCR4- cell population, whereas Wnt signaling activation favors CXCR4$^+$ progenitor cells.

Moving further in the identification of the origin of the different subpopulations of CMs, a more recent work from Zhang and colleagues, using *in vitro* differentiation of hPSCs into cardiac progenitor cells (Zhang et al., 2019b), showed that NKX2.5$^+$/TBX5$^+$ cells represent a FHF-like derived population, that predominantly differentiates into ventricular-like CMs that are genetically and functionally similar to left ventricular CMs, expressing *HAND1* and *KCNJ2* markers (Zhang et al., 2019b). They also identified *CORIN* as a specific cell surface marker for the NKX2.5$^+$/TBX5$^+$ subpopulation, enabling in this way the isolation of left ventricular CMs from a mixed population of hPSC-derived CMs. Finally, they also showed that the NKX2.5$^+$/TBX5$^-$ subpopulation represents a SHF-derived population that differentiates mainly into CMs (±78% cTNT$^+$). However, since 90% of those CMs showed atrial-like profile, expressing, among other genes, *PITX2* and *NR2F2*, it was suggested that this represents a posteriorly derived SHF population. Indeed, early studies in mice models, suggested the existence of sub-clusters of cells within the SHF progeny. Anterior SHF (aSHF) has been suggested to not contribute to atrium, being responsible for the development of OFT and right ventricle myocardium (Galli et al., 2008; Verzi et al., 2005). Verzi and colleagues showed that aSHF represented a subpopulation within the SHF progeny positive for *Mef2c* and *Isl1* was identified as a *pan*-SHF marker (Verzi et al., 2005). Additionally, posterior SHF (pSHF) was described to be responsible for the generation of atrial myocardium (Galli et al., 2008). The left and right sides of the pSHF population contribute to the left and right atrium (LAT and RAT), respectively, being *Pitx2c* an important mediator of this process, which is expressed in left and not in right atrium (Galli et al., 2008).

RA signaling has been demonstrated to play a central role in several steps of *in vivo* cardiovascular development, including atrial and sinus venosus specification (Ryckebusch et al., 2008), and thus the activation of this pathway has been successfully used as the main driver for atrial-like CMs differentiation from hPSCs (Devalla et al., 2015; Lee et al., 2017b; Lemme et al., 2018; Pei et al., 2017; Zhang et al., 2011) (Figure I-6). In fact, the anterior/posterior patterning in SHF can result in part from RAc signalling activity. Moreover, Lee and colleagues (Lee et al., 2017b) showed that atrial and ventricular CMs (left ventricular-like CMs), obtained from hPSC differentiation, are generated from different mesoderm populations and identified RALDH2 and CD235a as two markers that can be used to distinguish and specifically select mesodermal progenitors that are more prone to differentiate into atrial CMs or left ventricular-like CMs, respectively. These two mesodermal populations can be enriched through manipulation of BMP4 and Activin A concentrations during the first days of cardiac differentiation. Higher levels of Activin A provide an enrichment of the CD235a$^+$ cells and lower levels of Activin A the enrichment of

RALDH2^{+} cell population. Interestingly, by activating RA in RALDH2^{+} cells, atrial CMs were generated, otherwise the progenitor population evolved towards right ventricular-like CMs.

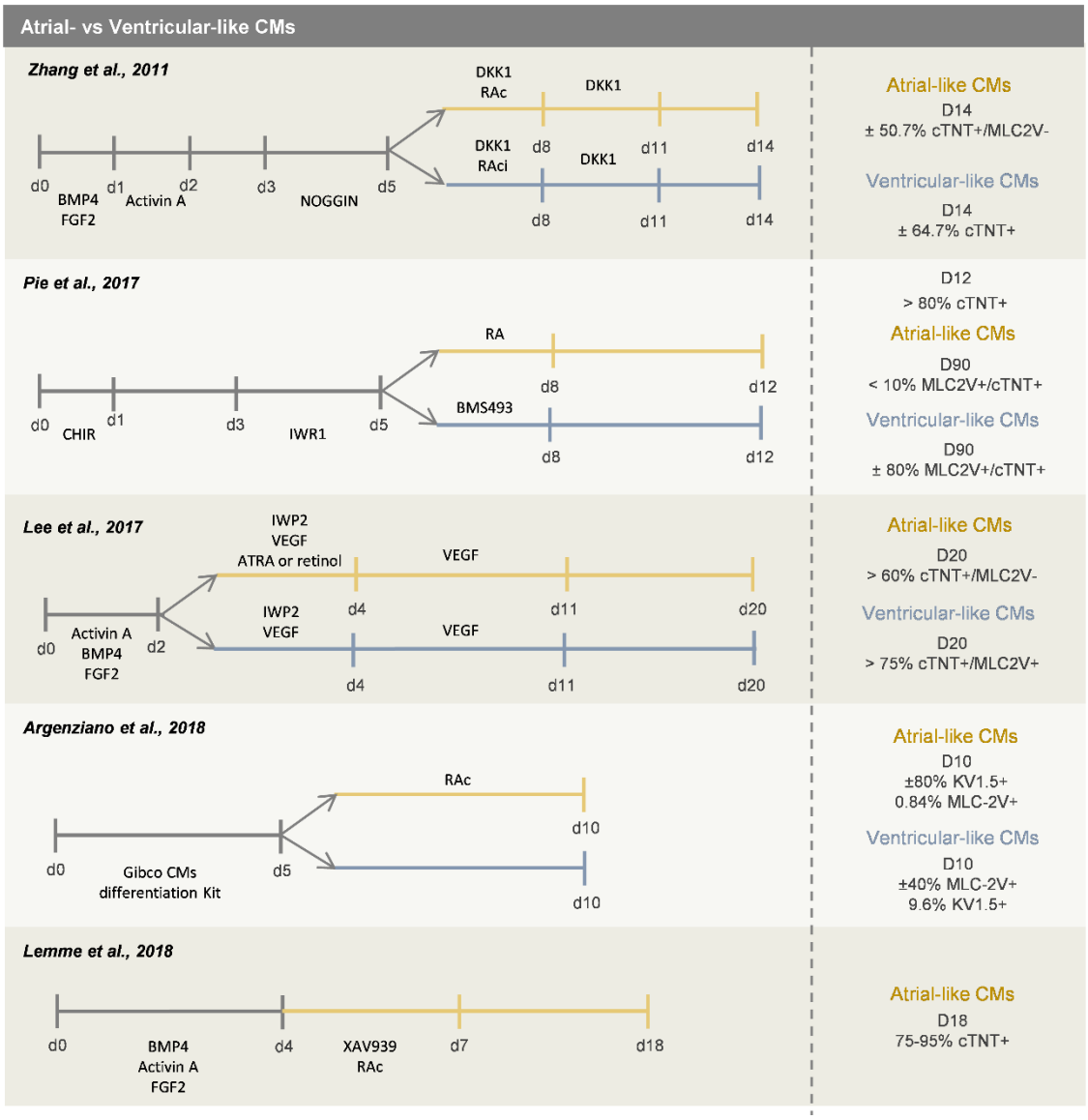

Figure I-6 Current *in vitro* strategies to generate atrial-like CM from hPSCs. ATRA, all-trans-retinoic acid.

Other relevant reports in this field have identified additional relevant markers to distinguish different subpopulations of CM progenitors. Specifically, the Leukemia Inhibitory Factor Receptor (*LIFR)* was identified as a cell surface marker that allow the identification of a cardiac mesoderm cell population responsible for the generation of ventricular CMs (Foo et al., 2018), and CD77^{+}/CD200^{-} cell-surface signature was described as a possible selective tool to specifically identify already differentiated ventricle CMs (Veevers et al., 2018). However, none of these studies mentioned if the generated ventricular CMs have a SHF or FHF mesoderm progenitor cell population origin. Additionally, *GFRA2* was identified as a marker that characterizes a cardiac progenitor cell population that resides in both SHF and FHF (Ishida et al., 2016). Interestingly, through hPSCs cardiac differentiation, the authors identified that the subpopulation GFRA2^{+}/KDR^{low}/PDGFRA^{+}/KIT^{-}, obtained after 4 days of differentiation, is a multipotent progenitor

population, whereas the subpopulation GFRA2^{+}/KDR^{-}/PDGFRA^{+}/KIT^{-}, present after 8 days of differentiation, is unipotent, presenting only cardiomyogenic fate potential. Additionally, CD82 has been also identified as a cardiac progenitor cell-surface marker, which represents cardiac progenitor cells that almost exclusively differentiate into CMs (Takeda et al., 2018a).

A recent report, which performed a single-cell transcriptomic analysis of the different stages of embryonic human heart development from 5 to 25 weeks of gestation, and studied individually each chamber specification, has now opened the possibility to confirm the specificity of already reported markers for each subtype of myocardium (Cui et al., 2019). Moreover, it can also reveal new markers, which can be used in the future to help the development of more precise CM subtype differentiation protocols and purification methodologies. Among the differentially expressed genes in atrial vs ventricular myocardium and right vs left segmentation, at 5 weeks of gestation, this study confirmed *MYL2* as a ventricular CM marker, common in both left and right ventricular CMs; *NR2F1* and *NR2F2* as atrial CM markers common to both left and right atrial CMs; *MYH7*, *HAND1* and *KCNJ2* as LV markers; *HEY2* as a RV marker; *PITX2* and *GJA5* as a LAT marker; and *CAV1* and *HCN4* as RAT markers. Interestingly, *MYL7*, also known as MLC2A, which is a commonly used marker for atrial CMs *in vitro*, was not differentially expressed among atrial and ventricular CMs, at least at this gestation stage. This could be in agreement with what is observed *in vitro* when differentiating hPSC into CMs, in which early ventricle CMs also express *MYL7*.

In summary, relevant information regarding specific markers and signaling pathways involved in atrial and ventricular CMs segmentation is now available, which can be further used to selectively produce a specific desired subpopulation of CMs. Overall, higher levels of Activin A in the presence of BMP signaling pathway activation during the first stage of mesoderm specification favor FHF cardiac progenitor cell generation and consequently LV-CMs specification. On the other hand, lower levels of Activin A in the presence of Wnt and BMP signaling pathway activation favor SHF progeny. These progenitor cells, after Wnt signaling inhibition, specify into ventricular CMs similar to RV-CMs. The activation of RA pathway during or after Wnt signaling inhibition for a short period of time is described as the main stimuli to favor atrial CMs specification from the same cardiac progenitor cell population.

I.3.3.2 SAN Cardiomyocytes

Up to date, the most important progress regarding the generation of conduction system CMs from hPSCs has been made for SAN pacemaker cells. SAN CMs are specified from the sinus venosus, that arise from a TBX18^{+}/NKX2.5^{-} progenitor population of cells (Mommersteeg et al., 2010), more specifically from the posterior SHF progenitor population, from where atrial CMs also arise (Figure I-5). With the progression of development, a gene regulatory network involving *TBX3*, which is responsible for the repression of atrial genes, and *SHOX2*, which is responsible for the repression of *NKX2.5*, allows SAN lineage specification. SAN cells also express *HCN4*, which confers the spontaneous electrical activity of these cells.

Generation of SAN-like pacemaker cells from hPSCs has been achieved by mimicking the developmental steps known to be involved in SAN specification *in vivo.* As already described above, by using a standard CM differentiation protocol, Zhang and colleagues identified a subpopulation of NKX2.5^{-}/TBX5^{+} cells that further differentiated into functional SAN-like CMs, expressing *SHOX2*, *TBX3* and *TBX18* (Zhang et al., 2019b), reinforcing the idea that SAN-like CMs arise from a NKX2.5^{-} population. Recently, Protze and colleagues (Protze et al., 2019) reported a directed differentiation protocol for generation of SAN-like CMs from hPSCs (Figure I-7). They first optimized the stage of mesoderm development, through manipulation of BMP4 and Activin A signaling pathways, to promote differentiation into posterior SHF mesoderm, as it was previously described (Lee et al., 2017b). Afterwards, they showed that RA and BMP4 favour the generation of SAN-like CMs from posterior SHF progenitor cells, and FGF and TGFβ pathways inhibition prevented generation of NKX2.5^{+} CMs. This optimized protocol allows the generation of 30-36% cTNT^{+}/NKX2.5^{-} SAN-like pacemaker cells, which were enriched to more than 80% by FACS, using the combination of SIRPA^{+}/CD90^{-}/NKX2.5-GFP^{-} markers. A more recent work demonstrated that the activation of canonical Wnt signaling in NKX2.5^{+} cardiac progenitor cells obtained after 5 days of differentiation, promotes the commitment of those cells into pacemaker-like CMs (Ren et al., 2019), which express several known markers of SAN cardiac cells, including *SHOX2*, *TBX18*, *HCN4* and *TBX3* and do not express *NKX2.5*. This protocol generates 54.2 % cTNT^{+} CMs, from which ± 80% are SHOX2^{+} and ± 50% are NKX2.5^{-}. The remaining cTNT^{-} cardiac cells were mainly epicardial-like cells, which is in agreement with recent studies that also report similar protocols to obtain epicardial cells from hPSCs, as it will be further explored in this chapter.

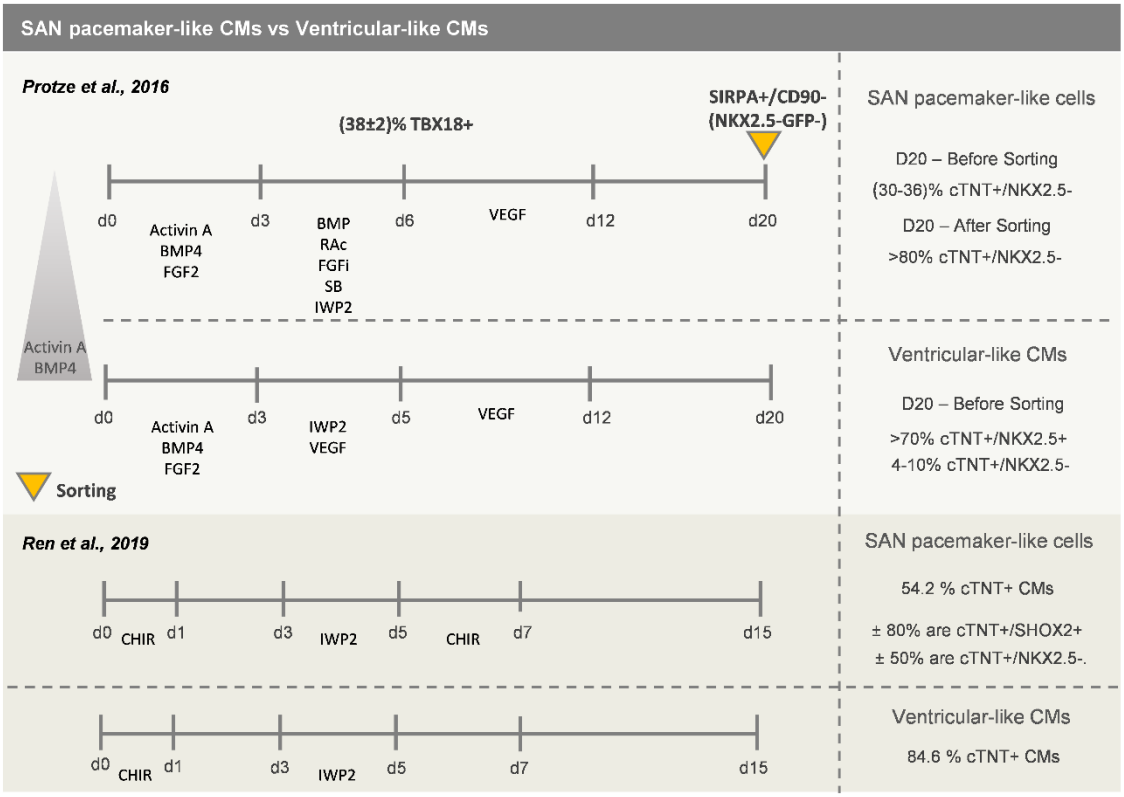

Figure I-7 Current in vitro strategies to generate SAN pacemaker-like CMs from hPSCs.

I.3.4 Generation of Non-CMs Cardiac Cells Present in Human Heart from hPSCs

I.3.4.1 Vascular Cardiac Cells

The protocols that have been described to obtain vascular cells *in vitro* from hPSCs (Figure I-8) are normally organized in three main steps, the first comprising cardiac mesoderm induction, followed by vascular progenitor cell specification and proliferation, and finally by ECs or pericyte/ vascular SMCs commitment and expansion. Since the first attempts to generate cardiovascular progenitor cells, and afterwards vascular cells, were not highly efficient, MACS or FACS-based purification methods were normally integrated with the differentiation protocols.

I.3.4.1.1 Endothelial Cells (ECs)

When generating ECs from hPSCs, the progenitor stage of ECs (EPCs) is normally controlled by CD34 and KDR expression and the most common used markers to assess mature ECs *in vitro* are CD31 and CD144. The first stage of mesoderm commitment normally takes two/three days and the most widely described approaches rely on the activation of the Wnt/β-catenin pathway, in some cases combined with the supplementation with BMP4 and Activin A growth factors (Farkas et al., 2020; Harding et al., 2017; Nguyen et al., 2016; Palpant et al., 2017; Patsch et al., 2015; Sahara et al., 2014; Sriram et al., 2015; Zhang et al., 2017). The inclusion of BMP4 activation during this first stage of differentiation has been described to enhance endothelial commitment by favoring the induction of KDR^+ precursor cells, which has been correlated with a higher percentage of endothelial progenitor cells at later stages of differentiation (Patsch et al., 2015; Sahara et al., 2014). Regarding the stage of vascular commitment, activation of the VEGF pathway through exogenous stimulus is the most widely used strategy. However, recent findings demonstrated that the addition of other cytokines or small molecules, such as (1) the TGFβ signalling inhibitor SB431542 (Orlova et al., 2014), (2) the inhibitor of Notch signaling DAPT (Farkas et al., 2020; Sahara et al., 2014), (3) the cAMP and protein kinase A pathways enhancer forskoline (Farkas et al., 2020; Patsch et al., 2015), and Tβ4 (Rosa et al., 2019), potentiate the effect of VEGF and promote EPCs proliferation and maintenance. The addition of BMP4 during the stage of vascular commitment, in combination with only VEGF (Sriram et al., 2015) or with VEGF/FGF2 (Harding et al., 2017; Palpant et al., 2015, 2017), VEGF/SB (Zhang et al., 2017), or VEGF/FGF2/DAPT (Nguyen et al., 2016) has also been used to favor the development of EPCs. The stepwise optimization of these two first stages to specify EPCs from hPSCs, in combination with a progression to more defined and serum-free protocols (Farkas et al., 2020; Harding et al., 2017; Rosa et al., 2019; Sriram et al., 2015; Zhang et al., 2017) improved the efficiency and reproducibility of the differentiation methods. With these more recent optimized protocols to generate EPCs, it is now possible to generate more than 80% $CD34^+/CD31^+$ EPCs within 5 days of differentiation without the need for any cell sorting strategy. After cell passage and culture in EC-specific culture medium, generally supplemented with VEGF, and after

successive passages in culture, these immature EPCs differentiate towards CD31⁺/CD144⁺ mature-like ECs.

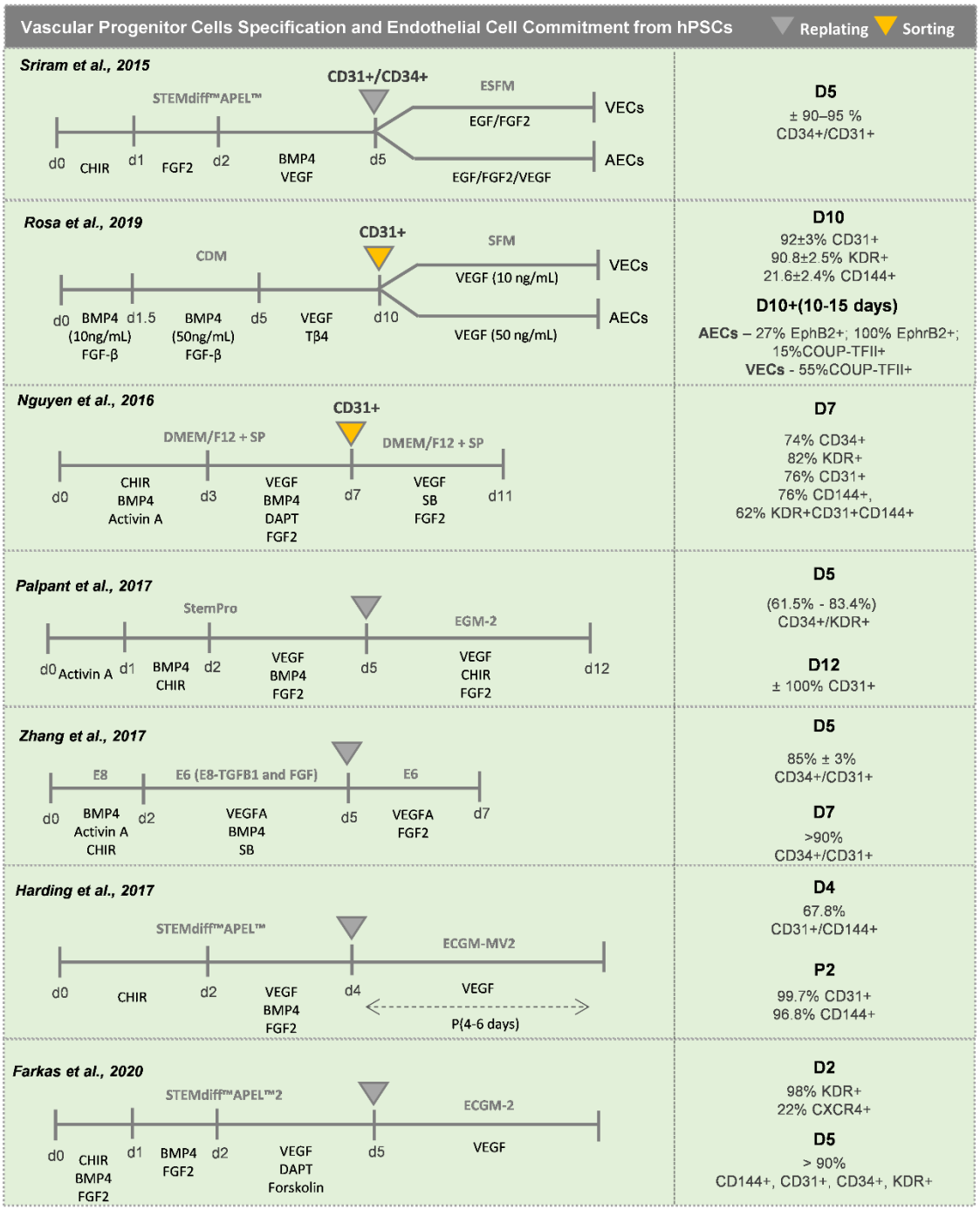

Figure I-8 Current *in vitro* strategies to generate vascular progenitor cells and endothelial cells (ECs) **from hPSCs and respective molecular markers**. VECs, Venous Endothelial Cells; AECs, Arterial Endothelial Cells; P, Passage; AA, Ascorbic Acid; DMEM/F12+SP, DMEM/F12 + chemically defined lipid concentrate + ITS + Glutamax + monothiol glycerol + AA; ECGM-MV2, Endothelial Cell Growth Medium MV2, PromoCell; ESFM, Endothelial Serum-Free Medium, GIBCO; ECGM-2, Endothelial Cell Growth Medium 2, PromoCell.

The differentiation strategies described so far include the derivation of a population of mesoderm-derived cardiovascular progenitors. However, in this case, the resulting population of vascular cells normally represents a heterogeneous mixture of ECs subtypes, which although sharing many features, also present functional and transcriptomic differences, depending on the lineage trajectory used to obtain them. For this reason, the development and deeper characterization of different sub-types of ECs is being now explored to improve the suitability of these cells for downstream applications, such us regenerative medicine and tissue engineering. Different groups are now optimizing protocols to generate in a more controlled and robust way different sub-populations of ECs, namely (1) vessel-like arterial and venous ECs (Rosa et al., 2019)(Sriram et al., 2015), (2) endocardial-like ECs, which were recently identified as $NKX2.5^{+}/CD31^{+}$ ECs and described to have the capacity to induce trabecular fate in CMs and the ability to undergo EndoMT to give rise to mesenchymal cells that share expression features with valvular interstitial cells (Misfeldt et al., 2009)(Mikryukov et al., 2021), and (3) hemogenic mesoderm-derived ECs, which have blood-forming capacity (Palpant et al., 2017). A recent protocol highlighted the generation of endocardial-like ECs from hPSCs (Mikryukov et al., 2021).

I.3.4.1.2 Vascular Smooth Muscle Cells (SMCs)

Different sources for SMCs progenitors have been identified in the heart, including cardiovascular progenitors derived from a SHF cell population and PECs. Regarding the development of SMCs from cardiovascular progenitors (Figure I-9), Cheung and colleagues (Cheung et al., 2014) reported an efficient protocol based on BMP4 and FGF2 supplementation for lateral plate mesoderm induction from hPSCs, followed by a 12 days period of SMCs specification using PDGF-BB and TGFβ1 growth factors. After this period, more than 80% of the cells were $CNN1^{+}/MYH11^{+}$ with SMCs showing a spindle or stellate shaped morphology. In addition, Patsch and co-workers (Patsch et al., 2015) showed that after mesoderm induction, the addition of Activin A and PDGF-BB generated ±90% $CD140a^{+}$ cells after 6 days of differentiation. Orlova and colleagues (Orlova et al., 2014) also described a method to obtain pericytes after vascular progenitor population specification, by culturing the $CD31^{-}$ fraction after sorting, in endothelial cell basal medium followed by medium supplementation with TGFβ3 and PDGF-BB for pericyte commitment. Regarding the generation of SMCs from PECs (Figure I-10), the majority of the protocols is based on the use of a combination of TGFβ1 and FGF2 (Bao et al., 2017; Witty et al., 2014a; Zhao et al., 2017), or TGFβ1 and PDGF-BB (Iyer et al., 2015) to generate a highly pure population of $ACTA2^{+}/CNN1^{+}/TAGLN^{+}$ SMCs.

Different methods have been described to assess vascular cell function. Regarding ECs, the capacity of tube formation in Matrigel is one of the most widely used functional tests. The capacity for acetylated low-density lipoprotein (Ac-LDL) uptake and response to pro-inflammatory cytokines, seen by the upregulation of the intracellular adhesion molecule-1 (ICAM1) upon TNF-α and IL-1β treatment, is also an important functional test (Orlova et al., 2014). Regarding SMCs, function can be evaluated *in vitro* by assessing the contractibility after stimulation with vasoconstrictive drugs or cytokines (e.g. endothelin1 and carbachol), and also by evaluating the

deposition of extracellular fibronectin following treatment with increasing concentrations of TGF-β1 and angiotensin II (Cheung et al., 2014).

I.3.4.2 Cardiac Fibroblasts

CFs present a highly variable morphology in culture and are mostly sheet or spindle-like shaped. Although there is not a specific marker for the identification of CFs, a combination of cytoskeletal, cell membrane, nuclear and extracellular markers have been used to identify these cells. Periostin (POSTN), fibronectin, and collagen types I, III, V, and VI are the main structural components produced by CFs present in cardiac tissue. Moreover, vimentin has been used as a cytoskeletal marker, *TCF21* as a nuclear marker and PDGFRα, *DDR2* and CD90 as cell membrane markers.

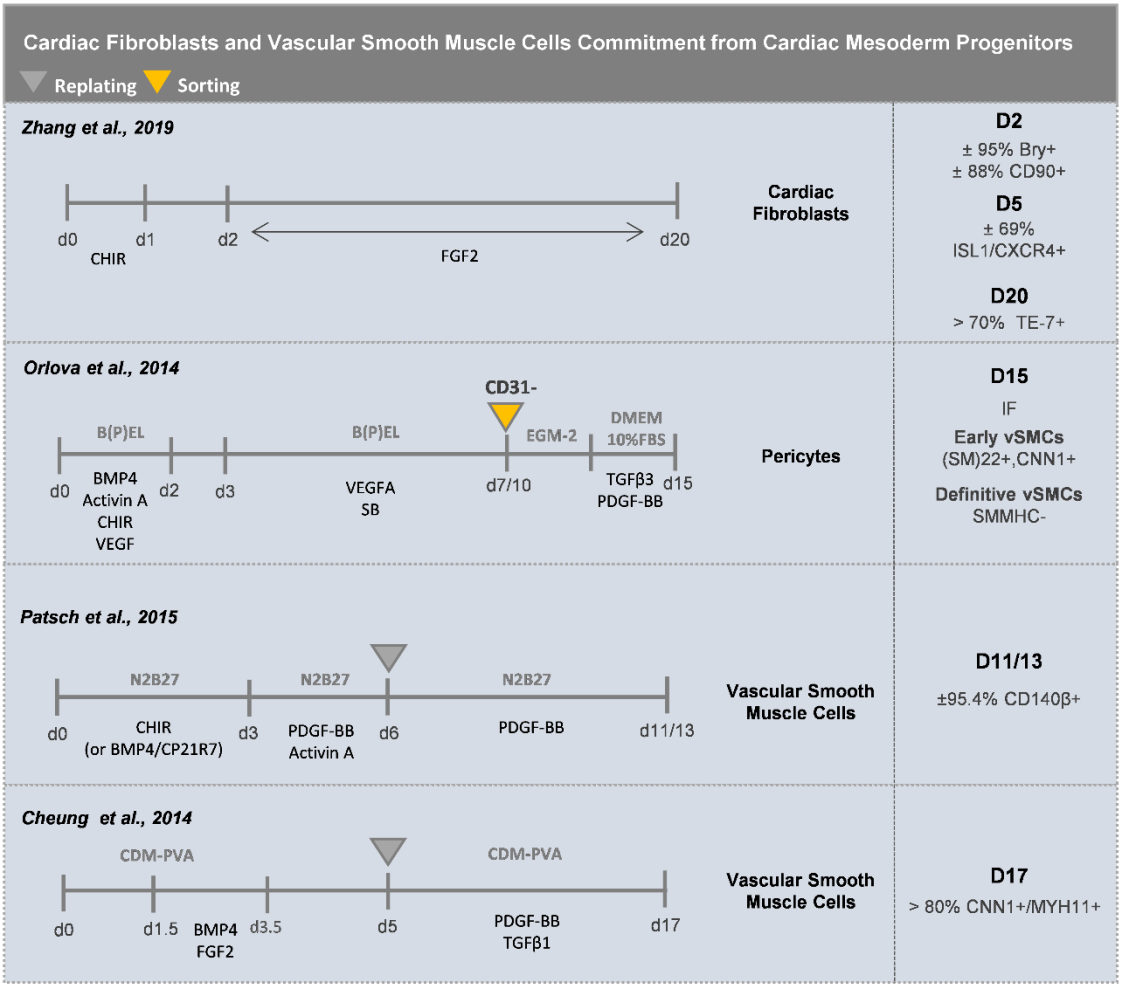

Figure I-9 Current *in vitro* strategies to generate cardiac fibroblasts (CFs) and vascular smooth muscle cells (SMCs) from cardiac mesoderm progenitors.

Cardiac fibroblasts are normally present as a minority among the overall cell population generated from hPSC differentiation protocols optimized to maximize the production of CMs. Thus, differentiation protocols have been developed to specifically derive CFs from hPSCs. In a recent study from Zhang and colleagues (Zhang et al., 2019a), a protocol for the generation of

CFs from SHF progenitors (ISL1$^+$/CXCR4$^+$) was reported. After generating mesoderm progenitor cells (Bry$^+$/CD90$^+$) by Wnt signalling activation, this population was exposed to FGF2 for 18 days, thus generating more than 70% of CFs (TE-7$^+$) (Figure I-9). Indirect differentiation protocols, that comprise a pre-differentiation stage of hPSCs into epicardial cells followed by a stage of differentiation into CFs, have been also explored to generate these type of cardiac cells (Bao et al., 2017; Iyer et al., 2015; Witty et al., 2014a; Zhao et al., 2017) (Figure I-10). For this purpose, the hPSC-derived epicardial cells (> 90% WT1$^+$cells) are exposed to FGF2 for 6-14 days to generate an almost pure population of POSTN$^+$ CF-like cells.

To assess CF function, the main evaluated parameter is the capacity of those cells for producing ECM proteins, particularly fibronectin and collagen I. Additionally, the capacity of CFs to convert into myofibroblasts (α-SMA$^+$ population with prominent fibers) upon injury can be evaluated, which has been recreated *in vitro* through TGFβ1 stimulation (Zhang et al., 2019a).

I.3.4.3 Epicardial Cells

As mentioned before, the most common markers used to identify PECs are *WT1, TCF21, TBX18, SCX and SEMA3D* (Cano et al., 2016; Katz et al., 2012; Lupu et al., 2020a). Witty and colleagues reported one of the first protocols for efficient differentiation of epicardial-like cells from hPSC (Witty et al., 2014a). They demonstrated that the combined activation of BMP and Wnt signaling in a KDR$^+$/PDGFRA$^+$ mesoderm cardiac progenitor population promotes the generation of more than 80% of WT1$^+$/TBX18$^+$ epicardial like-cells (Figure I-10). After several passages in culture these cells showed characteristic properties of the *in vivo* epicardium, namely the formation of epithelial-like sheets with tight junctions expressing ZO1 and expressing ALDH1A2, which is correlated with aldehyde dehydrogenase activity, an indication of their ability to synthesize RA. An alternative method to obtain epicardial like-cells was reported by Lyer et al (Iyer et al., 2015), that proposed the combination of Wnt, BMP and RA signaling activation in lateral plate mesoderm progenitor cells (KDR$^+$/ISL1$^+$) towards the generation of more than 60% of WT1$^+$ cells after 15 days of differentiation. These epicardial-like cells showed epithelial cell morphology and expression of the epicardial markers, *TBX18*, *WT1* and *TCF21*. At the same time, Boa and colleges (Bao et al., 2017) showed that the temporal modulation of the canonical WNT signaling via small molecules was sufficient for epicardial induction from hPSCs in chemically defined, xeno-free conditions. The activation of Wnt signaling for 2 days in a NKX2.5$^+$/ISL1$^+$ cardiac progenitor population was sufficient to generate more than 90% of WT1$^+$ epicardial-like cells. They also demonstrated that TGF-β-signaling-inhibition allows the long-term maintenance of self-renewing epicardial cells. Zhao and colleagues (Zhao et al., 2017) reinforced the idea that the sole combination of RA and Wnt signaling pathways activation in a ISL1$^+$/KDR$^+$ cardiac progenitor population of cells, was sufficient to generate more than 90% of WT1$^+$-epicardial-like cells.

One of the major features of PECs *in vivo* is their capacity for migration and spreading, surrounding the myocardium of the developing heart. After the establishment of this layer, some

cells undergo EMT to differentiate into SMCs and CFs. Thus, the potential of these cells to undergo EMT has been the main functional test to identify their presence.

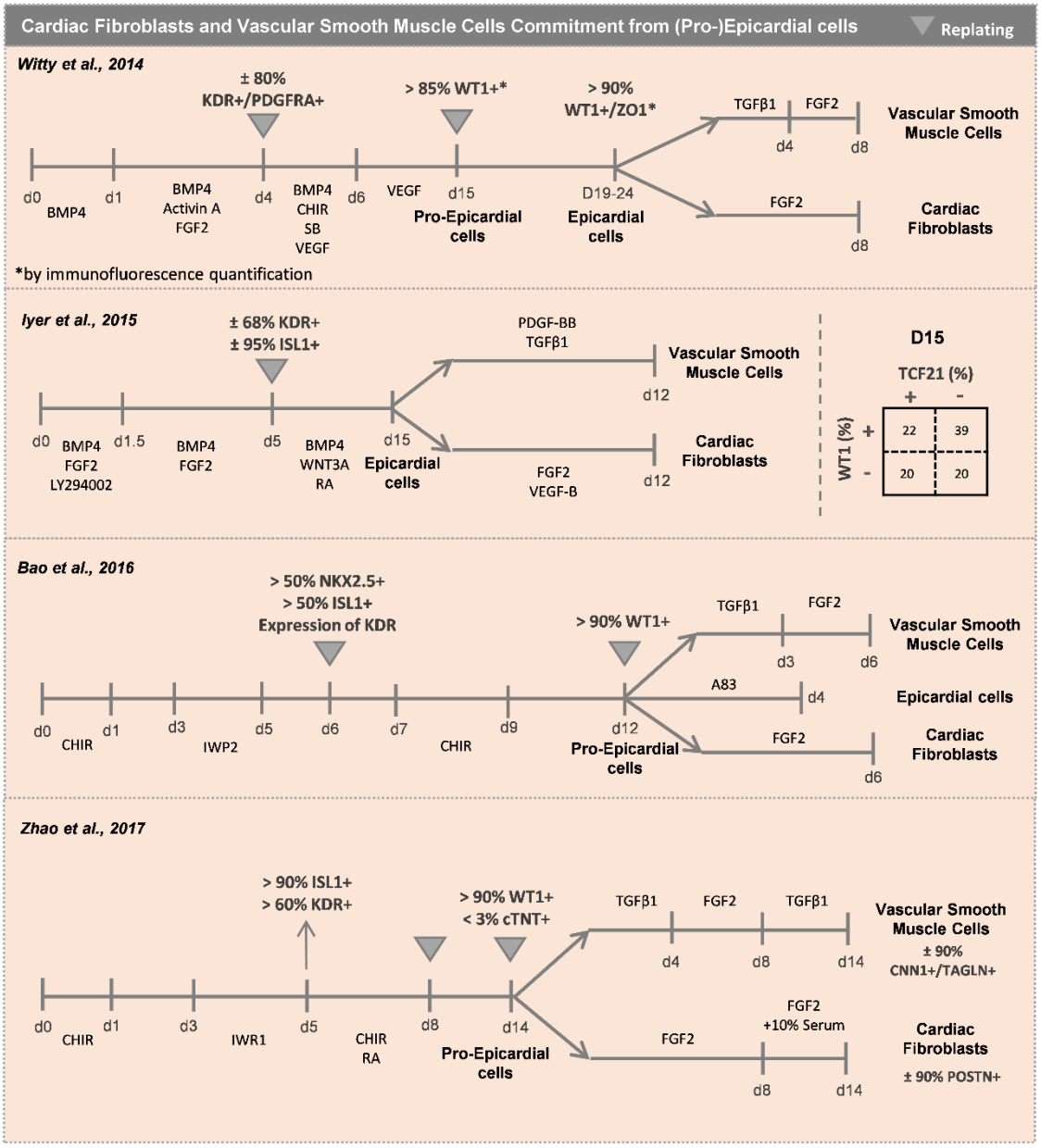

Figure I-10 Current in vitro strategies to generate cardiac fibroblasts (CFs) and vascular smooth muscle cells (SMCs) from pro-epicardial-like cells and respective molecular markers. RA, Retinoic Acid.

I.4 hPSC-derived CMs versus Adult CMs: Structural, Functional and Metabolic Aspects

One of the most relevant limitations of the hPSC-derived CMs generated through the methodologies described above, meaning without further maturation strategies, is the lack of structural, functional and metabolic maturation compared with adult CMs (Table I-2). This

represents a barrier for the utilization of these cells in a reliable way in *in vitro* applications, such as drug screening and disease modelling. Below are described the main differences observed in hPSC-CMs compared with adult CMs, in terms of structural, functional and metabolic properties.

I.4.1 Cardiomyocyte Structure and Morphology

Fetal and adult CMs present significantly different morphological characteristics, which impact cell functionality. Adult CMs show a rod shape with well-organized and aligned sarcomere structure (Figure I-11), which is the basal contractile unit of CMs. The sarcomeres are composed by Z-discs/bands and M-bands, which are present at the lateral boundaries and central part the contractile structure, respectively, and are aligned in parallel and connected by the intermediate filaments. Directly linked to the Z-band are the F-actin filaments (thin filaments). The myosin-based thick filaments do not directly interact with the Z-disc. The laminar arrangement of CMs within the cardiac tissue and the well-organized contractile apparatus, facilitates the excitation-contraction coupling, conduction velocity and generation of contractile force.

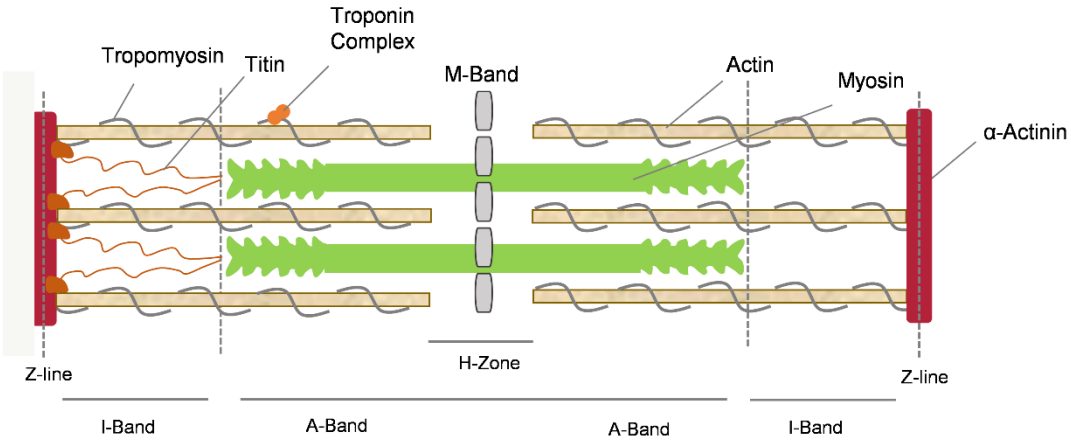

Figure I-11 Schematic representation of the sarcomere structure of CMs.

hPSC-CMs resemble fetal CMs which have a more circular shape, are smaller, and consequently, show a less organized contractile apparatus, which impacts CM function. Specifically, although Z-discs are normally observed in hPSC-CMs, they normally lack clear M-bands (Lundy et al., 2013). Additionally, It is known that during CM development, sarcomeric structure becomes more organized, occupying (40-52)% of CM area, and sarcomeric length increases to facilitate force-generation. In a relaxed adult human cardiac muscle cell, sarcomere length is about 2.2 μm, whereas hPSC-CMs, without any maturation strategy, show a sarcomere length that can go up to 1.65 μm (Lundy et al., 2013). The analysis of the alignment and density of myofiber and the sarcomere length is normally used to assess hPSC-CMs maturity *in vitro*.

During development, several myofibrillar protein isoforms switch, which modulates the contractile function of CMs and the maturity level. For example, the embryonic heart expresses an isoform designated slow skeletal troponin I (TNNI1), whereas adult hearts express cardiac troponin I (TNNI3). Also, the expression levels of β- myosin heavy chain (MYH7) in adult CMs is

normally much higher compared with the α-myosin heavy chain (MYH6). Due to that, one way to assess hPSC-CM maturity relies on monitoring expression of the TNNI3/TNNI1 and MYH7/MYH6 ratios.

Another important characteristic of adult CMs is the fact that they are 20-30% bi- or multinucleated, while early hPSC-CMs are normally mononucleated or have a percentage of multinucleation lower than 5% (Lundy et al., 2013).

I.4.2 Cardiomyocyte Functionality

Adult cardiomyocytes contraction occurs in response to an electrical stimulus, which begins in pacemaker cells and propagate throughout the whole muscle in a synchronous manner. The generation and propagation of AP is the result of the combined activity of several ion channels present on the cell membrane, which determine the ionic flow inward and outward the cell, and gap junctions, that allow the passage of ion flux throughout CMs (Figure I-12). The expression and function of these ion channels and gap junctions are crucial for the normal function of CMs and their expression and function are developmentally regulated.

Regarding how the electric impulse is propagated, when stimulated by an adjacent CM, the resting membrane potential rises to a threshold value that triggers the beginning of the depolarization process (Figure I-12A). During this phase, fast Na^+ channels open and induce a rapid influx of Na^+ ions to the interior of the cell, increasing in this way the membrane potential. When the maximum of depolarization is reached, Na^+ channels close and K^+ channels open, resulting in a small decrease in membrane potential, known as early repolarization. After this phase, called the plateau phase, the potassium flux is balanced by calcium influx, keeping the membrane potential relatively stable. As Ca^{2+} channels close, K^+ flux predominates and membrane potential returns to the resting value. This characterizes the action potential profile of a mature ventricle CM. It is during the plateau phase that the contraction occurs. The influx of calcium ions during that phase is not sufficient

Table I-2. Comparison between hPSC-derived and adult CMs. Summary of the main differences reported in the literature regarding CM structural, electrophysiological, contractile and metabolic functional parameters between early age hPSC-CMs and adult CMs.

	Immature hPSC-CMs	Adult CMs	Methods used to assess *in vitro*
Cell structure and organization (Morphology)			
Cell shape	Round	Rod-like	- RT-PCR for myofiber proteins expression level (TNNI3/TNNI1; MYH6/MYH7) - Immunostaining (cTNT/α-actinin/F-actin) – myofiber alignment and density - TEM – bands and discs identification - α-actinin/F-actin – Sarcomere Length
	Mainly Mononucleated	20-30% multinucleated	
Sarcomere Appearance	Disordered	Organized (Aligned along the longitudinal axis)	
Sarcomere Proteins (Isoform Switch)			
Myosin Heavy Chain (MHC)	β > α	β >> α	
Titin	N2BA	N2B	
Troponin I	ssTnI (TNNT1)	CTnI (TNNT3)	
Sarcomere Units			
Z-discs and I-bands	Formed	Formed	
H-zones and A-bands	Formed (prolonged differentiation)	Formed	
M-bands	Absent or low defined	Present	
Sarcomere Length	1.6 µm	2.2 µm	
Electrophysiology			
Upstroke velocity	2 to >200 V/s	300 V/s	- Action potential profile (Patch Clamp; MEA; Voltage sensitive dyes) - Immunostaining (cTNT/α-actinin/F-actin/Cx43)
Resting membrane potential	−20 to -60 mV	−80 to -90 mV	
Conduction velocity	2.1–20 cm/s	41–84 cm/s	
Upstroke Velocity	2–200 V/s	300 V/s	
Spontaneous automaticity	Exhibit	Absent	
Gap Junctions	Circunferencial distributed	Polarized to intercalated discs	
Conduction velocity	Slower (≈0.1 m/s) Inefficient	Faster (0.3–1.0 m/s) Efficient	
Contractility			
Contraction force	0.08-4 mN/mm2 for 3D cultivation; nN range for a single cell	40–80 mN/mm2 for muscle lines; µN range for a single cell	- Ca^{2+} Transients (fluorescence Ca^{2+} dyes) - Response to compounds that interfere with calcium handling process - TEM – for T-tubule observation - Caffein stimulation (caffeine induces calcium release from SR)
Ca^{2+} handling proteins (CASQ2, RyR2, and PLN)	Low or absent	Normal	
T-tubules	Normally not present	Present	
Metabolism			
ATP source (Metabolic Substrate)	Glycolysis (Glucose)	Fatty acid β-oxidation (fatty acids)	- TEM - mitochondria distribution, size and abundance) - ATP Production Assays **-** Metabolomic Analysis
Mitochondria	Irregularly distributed; paucity	High number, Localized along the sarcomeres, Well developed cristae, Regularly distributed; 20–40% of cell volume	

to trigger sarcomere contraction, but it is responsible for triggering the release of calcium from the sarcoplasmic reticulum (SR) to the cytoplasm. Specifically, the intracellular calcium binds to the ryanodine receptors (RyR) located on the SR membrane and stimulate the secretion of Ca^{2+} from the SR, a process known as calcium-induced calcium release (Figure I-12B). The increased availability of calcium allows cross-bridge formation in the myofilaments and makes the cell contraction possible. For the specific case of nodal CMs, it is described that the release of calcium from the SR is the trigger and not the consequence of calcium ion influx through the cell membrane (Kane and Terracciano, 2017). The presence of these ion channels and gap junctions in hPSC-derived CMs are not as expressive as they are in adult CMs. That, together with undeveloped cell-cell interactions and an immature sarcomere structure, confers hPSC-CMs immature electrophysiological features that directly affect action potential profile and contraction dynamics.

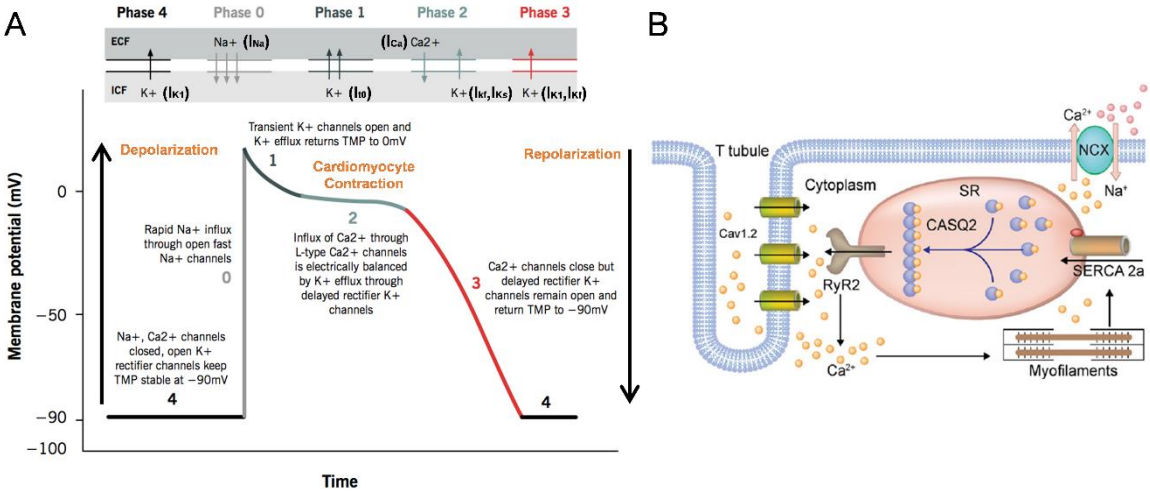

Figure I-12: Action potential profile of ventricle CMs and contraction event. (A) Schematic highlighting the different phases (0-4) of action potential profile of ventricular CMs and the most relevant ion channels and ion currents linked to each phase. Adapted from(Li et al., 2016) (B) Schematic of excitation-contraction coupling in CMs. Adapted from (Karakikes et al., 2015).

Compared to adult CMs, differences in the expression level of important ion channel subunits, particularly lower potassium repolarizing current IK1 and enhanced pacemaker current IF current, result in a higher resting membrane potential (~−60 mV), compared with the value observed in their mature counterparts (~−85/90 mV), and spontaneous contraction, which is not observed in adult CMs (Gintant et al., 2020). Additionally, a lower expression level of Na^+ channels in immature CMs leads to slower upstroke velocity, which in adult CMs is an extremely fast process (rate of depolarization ± 300 V/s). Regarding CM contraction, the information available in the literature is contradictory. In some studies, hPSC-CMs show evidences of supporting the presence of a functional SR-dependent Ca^{2+} handling. However, immature hPSC-CMs show slower and smaller Ca^{2+} transients due to very low or absent SR function, when compared with adult CMs, being the trigger of contraction mainly linked to the calcium that comes from the ion influx through cell membrane. Cell membrane in adult CMs display invaginations, named

Transverse tubules (T-tubules), which are crucial for a normal contraction behavior since they are involved in the process of triggering calcium release from SR. These structures, which fully develop about 1 month after birth, represent a hallmark of CM maturity. hPSC-CMs and fetal CMs generally lack T-tubules, which are also responsible for the slower excitation-contraction coupling process.

Conduction velocity is another important parameter that is also normally used to determine the maturity level of hPSC-CMs. In addition to the contribution of cell geometry, the distribution of gap junctions is an important factor that regulates conduction velocity. The gap junction protein connexin 43 and the N-cadherin adherent junctions are circumferentially distributed during fetal life, and as the post-natal heart matures, these proteins become progressively concentrated into intercalated disks at the ends of the cells. This sub cellular redistribution results in a much more accelerated conduction velocity. In immature hPSC-CMs, connexin 43 and N-cadherin are normally distributed circumferentially around all CM surface.

I.4.3 Cardiomyocyte Metabolism

During embryonic heart development, the metabolism of CMs changes from an almost complete dependency from glucose substrate as source of energy through glycolysis, to a predominantly fatty acid oxidative metabolism.

In immature CMs, mitochondria account only for a small fraction of the total volume of the cell, being glycolysis the major source (80%) of energy, with oxidative metabolism accounting for <15% of the total acetyl-CoA derived from energy substrates. As the development proceeds, mitochondria occupancy increases to 20–40% of the adult myocyte volume, and are distributed throughout the cell, aligned with myofibrillar proteins to facilitate energy production and excitation-contraction coupling during myocardial contraction. With the increase of mitochondrial oxidative capacity, fatty acid β-oxidation (80-90%) becomes the major source of energy in adult CMs. Similarly, to what happens in fetal CMs, hPSC-CMs rely mainly in glycolysis as primarily energy source. In fact, the majority of culture media used for CMs maintenance *in vitro* offer glucose as the main energy source, with almost no lipids present in their composition, which can limit the metabolic maturation of hPSC-CMs. Adding to that, in hPSC-CMs mitochondria normally are shown in a lower number and are less developed compared to what is observed in adult CMs and they are concentrated around the peri-nuclear area.

I.5 Engineering 3D Cardiac Microtissues to Better Mimic the Human Heart Environment

In the *in vivo* cardiac microenvironment, CMs are organized in a 3D structure, the integrity of which is maintained by ECM produced mainly by CFs, and are in close proximity with cardiac vascular cells, which play a critical role not only during the first stages of embryonic heart development but also in myocardium structural and functional maturation.

One of the main limitations that started to stand out in hPSC-CMs was the lack of structural and functional maturation compared with adult CMs as explored before in this chapter. Among different strategies that have been implemented *in vitro* to improve hPSC-CMs maturation, co-culture strategies of hPSC-CMs with other relevant cell types, as well as, 3D culture, have been explored. Regarding co-culture systems, simple models where hPSC-CMs are co-cultured with ECs and/or CFs has been extensively described in the literature. Co-culture of CMs with ECs (Lee et al., 2015) (Pasquier et al., 2017) (Abecasis et al., 2019) (Dunn et al., 2019) or CFs (Li et al., 2017b)(Kevin Range, 2012)(Beauchamp et al., 2020; Rupert et al., 2020) has been described to improve CMs structural and functional maturation. Particularly in the case of co-culture with CFs, although different studies had pointed out the electric coupling between CMs and CFs (Klesen et al., 2018), and how that affects the electric signal propagation in the heart, the majority of CMs-fibroblast co-culture systems demonstrated that paracrine signals secretion by fibroblasts and fibroblast-derived ECM are the main drivers of CM maturation (Li et al., 2017b) (Kevin Range, 2012). As a next level approach to promote not only hPSC-CM maturation but also as an attempt to develop more reliable cardiac models, the combination of multicellularity and 3D culture, has emerged as an interesting alternative to better mimic the complexity and dynamic network of interactions and signals that are present in the human heart tissue (Ma et al., 2015; Warmflash et al., 2014).

Different approaches to generate 3D cardiac MTs have been explored and reported in the literature. The two most promising approaches for *in vitro* applications are (1) hydrogel-based engineered heart tissues (EHT), and (2) cardiac spheroids obtained through self-assembly of cells in a scaffold-free environment (3D multicellular MTs). In both models, different cardiac cells, including ECs and CFs, which can be hPSC-derived or primary cultured cells, are combined with hPSC-derived CMs at a specific ratio. In the case of the EHT models, the composition of the hydrogel and the concentration of the ECM used are also important parameters to ensure tissue structure and functionality (Thavandiran et al., 2019).

I.5.1 3D Hydrogel-based Engineered Heart Tissues (EHT)

The development of EHT models has been described as a strategy to improve hPSC-CMs structural and functional maturation (Table I-3). The EHT models described in the literature are composed by hPSC-derived CMs alone (Goldfracht et al., 2019; Lemoine et al., 2017; Lu et al., 2017; Mannhardt et al., 2016) or in combination with primary fibroblast/stromal cells (Feric et al., 2019; Ronaldson-Bouchard et al., 2018a; Tiburcy et al., 2017) and endothelial cells (HUVECs) (Huang et al., 2020) normally embedded in an hydrogel-based matrix that is then shaped according to a specific format. One of the models that has been described is the ring-shaped EHT, in which the mixture is pipetted into circular casting molds, where the tissue condenses, and is then placed around passive-flexible holders (Thavandiran et al., 2019; Tiburcy et al., 2017; Voges et al., 2017). A different strategy relies on the development of elliptic shaped or strip-like cardiac tissues, which are anchored and stretched between two flexible pillars (Huang et al., 2020; Lemoine et al., 2017; Mannhardt et al., 2016; Mills et al., 2017a; Ronaldson-Bouchard et al.,

2018a; Schaaf et al., 2011). In this type of constructs, cells are exposed to mechanical load, an intrinsic attribute of these systems, through post deflection, which results in auxotonic contractile work. In addition to the mechanical load, these models have been also combined with other stimuli, such as electric impulses (Feric et al., 2019; Ronaldson-Bouchard et al., 2018a; Ruan et al., 2016) and/or different culture media (see Table I3-A) (Huang et al., 2020; Mills et al., 2017a; Tiburcy et al., 2017).

One of the main improvements regarding cardiac tissue maturation provided by these EHT constructs is the anisotropic arrangement of CMs in an elongated and well aligned manner, along the longitudinal axis of the tissue (Goldfracht et al., 2019; Mannhardt et al., 2016). In contrast to what is observed in parallel 2D monolayer culture systems, this type of EHT showed a better alignment of sarcomeres with clearly distinguishable Z-lines and I-, A- and H- zones (Huang et al., 2020; Mannhardt et al., 2016; Mills et al., 2017a; Ronaldson-Bouchard et al., 2018a). The observation of M-bands and T-tubules, which are normally absent in monolayer derived hPSC-CMs and are hallmarks of structural and functional maturation, have been observed in hPSC-CMs cultured in an electrically stimulated EHT model (Ronaldson-Bouchard et al., 2018a). Additionally, in these type of models it has been observed the presence of hPSC-CMs with sarcomere length around 2 µm (Huang et al., 2020; Mills et al., 2017a; Ronaldson-Bouchard et al., 2018a) which is close to the value observed *in vivo*. Myofibril protein switch to more mature isoforms was also reported in these EHT-systems, being observed increased ratios of MYH7/MYH6, MYL2/MYL7 and TNNI3/TNNI1 which is considered an indication of CMs maturation (Mannhardt et al., 2016; Mills et al., 2017a; Tiburcy et al., 2017). Moreover, through a transcriptomic analysis comparing 6 week-old EHT and 60 days-old 2D cultured CMs, Tiburcy and colleagues (Tiburcy et al., 2017) showed an increased expression level for adult-like CMs genes (genes that were preferential upregulated in adult heart sample), including *TNNI3, TTN, PLN*, and genes involved in “ventricular cardiac muscle tissue morphogenesis” in ETH.

Table I-3. Summary of studies reporting the generation of EHT models for *in vitro* applications. (A) Current strategies for the generation of EHT models, highlighting the main features of the constructs. (B) EHT models adapted to medium- to high- through screening setups and commercially available EHT platforms. HS, Horse Serum; FBS, Fetal Bovine Serum.

A	Cell Composition	Cell density (Cardiac Cells/EHT)	Hydrogel	Mechanical Load	Electrical Stimulation	Medium	Model	
Goldfracht et al., 2019	hPSC-CMs (≥ 80% cTNT^{+}) (D14-D20)	2 x 10^6	Porcine cardiac ECM	Passive stretcher device	No	IMDM + 20% FBS	Ring-shape	
Ruan et al. 2016	hPSC-CMs (73±3% cTNT^{+}) (D14-D21)	2 x 10^6	Collagen Type I (1.25 mg/mL)	Static Stress (constructs at a fixed static length)	2 Hz, 5 ms pulse (1 week)	RPMI+B27	Ring-shape	
Mannhardt et al., 2016 Lemoine et al., 2017 Ulmer et al., 2018	hPSC-CMs (D14)	1 x 10^6	Bovine fibrinogen (5 mg/ml)	Yes	No	DMEM + 10% HS + 10 mg/ml insulin	strip-like	
Lu et al., 2017	hPSC-CMs (> 90% cTNT+) (D12)	1.3 x10^6	-	No	No	RPMI+B27	Rectangular tissue holder	
Tiburcy et al., 2017	hESC-CMs (70%) + Human Foreskin Fibroblasts (30%)	1.5 x 10^6	Bovine Collagen (0.8mg/mL)	Yes	No	IMDM + 4% B27-INS + 100 ng/ml IGF1 + 10 ng/ml FGF2 + 5 ng/ml VEGF + 5 ng/ml TGFβ1	Ring-shape	
Ronaldson-Bouchard et al., 2018	hiPSC-CMs (75%) (D12) Human Dermal Fibroblasts (25%)	-	Human fibrinogen (20 mg/ml)	Yes	Increment regime of electric stimulation (0.33 Hz per day from 2 Hz to 6 Hz) (4 weeks)	RPMI+B27	strip-like	
B	**Medium- to High-throughput EHT models**							
Zhao et al., 2019 Feric et al., 2019	hPSC-CMs + hCFs (10:1)	1.1 x 10^5	Rat tail collagen (3 mg/mL)	Yes	Yes		Biowire^{TM} II (TARA Biosystems)	Strip-like Rectangular Chips (5mm×1mm×0.3mm)
Mills et al., 2017 Mills et al., 2019	hPSC-CMs* (D15)	5 × 10^4	Collagen I (2.6 mg/mL)	Yes	No	low glucose, high palmitate, no insulin	Heart-Dyno platform	Elliptic-shape Two elastomeric posts in each well (1 mm from each other) (96-Well plate)
Thavandiran et al., 2019	hPSC-CMs + hCFs (10:1)	7 x 10^4	Collagen I (2 mg/mL)	Yes	No		Cardiac MicroRings (CaMiRi)	Ring-shape Two elastomeric posts in each well (96-Well plate)
Turnbull et al., 2014 Lee et al., 2017	hPSC-CMs (D14-16) + human Foreskin Fibroblasts (1:1)	2 x 10^5	Bovine Collagen I (2 mg/mL)	Yes	No		Novoheart^{TM}	Strip-like Rectangular casting molds with two flexible PDMS pillars (10 mm from each other)
Huang et al., 2020	hiPSC -CMs (75%) (D20-22) + HUVECs (10%) + Human adult ventricular CFs (15%)	2.5 x 10^5 cells/cm2	Human fibrinogen (0.75 mg/mL) + rat tail type I collagen (2.25 mg/mL)	Yes	No	RPMI+B27 + T3 + IGF -1 + Dex	µTUG arrays	Elliptic-shape Two elastomeric posts in each microwell (interpillar spacing of 500 µm) (42 microwells of dimensions 400 µm x 800 µm x 200 µm)

Regarding electrophysiology and Ca^{2+} handling properties, EHT-CMs have been also described to show a higher expression of important ion channels and gap junctions involved in AP propagation and CMs contraction. Due to this improved functional and structural maturation, hPSC-CMs cultured in EHT models, showed also a higher sensitivity and predictivity for the effect of different classes of drugs when compared with the 2D cultured hPSC-CMs (Feric et al., 2019; Huebsch et al., 2016; Lemoine et al., 2017; Lu et al., 2017; Mannhardt et al., 2016; Ronaldson-Bouchard et al., 2018a; Saleem et al., 2020). This includes proarrhythmic and positive/negative inotropic drugs with a broad range of modes of action including modulation of ion channels, intracellular Ca^{2+} transients, myosin filaments function and β1- and β2-adrenoceptors, yielding results that were in good agreement with clinical observations. Additionally, EHT CMs were observed to present a higher resistance to drug toxicity (Lu et al., 2017) thus eliminating false positives detected in standard 2D culture systems (Mills et al., 2019).

It has been also described that EHT-CMs exhibit larger and a higher number of mitochondria, which show a more mature structure with well-developed cristae (Ulmer et al., 2018), and in some cases are located closed to sarcomeres (Huang et al., 2020; Mills et al., 2017a; Ronaldson-Bouchard et al., 2018a). A higher level of mitochondria content is linked with the improved metabolic maturation of hPSC-CMs, since adult CMs rely primarily on ATP production through oxidative phosphorylation of fatty acids. In fact, Ulmer and co-workers demonstrated that culturing hiPSC-CMs in a 3D-EHT format improves metabolic maturation through a switch from glycolysis to oxidative metabolism of glucose, lactate, and fatty acids, generating 2.3-fold more ATP by oxidation than 2D cultured hiPSC-CMs (Ulmer et al., 2018).

I.5.2 3D Scaffold-free Multicellular Cardiac Microtissues (MTs)

Scaffold-free 3D aggregation has also been explored as a strategy to develop 3D multicellular cardiac MTs through the combination of hPSC-CMs with hPSC-ECs/early vascular cells (EVCs) or primary ECs, and/or hPSC-CFs or primary CFs, at different proportions (Table I-4). Only recently it has been described a 3D multicellular MT that does not use primary ECs and CFs, and instead combines CMs/ECs/CFs derived from the same hPSC-derived mesoderm population (Giacomelli et al., 2020).

The introduction of CFs in 3D multicellular MTs has been described to facilitate aggregation and to generate more compact 3D cardiac spheroids (Giacomelli et al., 2020)(Beauchamp et al., 2020; Rupert et al., 2020)(Filippo Buono et al., 2020), likely through enhanced cell-cell adhesion. Additionally, the presence of CFs in these 3D MTs has been also described to contribute for ECM deposition, particularly collagen I, resulting in a stable collagen fibril structure, which was not observed in spheroids composed by hiPSC-CMs only (Richards et al., 2017). Additionally, and specifically in the cases where primary CFs are used for co-culture, the proportion of CFs and the level of activity of those cells have been also described as critical parameters to avoid pro-fibrotic

effects and arrhythmic behavior. It has been demonstrated that CFs are very sensitive to stiffness, which may be responsible for myofibroblast phenotype (Beauchamp et al., 2020; Rupert et al., 2020), and consequently be responsible for the generation of fibrotic environment. Interestingly, it has been also described that the origin of CFs has impact on the developed cardiac 3D co-culture model. In fact, Rupert and co-workers demonstrated that the use of dermal fibroblasts instead of CFs of heart origin compromise the generation of functional 3D cardiac models (Rupert et al., 2020).

The type and the percentage of ECs have been shown to impact the capacity of micro-vascularization network establishment inside the 3D multicellular MTs. It was previously observed that human umbilical vein endothelial cells (HUVECs) added to 3D cardiac spheroids did not spread inside the tissue (Richards et al., 2017). However, the addition of human adipose-derived stem cells (hADSCs) overcame that problem, contributing to the formation of a network of ECs, which was attributed to the pericyte-like function and pro-angiogenic properties of hADSCs. Interestingly, a different study performed by Pitaktong and colleagues showed that EVCs derived from hPSCs, a type of progenitor cells that can differentiate into both endothelial cells and pericytes, improved micro-vascularization inside 3D cardiac spheroids (Pitaktong et al., 2020). They observed that the integration of early vascular cells influences the morphology of the microvascular structure and distribution, and the overall cardiac function of the 3D cardiac tissue. In fact, when compared with the use of HUVECs, cardiac spheroids containing hPSC-EVCs presented a faster contraction, which they suggested to be related with the fact that EVCs secrete a great amount of angiogenic growth factors. They also concluded that the establishment of an appropriate balance between EVCs and CMs should be considered to obtain an optimal micro-vascularization while not compromising the cardiac function. In particular, they observed that the addition of 15% of EVCs in combination with 70% CMs and 15% CFs corresponded to the optimal 3D cardiac MT, since the contraction of the 3D MTs was not negatively affected and it allowed the formation of micro-vasculature inside the 3D structure. The same proportions have been also recently described for the generation of 3D tri-cellular cardiac MTs derived from hiPSCs (Giacomelli et al., 2020).

In addition to the impact of macrostructure arrangement and cell composition in the overall function of 3D cardiac multicellular MTs, the impact towards other aspects linked with hPSC-CMs maturation has also been studied in these models. Richard and colleagues observed an improved sarcomere organization, an increased adult cardiac troponin I and MYL2 expression, all hallmarks of CM maturation, in 3D multicellular MTs when compared with spheroids composed only by hPSC-CMs (Richards et al., 2017). In addition, Ravenscroft and co-workers (Ravenscroft et al., 2016), observed that the culture of hPSC-CMs in 3D multicellular MTs induced a significant increase in the expression of important genes related with cardiovascular function, nitric oxide production and microtubule and sarcomere assembly, highlighting the Ca^{2+} binding protein S100A1, which they suggested to play an important role in the contractile maturity of the multicellular cardiac MTs.

Table I-4. Summary of studies reporting the generation of 3D multicellular cardiac MTs. The table highlights 3D cardiac MT composition regarding the type and proportion of the different cell types, and the culture format used for MT generation. cTnI, Cardiac Troponin I; HUVECs, Human Umbilical Vein Endothelial Cells; EVCs, Early Vascular Cells; hACFs, human Adult Cardiac Fibroblasts; hSFs, human Skin Fibroblasts.

	Cardiac Microtissue Composition	Control		Cell Seeding Density	Culture Platform
Richards et al., 2017	hPSC-CMs (50%) – α-SA Human Ventricular CFs (29%) – Vimentin HUVECs (14%) – CD31 Human Adipose-derived Stem Cells (7%)	hiPSC-CMs Spheroids		$1.5x10^5$ cells/mold (±4300 cells/well)	Custom-made agarose molds containing 35 microwells (800 µm diameter, 800 µm deep)
Ravenscroft et al., 2016	hPSC-CMs/hESC-CMs (57%) – α-actinin, ACTN2 Human CFs (29%) - collagen I, COL1A1 Human Cardiac Microvascular ECs (14%) – CD31	hPSC-CMs Spheroids		500 cells/well	U-bottom ultra-low adhesion 96-well plate
Polonchuk et al., 2017	hPSC-CMs (50%) – cTNT Human Coronary Artery ECs (25%) – CD31 hiPSC-CFs (25%) – Vimentin	-		$1x10^4$/drop	96-well Hanging Drop Plates
Archer et al., 2018	hPSC-CMs (57%) – α-actinin and cTnI Primary Human Cardiac Microvascular ECs (29%) – CD31 Primary Human CFs (14%) – Vimentin and Collagen I	hPSC-CMs Monolayer		500 cells/well	Ultra-low attachment 384-well plate
Giacomelli et al., 2017	hPSC-CMs (85%) – cTNI hPSC-ECs (15%) – CD31	hPSC-CMs Spheroids	hPSC-CMs monolayer	5000 cells/well	V-bottom ultra-low adhesion 96-well plate
Giacomelli et al., 2020	hPSC-CMs (70%) – cTNI	hPSC-CMs (85%) + hPSC-ECs (15%)	hPSC-CMs (70%) + hPSC-ECs (15%) + hACFs (15%	5000 cells/well	V-bottom ultra-low adhesion 96-well plate
	hPSC-ECs (15%) – CD31 hPSC-CFs (15%) – COL1A1	hPSC-CMs (85%) + hPSC-CFs (15%)	hPSC-CMs (85%) + hPSC-ECs + hPSC-hSFs (15%)		
Pitaktong et al., 2020	hPSC-CMs (70%) – cTNT Human Adult Ventricular CFs (15%) – Vimentin hiPSC-EVCs* (15%) – Pericytes (NG2); ECs (CD31)	hiPSC-CMs (70%) + CFs (15%) + HUVECs (15%)	hiPSC-CMs (40%) + CFs (15%) + hPSC-EVCs (45%)	$3.3x10^4$ cells/well	U-bottom ultra-low adhesion 96-well plate
	* mixed population containing iPSC-ECs with iPSC-pericyte-like cells and other non-endothelial stromal-like cells				
Buono et al., 2020	hPSC-CMs (30%) – cTNT Human Cardiac Microvascular ECs (HCMECs) (50%) – VE-cadherin	Healthy hiPSC-CMs	Cardiomyopathy hiPSC-CMs	$1x10^5$/drop	60-well Hanging Drop Plates (Greiner HLA Terasaki)

	Human CFs (20%) – Vimentin					
Beauchamp et al., 2020	hPSC-CMs (80%) – Myosin Heavy Chain Human Fetal Cardiac Fibroblasts (20%) – Vimentin		hPSC-CMs Spheroids	hPSC-CMs monolayer	5000 cells/drop	GravityPlusTM hanging-drop system
Abecasis et al., 2020	hPSC-CMs (33%) – cTNT and α-actinin		hPSC-CMs Spheroids		Cell suspension microencapsulation using an electrostatic bead generator	
	hPSC-ECs + MCs (66%)	ECs (25-30%) – CD31 and VE-cadherin MCs: CFs – Vimentin + SMCs (25 – 45%) - α-SMA				

Aiming to reveal the individual and synergetic effect that each cardiac cell added to the multicellular MTs has on hPSC-CMs maturation, two different studies from the same group standout. In a study where hPSC-CMs and hPSC-ECs were co-cultured as 3D spheroids (Giacomelli et al., 2017), it was demonstrated that the inclusion of ECs and prolonged time in culture induced considerable changes in the expression of important structural and functional genes, including ion channels and calcium handling genes related with a higher degree of CM maturation when compared with 3D spheroids composed by CMs only and 2D cultured CMs. More recently, the addition of hPSC-CFs to the previous 3D cardiac MTs highlighted the additional improvements of that extra stimuli on CM structural, functional and metabolic maturation when compared with 3D-hPSC-CMs and 3D-hPSC-CMs+ECs (Giacomelli et al., 2020). Specifically, they observed a more mature ultrastructure, with higher sarcomere length and organization, regular Z-lines, I-bands, H-zones, M-lines, T-tubule-like structures and elongated mitochondria adjacent to sarcomeres. Regarding CM function, they demonstrated an improved mechanical contraction system and more mature Ca^{2+} handling properties. Moreover, the AP profiles showed a more mature behaviour, exhibiting a hyperpolarized resting membrane potential (RMP), higher upstroke velocity and fast transient repolarization after the AP peak (AP notch). Additionally, mitochondrial respiration capacity was also increased in these 3D multicellular MTs. Importantly, they showed that the improvements observed in hPSC-CM maturation resulted from the presence of both hPSC-ECs and hPSC-CFs, suggesting that the tri-cellular interaction is essential for the observed outcomes in terms of hPSC-CM maturation, and that hPSC-CFs outperformed the use of primary skin fibroblasts. Importantly, when studying the mechanistic network underlying the enhanced maturation observed in 3D co-cultured hPSC-CMs, the authors showed an upregulation of intracellular cAMP levels in hPSC-CMs which positively enhanced the Cx43 gap junction formation, promoting coupling between hPSC-CMs with hPSCs-CFs.

All of the aforementioned improvements regarding structural and functional maturation observed in 3D multicellular cardiac MTs were also reflected in an improved pharmacological response (Ravenscroft et al., 2016)(Abecasis et al., 2020). Ravenscroft and co-workers (Ravenscroft et al., 2016) observed an enhanced predictivity of the effect of positive and negative inotropic compounds in these MTs, when compared with hPSC-CM spheroids alone, in which, for some tested drugs, no effect was observed or the effect was not the expected one. These results demonstrated the superior relevance of 3D tri-cellular MTs compared to CM spheroids in which regards to the pharmacological correlation and relevance compared with *in vivo* known outcomes. It was also demonstrated that the improvement in pharmacological response requires both endothelial and fibroblast cells of cardiac origin. Additionally, these 3D tri-cellular MTs have been also proved to be a valuable tool to identify synergies between the cell types present in the cardiac spheroids in response to a specific compound by using different combinations of those three different cell types (Archer et al., 2018; Polonchuk et al., 2017).

I.6 *In vitro* Applications of hPSC-derived 3D Cardiac Microtissues (MTs)

The improvements achieved in the field of hPSC-derived cardiac MTs have increased the interest of applying those models in different *in vitro* applications, such as modelling of cardiac disorders, cardiotoxicity tests and for studying the therapeutic effects of developing drugs in the context of diseased phenotypes. Importantly, to increase the applicability of the hPSC-derived cardiac models, namely by the pharmaceutical industry, the integration of those models in medium- to high-throughput screening settings coupled with high content analytical setups, has also been the focus of attention. The miniaturization of 3D cardiac MTs is particularly relevant in cardiotoxicity and drug screening applications since, normally, large libraries of new compounds are tested at different concentrations and times of exposure, and, in this way, it is possible to maximize the amount of information collected with smaller and more cost-effective set ups.

I.6.1 *In vitro* Modelling of Cardiac Disorders – Challenges and Perspectives

A broad range of cardiovascular disorders, mainly cardiomyopathies and arrhythmic diseases has recently been modelled using hPSC-CMs (reviewed in (Brandao et al., 2017)). However, the majority of these studies still rely on hiPSC-CMs cultured in 2D monolayers. Although these models have been able to recapitulate some features of the pathologic phenotype and reveal important molecular insights about the disease mechanisms (Li et al., 2018), the *in vitro* recreation of the complete phenotype of the disease is still challenging mainly due to the functional immaturity of hPSC-CMs, which in part can hide some important features of the disorder being analysed, resulting in controversial findings. Additionally, the majority of the reported cardiac disease modelling studies uses a mixed population of CMs subtypes which can also interfere with the outcomes of the study. In this way, the use of hPSC-CMs of a specific subtype, atrial, ventricular and nodal, and also with left or right chamber specification, can level up the applicability of these models. Although, so far, the most studied cardiac diseases using hiPSC-CMs are ventricular disorders, the use of subtype-specific hiPSC-CMs can help the study of other disorders that affect a specific subtype of CM, such as atrial fibrillation, that has been already modelled *in vitro* using atrial-like hiPSC-CMs (Laksman et al., 2017). Additionally, inherited arrhythmias and cardiomyopathies that are chamber-specific, as it is the case of arrhythmogenic cardiomyopathy (ACM) (Corrado et al., 2020; Miles et al., 2019) and Brugada syndrome, can also benefit from the use of hPSC-CMs that recapitulate left or right ventricular chamber differences.

Another important limitation of this type of disease modeling studies is related with the fact that 2D monoculture of hPSC-CMs lacks the structural and multicellular complexity observed *in vivo*. In fact, although electrophysiological cardiac disorders affect specifically CMs, the introduction and use of 3D multicellular cardiac MTs can help on modelling other cardiac diseased phenotypes that have a non-CM component and study the eventual synergetic/indirect effect of that disorder on CMs. The

application of 3D tri-cellular MTs for cardiac disease modelling has been recently addressed in the literature. By using hiPSCs generated from a patient with ACM carrying a *PKP2* mutation, 3D tri-cellular MTs containing ACM-hPSC-CFs were generated (Giacomelli et al., 2020). In this study, the authors proved the role of CFs in ACM pathogenesis and clearly demonstrated the utility of using multicellular MTs for modelling this and potentially other cardiac diseases. Specifically, they showed that ACM-CFs possess a higher tendency to assume a myofibroblast-like identity and ACM-MTs showed a reduced Cx43 expression, which can impact the electrical conduction of CMs, being responsible for the induction of the arrhythmic behaviour observed in CMs. The use of 3D cardiac models per se has also been proved to benefit cardiac disease modelling studies. EHT constructs (Cashman et al., 2016; Goldfracht et al., 2019; Prondzynski et al., 2019; Zhao et al., 2019b) and 3D cultured hPSC-CMs (Shah et al., 2020) have been successfully used to recapitulate cardiac disease phenotypes showing in some cases that the use of more complex cardiac models can benefit and improve the liability of the outcomes taken from the disease modelling studies. Specifically, Goldfracht and colleagues, that studied catecholaminergic polymorphic ventricular tachycardia type 2 (CPVT2) and long QT syndrome type 2 (LQTS2) disorders using patient derived hPSC-CMs in a EHT model, showed that the arrhythmogenic potential of the generated CPVT2 and LQTS2 tissues was reduced in EHT constructs, compared to the same cells within single-cell models (Goldfracht et al., 2019), being more similar to what occurs *in vivo*. By using hiPSC-derived from a hypertrophic cardiomyopathy (HCM) patient carrying the α-actinin 2 (*ACTN2*) mutation, Prondzynski and colleagues also demonstrated the advantages of a 3D-EHT model over 2D cultured hPSC-CMs in recapitulating disease features (Prondzynski et al., 2019). In the EHT-HCM model it was possible to recapitulate several hallmarks of the disease including prolonged AP duration, increased contractility and hypertrophy. Also, upon modelling of LQTS2 cardiac disorder, Shah and co-workers revealed that clinical phenotypic differences observed in patients with this disease were also observed in hiPSC-CMs cultures as 3D aggregates but were not seen in homogenous cultures of hPSC-CMs, reinforcing the utility and necessity for more complex cardiac models in this field (Shah et al., 2020).

Apart from the benefits of using 3D models to study cardiac diseases with a genetic background, hPSC-derived 3D MTs have been also shown to be interesting models to recreate acute cardiac disorders, such as myocardium infarction (MI). By using a 3D multicellular MT (Richards et al., 2017) and by taking advantage of nutrient diffusion gradients inside the 3D model, Richards and colleagues were able to recreate different regions inside the aggregates with different oxygen levels, recapitulating this way the different areas observed in the post-MI heart. With this model, they also recreated major hallmarks of the acute post-MI cardiac environment, including fibrosis-like tissue phenotypes and the presence of unsynchronized calcium transients, and proved the applicability of these models for screening of drugs that can reverse/improve the heart damages after MI (Richards et al., 2020).

I.6.2 Cardiotoxicity Tests and Drug screening

Cardiovascular toxicity, along with hepatotoxicity, is still one of the primary reasons for candidate drugs to be discarded during the pre-clinical and clinical stages of the drug development pipeline (Onakpoya et al., 2016)(Van Norman, 2019), and it has been also one of the main causes for drugs withdrawal from the market (17% of drug withdrawal) (Siramshetty et al., 2016). Such events made clear that the standard methods that are being used to assess cardiac safety in pre-clinical stage, are not sufficiently accurate to predict how the human heart would respond to a putative compound nor informative enough regarding the mechanism of action of the tested drug. Therefore, current standard pre-clinical approaches need to be improved to better mimic the complexity of human heart, providing in this way more accurate and relevant results, and saving both time and money in the development process of a new drug. In fact, from all the new drugs that enter the drug development pipeline, less than 1% reaches the market. Moreover, a report from 2017 highlighted that the research-based pharmaceutical industry spends over $149.8 billion on R&D per year, and pre-clinical stage is the second most expensive phase regarding R&D costs, preceded by Phase III clinical Trials (IFPMA, 2017).

I.6.2.1 Pre-clinical Stage and Cardiotoxicity Assessment – Gold Standard Tests

The first step in a drug development pipeline is the pre-clinical phase, during which drug candidates undergo *in vitro* and animal *in vivo* testing. During the past years, animal models have been the gold standard to perform preliminary cardiotoxicity prediction studies. Nevertheless, since millions of animals are needed during the pre-clinical phase, animal tests represent a considerable cost, which, in 2015, was estimated to account for a total value of $11.3 billion (de Korte et al., 2020). Moreover, studies using animal models raise challenging ethical issues. Importantly, although tests performed in animals have been and will continue to be a valuable and indispensable tool in this context, the conclusions taken from these models must be interpreted with caution due to interspecies differences in which regards the frequency of contraction, expression of ion channels involved in AP profile and myofilament proteins involved in the contraction process (Milani-Nejad and Janssen, 2014; Nerbonne, 2004; Salama and London, 2007). However, *in vivo* animal models will be always necessary to provide valuable information regarding the effect at the whole organism level.

In addition to animal models, other simplified *in vitro* assays have been also applied during the pre-clinical stage. Long QT has been defined by FDA as the major cardiotoxicity issue (Braam et al., 2010) and it is commonly linked with interferences with Kv11.1 ion channel (encoded by the human ether-à-go-go-related gene (hERG)). This ion channel is a common target of a large spectrum of drugs, affecting the flux of K^+ ions by reducing the I_{kr} current (Perry et al., 2006) (Sala et al., 2017). This ion channel is negligible in mice, which has been responsible for misdetection of abnormalities in the behaviour of this channel in the past. Due to that, one of the assays that has been used in pre-

clinical *in vitro* tests to assess interaction with Kv11.1 channel is the hERG blockage assay. In this assay, immortalized cell lines are genetically manipulated to express hERG ion channel. Although these models have improved the prediction of cardiotoxicity, being a good indicative of arrhythmogenicity, they do not recapitulate the complex ion channel interactions that are presence in CMs, reducing the predictive value of this assay. Additionally, this assay it is commonly responsible for a high rate of false-positive/negative cardiotoxic compounds detection and therefore, for unnecessary drug discard at the pre-clinical stage. This problem highlights the need for the development of models that allow an integrated assessment of drug effect at multiple ion channels, pumps and exchangers.

Primary human CMs occupy also a place in pre-clinical phase in cardiotoxicity prediction studies. However, the availability and the maintenance in culture of those cells are very challenging since these are already post-mitotic cells and/or due to their almost immediate dedifferentiation in culture, which difficult their applicability (Sharma et al., 2017, 2018).

I.6.2.2 hPSC-derived Cardiac Models to Assess Cardiotoxicity *in vitro*

Due to the limitations that are still observed in the current assays used during the pre-clinical stage of drug development, hPSC-derived cardiac models are gaining attention as a potentially effective tool to be used as a complementary approach to the ones described above to increase the potential to predict the safety of newly developed drugs during early pre-clinical trials, in a diseased or healthy context. In fact, hPSC-CMs have the advantage of having a human origin, reflecting in this way specific species characteristics. Moreover, by using hiPSCs it is possible to generate patient-specific cardiac models, which is also a really important feature.

Although hPSCs-CMs are still described to present some immature functional features, namely differences in the expression profile of important ion channels, which can compromise the accuracy of drug effect prediction, the use of more complex and multicellular cardiac models has gain attention not only because these allow further maturation of hPSCs-CMs but also because they recapitulate better the heterogeneity in terms of cell composition of the human heart.

Since in drug screening applications normally a large number of compounds needs to be tested, the adaptation of already developed EHT models and 3D multicellular cardiac MTs to medium- to high-throughput screening (HTS) platforms is an important aspect that should be taken into consideration. 3D multicellular cardiac MTs can be easily generated in microscale platforms such as hanging drop microplates (Polonchuk et al., 2017), ultra-low attachment 96/384-well plates (Archer et al., 2018; Pitaktong et al., 2020; Ravenscroft et al., 2016) and micropatterned molds (Richards et al., 2017). As a major advantage of these platforms, the number of cardiac cells needed per each 3D MT is very small, with, in some cases, only 500 cardiac cells being used per each MT. Additionally, the 3D arrangement can provide superior predictions of the clinical outcome of a newly developed drug due to the inclusion of an extra variable to the system, the gradients of soluble molecules, which

better recreates what happens *in vivo*. In the case of EHT, the adaptation to a HTS format has been more challenging, mainly due to the size of the construct that should be compatible with a multi-well platform, to maximize the throughput of the system, and also due to the number of hPSC-derived cardiac cells needed for each cardiac MT. To overcome those limitations, small size EHT platforms have been described in the literature, including the Heart-Dyno platform (Mills et al., 2017a, 2019), the Cardiac MicroRings (CaMiRi) (Thavandiran et al., 2019) and the μTUG arrays (Huang et al., 2020). Some platforms are now commercially available, such as the case of the Biowire™ II platform (TARA Biosystems) (Feric et al., 2019; Zhao et al., 2019b) and the cardiac tissue strip model (Novoheart™) (Lee et al., 2017a; Turnbull et al., 2014) (see Table I-3B).

The incorporation of 3D cardiac MTs in HTS systems with automated assessment of relevant cellular readouts has also been focused. The definition of the main set of parameters that should be analysed in a specific cardiotoxicity screening assay is as critical as the selection of the best cardiac tissue model. Cardiotoxicity can result in two main outcomes, namely (1) physical damage, including morphological damage and loss of cell viability due to increased oxidative stress and DNA and mitochondrial damage; and/or (2) altered CM function, through electric conduction system disruption and/or interference with the contraction process (Sala et al., 2017). This former problem is normally caused by an interference with the flux of important ions, through blockage of ion channels, being responsible for arrythmias, QT prolongation (delayed ventricular repolarization) and decrease of contractile performance. Depending on the selected readouts, the type of information regarding the effect of the drug in CM function and structure will be different, which means that the readouts from the HTS platforms should be selected according to the biological question to be answered.

Cellular viability can be detected using different commercially available fluorescence or luminescence kits based on ATP depletion that are now also adapted to 3D models. The information obtained from cell viability tests is normally used to generate a dose-response cell viability curve after drug treatment at different concentrations, and from that curve it is possible to determine the LD50 value, which indicates the drug concentration at which there is a 50% loss in the number of viable hiPSC-CM. In addition, different fluorescence dyes have been used to assess cell membrane permeability, endoplasmic reticulum integrity and mitochondrial membrane potential. In this case, it is possible to quantify cell damage through a quantitative measurement of the average fluorescence intensity combined with a HTS imaging platform (Archer et al., 2018; Pointon et al., 2013).

In what concerns to CM function, the effect of drugs on electrophysiological behavior of CMs can be assessed directly using AP measurements or indirectly through evaluation of downstream effects that may be modulated by electrophysiological activity, specifically intracellular calcium transients or contraction behavior (Gintant et al., 2020) (Table I-5). Both of them have been considered physiologically relevant functional outputs to be used in pre-clinical safety evaluation of new drugs (Saleem et al., 2020)(Lu et al., 2019).

Different platforms and assays have been described in the literature to assess the functional behavior of hPSC-CM/cardiac models. Multielectrode arrays technology (MEA), which measures the extracellular voltage and/or electrical impedance to obtain information about CM contractibility and electrophysiology properties, is a commonly used platform (Zhang et al., 2016). However, these devices are generally not compatible with 3D cardiac tissues, since cells need to be in direct contact with the electrodes. Additionally, optical systems that rely on image-based contractile motion (bright field or fluorescent high-resolution videos) are also widely used systems to assess CM function and are compatible with 3D cardiac tissues (Table I-6). Voltage sensitive dyes coupled with a high-speed frame acquisition system, have been used to obtain, in an automated way, information regarding CM electrophysiological properties, including AP duration and conduction velocity parameters (Feric et al., 2019; Mckeithan et al., 2017; Turnbull et al., 2014). Brightfield videos of spontaneously beating cardiac tissues can be acquired and then be converted to beating profiles by means of different available softwares (Devarasetty et al., 2017; Lu et al., 2015; Ravenscroft et al., 2016; Richards et al., 2017; Sala et al., 2018), allowing the analysis of different contractility parameters such as beating frequency, amplitude and time of contraction, and relaxation time.

Table I-5. Direct and indirect methods used to assess electrophysiological behavior of CMs *in vitro*.

Method	Approach	Advantages	Disadvantages
DIRECT METHODS			
Transmembrane Action Potential (Intracellular)	Microelectrodes or whole-cell patch technique	Quantitative evaluation of the action potential profile	Low-throughput and Substantial technical expertise
Voltage sensitive optical probes	Fluorescent dyes or protein-based technology (genetic modified cell lines)	Compatible with high-throughput screening settings	Not possible to have information regarding RMP and Upstroke Velocity
Extracellular field potential	Multi-electrode Array (MEA)	Label free and non-invasive	Low sensitivity
INDIRECT METHODS			
Calcium Transients	Fluorescent dyes	User-friendly and high-throughput	Dye can interfere with cytosolic free calcium levels and consequently impact the calcium transient parameters
Contractility and motion	Optical measures of sarcomeres or cardiomyocytes length changes using: 1) Image-based analysis platforms 2) simpler image motion packages 3) force microscopy	User-friendly and high-throughput	Reduced redoubts

The improvement of the analysis of the contractile profiles generated from the video acquisition system has been also focused, envisaging to maximize the number of possible outcomes/parameters that can be extracted from the video records in an automated way (Hoang et al., 2018; Sala et al., 2018). Fluorescence-based methods have been used to collect calcium transient profiles through the use of calcium fluorescent dyes, such as Fura-2 (Ravenscroft et al., 2016) or Fluo-4 (Lu et al., 2015; Richards et al., 2017). From these profiles, it is possible to obtain parameters, such as amplitude, time to peak and time to calcium decay. In a more recent study, a triple transient measurement (TTM) system was described, which allows the simultaneous detection of contractility, cytosolic Ca^{2+} flux, and electrophysiology in hiPSC-CMs labeled with three different fluorescent dyes (van Meer et al., 2019). In the cases where the cardiac MT is anchored between two flexible structures, as it is the case of EHT models, analysis of the force of contraction can be provided by capturing *in situ* the post deflection or wire movements through acquisition of high-frame-rate bright field videos (Mills et al., 2019; Turnbull et al., 2014; Zhao et al., 2019b), or by using a fluorescent dye (Feric et al., 2019). This system is the only that allows the measurement of absolute force of contraction in a continuous way.

Before applying any new developed cardiac models in screening settings to test new compounds, it is is important to first validate these models using standard drugs with known effects on CM functional behavior. Due to that, for a set of selected drugs, it is necessary to assess the effect of different drug concentrations, different times of exposure and test also single vs multiple dosages effects on CM function, selecting one or more readouts to be analyzed for each tested parameter. Those results should then be compared with known effects registered in clinical observations, in order to assess the utility and accuracy of the developed model.

The development of scoring systems to help quantifying the effect of cardioactive compounds on hPSC-CMs has also been explored in these last years. For easy assessment of the cardiotoxicity risk, normally a color-coded scorecard is elaborated. For the establishment of the hazard scoring system, a set of known drugs is normally used as a pharmacological reference set. Additionally, depending on the selected parameters, different information such as CM function (contraction behavior, AP profile and Ca^{2+} handling) and/or CM morphology, can be taken from the readouts and the score matrix will be linked to those specific readouts. The selected parameters should reflect relevant changes related to the pharmacological effects and preferentially allow the discrimination of different levels of toxicity severity and different types of toxic effects (Kopljar et al., 2018; Sharma et al., 2018). In addition to the development and selection of the best methodologies to capture and quantify the effects of cardioactive compounds on hPSC-CMs, the development of strategies that help on the identification and interpretation of the readouts in order to define which type of cardiotoxicity is associated to a specific compound and elucidate the mechanism of action, is also a relevant topic that should be taken into consideration (Lee et al., 2017a).

Table I-6. Summary of the main experimental setups used to assess functional and morphological parameters in 2D cultured hPSC-CMs, 3D cardiac MTs and EHT models. fps, frames per second; bpm, beats per minute.

	Culture Format	Dye	Functional/Morphological analysis	
			Optical Recording /Software	Analyzed parameters
van Meer et al., 2019	2D and 3D spheroids	Simultaneous combination of three fluorescence dyes: 1. ANNINE- 6 plus 2. Rhod-3 3. CellMask Deep Red	>300 fps MuscleMotion (Sala et al., 2018)	1. Action potential (Amplitude, t_{APD}, t_{rise}) 2. Calcium flux (Amplitte, t_{peak}, t_{decay}) 3. Contraction (Amplitude, $t_{contraction}$, $t_{relaxation}$)
Turnbull et al., 2014 **Lee et al., 2017**	EHT	-	Post deflection (100 fps) LabView software	- Force of contraction (mN) - peak - Contraction parameters (time to peak, time to 90% relaxation, maximum rate of force increase and maxium rate of force decrease)
		Voltage-sensitive dye: di-4-ANEPPS	Video aquisition	Action Potential Duration (ms)
Mckeithan et al., 2017	2D	Voltage sensitive dye: Fluor 2.1. Cl	IC200 KIC instrument CyteSeer	- Beat rate - Action potential profile (APD25, APD50, APD75, and APD90)
Mills et al., 2019	EHT	-	Post deflection (10 s time-lapse capture) Vision.PointTracker	- Force of Contraction (µN) (peak) - Contraction parameters (rate (bpm), 50% activation (s); 50% relaxation (s))
Lu et al., 2017	EHT	FluoSpheres polystyrene microspheres	Imaris software	- Contraction speed (µm/s) - Contraction rate (bpm)
Zhao et al., 2019 **Feric et al., 2019**	EHT	1. Fluo-4 2. voltage-sensitive dye di-4-ANEPPS	Post deflection (500 fps) Image J SpotTracker plugin	1. Force of contraction and Ca^{2+} transient profile 2. Conduction velocity (cm/s)
Archer et al., 2018	3D	1. TMRE 2. ER-Tracker blue	Quantitative measurements of average fluorescence intensity (Columbus Image Data Analysis System, Perkin Elmer Inc.)	1. Mitochondrial membrane potential 2. Endoplasmic reticulum integrity
Pointon et al., 2013	2D	1. TMRE 2. ER-Tracker blue 3.TOTO-3	metaXpress	1. Mitochondrial membrane potential 2. Endoplasmic reticulum integrity 3. Membrane permeability

Richards et al., 2017	3D	Fluo-4 dye	Videos of the calcium transient of whole spheroids with a capture rate of 20 fps ImageJ software.	- **Calcium transient profile** (Normalized peak of calcium fluorescence, time to peak calcium (sec) and time to 50% calcium decay (sec))
		-	Videos of spontaneously beating spheroids from ImageJ Software	- **Beating profile** (rate of contraction (bpm) and contraction amplitude)

I.7 REFERENCES

Abecasis, B., Gomes-Alves, P., Rosa, S., Gouveia, P.J., Ferreira, L., Serra, M., and Alves, P.M. (2019). Unveiling the molecular crosstalk in a human induced pluripotent stem cell-derived cardiac model. Biotechnol. Bioeng. *116*, 1245–1252.

Abecasis, B., Canhão, P.G.M., Almeida, H. V., Calmeiro, T., Fortunato, E., Gomes-Alves, P., Serra, M., and Alves, P.M. (2020). Toward a Microencapsulated 3D hiPSC-Derived in vitro Cardiac Microtissue for Recapitulation of Human Heart Microenvironment Features. Front. Bioeng. Biotechnol. *8*, 1–16.

Acharya, A., Baek, S.T., Huang, G., Eskiocak, B., Goetsch, S., Sung, C.Y., Banfi, S., Sauer, M.F., Olsen, G.S., Duffield, J.S., et al. (2012). The bHLH transcription factor Tcf21 is required for lineage-specific EMT of cardiac fibroblast progenitors. Development *139*, 2139–2149.

Al-Mehdi, A.-B., Pastukh, V.M., Swiger, B.M., Reed, D.J., Patel, M.R., Bardwell, G.C., Pastukh, V. V, Alexeyev, M.F., and Gillespie, M.N. (2012). Perinuclear Mitochondrial Clustering Creates an Oxidant-Rich Nuclear Domain Required for Hypoxia-Induced Transcription. Sci. Signal. *5*, ra47–ra47.

Andersen, P., Tampakakis, E., Jimenez, D. V., Kannan, S., Miyamoto, M., Shin, H.K., Saberi, A., Murphy, S., Sulistio, E., Chelko, S.P., et al. (2018). Precardiac organoids form two heart fields via Bmp/Wnt signaling. Nat. Commun. *9*, 3140.

Archer, C.R., Sargeant, R., Basak, J., Pilling, J., Barnes, J.R., and Pointon, A. (2018). Characterization and Validation of a Human 3D Cardiac Microtissue for the Assessment of Changes in Cardiac Pathology. Sci. Rep. *8*, 10160.

Arthur, S.A., Blaydes, J.P., and Houghton, F.D. (2019). Glycolysis Regulates Human Embryonic Stem Cell Self-Renewal under Hypoxia through HIF-2α and the Glycolytic Sensors CTBPs. Stem Cell Reports *12*, 1–15.

Azarin, S.M., Lian, X., Larson, E.A., Popelka, H.M., de Pablo, J.J., and Palecek, S.P. (2012). Modulation of Wnt/β-catenin signaling in human embryonic stem cells using a 3-D microwell array. Biomaterials *33*, 2041–2049.

Bao, X., Lian, X., Hacker, T.A., Schmuck, E.G., Qian, T., Bhute, V.J., Han, T., Shi, M., Drowley, L., Plowright, A.T., et al. (2016). Long-term self-renewing human epicardial cells generated from pluripotent stem cells under defined xeno-free conditions. Nat. Biomed. Eng. *1*, 0003.

Bao, X., Lian, X., Hacker, T.A., Schmuck, E.G., Qian, T., Bhute, V.J., Han, T., Shi, M., Drowley, L., Plowright, A.T., et al. (2017). Long-term self-renewing human epicardial cells generated from

pluripotent stem cells under defined xeno-free conditions. Nat. Biomed. Eng. *1*, 1–12.

Barbosa, H.S.C., Fernandes, T.G., Dias, T.P., Diogo, M.M., and Cabral, J.M.S. (2012). New Insights into the Mechanisms of Embryonic Stem Cell Self-Renewal under Hypoxia: A Multifactorial Analysis Approach. PLoS One *7*, e38963.

Bargehr, J., Ong, L.P., Colzani, M., Davaapil, H., Hofsteen, P., Bhandari, S., Gambardella, L., Novère, N. Le, Iyer, D., Sampaziotis, F., et al. (2019). regeneration. Nat. Biotechnol. *37*.

Bauwens, C.L., Peerani, R., Niebruegge, S., Woodhouse, K.A., Kumacheva, E., Husain, M., and Zandstra, P.W. (2008). Control of Human Embryonic Stem Cell Colony and Aggregate Size Heterogeneity Influences Differentiation Trajectories. Stem Cells *26*, 2300–2310.

Bauwens, C.L., Song, H., Thavandiran, N., Ungrin, M., Massé, S., Nanthakumar, K., Seguin, C., and Zandstra, P.W. (2011). Geometric control of cardiomyogenic induction in human pluripotent stem cells. Tissue Eng. *17*, 1901–1909.

Bax, N.A.M., Van Oorschot, A.A.M., Maas, S., Braun, J., Van Tuyn, J., De Vries, A.A.F., Gittenberger-De Groot, A.C., and Goumans, M.J. (2011). In vitro epithelial-to-mesenchymal transformation in human adult epicardial cells is regulated by TGFβ-signaling and WT1. Basic Res. Cardiol. *106*, 829–847.

Beauchamp, P., Jackson, C.B., Ozhathil, L.C., Agarkova, I., Galindo, C.L., Sawyer, D.B., Suter, T.M., and Zuppinger, C. (2020). 3D Co-culture of hiPSC-Derived Cardiomyocytes With Cardiac Fibroblasts Improves Tissue-Like Features of Cardiac Spheroids. Front. Mol. Biosci. *7*, 1–17.

Bedada, F.B., Chan, S.S.K., Metzger, S.K., Zhang, L., Zhang, J., Garry, D.J., Kamp, T.J., Kyba, M., and Metzger, J.M. (2014). Acquisition of a quantitative, stoichiometrically conserved ratiometric marker of maturation status in stem cell-derived cardiac myocytes. Stem Cell Reports *3*, 594–605.

Birket, M.J., Ribeiro, M.C., Verkerk, A.O., Ward, D., Leitoguinho, A.R., den Hartogh, S.C., Orlova, V. V, Devalla, H.D., Schwach, V., Bellin, M., et al. (2015). Expansion and patterning of cardiovascular progenitors derived from human pluripotent stem cells. Nat. Biotechnol. *33*, 970–979.

Bonet, F., Pereira, P.N.G., Bover, O., Marques, S., Inácio, J.M., and Belo, J.A. (2018). CCBE1 is required for coronary vessel development and proper coronary artery stem formation in the mouse heart. Dev. Dyn. *247*, 1135–1145.

Braam, S.R., Tertoolen, L., van de Stolpe, A., Meyer, T., Passier, R., and Mummery, C.L. (2010). Prediction of drug-induced cardiotoxicity using human embryonic stem cell-derived cardiomyocytes. Stem Cell Res. *4*, 107–116.

Brade, T., Kumar, S., Cunningham, T.J., Chatzi, C., Zhao, X., Cavallero, S., Li, P., Sucov, H.M.,

Ruiz-Lozano, P., and Duester, G. (2011). Retinoic acid stimulates myocardial expansion by induction of hepatic erythropoietin which activates epicardial Igf2. Development *138*, 139–148.

Branco, M.A., Cotovio, J.P., Rodrigues, C.A.V., Vaz, S.H., Fernandes, T.G., Moreira, L.M., Cabral, J.M.S., and Diogo, M.M. (2019). Transcriptomic analysis of 3D Cardiac Differentiation of Human Induced Pluripotent Stem Cells Reveals Faster Cardiomyocyte Maturation Compared to 2D Culture. Sci. Rep. *9*, 1–13.

Brandao, K.O., Tabel, V.A., Atsma, D.E., Mummery, C.L., and Davis, R.P. (2017). Human pluripotent stem cell models of cardiac disease: From mechanisms to therapies. DMM Dis. Model. Mech. *10*, 1039–1059.

Bruneau, B.G., Logan, M., Davis, N., Levi, T., Tabin, C.J., Seidman, J.G., and Seidman, C.E. (1999). Chamber-specific cardiac expression of Tbx5 and heart defects in Holt- Oram syndrome. Dev. Biol. *211*, 100–108.

Brutsaert, D.L. (2003). Cardiac Endothelial-Myocardial Signaling: Its Role in Cardiac Growth, Contractile Performance, and Rhythmicity. Physiol. Rev. *83*, 59–115.

Burridge, P.W., Anderson, D., Priddle, H., Barbadillo Muñoz, M.D., Chamberlain, S., Allegrucci, C., Young, L.E., and Denning, C. (2007). Improved Human Embryonic Stem Cell Embryoid Body Homogeneity and Cardiomyocyte Differentiation from a Novel V-96 Plate Aggregation System Highlights Interline Variability. Stem Cells *25*, 929–938.

Burridge, P.W., Thompson, S., Millrod, M. a, Weinberg, S., Yuan, X., Peters, A., Mahairaki, V., Koliatsos, V.E., Tung, L., and Zambidis, E.T. (2011a). A Universal System for Highly Efficient Cardiac Differentiation of Human Induced Pluripotent Stem Cells That Eliminates Interline Variability. PLoS One *6*, e18293.

Burridge, P.W., Thompson, S., Millrod, M.A., Weinberg, S., Yuan, X., Peters, A., Mahairaki, V., Koliatsos, V.E., Tung, L., and Zambidis, E.T. (2011b). A universal system for highly efficient cardiac differentiation of human induced pluripotent stem cells that eliminates interline variability. PLoS One *6*.

Burridge, P.W., Keller, G., Gold, J.D., and Wu, J.C. (2012). Production of De Novo Cardiomyocytes: Human Pluripotent Stem Cell Differentiation and Direct Reprogramming. Cell Stem Cell *10*, 16–28.

Burridge, P.W., Matsa, E., Shukla, P., Lin, Z.C., Churko, J.M., Ebert, A.D., Lan, F., Diecke, S., Huber, B., Mordwinkin, N.M., et al. (2014a). Chemically defined generation of human cardiomyocytes. Nat. Methods *11*, 855–860.

Burridge, P.W., Matsa, E., Shukla, P., Lin, Z.C., Churko, J.M., Ebert, A.D., Lan, F., Diecke, S.,

Huber, B., Mordwinkin, N.M., et al. (2014b). Chemically defined generation of human cardiomyocytes. Nat. Methods *11*, 855–860.

Cai, C.-L., Liang, X., Shi, Y., Chu, P.-H., Pfaff, S.L., Chen, J., and Evans, S. (2003). Isl1 identifies a cardiac progenitor population that proliferates prior to differentiation and contributes a majority of cells to the heart. Dev. Cell *5*, 877–889.

Cai, C.-L., Martin, J.C., Sun, Y., Cui, L., Wang, L., Ouyang, K., Yang, L., Bu, L., Liang, X., Zhang, X., et al. (2008). A myocardial lineage derives from Tbx18 epicardial cells. Nature *454*, 104–108.

Camelliti, P., Borg, T.K., and Kohl, P. (2005). Structural and functional characterisation of cardiac fibroblasts. Cardiovasc. Res. *65*, 40–51.

Cano, E., Carmona, R., Ruiz-Villalba, A., Rojas, A., Chau, Y.Y., Wagner, K.D., Wagner, N., Hastie, N.D., Muñoz-Chápuli, R., and Pérez-Pomares, J.M. (2016). Extracardiac septum transversum/proepicardial endothelial cells pattern embryonic coronary arterio-venous connections. Proc. Natl. Acad. Sci. U. S. A. *113*, 656–661.

Carmona, R., González-Iriarte, M., Atencia, G., Wessels, A., Muñoz-Chápuli, R., Pérez Pomares, J.M., Carmona, R., González-Iriarte, M., Atencia, G., Wessels, A., et al. (2002). Origin of coronary endothelial cells from epicardial mesothelium in avian embryos. Int. J. Dev. Biol. *46*, 1005–1013.

Cashman, T.J., Josowitz, R., Johnson, B. V., Gelb, B.D., and Costa, K.D. (2016). Human engineered cardiac tissues created using induced pluripotent stem cells reveal functional characteristics of BRAF-mediated hypertrophic cardiomyopathy. PLoS One *11*, 1–17.

Chen, B., Dodge, M.E., Tang, W., Lu, J., Ma, Z., Fan, C.-W., Wei, S., Hao, W., Kilgore, J., Williams, N.S., et al. (2009). Small molecule–mediated disruption of Wnt-dependent signaling in tissue regeneration and cancer. Nat. Chem. Biol. *5*, 100–107.

Chen, Q., Zhang, H., Liu, Y., Adams, S., Eilken, H., Stehling, M., Corada, M., Dejana, E., Zhou, B., and Adams, R.H. (2016). Endothelial cells are progenitors of cardiac pericytes and vascular smooth muscle cells. Nat. Commun. *7*.

Chen, T.H.P., Chang, T.C., Kang, J.O., Choudhary, B., Makita, T., Tran, C.M., Burch, J.B.E., Eid, H., and Sucov, H.M. (2002). Epicardial induction of fetal cardiomyocyte proliferation via a retinoic acid-inducible trophic factor. Dev. Biol. *250*, 198–207.

Chen, V.C., Ye, J., Shukla, P., Hua, G., Chen, D., Lin, Z., Liu, J., Chai, J., Gold, J., Wu, J., et al. (2015a). Development of a scalable suspension culture for cardiac differentiation from human pluripotent stem cells. Stem Cell Res. *15*, 365–375.

Chen, V.C., Ye, J., Shukla, P., Hua, G., Chen, D., Lin, Z., Liu, J., Chai, J., Gold, J., Wu, J., et al.

(2015b). Development of a scalable suspension culture for cardiac differentiation from human pluripotent stem cells. Stem Cell Res. *15*, 365–375.

Cheung, C., Bernardo, A.S., Pedersen, R.A., and Sinha, S. (2014). Directed differentiation of embryonic origin-specific vascular smooth muscle subtypes from human pluripotent stem cells. Nat. Protoc. *9*, 929–938.

Chiquet, M., and Flück, M. (2001). Chapter 8 Early responses to mechanical stress: From signals at the cell surface to altered gene expression. In Cell and Molecular Response to Stress, pp. 97–110.

Corrado, D., van Tintelen, P.J., McKenna, W.J., Hauer, R.N.W., Anastastakis, A., Asimaki, A., Basso, C., Bauce, B., Brunckhorst, C., Bucciarelli-Ducci, C., et al. (2020). Arrhythmogenic right ventricular cardiomyopathy: evaluation of the current diagnostic criteria and differential diagnosis. Eur. Heart J. *41*, 1414–1429.

Correia, C., Koshkin, A., Duarte, P., Hu, D., Teixeira, A., Domian, I., Serra, M., and Alves, P.M. (2017). Distinct carbon sources affect structural and functional maturation of cardiomyocytes derived from human pluripotent stem cells. Sci. Rep. *7*, 8590.

Correia, C., Koshkin, A., Duarte, P., Hu, D., Carido, M., Sebastião, M.J., Gomes-Alves, P., Elliott, D.A., Domian, I.J., Teixeira, A.P., et al. (2018). 3D aggregate culture improves metabolic maturation of human pluripotent stem cell derived cardiomyocytes. Biotechnol. Bioeng. *115*, 630–644.

Cui, Y., Zheng, Y., Liu, X., Yan, L., Fan, X., Yong, J., Hu, Y., Dong, J., Li, Q., Wu, X., et al. (2019). Single-Cell Transcriptome Analysis Maps the Developmental Track of the Human Heart. Cell Rep. *26*, 1934-1950.e5.

Cyganek, L., Tiburcy, M., Sekeres, K., Gerstenberg, K., Bohnenberger, H., Lenz, C., Henze, S., Stauske, M., Salinas, G., Zimmermann, W.-H., et al. (2018). Deep phenotyping of human induced pluripotent stem cell–derived atrial and ventricular cardiomyocytes. JCI Insight *3*, e99941.

Dahlmann, J., Kensah, G., Kempf, H., Skvorc, D., Gawol, A., Elliott, D.A., Dräger, G., Zweigerdt, R., Martin, U., and Gruh, I. (2013). The use of agarose microwells for scalable embryoid body formation and cardiac differentiation of human and murine pluripotent stem cells. Biomaterials *34*, 2463–2471.

Desireddi, J.R., Farrow, K.N., Marks, J.D., Waypa, G.B., and Schumacker, P.T. (2010). Hypoxia Increases ROS Signaling and Cytosolic Ca 2+ in Pulmonary Artery Smooth Muscle Cells of Mouse Lungs Slices. Antioxid. Redox Signal. *12*, 595–602.

Dettman, R.W., Denetclaw, W., Ordahl, C.P., and Bristow, J. (1998). Common epicardial origin of coronary vascular smooth muscle, perivascular fibroblasts, and intermyocardial fibroblasts in the avian heart. Dev. Biol. *193*, 169–181.

Devalla, H.D., Schwach, V., Ford, J.W., Milnes, J.T., El-Haou, S., Jackson, C., Gkatzis, K., Elliott, D.A., Chuva de Sousa Lopes, S.M., Mummery, C.L., et al. (2015). Atrial-like cardiomyocytes from human pluripotent stem cells are a robust preclinical model for assessing atrial-selective pharmacology. EMBO Mol. Med. *7*, 394–410.

Devarasetty, M., Forsythe, S., Shupe, T., Soker, S., Bishop, C., Atala, A., and Skardal, A. (2017). Optical Tracking and Digital Quantification of Beating Behavior in Bioengineered Human Cardiac Organoids. Biosensors *7*, 24.

Devine, W.P., Wythe, J.D., George, M., Koshiba-Takeuchi, K., and Bruneau, B.G. (2014). Early patterning and specification of cardiac progenitors in gastrulating mesoderm. Elife *3*, 1–23.

Dhanasekaran, D.N., and Reddy, E.P. (2008). JNK signaling in apoptosis. Oncogene *27*, 6245–6251.

Dias, T.P., Pinto, S.N., Santos, J.I., Fernandes, T.G., Fernandes, F., Diogo, M.M., Prieto, M., and Cabral, J.M.S. (2018). Biophysical study of human induced Pluripotent Stem Cell-Derived cardiomyocyte structural maturation during long-term culture. Biochem. Biophys. Res. Commun. *499*, 611–617.

Döring, Y., Pawig, L., Weber, C., and Noels, H. (2014). The CXCL12/CXCR4 chemokine ligand/receptor axis in cardiovascular disease. Front. Physiol. *5*, 212.

Duim, S.N., Kurakula, K., Goumans, M.J., and Kruithof, B.P.T. (2015). Cardiac endothelial cells express Wilms' tumor-1. Wt1 expression in the developing, adult and infarcted heart. J. Mol. Cell. Cardiol. *81*, 127–135.

Duim, S.N., Smits, A.M., Kruithof, B.P.T., and Goumans, M.J. (2016). The roadmap of WT1 protein expression in the human fetal heart. J. Mol. Cell. Cardiol. *90*, 139–145.

Dunn, K.K., Reichardt, I.M., Simmons, A.D., Jin, G., Floy, M.E., Hoon, K.M., and Palecek, S.P. (2019). Coculture of Endothelial Cells with Human Pluripotent Stem Cell-Derived Cardiac Progenitors Reveals a Differentiation Stage-Specific Enhancement of Cardiomyocyte Maturation. Biotechnol. J. *14*, e1800725.

Dyer, L.A., and Kirby, M.L. (2009). Sonic hedgehog maintains proliferation in secondary heart field progenitors and is required for normal arterial pole formation. Dev. Biol. *330*, 305–317.

Evans, M.J., and Kaufman, M.H. (1981). Establishment in culture of pluripotential cells from mouse embryos. Nature *292*, 154–156.

Fan, D., Takawale, A., Lee, J., and Kassiri, Z. (2012). Cardiac fibroblasts, fibrosis and extracellular matrix remodeling in heart disease. Fibrogenesis Tissue Repair *5*, 15.

Farkas, S., Simara, P., Rehakova, D., Veverkova, L., and Koutna, I. (2020). Endothelial Progenitor Cells Produced From Human Pluripotent Stem Cells by a Synergistic Combination of Cytokines, Small Compounds, and Serum-Free Medium. Front. Cell Dev. Biol. *8*.

Feric, N.T., Pallotta, I., Singh, R., Bogdanowicz, D.R., Gustilo, M.M., Chaudhary, K.W., Willette, R.N., Chendrimada, T.P., Xu, X., Graziano, M.P., et al. (2019). Engineered Cardiac Tissues Generated in the Biowire II: A Platform for Human-Based Drug Discovery. Toxicol. Sci. *172*, 89–97.

Filippo Buono, M., von Boehmer, L., Strang, J., P Hoerstrup, S., Y Emmert, M., and Nugraha, B. (2020). Human Cardiac Organoids for Modeling Genetic Cardiomyopathy. Cells *9*.

Fisher, J.B., Pulakanti, K., Rao, S., and Duncan, S.A. (2017). GATA6 is essential for endoderm formation from human pluripotent stem cells. Biol. Open *6*, 1084–1095.

Fonoudi, H., Ansari, H., Abbasalizadeh, S., Larijani, M.R., Kiani, S., Hashemizadeh, S., Zarchi, A.S., Bosman, A., Blue, G.M., Pahlavan, S., et al. (2015a). A Universal and Robust Integrated Platform for the Scalable Production of Human Cardiomyocytes From Pluripotent Stem Cells. Stem Cells Transl. Med. *4*, 1482–1494.

Fonoudi, H., Ansari, H., Abbasalizadeh, S., Larijani, M.R., Kiani, S., Hashemizadeh, S., Zarchi, A.S., Bosman, A., Blue, G.M., Pahlavan, S., et al. (2015b). A Universal and Robust Integrated Platform for the Scalable Production of Human Cardiomyocytes From Pluripotent Stem Cells. Stem Cells Transl. Med. *4*, 1482–1494.

Foo, K.S., Lehtinen, M.L., Leung, C.Y., Lian, X., Xu, J., Keung, W., Geng, L., Kolstad, T.R.S., Thams, S., Wong, A.O., et al. (2018). Human ISL1 + Ventricular Progenitors Self-Assemble into an In Vivo Functional Heart Patch and Preserve Cardiac Function Post Infarction. Mol. Ther. *26*, 1644–1659.

Funa, N.S., Schachter, K.A., Lerdrup, M., Ekberg, J., Hess, K., Dietrich, N., Honoré, C., Hansen, K., and Semb, H. (2015a). β-Catenin Regulates Primitive Streak Induction through Collaborative Interactions with SMAD2/SMAD3 and OCT4. Cell Stem Cell *16*, 639–652.

Funa, N.S., Schachter, K.A., Lerdrup, M., Ekberg, J., Hess, K., Dietrich, N., Honoré, C., Hansen, K., and Semb, H. (2015b). β-Catenin Regulates Primitive Streak Induction through Collaborative Interactions with SMAD2/SMAD3 and OCT4. Cell Stem Cell *16*, 639–652.

Galdos, F.X., Guo, Y., Paige, S.L., Vandusen, N.J., Wu, S.M., and Pu, W.T. (2017). Cardiac Regeneration: Lessons from Development. Circ. Res. *120*, 941–959.

Galli, D., Domínguez, J.N., Zaffran, S., Munk, A., Brown, N.A., and Buckingham, M.E. (2008). Atrial myocardium derives from the posterior region of the second heart field, which acquires left-right identity as Pitx2c is expressed. Development *135*, 1157–1167.

Garg, P., Garg, V., Shrestha, R., Sanguinetti, M.C., Kamp, T.J., and Wu, J.C. (2018). Human Induced Pluripotent Stem Cell–Derived Cardiomyocytes as Models for Cardiac Channelopathies. Circ. Res. *123*, 224–243.

Gatenby, R.A., and Gillies, R.J. (2004). Why do cancers have high aerobic glycolysis? Nat. Rev. Cancer *4*, 891–899.

Giacomelli, E., Bellin, M., Sala, L., van Meer, B.J., Tertoolen, L.G.J., Orlova, V. V., and Mummery, C.L. (2017). Three-dimensional cardiac microtissues composed of cardiomyocytes and endothelial cells co-differentiated from human pluripotent stem cells. Dev. *144*, 1008–1017.

Giacomelli, E., Meraviglia, V., Campostrini, G., Cochrane, A., Cao, X., van Helden, R.W.J., Krotenberg Garcia, A., Mircea, M., Kostidis, S., Davis, R.P., et al. (2020). Human-iPSC-Derived Cardiac Stromal Cells Enhance Maturation in 3D Cardiac Microtissues and Reveal Non-cardiomyocyte Contributions to Heart Disease. Cell Stem Cell *26*, 862-879.e11.

Gintant, G., Kaushik, E.P., Feaster, T., Stoelzle-Feix, S., Kanda, Y., Osada, T., Smith, G., Czysz, K., Kettenhofen, R., Lu, H.R., et al. (2020). Repolarization studies using human stem cell-derived cardiomyocytes: Validation studies and best practice recommendations. Regul. Toxicol. Pharmacol. *117*, 104756.

Gittenberger-de Groot, A.C., Vrancken Peeters, M.-P.F.M., Bergwerff, M., Mentink, M.M.T., and Poelmann, R.E. (2000). Epicardial Outgrowth Inhibition Leads to Compensatory Mesothelial Outflow Tract Collar and Abnormal Cardiac Septation and Coronary Formation. Circ. Res. *87*, 969–971.

Goldfracht, I., Efraim, Y., Shinnawi, R., Kovalev, E., Huber, I., Gepstein, A., Arbel, G., Shaheen, N., Tiburcy, M., Zimmermann, W.H., et al. (2019). Engineered heart tissue models from hiPSC-derived cardiomyocytes and cardiac ECM for disease modeling and drug testing applications. Acta Biomater. *92*, 145–159.

Guadix, J.A., Carmona, R., Muñoz-Chápuli, R., and Pérez-Pomares, J.M. (2006). In vivo and in vitro analysis of the vasculogenic potential of avian proepicardial and epicardial cells. Dev. Dyn. *235*, 1014–1026.

Guadix, J.A., Orlova, V. V., Giacomelli, E., Bellin, M., Ribeiro, M.C., Mummery, C.L., Pérez-Pomares, J.M., and Passier, R. (2017). Human Pluripotent Stem Cell Differentiation into Functional Epicardial Progenitor Cells. Stem Cell Reports *9*, 1754–1764.

Gustafsson, M. V, Zheng, X., Pereira, T., Gradin, K., Jin, S., Lundkvist, J., Ruas, J.L., Poellinger, L., Lendahl, U., and Bondesson, M. (2005). Hypoxia Requires Notch Signaling to Maintain the Undifferentiated Cell State. Dev. Cell *9*, 617–628.

Halloin, C., Schwanke, K., Löbel, W., Franke, A., Szepes, M., Biswanath, S., Wunderlich, S.,

Merkert, S., Weber, N., Osten, F., et al. (2019). Continuous WNT Control Enables Advanced hPSC Cardiac Processing and Prognostic Surface Marker Identification in Chemically Defined Suspension Culture. Stem Cell Reports *13*, 366–379.

Hamad, S., Derichsweiler, D., Papadopoulos, S., Nguemo, F., Šarić, T., Sachinidis, A., Brockmeier, K., Hescheler, J., Boukens, B.J., and Pfannkuche, K. (2019). Generation of human induced pluripotent stem cell-derived cardiomyocytes in 2D monolayer and scalable 3D suspension bioreactor cultures with reduced batch-to-batch variations. Theranostics *9*, 7222–7238.

Hamm, M.J., Kirchmaier, B.C., and Herzog, W. (2016). Sema3d controls collective endothelial cell migration by distinct mechanisms via nrp1 and plxnD1. J. Cell Biol. *215*, 415–430.

Han, L., Chaturvedi, P., Kishimoto, K., Koike, H., Nasr, T., Iwasawa, K., Giesbrecht, K., Witcher, P.C., Eicher, A., Haines, L., et al. (2020). Single cell transcriptomics identifies a signaling network coordinating endoderm and mesoderm diversification during foregut organogenesis. Nat. Commun. *11*.

Harding, A., Cortez-Toledo, E., Magner, N.L., Beegle, J.R., Coleal-Bergum, D.P., Hao, D., Wang, A., Nolta, J.A., and Zhou, P. (2017). Highly Efficient Differentiation of Endothelial Cells from Pluripotent Stem Cells Requires the MAPK and the PI3K Pathways. Stem Cells *35*, 909–919.

Hatcher, C.J., Diman, N.Y.S.G., Kim, M.S., Pennisi, D., Song, Y., Goldstein, M.M., Mikawa, T., and Basson, C.T. (2004). A role for Tbx5 in proepicardial cell migration during cardiogenesis. Physiol. Genomics *18*, 129–140.

He, J.Q., Ma, Y., Lee, Y., Thomson, J.A., and Kamp, T.J. (2003). Human embryonic stem cells develop into multiple types of cardiac myocytes: Action potential characterization. Circ. Res. *93*, 32–39.

Hemmi, N., Tohyama, S., Nakajima, K., Kanazawa, H., Suzuki, T., Hattori, F., Seki, T., Kishino, Y., Hirano, A., Okada, M., et al. (2014). A Massive Suspension Culture System With Metabolic Purification for Human Pluripotent Stem Cell-Derived Cardiomyocytes. Stem Cells Transl. Med. *3*, 1473–1483.

Hirose, T., Karasawa, M., Sugitani, Y., Fujisawa, M., Akimoto, K., Ohno, S., and Noda, T. (2006). PAR3 is essential for cyst-mediated epicardial development by establishing apical cortical domains. Development *133*, 1389–1398.

Hoang, P., Huebsch, N., Bang, S.H., Siemons, B.A., Conklin, B.R., Healy, K.E., Ma, Z., and Jacquir, S. (2018). Quantitatively characterizing drug-induced arrhythmic contractile motions of human stem cell-derived cardiomyocytes. Biotechnol. Bioeng. *115*, 1958–1970.

Hofbauer, P., Jahnel, S., Papai, N., Giesshammer, M., Tavernini, K., Grdseloff, N., Penc, M.,

Meledeth, C., Deyett, A., Schmidt, C., et al. (2020). Cardioids reveal self-organizing principles of human cardiogenesis.

Hsiao, C., Tomai, M., Glynn, J., and Palecek, S.P. (2014). Effects of 3-D microwell culture on initial fate specification in human embryonic stem cells. AIChE J. *60*, 1225–1235.

Huang, C.Y., Peres Moreno Maia-Joca, R., Ong, C.S., Wilson, I., DiSilvestre, D., Tomaselli, G.F., and Reich, D.H. (2020). Enhancement of human iPSC-derived cardiomyocyte maturation by chemical conditioning in a 3D environment. J. Mol. Cell. Cardiol. *138*, 1–11.

Huber, I., Itzhaki, I., Caspi, O., Arbel, G., Tzukerman, M., Gepstein, A., Habib, M., Yankelson, L., Kehat, I., and Gepstein, L. (2007). Identification and selection of cardiomyocytes during human embryonic stem cell differentiation. FASEB J. *21*, 2551–2563.

Hudson, J., Titmarsh, D., Hidalgo, A., Wolvetang, E., and Cooper-White, J. (2012). Primitive Cardiac Cells from Human Embryonic Stem Cells. Stem Cells Dev. *21*, 1513–1523.

Huebsch, N., Loskill, P., Deveshwar, N., Spencer, C.I., Judge, L.M., Mandegar, M.A., Fox, C.B., Mohamed, T.M.A., Ma, Z., Mathur, A., et al. (2016). Miniaturized iPS-Cell-Derived Cardiac Muscles for Physiologically Relevant Drug Response Analyses. Sci. Rep. *6*, 1–12.

Huh, D., Kim, H.J., Fraser, J.P., Shea, D.E., Khan, M., Bahinski, A., Hamilton, G.A., and Ingber, D.E. (2013). Microfabrication of human organs-on-chips. Nat. Protoc. *8*, 2135–2157.

Hulsmans, M., Clauss, S., Xiao, L., Aguirre, A.D., King, K.R., Hanley, A., Hucker, W.J., Wülfers, E.M., Seemann, G., Courties, G., et al. (2017). Macrophages Facilitate Electrical Conduction in the Heart. Cell *169*, 510-522.e20.

Husain, M., Zandstra, P.W., Niebruegge, S., Kumacheva, E., Peerani, R., Woodhouse, K.A., and Bauwens, C.L. (2008). Control of Human Embryonic Stem Cell Colony and Aggregate Size Heterogeneity Influences Differentiation Trajectories. Stem Cells *26*, 2300–2310.

Hutson, M.R., Zeng, X.L., Kim, A.J., Antoon, E., Harward, S., and Kirby, M.L. (2010). Arterial pole progenitors interpret opposing FGF/BMP signals to proliferate or differentiate. Development *137*, 3001–3011.

Huynh, T., Chen, L., Terrell, P., and Baldini, A. (2007). A fate map of Tbx1 expressing cells reveals heterogeneity in the second cardiac field. Genesis *45*, 470–475.

Hwang, Y.S., Bong, G.C., Ortmann, D., Hattori, N., Moeller, H.C., and Khademhosseinia, A. (2009). Microwell-mediated control of embryoid body size regulates embryonic stem cell fate via differential expression of WNT5a and WNT11. Proc. Natl. Acad. Sci. U. S. A. *106*, 16978–16983.

IFPMA (2017). IFPMA-Facts-And-Figures-2017. Int. Fed. Pharmacutical Manuf. Asoc. 86.

Ishida, H., Saba, R., Kokkinopoulos, I., Hashimoto, M., Yamaguchi, O., Nowotschin, S., Shiraishi, M., Ruchaya, P., Miller, D., Harmer, S., et al. (2016). GFRA2 Identifies Cardiac Progenitors and Mediates Cardiomyocyte Differentiation in a RET-Independent Signaling Pathway. Cell Rep. *16*, 1026–1038.

Ishii, Y., Garriock, R.J., Navetta, A.M., Coughlin, L.E., and Mikawa, T. (2010). BMP signals promote proepicardial protrusion necessary for recruitment of coronary vessel and epicardial progenitors to the heart. Dev. Cell *19*, 307–316.

Iyer, D., Gambardella, L., Bernard, W.G., Serrano, F., Mascetti, V.L., Pedersen, R.A., Talasila, A., and Sinha, S. (2015). Robust derivation of epicardium and its differentiated smooth muscle cell progeny from human pluripotent stem cells. Development *142*, 1528–1541.

Kane, C., and Terracciano, C.M.N. (2017). Concise Review: Criteria for Chamber-Specific Categorization of Human Cardiac Myocytes Derived from Pluripotent Stem Cells. Stem Cells *35*, 1881–1897.

Kang, J., Gu, Y., Li, P., Johnson, B.L., Sucov, H.M., and Thomas, P.S. (2008). PDGF-A as an epicardial mitogen during heart development. Dev. Dyn. *237*, 692–701.

Karakikes, I., Ameen, M., Termglinchan, V., and Wu, J.C. (2015). Human Induced Pluripotent Stem Cell-Derived Cardiomyocytes: Insights Into Molecular, Cellular, and Functional Phenotypes. Circ. Res. *117*, 80–88.

Kastner, P., Grondona, J.M., Mark, M., Gansmuller, A., LeMeur, M., Decimo, D., Vonesch, J.L., Dollé, P., and Chambon, P. (1994). Genetic analysis of RXRα developmental function: Convergence of RXR and RAR signaling pathways in heart and eye morphogenesis. Cell *78*, 987–1003.

Kattman, S.J., Witty, A.D., Gagliardi, M., Dubois, N.C., Niapour, M., Hotta, A., Ellis, J., and Keller, G. (2011a). Stage-specific optimization of activin/nodal and BMP signaling promotes cardiac differentiation of mouse and human pluripotent stem cell lines. Cell Stem Cell *8*, 228–240.

Kattman, S.J., Witty, A.D., Gagliardi, M., Dubois, N.C., Niapour, M., Hotta, A., Ellis, J., and Keller, G. (2011b). Stage-Specific Optimization of Activin/Nodal and BMP Signaling Promotes Cardiac Differentiation of Mouse and Human Pluripotent Stem Cell Lines. Cell Stem Cell *8*, 228–240.

Kattman, S.J., Witty, A.D., Gagliardi, M., Dubois, N.C., Niapour, M., Hotta, A., Ellis, J., and Keller, G. (2011c). Stage-specific optimization of activin/nodal and BMP signaling promotes cardiac differentiation of mouse and human pluripotent stem cell lines. Cell Stem Cell *8*, 228–240.

Katz, T.C., Singh, M.K., Degenhardt, K., Rivera-Feliciano, J., Johnson, R.L., Epstein, J.A., and Tabin, C.J. (2012). Distinct Compartments of the Proepicardial Organ Give Rise to Coronary Vascular Endothelial Cells. Dev. Cell *22*, 639–650.

Kehat, I., Kenyagin-Karsenti, D., Snir, M., Segev, H., Amit, M., Gepstein, A., Livne, E., Binah, O., Itskovitz-Eldor, J., and Gepstein, L. (2001). Human embryonic stem cells can differentiate into myocytes with structural and functional properties of cardiomyocytes. J. Clin. Invest. *108*, 407–414.

Keith, B., and Simon, M.C. (2007). Hypoxia-Inducible Factors, Stem Cells, and Cancer. Cell *129*, 465–472.

Kempf, H., Olmer, R., Kropp, C., Rückert, M., Jara-Avaca, M., Robles-Diaz, D., Franke, A., Elliott, D.A., Wojciechowski, D., Fischer, M., et al. (2014a). Controlling Expansion and Cardiomyogenic Differentiation of Human Pluripotent Stem Cells in Scalable Suspension Culture. Stem Cell Reports *3*, 1132–1146.

Kempf, H., Olmer, R., Kropp, C., Rückert, M., Jara-Avaca, M., Robles-Diaz, D., Franke, A., Elliott, D.A., Wojciechowski, D., Fischer, M., et al. (2014b). Controlling Expansion and Cardiomyogenic Differentiation of Human Pluripotent Stem Cells in Scalable Suspension Culture. Stem Cell Reports *3*, 1132–1146.

Kempf, H., Olmer, R., Haase, A., Franke, A., Bolesani, E., Schwanke, K., Robles-Diaz, D., Coffee, M., Göhring, G., Dräger, G., et al. (2016a). Bulk cell density and Wnt/TGFbeta signalling regulate mesendodermal patterning of human pluripotent stem cells. Nat. Commun. *7*, 13602.

Kempf, H., Olmer, R., Haase, A., Franke, A., Bolesani, E., Dra, G., Po, O., Joos, T., Schwanke, K., Coffee, M., et al. (2016b). Bulk cell density and Wnt/TGFbeta signalling regulate mesendodermal patterning of human pluripotent stem cells.

Kensah, G., Zenker, M., Lang, A., Haghighi, F., Piekorz, R.P., Nakhaei-Rad, S., Ahmadian, M.R., Kutschka, I., and Dahlmann, J. (2018). bFGF-mediated pluripotency maintenance in human induced pluripotent stem cells is associated with NRAS-MAPK signaling. Cell Commun. Signal. *16*, 1–14.

Kerscher, P., Turnbull, I.C., Hodge, A.J., Kim, J., Seliktar, D., Easley, C.J., Costa, K.D., and Lipke, E.A. (2016). Direct hydrogel encapsulation of pluripotent stem cells enables ontomimetic differentiation and growth of engineered human heart tissues. Biomaterials *83*, 383–395.

Kevin Range, and D.M.Y.A.M. (2012). 基因的改变NIH Public Access. Bone *23*, 1–7.

Kim, K., Zhao, R., Doi, A., Ng, K., Unternaehrer, J., Cahan, P., Hongguang, H., Loh, Y.-H., Aryee, M.J., Lensch, M.W., et al. (2011). Donor cell type can influence the epigenome and differentiation potential of human induced pluripotent stem cells. Nat. Biotechnol. *29*, 1117–1119.

Kinney, M.A., Sargent, C.Y., and McDevitt, T.C. (2013). Temporal Modulation of β-Catenin Signaling by Multicellular Aggregation Kinetics Impacts Embryonic Stem Cell Cardiomyogenesis. Stem Cells Dev. *22*, 2665–2677.

Klesen, A., Jakob, D., Emig, R., Kohl, P., Ravens, U., and Peyronnet, R. (2018). Cardiac fibroblasts. Herzschrittmachertherapie + Elektrophysiologie *29*, 62–69.

Kopljar, I., Lu, H.R., Van Ammel, K., Otava, M., Tekle, F., Teisman, A., and Gallacher, D.J. (2018). Development of a Human iPSC Cardiomyocyte-Based Scoring System for Cardiac Hazard Identification in Early Drug Safety De-risking. Stem Cell Reports *11*, 1365–1377.

de Korte, T., Katili, P.A., Mohd Yusof, N.A.N., van Meer, B.J., Saleem, U., Burton, F.L., Smith, G.L., Clements, P., Mummery, C.L., Eschenhagen, T., et al. (2020). Unlocking Personalized Biomedicine and Drug Discovery with Human Induced Pluripotent Stem Cell–Derived Cardiomyocytes: Fit for Purpose or Forever Elusive? Annu. Rev. Pharmacol. Toxicol. *60*, 529–551.

Krishnan, J., Ahuja, P., Bodenmann, S., Knapik, D., Perriard, E., Krek, W., and Perriard, J.-C. (2008). Essential role of developmentally activated hypoxia-inducible factor 1alpha for cardiac morphogenesis and function. Circ. Res. *103*, 1139–1146.

Kwee, L., Baldwin, H.S., Shen, H.M., Stewart, C.L., Buck, C., Buck, C.A., and Labow, M.A. (1995). Defective development of the embryonic and extraembryonic circulatory systems in vascular cell adhesion molecule (VCAM-1) deficient mice. Development *121*, 489–503.

Laco, F., Woo, T.L., Zhong, Q., Szmyd, R., Ting, S., Khan, F.J., Chai, C.L.L., Reuveny, S., Chen, A., and Oh, S. (2018). Unraveling the Inconsistencies of Cardiac Differentiation Efficiency Induced by the GSK3β Inhibitor CHIR99021 in Human Pluripotent Stem Cells. Stem Cell Reports *10*, 1851–1866.

Laflamme, M.A., Chen, K.Y., Naumova, A. V., Muskheli, V., Fugate, J.A., Dupras, S.K., Reinecke, H., Xu, C., Hassanipour, M., Police, S., et al. (2007). Cardiomyocytes derived from human embryonic stem cells in pro-survival factors enhance function of infarcted rat hearts. Nat. Biotechnol. *25*, 1015–1024.

Laksman, Z., Wauchop, M., Lin, E., Protze, S., Lee, J., Yang, W., Izaddoustdar, F., Shafaattalab, S., Gepstein, L., Tibbits, G.F., et al. (2017). Modeling Atrial Fibrillation using Human Embryonic Stem Cell-Derived Atrial Tissue. Sci. Rep. *7*, 1–11.

Lavine, K.J., Yu, K., White, A.C., Zhang, X., Smith, C., Partanen, J., and Ornitz, D.M. (2005). Endocardial and epicardial derived FGF signals regulate myocardial proliferation and differentiation in vivo. Dev. Cell *8*, 85–95.

Lee, D.S., Chen, J.H., Lundy, D.J., Liu, C.H., Hwang, S.M., Pabon, L., Shieh, R.C., Chen, C.C., Wu, S.N., Yan, Y.T., et al. (2015). Defined MicroRNAs Induce Aspects of Maturation in Mouse and Human Embryonic-Stem-Cell-Derived Cardiomyocytes. Cell Rep. *12*, 1960–1967.

Lee, E.K., Tran, D.D., Keung, W., Chan, P., Wong, G., Chan, C.W., Costa, K.D., Li, R.A., and Khine, M. (2017a). Machine Learning of Human Pluripotent Stem Cell-Derived Engineered Cardiac

Tissue Contractility for Automated Drug Classification. Stem Cell Reports *9*, 1–13.

Lee, J.H., Protze, S.I., Laksman, Z., Backx, P.H., and Keller, G.M. (2017b). Human Pluripotent Stem Cell-Derived Atrial and Ventricular Cardiomyocytes Develop from Distinct Mesoderm Populations. Cell Stem Cell *21*, 179-194.e4.

Lee, J.H., Protze, S.I., Laksman, Z., Backx, P.H., and Keller, G.M. (2017c). Human Pluripotent Stem Cell-Derived Atrial and Ventricular Cardiomyocytes Develop from Distinct Mesoderm Populations. Cell Stem Cell *21*, 179-194.e4.

Lemme, M., Ulmer, B.M., Lemoine, M.D., Zech, A.T.L., Flenner, F., Ravens, U., Reichenspurner, H., Rol-Garcia, M., Smith, G., Hansen, A., et al. (2018). Atrial-like Engineered Heart Tissue: An In Vitro Model of the Human Atrium. Stem Cell Reports *11*, 1378–1390.

Lemoine, M.D., Mannhardt, I., Breckwoldt, K., Prondzynski, M., Flenner, F., Ulmer, B., Hirt, M.N., Neuber, C., Horváth, A., Kloth, B., et al. (2017). Human iPSC-derived cardiomyocytes cultured in 3D engineered heart tissue show physiological upstroke velocity and sodium current density. Sci. Rep. *7*, 1–11.

Lescroart, F., Chabab, S., Lin, X., Rulands, S., Paulissen, C., Rodolosse, A., Auer, H., Achouri, Y., Dubois, C., Bondue, A., et al. (2014). Early lineage restriction and regional segregation during mammalian heart development. *16*, 829–840.

Li, J., Miao, L., Zhao, C., Qureshi, W.M.S., Shieh, D., Guo, H., Lu, Y., Hu, S., Huang, A., Zhang, L., et al. (2017a). CDC42 is required for epicardial and pro-epicardial development by mediating FGF receptor trafficking to the plasma membrane. Dev. *144*, 1635–1647.

Li, P., Cavallero, S., Gu, Y., Chen, T.H.P., Hughes, J., Hassan, A.B., Brüning, J.C., Pashmforoush, M., and Sucov, H.M. (2011). IGF signaling directs ventricular cardiomyocyte proliferation during embryonic heart development. Development *138*, 1795–1805.

Li, S., Pan, H., Tan, C., Sun, Y., Song, Y., Zhang, X., Yang, W., Wang, X., Li, D., Dai, Y., et al. (2018). Mitochondrial Dysfunctions Contribute to Hypertrophic Cardiomyopathy in Patient iPSC-Derived Cardiomyocytes with MT-RNR2 Mutation. Stem Cell Reports *10*, 808–821.

Li, X., Zhang, R., Zhao, B., Lossin, C., and Cao, Z. (2016). Cardiotoxicity screening: a review of rapid-throughput in vitro approaches. Arch. Toxicol. *90*, 1803–1816.

Li, Y., Asfour, H., Bursac, N., and Author, A.B. (2017b). Age-dependent Functional Crosstalk Between Cardiac Fibroblasts and Cardiomyocytes in a 3D Engineered Cardiac Tissue Graphical abstract HHS Public Access Author manuscript. Acta Biomater *55*, 120–130.

Lian, X., Hsiao, C., Wilson, G., Zhu, K., Hazeltine, L.B., Azarin, S.M., Raval, K.K., Zhang, J.,

Kamp, T.J., and Palecek, S.P. (2012a). Robust cardiomyocyte differentiation from human pluripotent stem cells via temporal modulation of canonical Wnt signaling. Proc. Natl. Acad. Sci. U. S. A. *109*, E1848-57.

Lian, X., Hsiao, C., Wilson, G., Zhu, K., Hazeltine, L.B., Azarin, S.M., Raval, K.K., Zhang, J., Kamp, T.J., and Palecek, S.P. (2012b). Robust cardiomyocyte differentiation from human pluripotent stem cells via temporal modulation of canonical Wnt signaling. Proc. Natl. Acad. Sci. U. S. A. *109*, E1848-57.

Lian, X., Hsiao, C., Wilson, G., Zhu, K., Hazeltine, L.B., Azarin, S.M., Raval, K.K., Zhang, J., Kamp, T.J., and Palecek, S.P. (2012c). Robust cardiomyocyte differentiation from human pluripotent stem cells via temporal modulation of canonical Wnt signaling. Proc. Natl. Acad. Sci. *109*, E1848–E1857.

Lian, X., Zhang, J., Azarin, S.M., Zhu, K., Hazeltine, L.B., Bao, X., Hsiao, C., Kamp, T.J., and Palecek, S.P. (2013). Directed cardiomyocyte differentiation from human pluripotent stem cells by modulating Wnt/β-catenin signaling under fully defined conditions. Nat. Protoc. *8*, 162–175.

Lian, X., Bao, X., Zilberter, M., Westman, M., Fisahn, A., Hsiao, C., Hazeltine, L.B., Dunn, K.K., Kamp, T.J., and Palecek, S.P. (2015). Chemically defined, albumin-free human cardiomyocyte generation. Nat. Methods *12*, 595–596.

Litviňuková, M., Talavera-López, C., Maatz, H., Reichart, D., Worth, C.L., Lindberg, E.L., Kanda, M., Polanski, K., Heinig, M., Lee, M., et al. (2020). Cells of the adult human heart. Nature.

Liu, J., Laksman, Z., and Backx, P.H. (2016). The electrophysiological development of cardiomyocytes. Adv. Drug Deliv. Rev. *96*, 253–273.

Loh, K.M., Ang, L.T., Zhang, J., Kumar, V., Ang, J., Auyeong, J.Q., Lee, K.L., Choo, S.H., Lim, C.Y.Y., Nichane, M., et al. (2014a). Efficient endoderm induction from human pluripotent stem cells by logically directing signals controlling lineage bifurcations. Cell Stem Cell *14*, 237–252.

Loh, K.M., Ang, L.T., Zhang, J., Kumar, V., Ang, J., Auyeong, J.Q., Lee, K.L., Choo, S.H., Lim, C.Y.Y., Nichane, M., et al. (2014b). Efficient endoderm induction from human pluripotent stem cells by logically directing signals controlling lineage bifurcations. Cell Stem Cell *14*, 237–252.

Loh, K.M.M., Chen, A., Koh, P.W.W., Deng, T.Z.Z., Sinha, R., Tsai, J.M.M., Barkal, A.A.A., Shen, K.Y.Y., Jain, R., Morganti, R.M.M., et al. (2016a). Mapping the Pairwise Choices Leading from Pluripotency to Human Bone, Heart, and Other Mesoderm Cell Types. Cell *166*, 451–467.

Loh, K.M.M., Chen, A., Koh, P.W.W., Deng, T.Z.Z., Sinha, R., Tsai, J.M.M., Barkal, A.A.A., Shen, K.Y.Y., Jain, R., Morganti, R.M.M., et al. (2016b). Mapping the Pairwise Choices Leading from Pluripotency to Human Bone, Heart, and Other Mesoderm Cell Types. Cell *166*, 451–467.

Lu, H.F., Leong, M.F., Lim, T.C., Chua, Y.P., Lim, J.K., Du, C., and Wan, A.C.A. (2017). Engineering a functional three-dimensional human cardiac tissue model for drug toxicity screening. Biofabrication *9*, 025011.

Lu, H.R., Whittaker, R., Price, J.H., Vega, R., Pfeiffer, E.R., Cerignoli, F., Towart, R., and Gallacher, D.J. (2015). High throughput measurement of Ca++ dynamics in human stem cell-derived cardiomyocytes by kinetic image cytometery: A cardiac risk assessment characterization using a large panel of cardioactive and inactive compounds. Toxicol. Sci. *148*, 503–516.

Lu, H.R., Zeng, H., Kettenhofen, R., Guo, L., Kopljar, I., Van Ammel, K., Tekle, F., Teisman, A., Zhai, J., Clouse, H., et al. (2019). Assessing Drug-Induced Long QT and Proarrhythmic Risk Using Human Stem-Cell-Derived Cardiomyocytes in a Ca2+ Imaging Assay: Evaluation of 28 CiPA Compounds at Three Test Sites. Toxicol. Sci. *170*, 345–356.

Lundy, S.D., Zhu, W.-Z., Regnier, M., and Laflamme, M. a. (2013). Structural and Functional Maturation of Cardiomyocytes Derived from Human Pluripotent Stem Cells. Stem Cells Dev. *22*, 1991–2002.

Lupu, I.-E., Redpath, A.N., and Smart, N. (2020a). Spatiotemporal Analysis Reveals Overlap of Key Proepicardial Markers in the Developing Murine Heart. Stem Cell Reports *14*, 770–787.

Lupu, I.-E., Redpath, A.N., and Smart, N. (2020b). Spatiotemporal Analysis Reveals Overlap of Key Proepicardial Markers in the Developing Murine Heart. Stem Cell Reports *14*, 770–787.

Ma, Z., Wang, J., Loskill, P., Huebsch, N., Koo, S., Svedlund, F.L., Marks, N.C., Hua, E.W., Grigoropoulos, C.P., Conklin, B.R., et al. (2015). Self-organizing human cardiac microchambers mediated by geometric confinement. Nat. Commun. *6*, 7413.

Maddah, M., Heidmann, J.D., Mandegar, M.A., Walker, C.D., Bolouki, S., Conklin, B.R., and Loewke, K.E. (2015). A non-invasive platform for functional characterization of stem-cell-derived cardiomyocytes with applications in cardiotoxicity testing. Stem Cell Reports *4*, 621–631.

Mannhardt, I., Breckwoldt, K., Letuffe-Brenière, D., Schaaf, S., Schulz, H., Neuber, C., Benzin, A., Werner, T., Eder, A., Schulze, T., et al. (2016). Human Engineered Heart Tissue: Analysis of Contractile Force. Stem Cell Reports *7*, 29–42.

Mannhardt, I., Saleem, U., Mosqueira, D., Loos, M.F., Ulmer, B.M., Lemoine, M.D., Larsson, C., Améen, C., de Korte, T., Vlaming, M.L.H., et al. (2020). Comparison of 10 Control hPSC Lines for Drug Screening in an Engineered Heart Tissue Format. Stem Cell Reports *15*, 983–998.

Martin, G.R. (1981). Isolation of a pluripotent cell line from early mouse embryos cultured in medium conditioned by teratocarcinoma stem cells. Proc. Natl. Acad. Sci. U. S. A. *78*, 7634–7638.

Mazumdar, J., O'Brien, W.T., Johnson, R.S., LaManna, J.C., Chavez, J.C., Klein, P.S., and Simon, M.C. (2010). O2 regulates stem cells through Wnt/β-catenin signalling. Nat. Cell Biol. *12*, 1007–1013.

Mckeithan, W.L., Savchenko, A., Yu, M.S., Cerignoli, F., Bruyneel, A.A.N., Price, J.H., Colas, A.R., Miller, E.W., Cashman, J.R., and Mercola, M. (2017). An Automated Platform for Assessment of Congenital and Drug-Induced Arrhythmia with hiPSC-Derived Cardiomyocytes. *8*, 1–12.

van Meer, B.J., Krotenberg, A., Sala, L., Davis, R.P., Eschenhagen, T., Denning, C., Tertoolen, L.G.J., and Mummery, C.L. (2019). Simultaneous measurement of excitation-contraction coupling parameters identifies mechanisms underlying contractile responses of hiPSC-derived cardiomyocytes. Nat. Commun. *10*, 1–9.

Meilhac, S.M., Esner, M., Kelly, R.G., Nicolas, J.F., and Buckingham, M.E. (2004). The clonal origin of myocardial cells in different regions of the embryonic mouse heart. Dev. Cell *6*, 685–698.

Merki, E., Zamora, M., Raya, A., Kawakami, Y., Wang, J., Zhang, X., Burch, J., Kubalak, S.W., Kaliman, P., Belmonte, J.C.I., et al. (2005). Epicardial retinoid X receptor α is required for myocardial growth and coronary artery formation. Proc. Natl. Acad. Sci. U. S. A. *102*, 18455–18460.

Metsalu, T., and Vilo, J. (2015). ClustVis: A web tool for visualizing clustering of multivariate data using Principal Component Analysis and heatmap. Nucleic Acids Res. *43*, W566–W570.

Mi, H., Muruganujan, A., Casagrande, J.T., and Thomas, P.D. (2013). Large-scale gene function analysis with the panther classification system. Nat. Protoc. *8*, 1551–1566.

Mikryukov, A.A., Miao, Y., Gu, M., Keller, G.M., Mikryukov, A.A., Mazine, A., Wei, B., Yang, D., Miao, Y., and Gu, M. (2021). Article BMP10 Signaling Promotes the Development of Endocardial Cells from Human Pluripotent Stem Cell-Derived Cardiovascular Progenitors Article BMP10 Signaling Promotes the Development of Endocardial Cells from Human Pluripotent Stem Cell-Derived Cardio. Stem Cell 1–16.

Milani-Nejad, N., and Janssen, P.M.L. (2014). Small and large animal models in cardiac contraction research: Advantages and disadvantages. Pharmacol. Ther. *141*, 235–249.

Miles, C., Finocchiaro, G., Papadakis, M., Gray, B., Westaby, J., Ensam, B., Basu, J., Parry-Williams, G., Papatheodorou, E., Paterson, C., et al. (2019). Sudden Death and Left Ventricular Involvement in Arrhythmogenic Cardiomyopathy. Circulation *139*, 1786–1797.

Mills, R.J., Titmarsh, D.M., Koenig, X., Parker, B.L., Ryall, J.G., Quaife-Ryan, G.A., Voges, H.K., Hodson, M.P., Ferguson, C., Drowley, L., et al. (2017a). Functional screening in human cardiac organoids reveals a metabolic mechanism for cardiomyocyte cell cycle arrest. Proc. Natl. Acad. Sci. U. S. A. *114*, E8372–E8381.

Mills, R.J., Titmarsh, D.M., Koenig, X., Parker, B.L., Ryall, J.G., Quaife-Ryan, G.A., Voges, H.K., Hodson, M.P., Ferguson, C., Drowley, L., et al. (2017b). Functional screening in human cardiac organoids reveals a metabolic mechanism for cardiomyocyte cell cycle arrest. Proc. Natl. Acad. Sci. U. S. A. *114*, E8372–E8381.

Mills, R.J., Parker, B.L., Quaife-Ryan, G.A., Voges, H.K., Needham, E.J., Bornot, A., Ding, M., Andersson, H., Polla, M., Elliott, D.A., et al. (2019). Drug Screening in Human PSC-Cardiac Organoids Identifies Pro-proliferative Compounds Acting via the Mevalonate Pathway. Cell Stem Cell *24*, 895-907.e6.

Miranda, C.C., Fernandes, T.G., Diogo, M.M., and Cabral, J.M.S. (2018). Towards multi-organoid systems for drug screening applications. Bioengineering *5*, 1–17.

Misfeldt, A.M., Boyle, S.C., Tompkins, K.L., Bautch, V.L., Labosky, P.A., and Baldwin, H.S. (2009). Endocardial cells are a distinct endothelial lineage derived from Flk1+ multipotent cardiovascular progenitors. Dev. Biol. *333*, 78–89.

Mithal, A., Capilla, A., Heinze, D., Berical, A., Villacorta-Martin, C., Vedaie, M., Jacob, A., Abo, K., Szymaniak, A., Peasley, M., et al. (2020). Generation of mesenchyme free intestinal organoids from human induced pluripotent stem cells. Nat. Commun. *11*.

Mohr, J.C., Zhang, J., Azarin, S.M., Soerens, A.G., de Pablo, J.J., Thomson, J. a, Lyons, G.E., Palecek, S.P., and Kamp, T.J. (2010). The microwell control of embryoid body size in order to regulate cardiac differentiation of human embryonic stem cells. Biomaterials *31*, 1885–1893.

Mohyeldin, A., Garzón-Muvdi, T., and Quiñones-Hinojosa, A. (2010). Oxygen in stem cell biology: a critical component of the stem cell niche. Cell Stem Cell *7*, 150–161.

Mommersteeg, M.T.M., Domínguez, J.N., Wiese, C., Norden, J., De Gier-De Vries, C., Burch, J.B.E., Kispert, A., Brown, N.A., Moorman, A.F.M., and Christoffels, V.M. (2010). The sinus venosus progenitors separate and diversify from the first and second heart fields early in development. Cardiovasc. Res. *87*, 92–101.

Moriyama, M., Moriyama, H., Uda, J., Kubo, H., Nakajima, Y., Goto, A., Morita, T., and Hayakawa, T. (2017). BNIP3 upregulation via stimulation of ERK and JNK activity is required for the protection of keratinocytes from UVB-induced apoptosis. Cell Death Dis. *8*, e2576.

Nahirney, P.C., Mikawa, T., and Fischman, D.A. (2003). Evidence for an extracellular matrix bridge guiding proepicardial cell migration to the myocardium of chick embryos. Dev. Dyn. *227*, 511–523.

Nakano, A., Nakano, H., Smith, K.A., and Palpant, N.J. (2016). The developmental origins and lineage contributions of endocardial endothelium. Biochim. Biophys. Acta - Mol. Cell Res. *1863*,

1937–1947.

Navarrete, E.G., Liang, P., Lan, F., Sanchez-Freire, V., Simmons, C., Gong, T., Sharma, A., Burridge, P.W., Patlolla, B., Lee, A.S., et al. (2013). Screening drug-induced arrhythmia events using human induced pluripotent stem cell-derived cardiomyocytes and low-impedance microelectrode arrays. Circulation *128*, 3–13.

Nerbonne, J. (2004). Studying Cardiac Arrhythmias in the Mouse—A Reasonable Model for Probing Mechanisms? Trends Cardiovasc. Med. *14*, 83–93.

Nguyen, M.T.X., Okina, E., Chai, X., Tan, K.H., Hovatta, O., Ghosh, S., and Tryggvason, K. (2016). Differentiation of Human Embryonic Stem Cells to Endothelial Progenitor Cells on Laminins in Defined and Xeno-free Systems. Stem Cell Reports *7*, 802–816.

Niebruegge, S., Bauwens, C.L., Peerani, R., Thavandiran, N., Masse, S., Sevaptisidis, E., Nanthakumar, K., Woodhouse, K., Husain, M., Kumacheva, E., et al. (2009). Generation of human embryonic stem cell-derived mesoderm and cardiac cells using size-specified aggregates in an oxygen-controlled bioreactor. Biotechnol. Bioeng. *102*, 493–507.

Van Norman, G.A. (2019). Limitations of Animal Studies for Predicting Toxicity in Clinical Trials: Is it Time to Rethink Our Current Approach? JACC Basic to Transl. Sci. *4*, 845–854.

Ogaki, S., Morooka, M., Otera, K., and Kume, S. (2015). A cost-effective system for differentiation of intestinal epithelium from human induced pluripotent stem cells. Sci. Rep. *5*, 1–11.

Onakpoya, I.J., Heneghan, C.J., and Aronson, J.K. (2016). Post-marketing withdrawal of 462 medicinal products because of adverse drug reactions: A systematic review of the world literature. BMC Med. *14*, 1–11.

Orlova, V. V., Van Den Hil, F.E., Petrus-Reurer, S., Drabsch, Y., Ten Dijke, P., and Mummery, C.L. (2014). Generation, expansion and functional analysis of endothelial cells and pericytes derived from human pluripotent stem cells. Nat. Protoc. *9*, 1514–1531.

Pae, S.H., Dokic, D., and Dettman, R.W. (2008). Communication between integrin receptors facilitates epicardial cell adhesion and matrix organization. Dev. Dyn. *237*, 962–978.

Paige, S.L., Osugi, T., Afanasiev, O.K., Pabon, L., Reinecke, H., and Murry, C.E. (2010). Endogenous wnt/β-Catenin signaling is required for cardiac differentiation in human embryonic stem cells. PLoS One *5*.

Palpant, N.J., Pabon, L., Roberts, M., Hadland, B., Jones, D., Jones, C., Moon, R.T., Ruzzo, W.L., Bernstein, I., Zheng, Y., et al. (2015). Inhibition of β-catenin signaling respecifies anterior-like endothelium into beating human cardiomyocytes. Dev. *142*, 3198–3209.

Palpant, N.J., Pabon, L., Friedman, C.E., Roberts, M., Hadland, B., Zaunbrecher, R.J., Bernstein, I., Zheng, Y., and Murry, C.E. (2017). Generating high-purity cardiac and endothelial derivatives from patterned mesoderm using human pluripotent stem cells. Nat. Protoc. *12*, 15–31.

Pasquier, J., Gupta, R., Rioult, D., Hoarau-Véchot, J., Courjaret, R., Machaca, K., Al Suwaidi, J., Stanley, E.G., Rafii, S., Elliott, D.A., et al. (2017). Coculturing with endothelial cells promotes in vitro maturation and electrical coupling of human embryonic stem cell–derived cardiomyocytes. J. Hear. Lung Transplant. *36*, 684–693.

Patsch, C., Challet-Meylan, L., Thoma, E.C., Urich, E., Heckel, T., O'Sullivan, J.F., Grainger, S.J., Kapp, F.G., Sun, L., Christensen, K., et al. (2015). Generation of vascular endothelial and smooth muscle cells from human pluripotent stem cells. Nat. Cell Biol. *17*, 994–1003.

Pei, D., Xu, J., Zhuang, Q., Tse, H.-F., and Esteban, M.A. (2010). Induced pluripotent stem cell technology in regenerative medicine and biology. Adv. Biochem. Eng. Biotechnol. *123*, 127–141.

Pei, F., Jiang, J., Bai, S., Cao, H., Tian, L., Zhao, Y., Yang, C., Dong, H., and Ma, Y. (2017). Chemical-defined and albumin-free generation of human atrial and ventricular myocytes from human pluripotent stem cells. Stem Cell Res. *19*, 94–103.

Pennisi, D.J., Ballard, V.L.T., and Mikawa, T. (2003). Epicardium is required for the full rate of myocyte proliferation and levels of expression of myocyte mitogenic factors FGF2 and its receptor, FGFR-1, but not for transmural myocardial patterning in the embryonic chick heart. Dev. Dyn. *228*, 161–172.

Peralta, M., Steed, E., Harlepp, S., González-Rosa, J.M., Monduc, F., Ariza-Cosano, A., Cortés, A., Rayón, T., Gómez-Skarmeta, J.L., Zapata, A., et al. (2013). Heartbeat-driven pericardiac fluid forces contribute to epicardium morphogenesis. Curr. Biol. *23*, 1726–1735.

Perry, M., Stansfeld, P.J., Leaney, J., Wood, C., de Groot, M.J., Leishman, D., Sutcliffe, M.J., and Mitcheson, J.S. (2006). Drug Binding Interactions in the Inner Cavity of hERG Channels: Molecular Insights from Structure-Activity Relationships of Clofilium and Ibutilide Analogs. Mol. Pharmacol. *69*, 509–519.

Pinto, A.R., Ilinykh, A., Ivey, M.J., Kuwabara, J.T., D'Antoni, M.L., Debuque, R., Chandran, A., Wang, L., Arora, K., Rosenthal, N.A., et al. (2016). Revisiting Cardiac Cellular Composition. Circ. Res. *118*, 400–409.

Pitaktong, I., Lui, C., Lowenthal, J., Mattson, G., Jung, W.-H., Bai, Y., Yeung, E., Ong, C.S., Chen, Y., Gerecht, S., et al. (2020). Early Vascular Cells Improve Microvascularization Within 3D Cardiac Spheroids. Tissue Eng. Part C Methods *26*, 80–90.

Plavicki, J.S., Hofsteen, P., Yue, M.S., Lanham, K.A., Peterson, R.E., and Heideman, W. (2014).

Multiple modes of proepicardial cell migration require heartbeat. BMC Dev. Biol. *14*.

Pointon, A., Abi-gerges, N., Cross, M.J., and Sidaway, J.E. (2013). Phenotypic profiling of structural cardiotoxins in vitro reveals dependency on multiple mechanisms of toxicity. Toxicol. Sci. *132*, 317–326.

Polonchuk, L., Chabria, M., Badi, L., Hoflack, J.C., Figtree, G., Davies, M.J., and Gentile, C. (2017). Cardiac spheroids as promising in vitro models to study the human heart microenvironment. Sci. Rep. *7*, 1–12.

Prajapati, C., Pölönen, R.P., and Aalto-Setälä, K. (2018). Simultaneous recordings of action potentials and calcium transients from human induced pluripotent stem cell derived cardiomyocytes. Biol. Open *7*.

Prondzynski, M., Lemoine, M.D., Zech, A.T., Horváth, A., Di Mauro, V., Koivumäki, J.T., Kresin, N., Busch, J., Krause, T., Krämer, E., et al. (2019). Disease modeling of a mutation in α-actinin 2 guides clinical therapy in hypertrophic cardiomyopathy. EMBO Mol. Med. *11*, 1–18.

Protze, S.I., Liu, J., Nussinovitch, U., Ohana, L., Backx, P.H., Gepstein, L., and Keller, G.M. (2017). Sinoatrial node cardiomyocytes derived from human pluripotent cells function as a biological pacemaker. Nat. Biotechnol. *35*, 56–68.

Protze, S.I., Lee, J.H., and Keller, G.M. (2019). Human Pluripotent Stem Cell-Derived Cardiovascular Cells: From Developmental Biology to Therapeutic Applications. Cell Stem Cell *25*, 311–327.

Quail, D.F., Taylor, M.J., Walsh, L.A., Dieters-Castator, D., Das, P., Jewer, M., Zhang, G., and Postovit, L. (2011). Low oxygen levels induce the expression of the embryonic morphogen Nodal. Mol. Biol. Cell *22*, 4809–4821.

Rao, J., Pfeiffer, M.J., Frank, S., Adachi, K., Piccini, I., Quaranta, R., Araúzo-Bravo, M., Schwarz, J., Schade, D., Leidel, S., et al. (2016). Stepwise Clearance of Repressive Roadblocks Drives Cardiac Induction in Human ESCs. Cell Stem Cell *18*, 341–353.

Ravenscroft, S.M., Pointon, A., Williams, A.W., Cross, M.J., and Sidaway, J.E. (2016). Cardiac non-myocyte cells show enhanced pharmacological function suggestive of contractile maturity in stem cell derived cardiomyocyte microtissues. Toxicol. Sci. *152*, 99–112.

Red-Horse, K., Ueno, H., Weissman, I.L., and Krasnow, M. (2010). Coronary arteries form by developmental reprogramming of venous cellsNIH Public Access. Nat Immunol *464*, 549–553.

Ren, J., Han, P., Ma, X., Farah, E.N., Bloomekatz, J., Zeng, X.X.I., Zhang, R., Swim, M.M., Witty, A.D., Knight, H.G., et al. (2019). Canonical Wnt5b Signaling Directs Outlying Nkx2.5+ Mesoderm into

Pacemaker Cardiomyocytes. Dev. Cell *50*, 729-743.e5.

Richards, D.J., Coyle, R.C., Tan, Y., Jia, J., Wong, K., Toomer, K., Menick, D.R., and Mei, Y. (2017). Inspiration from heart development: Biomimetic development of functional human cardiac organoids. Biomaterials *142*, 112–123.

Richards, D.J., Li, Y., Kerr, C.M., Yao, J., Beeson, G.C., Coyle, R.C., Chen, X., Jia, J., Damon, B., Wilson, R., et al. (2020). Human cardiac organoids for the modelling of myocardial infarction and drug cardiotoxicity. Nat. Biomed. Eng. *4*, 446–462.

Risebro, C.A., Vieira, J.M., Klotz, L., and Riley, P.R. (2015). Characterisation of the human embryonic and foetal epicardium during heart development. Dev. *142*, 3630–3636.

Rodgers, L.S., Lalani, S., Runyan, R.B., and Camenisch, T.D. (2008). Differential growth and multicellular villi direct proepicardial translocation to the developing mouse heart. Dev. Dyn. *237*, 145–152.

Ronaldson-Bouchard, K., Ma, S.P., Yeager, K., Chen, T., Song, L.J., Sirabella, D., Morikawa, K., Teles, D., Yazawa, M., and Vunjak-Novakovic, G. (2018a). Advanced maturation of human cardiac tissue grown from pluripotent stem cells. Nature *556*, 239–243.

Ronaldson-Bouchard, K., Ma, S.P., Yeager, K., Chen, T., Song, L., Sirabella, D., Morikawa, K., Teles, D., Yazawa, M., and Vunjak-Novakovic, G. (2018b). Advanced maturation of human cardiac tissue grown from pluripotent stem cells. Nature *556*, 239–243.

Rosa, S., Praça, C., Pitrez, P.R., Gouveia, P.J., Aranguren, X.L., Ricotti, L., and Ferreira, L.S. (2019). Functional characterization of iPSC-derived arterial- and venous-like endothelial cells. Sci. Rep. *9*, 1–15.

Rossi, G., Broguiere, N., Miyamoto, M., Kelly, R.G., Kwon, C., Lutolf, M.P., Rossi, G., Broguiere, N., Miyamoto, M., Boni, A., et al. (2021). Article Capturing Cardiogenesis in Gastruloids Article Capturing Cardiogenesis in Gastruloids. Stem Cell 1–11.

Ruan, J.-L., Tulloch, N.L., Razumova, M. V., Saiget, M., Muskheli, V., Pabon, L., Reinecke, H., Regnier, M., and Murry, C.E. (2016). Mechanical Stress Conditioning and Electrical Stimulation Promote Contractility and Force Maturation of Induced Pluripotent Stem Cell-Derived Human Cardiac Tissue. Circulation *134*, 1557–1567.

Rupert, C.E., Kim, T.Y., Choi, B.R., and Coulombe, K.L.K. (2020). Human Cardiac Fibroblast Number and Activation State Modulate Electromechanical Function of hiPSC-Cardiomyocytes in Engineered Myocardium. Stem Cells Int. *2020*.

Ruttkay-Nedecky, B., Nejdl, L., Gumulec, J., Zitka, O., Masarik, M., Eckschlager, T., Stiborova,

M., Adam, V., and Kizek, R. (2013). The role of metallothionein in oxidative stress. Int. J. Mol. Sci. *14*, 6044–6066.

Ryckebusch, L., Wang, Z., Bertrand, N., Lin, S.C., Chi, X., Schwartz, R., Zaffran, S., and Niederreither, K. (2008). Retinoic acid deficiency alters second heart field formation. Proc. Natl. Acad. Sci. U. S. A. *105*, 2913–2918.

Sahara, M., Hansson, E.M., Wernet, O., Lui, K.O., Später, D., and Chien, K.R. (2014). Manipulation of a VEGF-Notch signaling circuit drives formation of functional vascular endothelial progenitors from human pluripotent stem cells. Cell Res. *24*, 820–841.

Sala, L., Bellin, M., and Mummery, C.L. (2017). Integrating cardiomyocytes from human pluripotent stem cells in safety pharmacology: has the time come? Br. J. Pharmacol. *174*, 3749–3765.

Sala, L., Van Meer, B.J., Tertoolen, L.G.J., Bakkers, J., Bellin, M., Davis, R.P., Denning, C., Dieben, M.A.E., Eschenhagen, T., Giacomelli, E., et al. (2018). Musclemotion: A versatile open software tool to quantify cardiomyocyte and cardiac muscle contraction in vitro and in vivo. Circ. Res. *122*, e5–e16.

Salama, G., and London, B. (2007). Mouse models of long QT syndrome. J. Physiol. *578*, 43–53.

Saleem, U., van Meer, B.J., Katili, P.A., Yusof, N.A.N.M., Mannhardt, I., Garcia, A.K., Tertoolen, L., de Korte, T., Vlaming, M.L.H., McGlynn, K., et al. (2020). Blinded, multi-centre evaluation of drug-induced changes in contractility using human induced pluripotent stem cell-derived cardiomyocytes. Toxicol. Sci.

Schaaf, S., Shibamiya, A., Mewe, M., Eder, A., Stöhr, A., Hirt, M.N., Rau, T., Zimmermann, W.H., Conradi, L., Eschenhagen, T., et al. (2011). Human engineered heart tissue as a versatile tool in basic research and preclinical toxicology. PLoS One *6*.

Schier, A.F. (2009). Nodal morphogens. Cold Spring Harb. Perspect. Biol. *1*, a003459.

Sengbusch, J.K., He, W., Pinco, K.A., and Yang, J.T. (2002). Dual functions of α4β1 integrin in epicardial development: Initial migration and long-term attachment. J. Cell Biol. *157*, 873–882.

Shadrin, I.Y., Allen, B.W., Qian, Y., Jackman, C.P., Carlson, A.L., Juhas, M.E., and Bursac, N. (2017). Cardiopatch platform enables maturation and scale-up of human pluripotent stem cell-derived engineered heart tissues. Nat. Commun. *8*.

Shah, D., Prajapati, C., Penttinen, K., Cherian, R.M., Koivumäki, J.T., Alexanova, A., Hyttinen, J., and Aalto-Setälä, K. (2020). hiPSC-Derived Cardiomyocyte Model of LQT2 Syndrome Derived from Asymptomatic and Symptomatic Mutation Carriers Reproduces Clinical Differences in

Aggregates but Not in Single Cells. Cells *9*.

Sharma, A., Burridge, P.W., McKeithan, W.L., Serrano, R., Shukla, P., Sayed, N., Churko, J.M., Kitani, T., Wu, H., Holmström, A., et al. (2017). High-throughput screening of tyrosine kinase inhibitor cardiotoxicity with human induced pluripotent stem cells. Sci. Transl. Med. *9*.

Sharma, A., McKeithan, W.L., Serrano, R., Kitani, T., Burridge, P.W., del Álamo, J.C., Mercola, M., and Wu, J.C. (2018). Use of human induced pluripotent stem cell–derived cardiomyocytes to assess drug cardiotoxicity. Nat. Protoc. *13*, 3018–3041.

Sheng, X., Reppel, M., Nguemo, F., Mohammad, F.I., Kuzmenkin, A., Hescheler, J., and Pfannkuche, K. (2012). Human Pluripotent Stem Cell-Derived Cardiomyocytes: Response to TTX and Lidocain Reveals Strong Cell to Cell Variability. PLoS One *7*, 1–12.

Sherwood, R.I., Maehr, R., Mazzoni, E.O., and Melton, D.A. (2011). Wnt signaling specifies and patterns intestinal endoderm. Mech. Dev. *128*, 387–400.

Silva, A.C., Matthys, O.B., Joy, D.A., Kauss, M.A., Natarajan, V., Lai, M.H., Turaga, D., Alexanian, M., Bruneau, B.G., and McDevitt, T.C. (2020). Developmental co-emergence of cardiac and gut tissues modeled by human iPSC-derived organoids. BioRxiv 2020.04.30.071472.

Siramshetty, V.B., Nickel, J., Omieczynski, C., Gohlke, B.O., Drwal, M.N., and Preissner, R. (2016). WITHDRAWN - A resource for withdrawn and discontinued drugs. Nucleic Acids Res. *44*, D1080–D1086.

Skardal, A., Murphy, S. V., Devarasetty, M., Mead, I., Kang, H.W., Seol, Y.J., Zhang, Y.S., Shin, S.R., Zhao, L., Aleman, J., et al. (2017). Multi-tissue interactions in an integrated three-tissue organ-on-a-chip platform. Sci. Rep. *7*, 1–16.

Smith, C.L., Baek, S.T., Sung, C.Y., and Tallquist, M.D. (2011). Epicardial-derived cell epithelial-to-mesenchymal transition and fate specification require PDGF receptor signaling. Circ. Res. *108*.

Später, D., Abramczuk, M.K., Buac, K., Zangi, L., Stachel, M.W., Clarke, J., Sahara, M., Ludwig, A., and Chien, K.R. (2013). A HCN4+ cardiomyogenic progenitor derived from the first heart field and human pluripotent stem cells. Nat. Cell Biol. *15*, 1098–1106.

Spence, J.R., Mayhew, C.N., Rankin, S.A., Kuhar, M.F., Vallance, J.E., Tolle, K., Hoskins, E.E., Kalinichenko, V. V., Wells, S.I., Zorn, A.M., et al. (2011). Directed differentiation of human pluripotent stem cells into intestinal tissue in vitro. Nature *470*, 105–110.

Spencer, C.I., Baba, S., Nakamura, K., Hua, E.A., Sears, M.A.F., Fu, C.C., Zhang, J., Balijepalli, S., Tomoda, K., Hayashi, Y., et al. (2014). Calcium transients closely reflect prolonged action potentials in iPSC models of inherited cardiac arrhythmia. Stem Cell Reports *3*, 269–281.

Sriram, G., Tan, J.Y., Islam, I., Rufaihah, A.J., and Cao, T. (2015). Efficient differentiation of human embryonic stem cells to arterial and venous endothelial cells under feeder- and serum-free conditions. Stem Cell Res. Ther. *6*, 1–17.

Stuckmann, I., Evans, S., and Lassar, A.B. (2003). Erythropoietin and retinoic acid, secreted from the epicardium, are required for cardiac myocyte proliferation. Dev. Biol. *255*, 334–349.

Sucov, H.M., Dyson, E., Gumeringer, C.L., Price, J., Chien, K.R., and Evans, R.M. (1994). RXRα mutant mice establish a genetic basis for vitamin A signaling in heart morphogenesis. Genes Dev. *8*, 1007–1018.

Sugi, Y., and Lough, J. (1994). Anterior endoderm is a specific effector of terminal cardiac myocyte differentiation of cells from the embryonic heart forming region. Dev. Dyn. *200*, 155–162.

Takahashi, K., and Yamanaka, S. (2006). Induction of Pluripotent Stem Cells from Mouse Embryonic and Adult Fibroblast Cultures by Defined Factors. Cell *126*, 663–676.

Takahashi, K., Tanabe, K., Ohnuki, M., Narita, M., Ichisaka, T., Tomoda, K., and Yamanaka, S. (2007). Induction of pluripotent stem cells from adult human fibroblasts by defined factors. Cell *131*, 861–872.

Takayama, K., Negoro, R., Yamashita, T., Kawai, K., Ichikawa, M., Mori, T., Nakatsu, N., Harada, K., Ito, S., Yamada, H., et al. (2019). Generation of Human iPSC–Derived Intestinal Epithelial Cell Monolayers by CDX2 Transduction. Cmgh *8*, 513–526.

Takeda, M., Kanki, Y., Masumoto, H., Funakoshi, S., Hatani, T., Fukushima, H., Izumi-Taguchi, A., Matsui, Y., Shimamura, T., Yoshida, Y., et al. (2018a). Identification of Cardiomyocyte-Fated Progenitors from Human-Induced Pluripotent Stem Cells Marked with CD82. Cell Rep. *22*, 546–556.

Takeda, M., Miyagawa, S., Fukushima, S., Saito, A., Ito, E., Harada, A., Matsuura, R., Iseoka, H., Sougawa, N., Mochizuki-Oda, N., et al. (2018b). Development of In Vitro Drug-Induced Cardiotoxicity Assay by Using Three-Dimensional Cardiac Tissues Derived from Human Induced Pluripotent Stem Cells. Tissue Eng. Part C Methods *24*, 56–67.

Takeda, M., Miyagawa, S., Fukushima, S., Saito, A., Ito, E., Harada, A., Matsuura, R., Iseoka, H., Sougawa, N., Mochizuki-Oda, N., et al. (2018c). Development of in vitro drug-induced cardiotoxicity assay by using three-dimensional cardiac tissues derived from human induced pluripotent stem cells. Tissue Eng. - Part C Methods *24*, 56–67.

Tan, J.Y., Sriram, G., Rufaihah, A.J., Neoh, K.G., and Cao, T. (2013). Efficient derivation of lateral plate and paraxial mesoderm subtypes from human embryonic stem cells through GSKi-mediated differentiation. Stem Cells Dev. *22*, 1893–1906.

Tewary, M., Dziedzicka, D., Ostblom, J., Prochazka, L., and Shakiba, N. (2018). High-throughput micro-patterning platform reveals Nodal- dependent dissection of peri-gastrulation-associated versus pre- neurulation associated fate patterning.

Thavandiran, N., Hale, C., Blit, P., Sandberg, M.L., McElvain, M.E., Gagliardi, M., Sun, B., Witty, A., Graham, G., Mcintosh, M., et al. (2019). Functional arrays of human pluripotent stem cell-derived cardiac microtissues. BioRxiv 566059.

Thomson, J.A. (1998). Embryonic Stem Cell Lines Derived from Human Blastocysts. Science (80-.). *282*, 1145–1147.

Tiburcy, M., Hudson, J.E., Balfanz, P., Schlick, S., Meyer, T., Chang Liao, M.-L., Levent, E., Raad, F., Zeidler, S., Wingender, E., et al. (2017). Defined Engineered Human Myocardium With Advanced Maturation for Applications in Heart Failure Modeling and Repair. Circulation *135*, 1832–1847.

Ting, S., Chen, A., Reuveny, S., and Oh, S. (2014). An intermittent rocking platform for integrated expansion and differentiation of human pluripotent stem cells to cardiomyocytes in suspended microcarrier cultures. Stem Cell Res. *13*, 202–213.

Tirosh-Finkel, L., Zeisel, A., Brodt-Ivenshitz, M., Shamai, A., Yao, Z., Seger, R., Domany, E., and Tzahor, E. (2010). BMP-mediated inhibition of FGF signaling promotes cardiomyocyte differentiation of anterior heart field progenitors. Development *137*, 2989–3000.

Turnbull, I.C., Karakikes, I., Serrao, G.W., Backeris, P., Lee, J.J., Xie, C., Senyei, G., Gordon, R.E., Li, R.A., Akar, F.G., et al. (2014). Advancing functional engineered cardiac tissues toward a preclinical model of human myocardium. FASEB J. *28*, 644–654.

Tzahor, E. (2007). Wnt/β-Catenin Signaling and Cardiogenesis: Timing Does Matter. Dev. Cell *13*, 10–13.

Ulmer, B.M., Stoehr, A., Schulze, M.L., Patel, S., Gucek, M., Mannhardt, I., Funcke, S., Murphy, E., Eschenhagen, T., and Hansen, A. (2018). Contractile Work Contributes to Maturation of Energy Metabolism in hiPSC-Derived Cardiomyocytes. Stem Cell Reports *10*, 834–847.

Uosaki, H., Fukushima, H., Takeuchi, A., Matsuoka, S., Nakatsuji, N., Yamanaka, S., and Yamashita, J.K. (2011). Efficient and Scalable Purification of Cardiomyocytes from Human Embryonic and Induced Pluripotent Stem Cells by VCAM1 Surface Expression. PLoS One *6*, e23657.

Varum, S., Momcilović, O., Castro, C., Ben-Yehudah, A., Ramalho-Santos, J., and Navara, C.S. (2010). Enhancement of human embryonic stem cell pluripotency through inhibition of the mitochondrial respiratory chain. Stem Cell Res. *3*, 142–156.

Veevers, J., Farah, E.N., Corselli, M., Witty, A.D., Palomares, K., Vidal, J.G., Emre, N., Carson,

C.T., Ouyang, K., Liu, C., et al. (2018). Cell-Surface Marker Signature for Enrichment of Ventricular Cardiomyocytes Derived from Human Embryonic Stem Cells. Stem Cell Reports *11*, 828–841.

Veldhuizen, J., Cutts, J., Brafman, D.A., Migrino, R.Q., and Nikkhah, M. (2020). Engineering anisotropic human stem cell-derived three-dimensional cardiac tissue on-a-chip. Biomaterials *256*, 120195.

Verzi, M.P., McCulley, D.J., De Val, S., Dodou, E., and Black, B.L. (2005). The right ventricle, outflow tract, and ventricular septum comprise a restricted expression domain within the secondary/anterior heart field. Dev. Biol. *287*, 134–145.

Voges, H.K., Mills, R.J., Elliott, D.A., Parton, R.G., Porrello, E.R., and Hudson, J.E. (2017). Development of a human cardiac organoid injury model reveals innate regenerative potential. Development *144*, 1118–1127.

Volz, K.S., Jacobs, A.H., Chen, H.I., Poduri, A., McKay, A.S., Riordan, D.P., Kofler, N., Kitajewski, J., Weissman, I., and Red-Horse, K. (2015). Pericytes are progenitors for coronary artery smooth muscle. Elife *4*, 1–22.

Vrancken Peeters, M.P.F.M., Gittenberger-de Groot, A.C., Mentink, M.M.T., and Poelmann, R.E. (1999). Smooth muscle cells and fibroblasts of the coronary arteries derive from epithelial-mesenchymal transformation of the epicardium. Anat. Embryol. (Berl). *199*, 367–378.

Warmflash, A., Sorre, B., Etoc, F., Siggia, E.D., and Brivanlou, A.H. (2014). A method to recapitulate early embryonic spatial patterning in human embryonic stem cells. Nat. Methods *11*, 847–854.

Watt, A.J., Battle, M.A., Li, J., and Duncan, S.A. (2004). GATA4 is essential for formation of the proepicardium and regulates cardiogenesis. Proc. Natl. Acad. Sci. U. S. A. *101*, 12573–12578.

van Weerd, J.H., and Christoffels, V.M. (2016). The formation and function of the cardiac conduction system. Development *143*, 197–210.

Wengerhoff, S.M., Weiss, A.R., Dwyer, K.L., and Dettman, R.W. (2010). A migratory role for EphrinB ligands in avian epicardial mesothelial cells. Dev. Dyn. *239*, 598–609.

Wessels, A., van den Hoff, M.J.B., Adamo, R.F., Phelps, A.L., Lockhart, M.M., Sauls, K., Briggs, L.E., Norris, R.A., van Wijk, B., Perez-Pomares, J.M., et al. (2012). Epicardially derived fibroblasts preferentially contribute to the parietal leaflets of the atrioventricular valves in the murine heart. Dev. Biol. *366*, 111–124.

Witty, A.D., Mihic, A., Tam, R.Y., Fisher, S.A., Mikryukov, A., Shoichet, M.S., Li, R.K., Kattman, S.J., and Keller, G. (2014a). Generation of the epicardial lineage from human pluripotent stem cells.

Nat. Biotechnol. *32*, 1026–1035.

Witty, A.D., Mihic, A., Tam, R.Y., Fisher, S.A., Mikryukov, A., Shoichet, M.S., Li, R.K., Kattman, S.J., and Keller, G. (2014b). Generation of the epicardial lineage from human pluripotent stem cells. Nat. Biotechnol. *32*, 1026–1035.

Witty, A.D., Mihic, A., Tam, R.Y., Fisher, S.A., Mikryukov, A., Shoichet, M.S., Li, R.K., Kattman, S.J., and Keller, G. (2014c). Generation of the epicardial lineage from human pluripotent stem cells. Nat. Biotechnol. *32*, 1026–1035.

Wolling, H., Konze, S.A., Höfer, A., Erdmann, J., Pich, A., Zweigerdt, R., and Buettner, F.F.R. (2018). Quantitative Secretomics Reveals Extrinsic Signals Involved in Human Pluripotent Stem Cell Cardiomyogenesis. Proteomics *18*, 1800102.

Wu, B., Zhang, Z., Lui, W., Chen, X., Wang, Y., Chamberlain, A.A., Moreno-Rodriguez, R.A., Markwald, R.R., O'Rourke, B.P., Sharp, D.J., et al. (2012). Endocardial Cells Form the Coronary Arteries by Angiogenesis through Myocardial-Endocardial VEGF Signaling. Cell *151*, 1083–1096.

Wu, H., Lee, S.H., Gao, J., Liu, X., and Iruela-Arispe, M.L. (1999). Inactivation of erythropoietin leads to defects in cardiac morphogenesis. Development *126*, 3597–3605.

Wu, M., Smith, C.L., Hall, J.A., Lee, I., Luby-Phelps, K., and Tallquist, M.D. (2010). Epicardial Spindle Orientation Controls Cell Entry into the Myocardium. Dev. Cell *19*, 114–125.

Xu, C., Police, S., Rao, N., and Carpenter, M.K. (2002). Characterization and enrichment of cardiomyocytes derived from human embryonic stem cells. Circ. Res. *91*, 501–508.

Yang, X., and Papoian, T. (2018). Moving beyond the comprehensive in vitro proarrhythmia assay: Use of human-induced pluripotent stem cell-derived cardiomyocytes to assess contractile effects associated with drug-induced structural cardiotoxicity. J. Appl. Toxicol. 1–11.

Yang, J.T., Rayburn, H., and Hynes, R.O. (1995). Cell adhesion events mediated by α4 integrins are essential in placental and cardiac development. Development *121*, 549–560.

Yang, L., Soonpaa, M.H., Adler, E.D., Roepke, T.K., Kattman, S.J., Kennedy, M., Henckaerts, E., Bonham, K., Abbott, G.W., Linden, R.M., et al. (2008). Human cardiovascular progenitor cells develop from a KDR+ embryonic-stem-cell-derived population. Nature *453*, 524–528.

Yin, F., zhang, xu, Wang, L., Wang, Y., Zhu, Y., Li, Z., Tao, T., Chen, W., Yu, H., and Qin, J. (2020). HiPSC-derived multi-organoids on chip system for safety assessment of antidepressant drug. Lab Chip.

Yu, J., Vodyanik, M.A., Smuga-Otto, K., Antosiewicz-Bourget, J., Frane, J.L., Tian, S., Nie, J., Jonsdottir, G.A., Ruotti, V., Stewart, R., et al. (2007). Induced pluripotent stem cell lines derived from

human somatic cells. Science (80-.). *318*, 1917–1920.

Zhang, H., Lui, K.O., and Zhou, B. (2018a). Endocardial cell plasticity in cardiac development, diseases and regeneration. Circ. Res. *122*, 774–789.

Zhang, J., Wilson, G.F., Soerens, A.G., Koonce, C.H., Yu, J., Palecek, S.P., Thomson, J.A., and Kamp, T.J. (2009). Functional Cardiomyocytes Derived From Human Induced Pluripotent Stem Cells. Circ. Res. *104*, 564–574.

Zhang, J., Schwartz, M.P., Hou, Z., Bai, Y., Ardalani, H., Swanson, S., Steill, J., Ruotti, V., Elwell, A., Nguyen, B.K., et al. (2017). A Genome-wide Analysis of Human Pluripotent Stem Cell-Derived Endothelial Cells in 2D or 3D Culture. Stem Cell Reports *8*, 907–918.

Zhang, J., Tao, R., Campbell, K.F., Carvalho, J.L., Ruiz, E.C., Kim, G.C., Schmuck, E.G., Raval, A.N., da Rocha, A.M., Herron, T.J., et al. (2019a). Functional cardiac fibroblasts derived from human pluripotent stem cells via second heart field progenitors. Nat. Commun. *10*.

Zhang, J.Z., Termglinchan, V., Shao, N.Y., Itzhaki, I., Liu, C., Ma, N., Tian, L., Wang, V.Y., Chang, A.C.Y., Guo, H., et al. (2019b). A Human iPSC Double-Reporter System Enables Purification of Cardiac Lineage Subpopulations with Distinct Function and Drug Response Profiles. Cell Stem Cell *24*, 802-811.e5.

Zhang, M., Schulte, J.S., Heinick, A., Piccini, I., Rao, J., Quaranta, R., Zeuschner, D., Malan, D., Kim, K.-P., Röpke, A., et al. (2015). Universal cardiac induction of human pluripotent stem cells in two and three-dimensional formats: implications for in vitro maturation. Stem Cells *33*, 1456–1469.

Zhang, Q., Jiang, J., Han, P., Yuan, Q., Zhang, J., Zhang, X., Xu, Y., Cao, H., Meng, Q., Chen, L., et al. (2011). Direct differentiation of atrial and ventricular myocytes from human embryonic stem cells by alternating retinoid signals. Cell Res. *21*, 579–587.

Zhang, R.R., Koido, M., Tadokoro, T., Ouchi, R., Matsuno, T., Ueno, Y., Sekine, K., Takebe, T., and Taniguchi, H. (2018b). Human iPSC-Derived Posterior Gut Progenitors Are Expandable and Capable of Forming Gut and Liver Organoids. Stem Cell Reports *10*, 780–793.

Zhang, X., Guo, L., Zeng, H., White, S.L., Furniss, M., Balasubramanian, B., Lis, E., Lagrutta, A., Sannajust, F., Zhao, L.L., et al. (2016). Multi-parametric assessment of cardiomyocyte excitation-contraction coupling using impedance and field potential recording: A tool for cardiac safety assessment. J. Pharmacol. Toxicol. Methods *81*, 201–216.

Zhao, J., Cao, H., Tian, L., Huo, W., Zhai, K., Wang, P., Ji, G., and Ma, Y. (2017). Efficient Differentiation of TBX18+/WT1+ Epicardial-Like Cells from Human Pluripotent Stem Cells Using Small Molecular Compounds. Stem Cells Dev. *26*, 528–540.

Zhao, M., Tang, Y., Zhou, Y., and Zhang, J. (2019a). Deciphering Role of Wnt Signalling in Cardiac Mesoderm and Cardiomyocyte Differentiation from Human iPSCs: Four-dimensional control of Wnt pathway for hiPSC-CMs differentiation. Sci. Rep. *9*, 19389.

Zhao, Y., Rafatian, N., Feric, N.T., Cox, B.J., Aschar-Sobbi, R., Wang, E.Y., Aggarwal, P., Zhang, B., Conant, G., Ronaldson-Bouchard, K., et al. (2019b). A Platform for Generation of Chamber-Specific Cardiac Tissues and Disease Modeling. Cell *176*, 913-927.e18.

Zhou, B., Ma, Q., Rajagopal, S., Wu, S.M., Domian, I., Rivera-, J., Jiang, D., Gise, A. Von, Ikeda, S., Chien, K.R., et al. (2009). NIH Public Access. *454*, 109–113.

Zwi, L., Caspi, O., Arbel, G., Huber, I., Gepstein, A., Park, I.H., and Gepstein, L. (2009). Cardiomyocyte differentiation of human induced pluripotent stem cells. Circulation *120*, 1513–1523.

II. TRANSCRIPTOMIC ANALYSIS OF 3D CARDIAC DIFFERENTIATION FROM HUMAN PLURIPOTENT STEM CELLS REVEALS FASTER CARDIOMYOCYTE COMMITMENT COMPARED WITH 2D MONOLAYER CULTURE SYSTEM

The content of this chapter was adapted from the publications:

Mariana A. Branco, João P. Cotovio, Carlos A.V. Rodrigues, Sandra H. Vaz, Tiago G. Fernandes, Leonilde M. Moreira, Joaquim M. S. Cabral, Maria Margarida Diogo "Transcriptomic analysis of 3D Cardiac Differentiation of Human Induced Pluripotent Stem Cells Reveals Faster Cardiomyocyte Maturation Compared to 2D Culture", Scientific Reports, 2019, https://doi.org/10.1038/s41598-019-45047-9

Mariana A. Branco, Tiago P. Dias, João P. Cotovio, Carlos A.V. Rodrigues, Tiago G. Fernandes, Joaquim M.S. Cabral, Maria Margarida Diogo "3D Microwell Platform for Cardiomyocyte Differentiation of Human Pluripotent Stem Cells" Methods in Molecular Biology, Springer, New York, 2020. https://doi.org/10.1007/7651_2020_336

II.1 ABSTRACT

Human PSCs represent an almost limitless source of cells, and, in the past years, different protocols have been described in the literature to generate hPSC-derived CMs with high specificity, both in 2D and 3D conditions. In this chapter it was established a novel 3D platform for CM production from hPSC, solely through temporal modulation of the Wnt signalling pathway and using a microwell platform to generate size controlled aggregates. The platform includes a pre-differentiation stage were hPSCs are allowed to form and proliferate as 3D aggregates for 3 days before the beginning of the differentiation process. In order to find the best condition that maximizes the generation of CMs in this platform, the aggregate size at the begging of differentiation and the concentration of the small molecule used in the step of Wnt signalling activation, was optimized. From that, an efficient protocol was establishment, which generates more than 85% $cTNT^+$ cells after 15 days of differentiation, corresponding to 20-25 million CMs per microwell plate. Additionally, and equally important when envisaging the applicability of the platform, low variability between biological runs was observed, making this platform a simple and robust process to generate CMs from hPSCs. The impact of performing the differentiation process in a 3D environment in comparison with 2D culture system, was characterized by transcriptomic analysis, using data collected from sequential stages of 2D and 3D CM differentiation. This analysis demonstrated that performing the initial period of hPSC aggregation before cardiac differentiation primed hPSCs towards an earlier mesendoderm stage, via TGF-β/Nodal signal stabilization, which was suggested to be responsible for a faster cardiac commitment of hPSCs and to an earlier CM structural and functional maturation when compared with CMs obtained from the monolayer culture. The generated hPSC-CMs can be used in different applications, namely disease modeling, drug screening and cardiotoxicity assays, and/or be integrated in more complex *in vitro* cardiac models.

II.2 INTRODUCTION

Human ESCs and hiPSCs offer an almost limitless source of cells for clinical translation applications. Particularly, CMs obtained from *in vitro* differentiation of hiPSCs have been considered an attractive tool for disease modelling and drug screening applications (Takeda et al., 2018b; Yang and Papoian, 2018).

The identification of key signaling pathways and the transcriptional network linked to embryonic heart development, guided the establishment of a number of *in vitro* models for cardiac differentiation from hPSCs. Through the sequential addition of growth factors and/or small molecules, the critical stages of cardiac specification have been recapitulated to some extent using 2D *in vitro* models (Birket et al., 2015; Kattman et al., 2011b; Lian et al., 2012b; Rao et al., 2016). However, human heart development is a complex process in which spatial gradients of molecules and biophysical stimuli, that occur due to the 3D configuration of the embryo, are crucial to determine the final heart tissue structure and function (Ma et al., 2015; Warmflash et al., 2014). Therefore, these processes are not well recapitulated in the commonly used 2D differentiation platforms.

Aiming at better mimicking the microenvironment of *in vivo* heart development, 3D platforms for *in vitro* cardiac differentiation and maturation have emerged in the past few years. However, and despite the existence of different reported protocols for hPSC differentiation into CMs as 3D aggregates (Chen et al., 2015b; Fonoudi et al., 2015b; Kempf et al., 2014b; Zhang et al., 2015), the development of an efficient, controlled and reproducible process of 3D-CM differentiation has been challenging.

3D culture of hiPSCs has been shown to favor transcriptional changes that improve differentiation into specific lineages (Azarin et al., 2012; Hsiao et al., 2014; Husain et al., 2008; Mohr et al., 2010), but the mechanisms behind this effect have not yet been completely understood. Additionally, the sole impact that 3D culture exerts throughout the process of hiPSC-CM differentiation, from the moment 3D aggregates are generated until the stage of CM maturation remains also poorly understood. In fact, as an example of the relevance of the culture format in this process, a recent study that performed 3D aggregation of cardiac progenitor cells obtained in 2D culture system, showed the benefits of 3D culture at early stages of cardiac differentiation regarding structural and metabolic maturation of the final hPSC-CMs (Correia et al., 2018). Thus, overall, the development of a platform that takes advantage of the knowledge regarding 3D culture of hiPSCs to establish a robust and straightforward cardiac differentiation protocol has not yet been reported.

In this context, in this chapter a study was performed to acquire a more profound understanding of the impact of 3D culture on pluripotency maintenance and priming of hPSC, using for that a forced aggregation platform as previously described (Dahlmann et al., 2013), and that knowledge was further used to develop a simple, efficient and robust 3D platform for hiPSC differentiation towards CMs, using the temporal modulation of the Wnt signalling pathway. RNA sequencing (RNA-seq) was then used to generate global gene expression profiles for sequential stages of cardiac differentiation of

both 3D aggregates and parallel monolayer 2D culture conditions. Expression profiling data analyses revealed that the initial period of hiPSC 3D aggregation before cardiac differentiation induces significant transcriptional changes that favor the cardiac differentiation process by priming hiPSCs to mesendoderm lineages. Also, the generated data suggests that the CMs obtained in this 3D microenvironment mature earlier when compared with the ones obtained in 2D conditions, as a cardiac monolayer.

II.3 MATERIALS AND METHODS

II.3.1 hiPSC Maintenance

In this work, the experiments for optimization of the 3D CM differentiation platform were performed using the hiPSC line iPS-DF6-9-9T.B, provided by WiCell Bank. This cell line was reprogramed from foreskin fibroblasts with a karyotype 46, XY that were collected from healthy donors using defined factors in the Laboratory of Dr. James Thomson, at University of Wisconsin. For the validation of the 3D differentiation platform, two additional hiPSC lines were used, the hiPSC line F002.1A.13, derived from a healthy female donor using a standard protocol (Takahashi et al., 2007) and provided by TCLab (Tecnologias Celulares para Aplicação Médica, Unipessoal, Lda.) and the Gibco® Human Episomal iPSC line (iPSC6.2) (Burridge et al., 2011b). The hiPSCs were maintained in mTeSR™1 (StemCell Technologies) in six-well plates coated with Matrigel™ (Corning). Medium was changed daily. Cells were routinely passaged every three to four days using 0.5mM EDTA solution (Thermo Fisher Scientific).

II.3.2 hiPSC Cardiomyocyte differentiation in 2D and 3D culture conditions

Pre-differentiation period. For 2D monolayer culture, cells were seeded onto Matrigel-coated 12-well tissue culture plates at a cell density of $4x10^5$ cells/well. Culture medium was changed daily until a confluence of around 90-95%. For 3D aggregates formation, cells were incubated with ROCK inhibitor (ROCKi, Y-27632, 10μM, StemCell Technologies) at 37ºC for 1 h and then treated with accutase (Sigma) for 7 min at 37ºC. After dissociation, cells were quickly re-aggregated using microwell plates (AggreWell™800, StemCell Technologies) according to the manufacturer's instructions. Cells were plated at different densities in 1.5 mL/well of mTeSR™1 supplemented with 10μM ROCKi. 24 hours later, the total volume of medium was replaced and cells were maintained in mTeSR™1 without ROCKi for an additional two days.

hiPSCs differentiation. For hiPSCs differentiation into CMs, in both 2D and 3D culture conditions, an adapted GiWi protocol was used (Lian et al., 2013). RPMI 1640 medium (Thermo Fisher Scientific) was used as basal medium. From day 0 to day 7, cells were cultured in RPMI supplemented with 2%(v/v) B-27 minus insulin (Thermo Fisher Scientific), and from day 7 until the

end of differentiation, cells were cultured in RPMI supplemented with 2%(v/v) B-27 (Thermo Fisher Scientific). At day 0 of differentiation, the Wnt signaling pathway was activated using the GSK3 inhibitor CHIR99021 (Stemgent) at a final concentration of 6 µM in 2D and 11 µM in 3D culture conditions. After 24 hours, medium was changed. At day 3, cells were cultured in basal medium supplemented with Wnt inhibitor IWP-4 (Stemgent) at a final concentration of 5 µM, for two days. At day 7, medium was changed and in the case of the 3D culture, aggregates were flushed from the AggreWell™800 plate and transferred to 6-Well Ultra-Low Attachment plates. Thereafter, medium was changed every 3 days until cell harvest.

Aggregate size monitoring. To monitor aggregate size throughout time in culture, several images were acquired at different time points using a Leica DMI 3000B microscope with a Nikon DXM 1200F digital camera. Aggregates were measured using ImageJ Software.

II.3.3 Expression profiling with RNA sequencing

Sample collection and RNA extraction. Cell samples from 2D monolayer and 3D aggregate culture at different stages of cardiac differentiation were singularized with 0.25% trypsin-EDTA at 37ºC for 7-15 min. For enzymatic digestion neutralization, RPMI+10% FBS was added. After centrifugation and washing cells with PBS, the cell pellet was frozen at -80ºC. Total RNA from the samples was extracted using High Pure RNA Isolation Kit (Roche, Cat. 11828665001), according to manufacturer´s instructions.

RNA-seq sample preparation and sequencing. RNA libraries were prepared for sequencing using Lexogen QuantSeq 3'mRNA-Seq Library Prep Kit FWD for Illumina, using standard protocols. Briefly, 500 ng of total RNA were primed with the oligo dT primer containing Illumina-compatible linker sequences. After first strand synthesis, the RNA was removed and the second strand synthesized with Illumina-compatible random primers. After magnetic bead-based purification, the libraries were PCR amplified introducing the sequences required for cluster generation. Sequencing was performed using HiSeq (50 cycles protocol) or NextSeq (75 cycles protocol) platforms. Sequencer Software HiSeq Control Software 2.2.58 was used for base calling of samples processed on Illumina HiSeq 2000. Base calling of samples processed in NextSeq Sequencer was performed with the Real-Time Analysis (RTA) v2.

RNA-seq Data Analysis. Sample read quality, reads mapping and counting were performed by a standard protocol from BlueBee Genomics Platform (http://www.bluebee.com/).

Differential Gene Expression Analysis. The DESeq2 (version 1.16.1) package of R was used to perform RNA-Seq read counts matrix data normalization and differentially expressed genes (DEG) analysis. Information about DESeq2 package is available online at https://bioconductor.org/packages/release/bioc/html/DESeq2.html.

Gene Ontology analysis and data representation. Gene ontology (GO) terms were identified using the PANTHER (protein annotation through evolutionary relationship) classification system (version 13.1) (Mi et al., 2013). GO terms were identified by analyzing differentially expressed genes using the following settings: GO Biological Process, test type FISHER, reference list Homo Sapiens and FDR<0.05. Heat maps and PCA using a selection of enriched genes were generated in the web tool ClustVis (Metsalu and Vilo, 2015) and in R.

All the supplementary tables (Table Sx) referred throughout the Results section are available on-line at https://www.nature.com/articles/s41598-019-45047-9

II.3.4 Flow Cytometry Analysis

Sample collection. For flow cytometry analysis, cells were washed with PBS and then incubated with accutase in the case of hiPSC, or singularized with 0.25% trypsin-EDTA, in the case of differentiating hiPSC, at 37ºC for (7-15) min. For enzymatic digestion neutralization, FBS-containing medium was added. After centrifugation and washing the cell pellet, cells were fixed with 2% paraformaldehyde (PFA) reagent for 20 minutes at room temperature (RT) or stored at 4ºC.

hiPSC Staining (Intracellular and Surface markers). For intracellular staining, samples were centrifuged at 1000 rpm for 5 minutes and washed twice with 1% normal goat serum (NGS) solution in PBS. Then, cells were incubated in 1:1 of 3% NGS and 1% saponin (Sigma) in PBS, at RT for 15 min, for cell membrane permeabilization. After washing 3 times with 1% NGS, primary antibody was diluted in 3% NGS, and cells incubated at RT for 90 min. After incubation, cells were then washed with 1% NGS, and after centrifugation, cell pellet was resuspended and incubated with secondary antibody diluted in 1% NGS, at RT for 45 min in the dark. Cells were washed twice with 1% NGS, centrifuged and resuspended in PBS for a final volume of 300 µL/FACS tube. For staining cell surface markers, cells were washed twice with PBS and re-suspended in primary antibody (Table II-1) diluted in FACS buffer, at approximately 500,000 cells per condition, and incubated for 30 min at RT. Afterwards, cells were washed with PBS and re-suspended in secondary antibody diluted in FACS buffer for another 15 min, at RT in the dark. In the case of conjugated antibodies, a single incubation period of 20 minutes at RT in the dark was performed. Finally, cells were washed twice with PBS for a final volume of 300 µL/FACS tube.

hiPSC-derived cells. Samples previously stored in 2% PFA were centrifuged at 1000 rpm for 3 minutes and then incubated with 90% (v/v) cold methanol at 4ºC for 15 min. Cells were then washed 3 times with flow cytometry buffer 1 (FB1), constituted by 0.5% bovine serum albumin (BSA) solution in PBS. Cell pellet was resuspended and incubated with the primary antibody diluted in FB2, constituted by 0.1% Triton X-100 in FB1, at room temperature for 1 h. After incubation, cells were washed with FB2 and cell pellet was resuspended and incubated in the secondary antibody diluted

in FB2, at room temperature for 30 min in the dark. Cells were washed twice with FB2. Cell pellet was resuspended in FB1 for a final volume of 300 µL/FACS tube.

Data acquisition and analysis. Flow cytometry was performed using a FACSCalibur™ flow cytometer (by Becton Dickinson) and data analysis was performed using the Flowing Software 2.0.

II.3.5 Immunostaining Analysis

Sample preparation. In the case of immunostaining for replated cells, 3D aggregates or 2D monolayer cultures were singularized with 0.25% trypsin-EDTA at 37ºC for (7-15) min. For enzymatic digestion neutralization, FBS-containing medium was added. After centrifugation and washing the cell pellet, cells were resuspended in RPMI+B27 with ROCK inhibitor (10µM) and replated on Matrigel-coated coverslips. Replated samples or 3D aggregates were fixed in 4% PFA at 4ºC for 30 min. After PFA removal, cells were stored in PBS at 4ºC for further analysis. 3D aggregates were incubated in 15% (m/v) sucrose in PBS, at 4ºC overnight and afterwards embedded in 7.5%/15% gelatin/sucrose and frozen in isopenthane at -80ºC. Aggregates with twelve-µm sections were cut on a cryostat-microtome (Leica CM3050S, Leica Microsystems), collected on Superfrost™ Microscope Slides (Thermo Scientific) and stored at -20ºC. Sections were de-gelatinized for 45 min in PBS at 37ºC before immunostaining.

Staining. 3D aggregate sections and replated cells in coverslips were incubated in 0.1 M Glycine (Millipore) for 10 min at room temperature to remove PFA residues, permeabilized with 0.1% Triton X-100 (Sigma) at room temperature for 10 min and blocked with 10% fetal goat serum (FGS, Gibco) in TBST (20 mM Tris-HCl pH 8.0, 150 mM NaCl and 0.05% Tween-20, Sigma), at room temperature for 30 min. Cells were then incubated with the primary antibody diluted in blocking solution (Table II-1) at 4ºC overnight. Secondary antibodies were added for 30 min and nuclear counterstaining was performed using 4',6-diamidino-2-phenylindole (DAPI, 1.5µg/mL, Sigma), at room temperature for 5 min. After brief drying, sections were mounted in Mowiol (Sigma).

Image acquisition and analysis Immunofluorescence staining images were acquired with a LSM 710 Confocal Laser Point-Scanning Microscope (by Zeiss) for 3D aggregate sections and for replated cells from 2D cultures. Data analysis was performed using ZEN Imaging Software (by Zeiss) and ImageJ Software.

Table II-1: List of antibodies used in Flow Cytometry and Immunostaining analysis

Antibody	Source	Reference	Isotype	Dilution
CD31	Dako	M0823	Mouse IgG	1:100 (IS) 1:40 (FC)
cTNT	Thermo Fisher	MA5-12960	Mouse IgG	1:200 (IS) 1:800 (FC)
α-SMA	Sigma-Aldrish	161208D	Rabbit IgG	1:200 (IS/FC)

CD90-PE	Biolegend	328110	Mouse IgG	1:6 (FC)
CX43	Sigma-Aldrish	C6219	Rabbit IgG	1:400 (IS)
OCT4	Millipore	288465	Mouse IgG	1:200 (IS/FC)
Calponin	Abcam	ab700	Mouse IgG1	1:200 (FC)
Ki-67	Abcam	ab833	Rabbit IgG	1:50 (IS)
TRA-1-60 - PE	Miltenyi Biotec	130-100-347	Human IgG	1:11 (FC)
SSEA-4 - PE	Miltenyi Biotec	130-098-369	Human IgG	1:11 (FC)

II.3.6 Live/Dead assay

Cells were washed with PBS and then incubated with accutase, in the case of hiPSC, or singularized with 0.25% trypsin-EDTA, in the case of differentiating hiPSC, at 37ºC for (7-15) min. For enzymatic digestion neutralization, FBS-containing medium was added. After centrifugation and washing the cell pellet, cells were incubated with LIVE/DEAD™ Fixable Dead Cell Stain Kit (Invitrogen) for 15 min. After that period, cells were washed with PBS, resuspended in PBS for a final volume of 300 µL/FACS tube and run in flow cytometer for cell viability data acquisition.

II.3.7 Total protein extraction and Immunoblotting

hiPSCs were collected and lysed using ice-cold lysis buffer (10 mM Tris-HCl, pH 7.6, 5 mM MgCl2, 1.5 mM potassium acetate, 1% Nonidet P-40, 2 mM DTT) and 1X Halt Protease and Phosphatase Inhibitor Cocktail (Thermo Fisher Scientific, Inc.) for 30 min at 4 °C. Samples were then sonicated for 30 sec in ultrasound and then centrifuged for 10 min at 10,000g and 4°C, saving the supernatant. Total protein content was measured using the BioRad protein assay kit (Bio-Rad Laboratories, Hercules, CA, USA), according to the manufacturer's specifications. Protein extracts were then denatured with 6x loading buffer. Equivalent amounts of protein (100 µg) were separated in 8% SDS-PAGE gel electrophoresis and then transferred onto a nitrocellulose membrane. The membranes were further blocked with 5% milk in TBS (25 mM Tris-HCl, 150 mM NaCl, pH 7.6), during 1 h at room temperature and further incubated overnight at 4°C, with gentle agitation, with the primary antibody HIF1α (ReD Systems, MAB1536) prepared in 5% milk in 1xTBS. Membranes were incubated with anti-mouse IgG secondary antibody conjugated with horseradish peroxidase (1:5000, Bio-Rad Laboratories) for 2h at RT. Membranes were processed for protein detection using SuperSignal substrate (Pierce, Thermo Fisher Scientific). Finally, the relative intensities of protein bands were analyzed using ImageLab Version 5.1 densitometric analysis program (Bio-Rad Laboratories). In order to normalize the amount of protein per lane, Ponceau staining was used. Protein Ladder, 10 to 250 kDa (catalog number, 26619), was used as protein molecular weight control.

II.3.8 Glucose consumption and Lactate production rate analysis

To determine glucose consumption rate and lactate production rate, mTeSR1 exhausted medium from day 0 hiPSC cultures under 2D and 3D conditions was collected. Glucose and lactate concentrations from cell-free supernatants were analyzed using an YSI 2700 Select™ Biochemistry Analyzer (YSI Incorporated Life Sciences, USA). Fresh mTeSR™1 was used to determine the concentration of glucose initially present in the culture media. The yield of lactate production from glucose consumption was calculated for each day as ΔLac/ΔGlc, where ΔLac is the production of lactate during that day and ΔGlc is the consumption of glucose during the same period.

II.3.9 Quantitative real time (qRT)-PCR

Total RNA from cell samples of sequential stages of CMs differentiation was extracted using High Pure RNA Isolation Kit (Roche) according to manufacturer´s instructions, and converted into cDNA with High Capacity cDNA Reverse Transcription Kit (Thermo Fisher Scientific). PCR reactions were performed with Taqman™ Gene Expression Assays (Thermo Fisher Scientific) or SYBR Green Master Mix (Nzytech) (Table II-2). Reactions were run in triplicate in ViiA7 Real-Time PCR Systems (Applied BioSystems). For each analysed time point, gene expression was normalized against the expression of the housekeeping gene glyceraldehyde-3-phosohate dehydrogenase (*GAPDH*) and results analyzed with QuantStudio™ RT-PCR Software.

Table II-2 List of primers used in qRT-PCR analysis

TAQMAN	
Gene	**Assay ID**
GAPDH	Hs02758991_g1
OCT4	Hs00999634_gH
T	Hs00610080_m1
ISL1	Hs01099687_m1
NKX2-5	Hs00231763_m1
TNNT2	Hs00165960_m1
TNNI3	Hs00165957_m1
SYBERGREEN	
GENE	**PRIMER (5´>3´)**
FOXA2	FW - GGGAGCGGTGAAGATGGA RV - TCATGTTGCTCACGGAGGAGTA

LEFTY1	FW - GAAGTGTTCGAGGGTACCAGG RV - AAAACTGAGCAAGGGCTCTCC
NODAL	FW – CCCAAGCAGTACAACGCCTA RV – TGCATGGTTGGTCGGATGAA
CER1	FW - TTCTCAGGGGGTCATCTTGC RV - ATGAACAGACCCGCATTTCC
JUN	FW - TTCTATGACGATGCCCTCAACGC RV - GCTCTGTTTCAGGATCTTGGGGTTAC
FOS	FW - GCATCTGCAGCGAGCATCTGAGAA RV – AGAGCTGGGTAGGAGCACGGTCACT
PGK1	FW - CAAGAAGTATGCTGAGGCTGTCA RV - CAAATACCCCCACAGGACCAT
BNIP3	FW - CAGGGCTCCTGGGTAGAACT RV - CTCCGTCCAGACTCATGCTG
GDF3	FW - CATGCCGTTGACCCAGAGAT RV - ACCCACACCCACATTCATCG

II.3.10 Patch-clamp recordings

Whole cell patch-clamp recordings were obtained for CMs dissociated from 3D aggregates at day 30 of differentiation using an upright microscope (Zeiss Axioskop 2FS) equipped with differential interference contrast optics using a Zeiss AxioCam MRm camera and a x40 IR-Achroplan objective. Spontaneous AP from CMs dissociated from 3D aggregates were recorded in the current-clamp mode using a Axopatch 200B (Axon Instruments) amplifier. The patch pipette (4- to 7-M resistance) was filled with an internal solution containing (in mM) 125 K-gluconate, 11 KCl, 0.1 CaCl2, 2 MgCl2, 1 EGTA, 10 HEPES, 2 MgATP, 0.3 NaGTP, and 10 phosphocreatine, pH 7.3, adjusted with 1 M NaOH, 280–290 mosM. The bath recording solution consisted of (in mM) 124 NaCl, 3 KCl, 1.25 NaH_2PO_4, 26 $NaHCO_3$, 1 $MgSO_4$, 2 $CaCl_2$, and 10 glucose, gassed with 95% O2-5% CO2, pH 7.4. The recordings were performed at 37 °C and the offset potentials were nulled before gigaseal formation. APs were recorded right after establishing whole-cell configuration. Acquired signals were filtered using an in-built, 2-kHz, 3-pole Bessel filter, and data were digitized at 5 or 10 kHz under control of the pCLAMP 10 (Molecular Devices) software program. AP duration (APD) was analyzed at 50% and 90% repolarization (APD_{50} and APD_{90}, respectively). Parameters from 5 consecutive APs were averaged.

II.4 RESULTS

II.4.1 Forced aggregation of hPSCs on microwells promotes an efficient generation of cardiomyocytes

To develop a platform for 3D cardiac differentiation of hiPSCs, it was used the temporal modulation of the Wnt signaling pathway (Lian et al., 2012c) as the differentiation protocol and a factorial design approach (Barbosa et al., 2012) to optimize the differentiation process. According to this differentiation method, mesoderm induction is performed by activation of canonical Wnt signaling using, among others, the small molecule CHIR that will allow the stabilization and consequent translocation of β-catenin into the nucleus, followed by Wnt signaling inhibition using for example IWP4 or IWP2 small molecules that will block Wnt protein secretion and activity (Chen et al., 2009). In order to generate size-controlled aggregates, forced aggregation of singularized hiPSCs in the commercially available Aggrewell™ 800 plates was performed. Aggregate size was controlled using different cell seeding densities, and hiPSC aggregates were maintained during 48 hours in mTeSR1, before starting the differentiation process (D0) (Figure II-1A and B). For CM differentiation, the period of Wnt signaling activation, using the small molecule CHIR, occurred from D0 to D1 followed by a step of Wnt signaling inhibition between D3 and D5, using the small molecule IWP4.

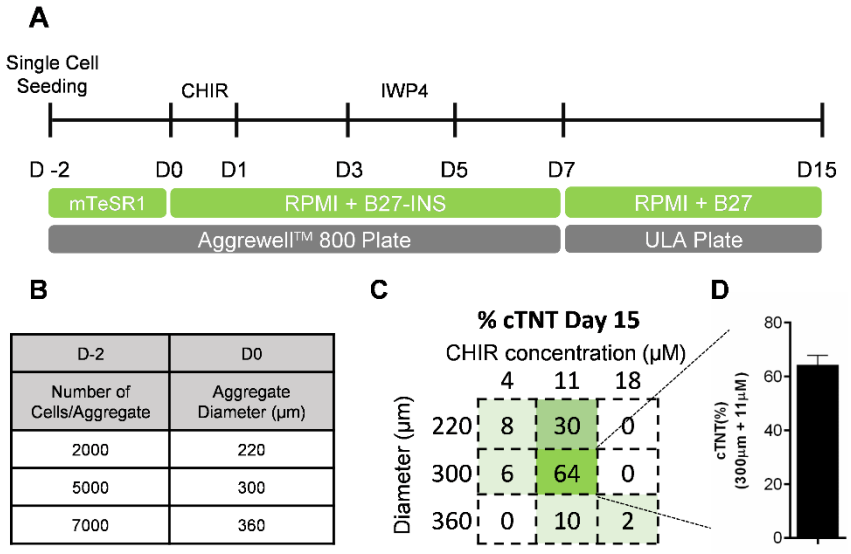

D-2	D0
Number of Cells/Aggregate	Aggregate Diameter (µm)
2000	220
5000	300
7000	360

Figure II-1: Forced aggregation of hiPSCs in a microwell plate promotes an efficient generation of CMs. (A) Schematic representation of CM differentiation protocol from hiPSC in a 3D culture system, using the temporal modulation of Wnt signaling. AggreWell™800 plates were used to obtain size-controlled aggregates. ULA – Ultra Low Attachment plates. (B) Correspondence between cell seeding densities at day -2 (D-2) used in the factorial design and aggregate diameters at day 0 (D0). (C) Percentage of cTNT positive cells after 15 days of differentiation for the experimental runs of the factorial design. CHIR concentration ranges from 4 µM to 18 µM (centered in 11 µM), and aggregate diameter between 220 µm and 360 µm (centered in 300 µm). Each of the tested combinations was performed once, excluding the centered point of the factorial design in which n=4

independent experiments were performed. (D) Percentage of $cTNT^+$ cells at D15 of cardiac differentiation for the centered point of the factorial design (aggregate diameter of 300µm and CHIR concentration of 11 µM). Data are represented as mean ± SEM, n=4 independent experiments.

The cardiac differentiation process was optimized by testing the combined effect of the small molecule CHIR concentration, ranging from 4 µM to 18 µM, and aggregates diameter at day 0, ranging from 220 µm to 360 µm, with the model centred in the culture condition corresponding to 11µM CHIR and 300 µm, respectively. The concentration of the Wnt signaling inhibitor IWP4, used for inhibition of Wnt signaling, was fixed for all the experiments at a concentration of 5 µM. CMs differentiation efficiency was evaluated as the percentage of cells expressing the CM marker cTNT at day 15 of differentiation. The experimental results obtained for the different tested conditions are represented in Figure II-1C. The centered condition (11µM CHIR, 300 µm) was the one that yielded the highest percentage of $cTNT^+$ cells after 15 days of differentiation, resulting in an average of 64 ± 4% $cTNT^+$ cells (Figure II-1D). From the quadratic model generated from the experimental results (Figure II-2A and B), only the quadratic term of CHIR concentration and aggregate diameter had statistical significance (Figure II-2C), which resulted in a maximum value for the considered output of the model ($cTNT^+$ cells at day 15) for a specific aggregate diameter and CHIR concentration. The optimal condition that allowed reaching a percentage of $cTNT^+$ cells between 50-66% was obtained when initiating the integrated process with an aggregate diameter of 289 ± 12 µm and a CHIR concentration of 10.8 ± 0.5 µM, which is in fact close to the centered point used in the factorial design.

The optimized cardiac differentiation platform was validated using the DF6-9-9T.B cell line, the one used for the factorial design optimization process, and two additional hiPSC cell lines, iPSC6.2 and F002.1A.13, proving the reproducibility and robustness of the platform (Figure II-3B). Additionally, a time-course analysis of cardiac differentiation markers until day 20 was performed, confirming the normal progression of cardiac differentiation (Figure II-3A). In addition to the parameters that were optimized through the factorial design, it was verified that by decreasing to 24 hours (D-1) the culture period before initiating the differentiation, the efficiency of CMs differentiation drastically dropped (Figure II-3C), reinforcing the importance of the step of expansion of 3D hiPSC aggregates. It was also confirmed that by extending the optimal aggregate diameter to the range of 280 - 310 µm, the CMs differentiation efficiency was not compromised.

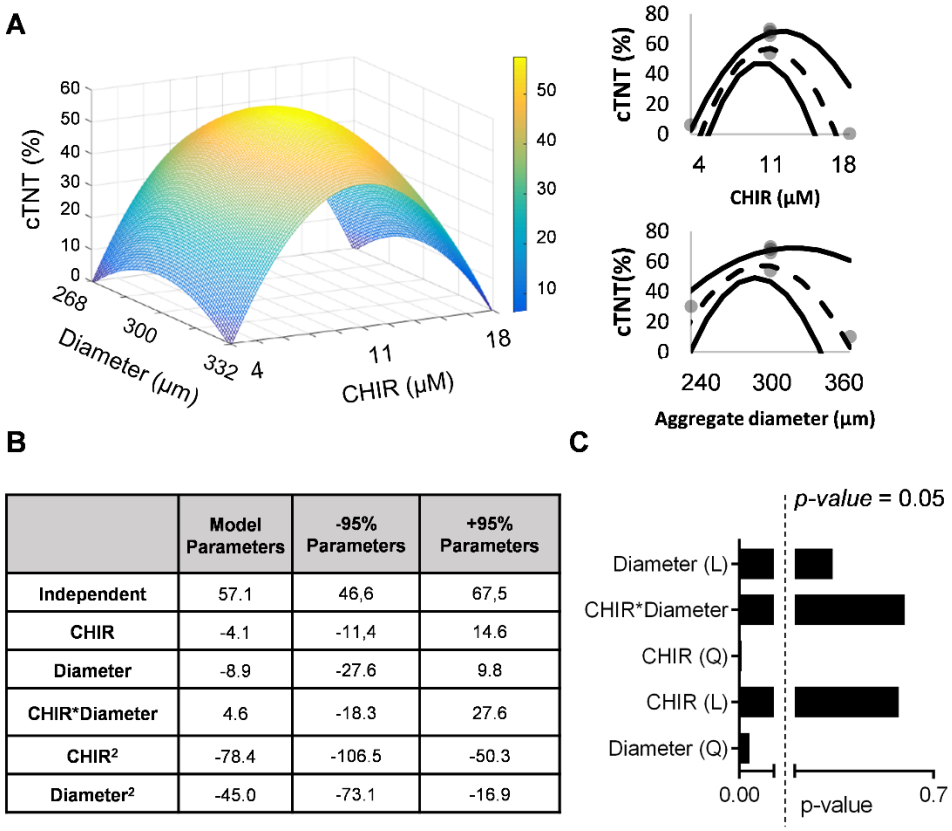

	Model Parameters	-95% Parameters	+95% Parameters
Independent	57.1	46,6	67,5
CHIR	-4.1	-11,4	14.6
Diameter	-8.9	-27.6	9.8
CHIR*Diameter	4.6	-18.3	27.6
CHIR²	-78.4	-106.5	-50.3
Diameter²	-45.0	-73.1	-16.9

Figure II-2: Determination of the optimal initial aggregate diameter and small molecule CHIR concentration that maximizes CM differentiation efficiency. (A) 3D representation of the quadratic model relating initial aggregate diameter and small molecule CHIR concentration with the percentage of cTNT$^+$ CMs after 15 days of differentiation. (B) Parameters of the quadratic model generated from the factorial design, which correlate the percentage of cTNT positive cells after 15 days of differentiation with CHIR concentration and aggregate diameter at D0. R^2=0.84. (C) Evaluation of the statistically significant contribution of each factor of the quadratic model. Only the quadratic terms of CHIR and aggregate diameter were statistically significant (p-values<0.05).

Also, although not directly optimized in this work, the cell density (cells/mL), and consequently the volume of culture medium used per well, mainly in the first steps of differentiation, can impact the concentration of important soluble factors in our platform (Kempf et al., 2016a). In fact, since only the Wnt signaling pathway is being directly manipulated, the combination of this extrinsic manipulation with the endogenous activity of TGF-β/Nodal/Activin and BMP ligands is crucial for determining the outcome of the differentiation process (Kempf et al., 2016b)(Kattman et al., 2011c; Lian et al., 2012c; Rao et al., 2016), and should be taken into consideration.

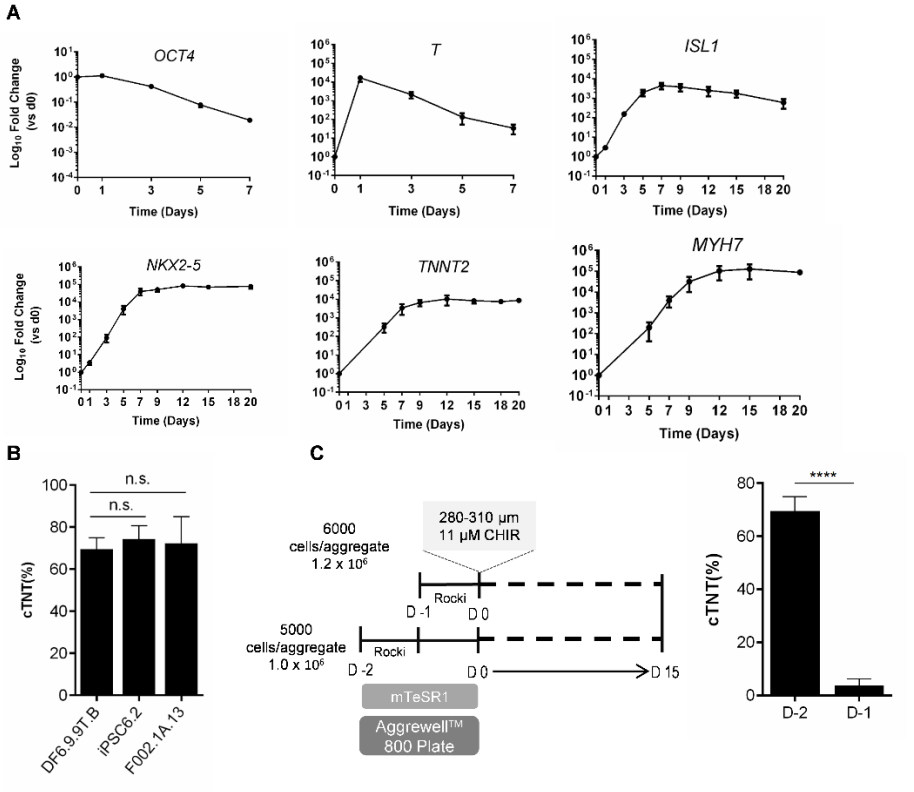

Figure II-3: Gene expression analysis and validation of the developed 3D CM differentiation platform. (A) Expression profile of key genes during the time-course of 3D cardiac differentiation at the indicated time points, between day 0 and day 20, for a selected set of genes: pluripotency (*OCT4*), primitive streak (*T*), cardiac mesoderm (*ISL1* and *NKX2-5*) and cardiomyocyte (*TNNT2* and *MYH7*) markers. Values are normalized to *GAPDH* and relative to D0. Data are represented as mean ± SEM, n=4 independent experiments. (B) Validation of the optimal conditions (aggregate size: 290 µM; CHIR concentration: 11uM) with the DF6.9.9T.B cell line and two other hiPSC cell lines (F002.1A.13 and iPSC6.2). Data are represented as mean ± SEM, n=3 independent experiments for F002.1A.13 and iPSC6.2 lines and n=6 independent experiments for DF6.9.9T.B cell line. n.s. – no statistically significant (p-value > 0.05). (C) Percentage of cTNT^{+} cells after 15 days of differentiation for both culture conditions for 1 day (D-1) and 2 days (D-2) of pre-differentiation period. Data are represented as mean ± SEM, n=6 independent experiments in the D-2 condition and n=3 independent experiments in the D-1 condition.

II.4.2 3D culture of hiPSCs under pluripotency maintenance medium primes hiPSC towards mesendoderm lineage

In order to reveal the main impact of 3D culture towards cardiac differentiation, a transcriptomic analysis of sequential stages of the 3D differentiation protocol was performed (Table S1), using 2D cardiac differentiation, based also on the temporal modulation of the Wnt signaling, as control (Dias et al., 2018; Lian et al., 2012b).

The first stage of hiPSC culture before cardiac induction involves a short period of hiPSCs expansion for both 2D and 3D culture conditions (Figure II-4A), which from now on will be designated as the pre-differentiation period. At D0 of the 2D platform, cells are 90-95% confluent while in the 3D culture, aggregates have ± 300 µm of diameter, as previously optimized. As confirmed by principal component analysis (PCA) (Figure II-4B), gene expression of D0 hiPSC population for both 2D ("2D-D0") and 3D ("3D-D0") differentiation culture formats, showed considerable differences when compared with the "hiPSC seeding" population (initial hiPSCs seeded in 2D and 3D platforms), mainly discriminated by PC2 (16% of total variance), which is presumably related with the degree of cell confluence and/or cell to cell communication. Differences at the gene expression level between "3D-D0" and "2D-D0" are also evident, and were mainly discriminated by PC1 (58% of total variance), which explains the majority of the observed differences in the analyzed dataset and seems to be linked with the culture format (2D versus 3D) (Figure II-4B and C).

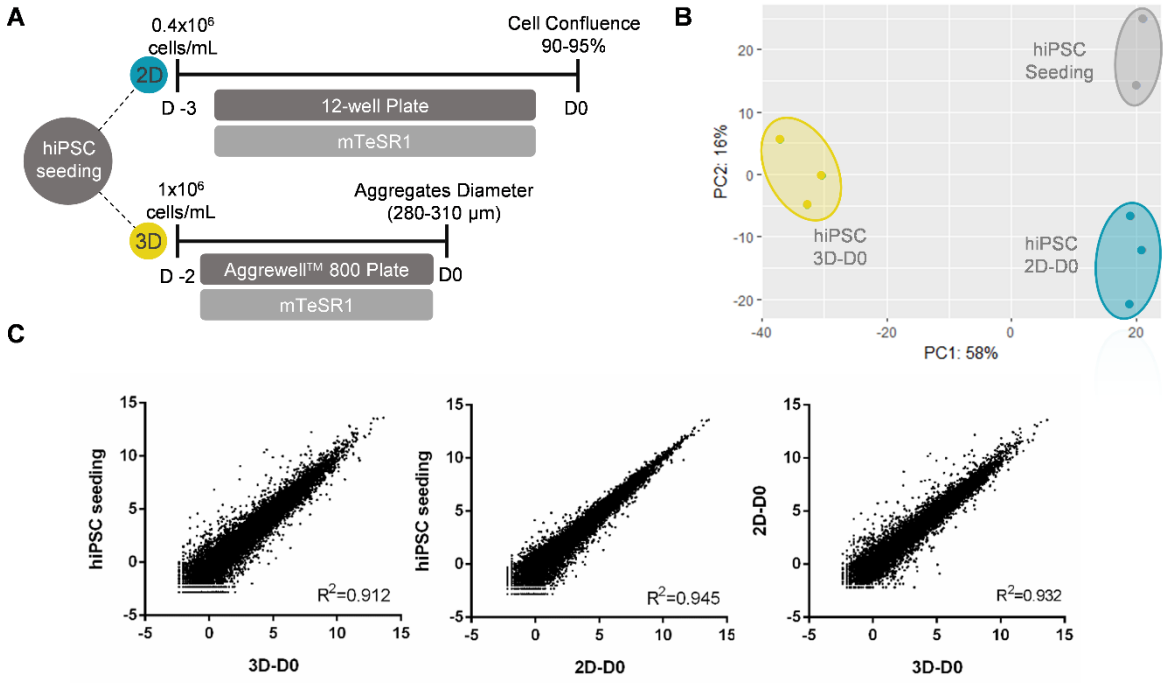

Figure II-4: Characterization of the hPSC cardiac pre-differentiation period. (A) Schematic representation of hPSC culture, before cardiac differentiation, in both 2D and 3D culture strategies. In 2D monolayer, hiPSC were seeded at a density of $0.4x10^6$ cells/mL, reaching 90-95% confluence after 3 days of culture. In the 3D culture platform, hiPSC were seeded at a density of $1x10^6$ cells/mL, reaching at D0 of differentiation a diameter ranging from 280-310 µm. (B) PCA based on whole RNA-seq data from three different conditions: hiPSCs used for seeding (hiPSC seeding, common for both culture strategies) (n=2, independent experiments), 3D day 0 (3D-D0) and 2D day 0 (2D-D0) (n=3, independent experiments). (C) Correlation coefficients for 2D-D0 vs hiPSC seeding, 3D-D0 vs hiPSC seeding and 3D-D0 vs 2D-D0 show that gene expression for D0 of both culture strategies is significantly correlated with hiPSC seeding population, as expected. However, in the 3D system there are already some genes that appear far from the linear correlation. Values used for the graph are Log_2 (CPM) for all RNA-seq data.

To understand those differences, a comparative analysis between “3D-D0” and “hiPSC seeding” expression profile was performed (Table S2 “DE gene list”). Gene ontology (GO) analysis using the upregulated genes shows that the most enriched biological process in the 3D culture format was related with response to hypoxia (Figure II-5A and Table S2 “GO - 3D D0 vs hiPSC seeding - up”). Since 3D hiPSC aggregates had already ±300 µm of diameter at D0, it is not surprising the activation of genes involved in hypoxic response as a result of oxygen diffusion limitations throughout the entire aggregate (Gatenby and Gillies, 2004). To demonstrate the existence of an hypoxic environment inside the 3D aggregates, the expression level of the HIF1α protein, which is the master transcriptional regulator of hypoxic response (Keith and Simon, 2007), was quantified in both “2D-D0” and “3D-D0” cell populations. The results revealed a significant increase in HIF1α protein expression levels in 3D aggregates as compared to the 2D monolayer (Figure II-5B). Since gradients of oxygen and nutrients inside the 3D aggregates could potentially compromise cell viability, we quantified the percentage of viable cells in 3D-D0 aggregates and compared with the “2D-D0” population, confirming that the viability of the cells was not affected by 3D culture (Figure II-5C).

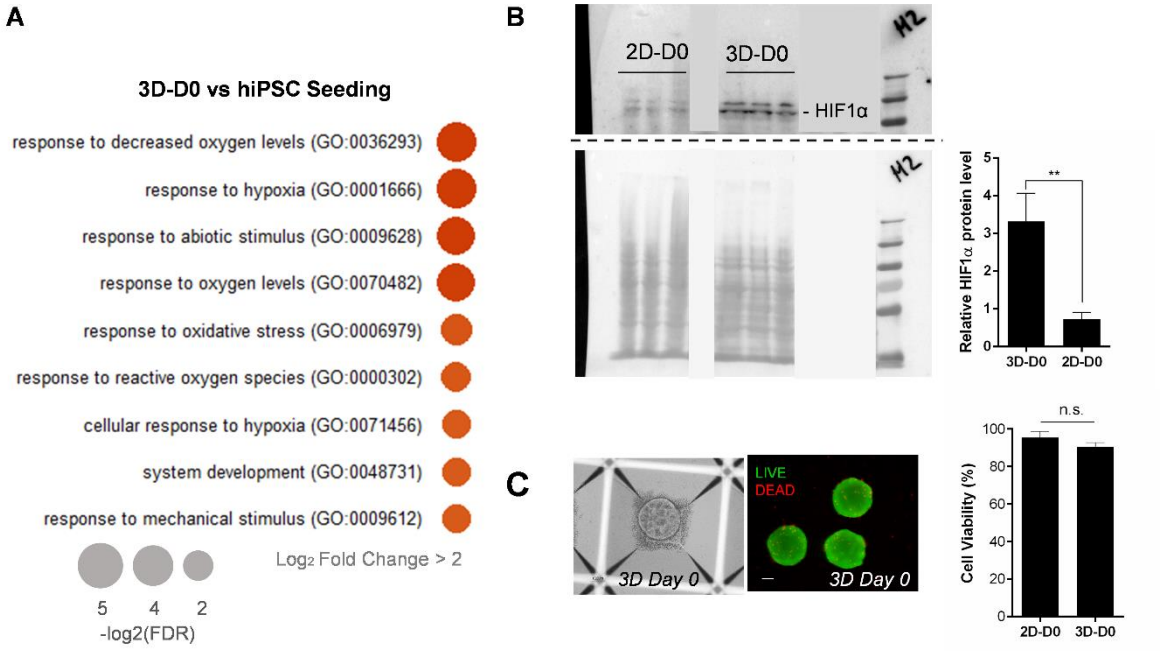

Figure II-5: Effect of hypoxia on 3D cultured hPSCs. (A) Top gene ontology (GO) terms for biological processes identified (FDR < 0.05) of differentially upregulated genes (Log_2 FC > 2 and adjusted *p-value* < 0.05) for 3D-D0 versus hiPSC seeding. (B) Western blot (left) and quantification (right) of HIF1α protein expression in 2D-D0 and 3D-D0 conditions. Data are represented as mean ± SEM, n=3 independent experiments. (C) Bright field and live/dead staining of aggregates at D0 of differentiation, showing high cell viability and no evidences of necrotic areas. Scale bar, 100 µm (left). Flow Cytometry analysis of viable cells at D0 of differentiation in both 2D and 3D culture conditions, proving that 3D culture does not compromise cell viability (right). Data are represented as mean ± SEM, n=3 independent experiments.

To highlight the genes that were upregulated in the “3D-D0” cell population vs the “hiPSCs seeding” population, a volcano plot was generated (Figure II-6D). Among the upregulated genes, *PGK1*, *LDHA*, *BNIP3* and *JUN* stood out, within the group of genes that show a higher and more significant upregulation. The higher expression level of those genes in 3D-D0 aggregates, when compared not only to “hiPSC seeding” cells but also to 2D-D0 monolayer cells, was confirmed by qRT-PCR, (Figure II-6E). In agreement with the hypothesis of an hypoxic response inside the 3D aggregates, the aforementioned genes are known direct or indirect targets of HIF1α activation network. Specifically, *PGK1* and *LDHA* are genes involved in glycolysis, which suggests that in the 3D environment the rate of glycolysis is higher compared with both “2D-D0” and “hiPSCs seeding” conditions. GO analysis of the downregulated genes in “3D-D0” and “2D-D0” environments compared to “hiPSCs seeding” population, revealed that some of the downregulated genes in the 3D-D0 population are related with the oxidative phosphorylation and mitochondrial respiratory chain (Figure II-6F and G), reinforcing the proposal of a higher rate of glycolysis in 3D-D0 aggregates. Finally, glucose consumption and lactate production rates were analyzed in both “2D-D0” and “3D-D0” conditions. The results revealed an equivalent specific glucose consumption rate in 2D-D0 and 3D-D0 conditions, however a statistically significant higher specific lactate production rate in hiPSCs present in the 3D-D0 aggregates was observed when compared with the cells in 2D monolayer. This results on a higher yield of lactate production/glucose consumption which is indicative of a higher level of glycolysis in 3D-D0 aggregates (Figure II-6H). In fact, hypoxia is a known trigger of metabolic changes in hPSCs and it is also described to be involved in pluripotency maintenance by promoting glycolysis and preventing mitochondrial respiration (Arthur et al., 2019; Varum et al., 2010).

The activation of MAPK/JNK/ERK signaling is also evident in “3D-D0” aggregates when compared with “hiPSC seeding” and “2D-D0”, with the upregulation of *JUN, FOSB, FOS and EGR1* gene expression. The possible activation of this pathway, which is involved in the transcription of a wide range of cell proliferation and apoptotic genes (Dhanasekaran and Reddy, 2008), can be also a consequence of reduced oxygen levels, specifically due to an increased concentration of ROS inside the cells (Moriyama et al., 2017). Additionally, JNK/ERK signaling pathway can be indirectly activated as a result of the increased cytosolic concentration of Ca^{2+} triggered by ROS (Desireddi et al., 2010), since Ca^{2+} has been described to be involved in MAPK JNK/ERK signaling activation (Chiquet and Flück, 2001). In fact, the calcium voltage channel Cav1.2 encoded by *CACNA1C*, is upregulated in 3D-D0 aggregates, as well as *CXCR4,* which is described to be involved in the regulation of Ca^{2+} mobilization and activation of MAPK signaling (Döring et al., 2014). MAPK/JNK pathway had been reported to be involved in the maintenance of stemness of hPSCs but activation of this pathway has also been reported to be linked with the initiation of hPSCs differentiation (Kensah et al., 2018).

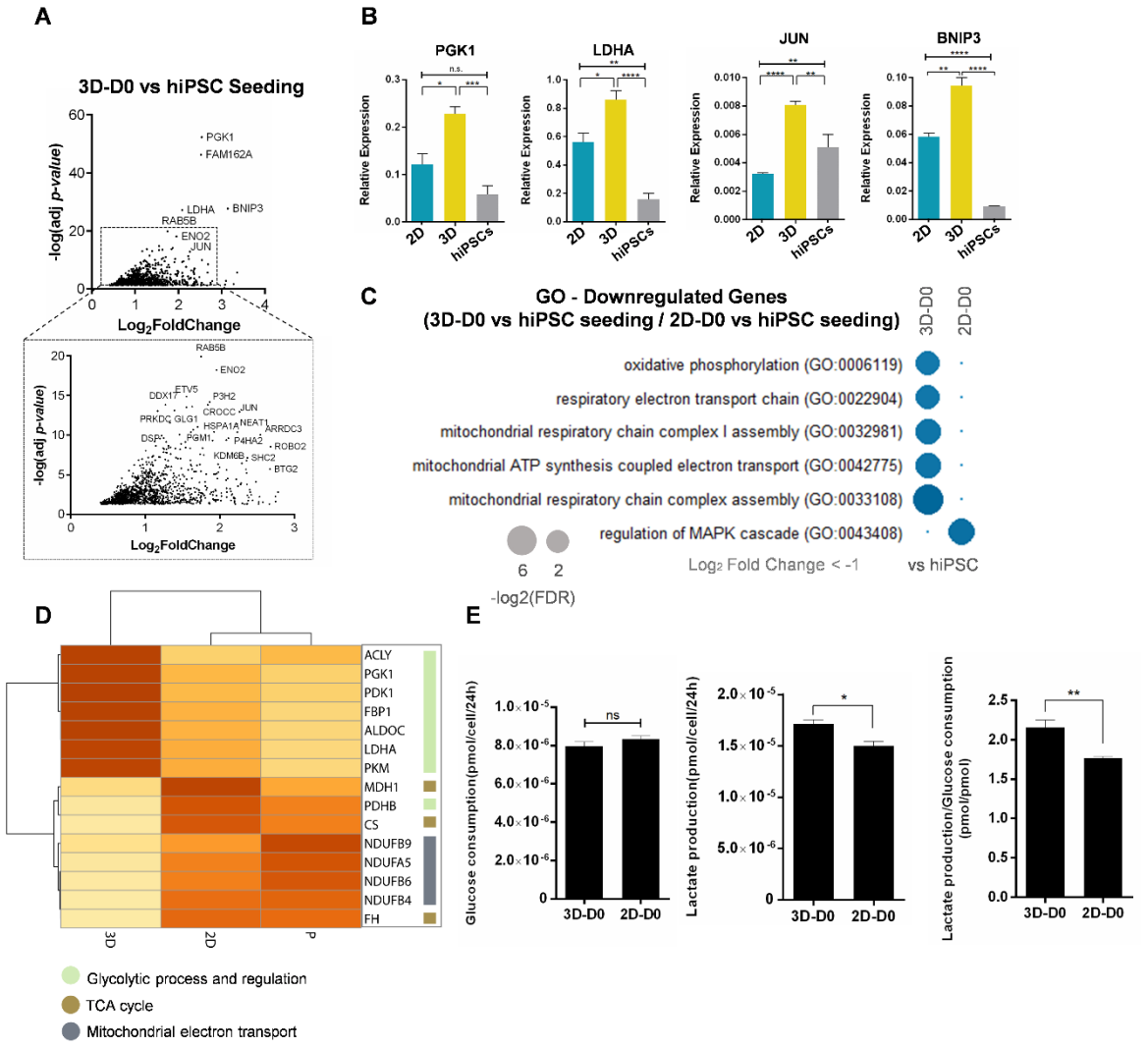

Figure II-6 Effect of 3D culture on hPSCs pluripotency stage. (A) Volcano Plot highlighting the most significant upregulated genes for 3D-D0 versus hiPSC seeding populations (Log_2FoldChange > 1 and Adjusted *p-value* > 0.05). (B) Expression profile of *PGK1, LDHA, BNIP3* and *JUN* genes for the three different populations: 3D-D0, 2D-D0 and hiPSCs seeding. Values are normalized to *GAPDH*. Data are represented as mean ± SEM, of at least n=3 independent experiments. Student´s t-test (two-tailed) statistics, * p<0.05, ** p<0.005, *** p<0.0005. (C) Gene ontology (GO) biological processes terms related with oxidative phosphorylation and mitochondrial respiratory chain identified (FDR < 0.05) for the differentially downregulated genes (Log2 FC < -1 and adjusted p-value < 0.05) of 3D-D0 versus hiPSC seeding and 2D-D0 versus hiPSC seeding. (D) Heat map highlighting differentially expressed genes in 3D-D0 versus hiPSC seeding populations (Log2 FC > 1 and adjusted p-value < 0.05) related with glycolysis metabolism and TCA cycle. Average CPM values of 3 replicates were used for each condition. (E) Glucose consumption rate (pmol/cell/24hours), lactate production rate (pmol/cell/24hours) and yield of lactate produced/glucose consumed, at D0 of differentiation for both 3D aggregates and 2D monolayer. Data are represented as mean ± SEM, n=3 independent experiments. Student´s t-test (two-tailed) statistics, * p<0.05, ** p<0.005, n.s., no statistically significant (p-value > 0.05).

Additionally, a differential gene expression analysis between “3D-D0” and “2D-D0” was performed (Table S2 “DE gene list”). From the GO analysis focused on the most significantly upregulated genes, the main differences were related with regulation of Nodal signaling, SMAD protein signal transduction and the induction of PS (Figure II-7A and Table S2 “GO - 3D-D0 vs 2D-D0 - up”). Within the upregulated genes, ligands of Nodal signaling, including *NODAL* and *GDF3*, as well as their direct targets, *LEFTY1*, *LEFTY2* and *CER1,* that act in a negative feedback loop (Schier, 2009), stood out (Figure II-7B). The upregulation of some of these genes, namely *GDF3*, *CER1*, *LEFTY1* and *NODAL*, was confirmed by qRT-PCR, corroborating the RNA-seq data (Figure II-7C). Interestingly, Nodal signaling is not upregulated in “3D-D0” vs “hiPSC seeding” and instead it is down-regulated in “2D-D0” vs “hiPSCs seeding”, meaning that 3D culture of hiPSC potentially induced the stabilization of Nodal signal.

Although Activin/Nodal signaling is described to be involved in pluripotency maintenance of hPSCs, it is also described to be responsible for driving early cell fate decisions along the mesendodermal lineages (Schier, 2009). The upregulation of *FOXA2* in “3D-D0” aggregates compared with “2D-D0” (Figure II-7C), which is also expressed in early/anterior PS (Pei et al., 2010), combined with TGF-β/Nodal signaling activity, strengthens the hypothesis of hiPSC priming to mesendoderm lineages in 3D conditions.

In summary, our results suggest that culture of hiPSCs as 3D aggregates, in a forced aggregation platform, results in oxygen gradients inside the aggregates, which are responsible for (1) stabilization of TGF-β/ Nodal pathway, (2) upregulation of MAPK/ JNK/ ERK pathway and (3) increase in glycolysis metabolism, culminating in a balance between pluripotency maintenance and hiPSCs priming towards differentiation, particularly into the mesendoderm lineage (Figure II-7D).

II.4.3 3D cardiac differentiation allows a faster structural and functional maturation of hiPSC-CMs when compared with 2D culture

To understand the impact of 3D culture during the progress of cardiac differentiation, it was analyzed the differentially expressed genes in 3D aggregates throughout the differentiation process, when compared with the 2D monolayer differentiation. Using a set of known genes involved in cardiogenesis and cardiomyocyte maturation, a PCA analysis (Table S3 “PCA 3D and 2D (D0-D20)”) was performed, which highlighted differences regarding the progression of cardiac differentiation when comparing both culture systems (Figure II-8A).

During the first 7 days of cardiac differentiation, 3D aggregates remain inside the microwell platform, which seems to be responsible for a prolonged oxidative stress and activation of hypoxic response. In fact, the transcriptional activation of metallothionein protein-coding genes during the first days of 3D cardiac differentiation, including *MT1G*, *MT1H*, *MT1E*, *MT2A*, *MT1F*, *MT1X*, which prevent cells from apoptosis (Ruttkay-Nedecky et al., 2013), reinforce the hypothesis of an oxidative stress response.

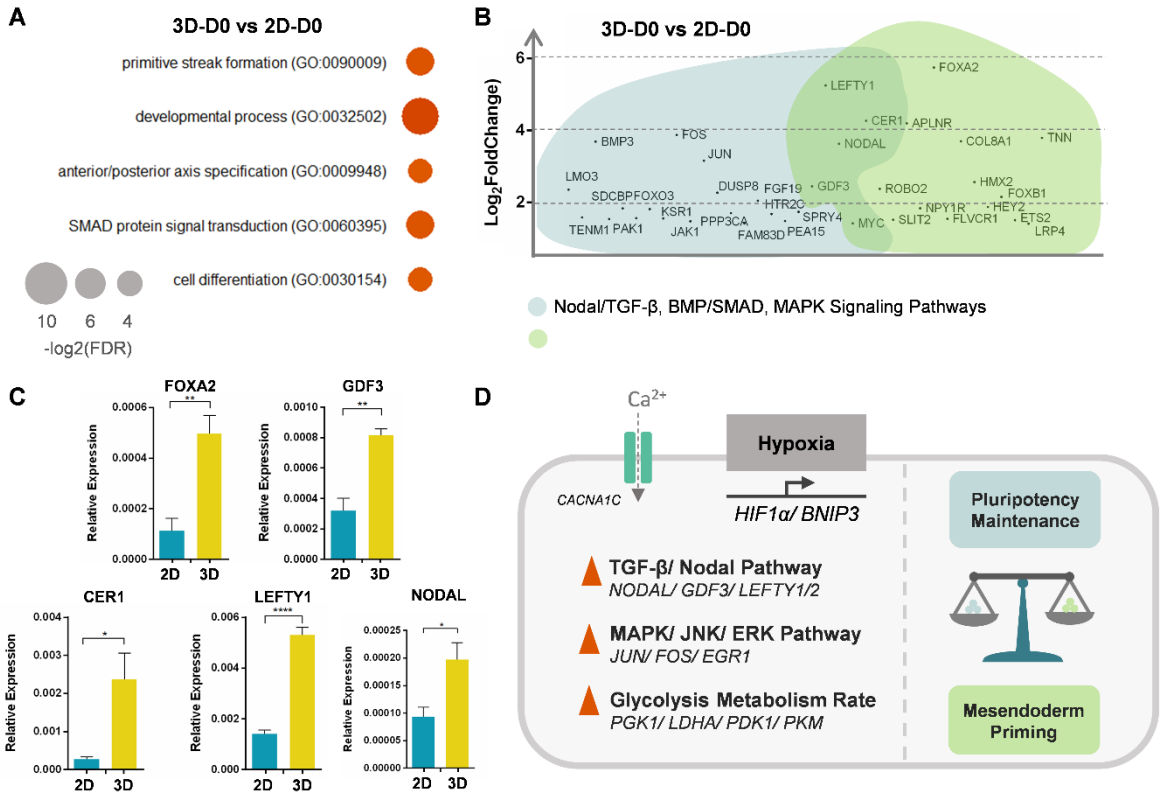

Figure II-7: Side by side comparison between 2D-D0 and 3D-D0 cell populations. (A) Top gene ontology (GO) biological processes terms identified (FDR < 0.05) for the differentially upregulated genes (Log2 FC > 2 and adjusted p-value < 0.05) of 3D-D0 versus 2D-D0. (B) Graphical representation highlighting a set of the upregulated genes in 3D-D0 versus 2D-D0 comparison, related with the enriched biological processes "Embryonic development / Primitive streak formation / Heart development" and "Nodal/TGF-β, BMP/SMAD and MAPK Signaling Pathways", which stands out from the GO analysis (Log_2FoldChange > 1 and adjusted p-value > 0.05). (C) Expression profile of *FOXA2, GDF3, CER1, NODAL* and *LEFTY1* genes in 3D-D0 and 2D-D0 populations. Values are normalized to *GAPDH*. Data are represented as mean ± SEM, of at least n=3 independent experiments. Student´s t-test (two-tailed) statistics, * p<0.05, ** p<0.005, *** p<0.0005. (D) Schematic representation of the proposed signaling network involved in hiPSCs culture as 3D aggregates in a forced aggregation platform. Oxygen gradients inside the spheroids trigger a hypoxic stimuli which is responsible for (1) stabilization of TGF-β/ Nodal pathway, (2) upregulation of MAPK/ JNK/ ERK pathway and (3) increase in glycolysis metabolism, culminating in a balance between pluripotency maintenance and hiPSCs priming towards differentiation, particularly into mesendoderm lineage.

At day 1 of differentiation, a GO analysis was performed focusing on the most significantly upregulated genes in 3D-D1 aggregates and 2D-D1 monolayer when compared to "3D-D0" and "2D-D0" populations, respectively (Figure II-8B). This analysis revealed that the most upregulated genes in "3D-D1" were statistically more related with "tissue development process" and "cardiac tissue specification" biological processes, and in "2D-D1" they were more related with "gastrulation", "primitive streak formation" and "anterior/posterior pattern specification" biological processes. This

corroborates the idea that 3D aggregates at day 0 of differentiation are more primed for mesendoderm differentiation and, consequently, cardiac differentiation progresses faster. Focusing our analysis only on transcription factors (TFs), RNA-seq data indicates that TFs known to be related with cardiac differentiation, such as *MESP1*, *GATA4*, *TBX3*, *MSX2*, were already upregulated at D1 of differentiation in 3D aggregates (Figure II-8C). Additionally, a higher expression of the gene *T,* which is one of the most important genes involved in mesendoderm specification, in 3D-D1 aggregates when compared with 2D-D1 monolayer, was further confirmed by qRT-PCR analysis (Figure II-8D). Also, the Wnt/β-catenin target genes, *AXIN2* and *DKK1,* were statistically significantly upregulated in the 3D aggregates when compared with 2D monolayer, at day 1 of differentiation, suggesting a higher degree of canonical Wnt signaling activation (Table S3 “DE gene list”).

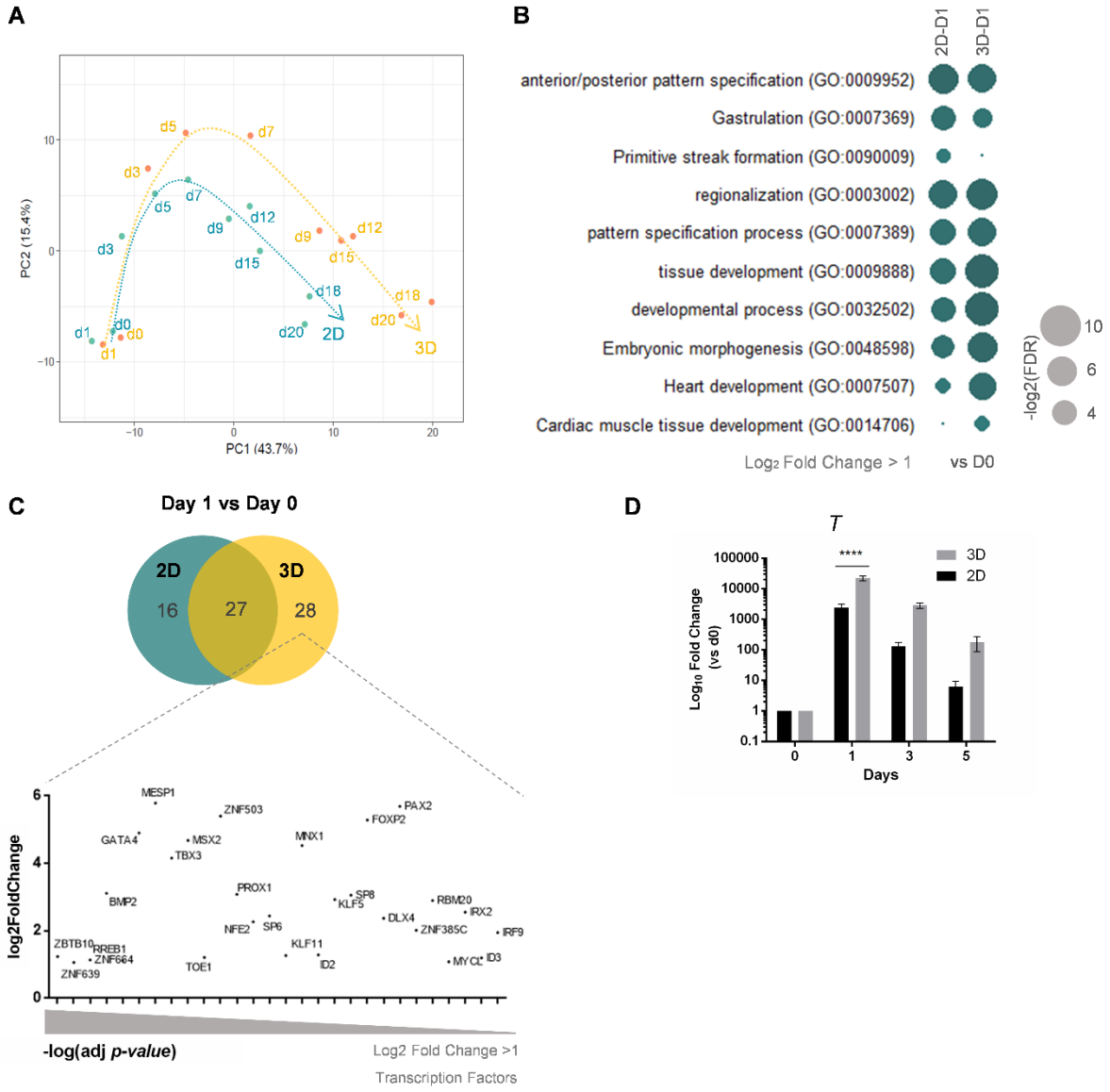

Figure II-8: Impact of 3D culture during the first days of hPSCs CM differentiation, compared with 2D monolayer differentiation. (A) PCA of RNA-seq data in counts per million (CPM) using a subset of 254 genes linked to cardiac differentiation progression, CM functional and structural maturation, CM metabolism, Wnt, TGF-β and FGF signaling pathways and other cardiac cells. Orange and blue arrows describe the pathway followed by 3D and 2D cardiac differentiation, respectively, until day 20 of differentiation. (B) Top gene ontology (GO) terms for biological processes identified (FDR < 0.05) of differentially upregulated genes (Log_2 FC > 1 and adjusted *p-value* < 0.05) for 3D-D1 versus hiPSC seeding, and 2D-D1 versus hiPSC seeding. (**C**) Venn diagram representing the number of transcription factors upregulated (Log2 FC > 1 and adjusted p-value < 0.05) in 3D-D1 and 2D-D1 versus 3D-D0 and 2D-D0, respectively, highlighting the ones that are only upregulated in 3D-D1 (bottom). (**D**) qRT-PCR analysis of the first 5 days of cardiac differentiation in both 3D and 2D, for mesendoderm gene T, highlighting the statistically significant higher expression of T after CHIR induction (day 1) in 3D aggregates compared with 2D monolayer. Values are normalized to GAPDH and relative to D0. Data are

represented as mean ± SEM, n=4 independent experiments. Student´s t-test (two-tailed) statistics, **** p<0.00005.

Moving along the cardiac differentiation process, at day 5 of differentiation it was verified that a set of genes related with the cardiac development and sarcomere structure and function were upregulated in the 3D aggregates (Table S3 "DE gene list"), including *MEF2C*, *MYH6*, *ACTC1*, *ATP1A2, CACNA1D, RYR2, TNNT2 and TNNI1* (Figure II-9A).

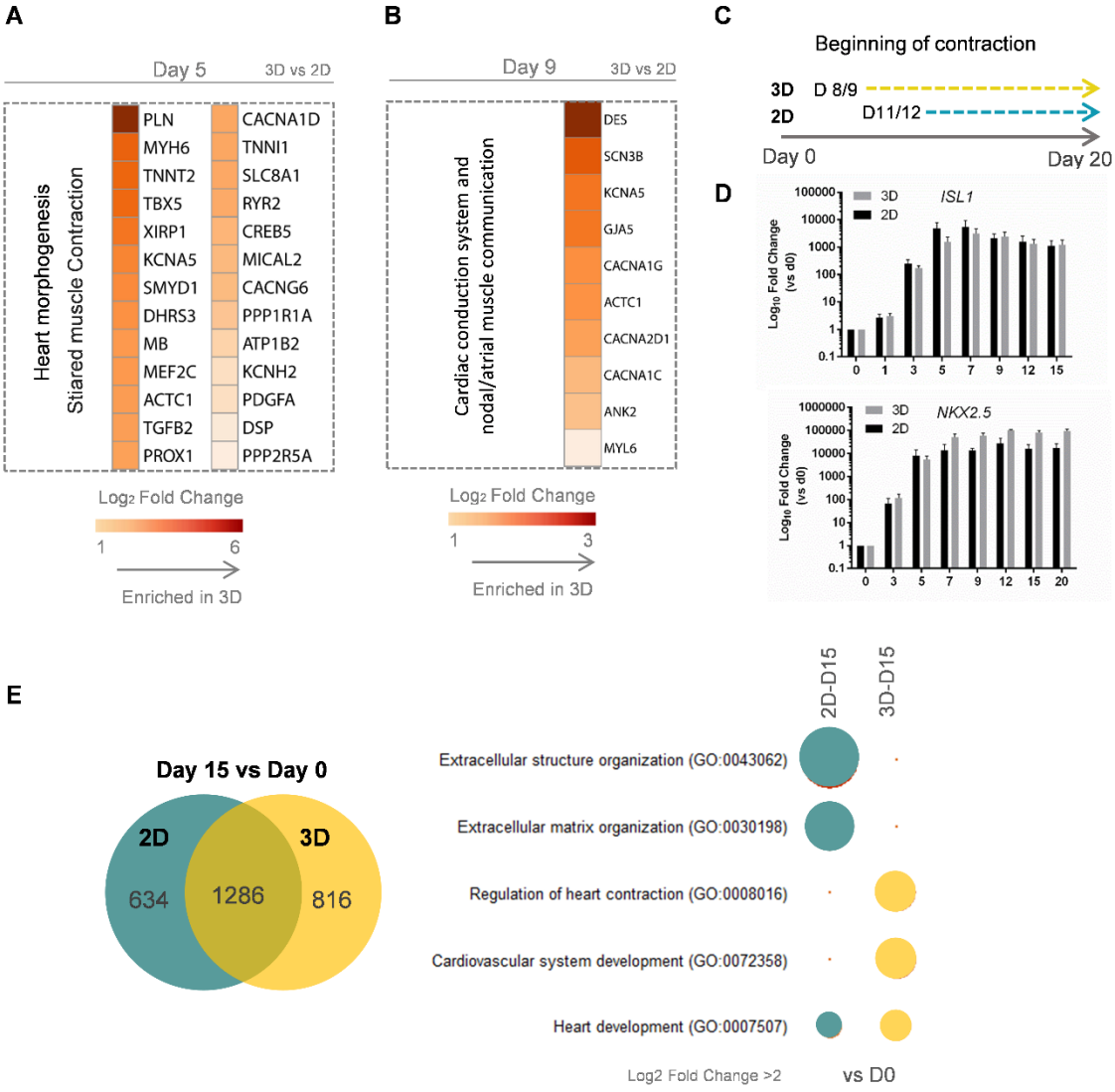

Figure II-9: Impact of 3D culture on later stages of CM differentiation, compared with 2D monolayer differentiation. (A-B) Heat map highlighting the differentially expressed genes (Log_2 FC > 1 and adjusted p-value < 0.05) related with the most significant GO terms for (A) 3D-D5 vs 2D-D5 and (B) 3D-D9 vs 2D-D9. See Table S3 for full DE gene list. (C) Schematic representation highlighting the moment of begging of contraction in both 3D aggregates and 2D monolayer. (D) Expression profile of cardiac progenitor genes *ISL1* and *NKX2-5* throughout the entire process of cardiac differentiation. Values are normalized to *GAPDH* and relative to day 0. Data are represented as mean ± SEM, n=3 independent experiments. (E) Venn diagram (top) representing the

number of genes (Log2 FC > 2 and adjusted p-value < 0.05) in 3D-D15 and 2D-D15 versus 3D-D0 and 2D-D0, respectively, and GO analysis (bottom) with the upregulated genes that are only present in 3D-D15 or 2D-D15.

At day 9 of differentiation, the differential expression analysis between 3D and 2D cardiac differentiation conditions (Table S3 “DE gene list”), revealed an enrichment in 3D aggregates of GO terms related with cardiac conduction system and nodal/atrial muscle communication. Specifically, the protein-coding genes *CACNA1C*, *GJA5*, *CACNA1G, SCN3B, KCNA5* and *ANK2* were upregulated (Figure II-9B). In fact, most of these genes are described to be present in atrial CMs or in the nodal/conduction system myocytes. *GJA5* gene, that encodes for the Cx40 gap junction, and *KCNA5*, that encodes for the ion channel Kv1.5, are described as cell markers for atrial CMs (Cyganek et al., 2018; Lee et al., 2017c), being almost absent in the ventricular working myocardium. Additionally, *GJA5* is largely expressed in the conduction system myocytes, which includes the HIS bundles, the left and right bundle branches (LBB and RBB) and purkinje fibers, enabling a fast conduction of the impulse between the AVN and ventricular working myocytes (van Weerd and Christoffels, 2016). The calcium channel Cav3.1, encoded by *CACNA1G*, is preferentially expressed in nodal/pacemaker myocytes although it is also abundantly expressed in atrial CMs and purkinje cells (Garg et al., 2018; Liu et al., 2016). Interestingly, it is at day 8/9 of differentiation that 3D aggregates start to contract, in contrast with 2D monolayer culture, in which the beginning of contraction only starts at day 11/12 of differentiation (Figure II-9C). Despite this apparent earlier expression of structural and functional CM genes in 3D aggregates, RNA-seq data did not show a delay in the expression of cardiac progenitor markers, namely *ISL1* and *NKX2-5,* in 2D monolayer vs 3D aggregates, a result further confirmed by qRT-PCR analysis (Figure II-9D).

At day 15 of differentiation, from a GO analysis of genes that were only upregulated in 3D aggregates or 2D monolayer, it was possible to observe that, in the case of 3D aggregates, regulation of heart contraction and cardiovascular system development appear as upregulated biological process, whereas in the case of 2D monolayer those terms were not represented and instead terms related with extracellular matrix organization and structure were highlighted (Figure II-9E).

A differential expression analysis comparing both cardiac tissues at day 20 of differentiation (Table S3 “DE gene list”, “GO - 3D-D20 vs 2D-D20 - up”) revealed an upregulation of genes related with endothelial differentiation/endothelium formation, such as *KDR*, *CDH5*, *PECAM1*, *CD34* and *GJA4* (Figure II-10A) in the 3D aggregates. The presence of $CD31^{+}$ endothelial cells in 3D aggregates was further validated by immunostaining of aggregate sections (Figure II-10B). In addition, genes involved in heart contraction, action potential and signal conduction, such as *KCNJ11*, *GJA5*, *CACNA2D2*, *CACNA1G*, *ATP1A2, MYOM1* and *MB*, were also upregulated in the 3D aggregates, suggesting a higher degree of functional maturation. In the 2D monolayer cardiac tissue, different protein-coding genes of ECM were upregulated, including different collagens (*COL1A1, COL4A1, COL5A1, COL9A1*) lumican (*LUM*), laminin (*LAMA5*), fibronectin (*FN1*) and vitronectin (*VTN*). The upregulation of ECM protein-coding genes throughout the process of cardiac differentiation was

already reported for 2D monolayer cardiac differentiation (Wolling et al., 2018), as well as the upregulation in 2D monolayer compared with 3D aggregates (Correia et al., 2018). The increased expression of these genes can be related with a higher content of fibroblast-like cells in the 2D monolayer since they are the main producers of ECM (Fan et al., 2012). In addition to this, in 2D cardiac tissue, expression profiling results suggested also the upregulation of protein-coding genes for skeletal muscle myocytes, namely *TNNT1*, and the upregulation of *ACTN1* and *TAGLN2*, which suggests higher content of smooth muscle cells compared with the 3D cardiac aggregates. In fact, immunostaining of replated 3D aggregates and 2D monolayer suggests a higher prevalence of smooth muscle cells in the 2D culture system (Figure II-10C), which was further confirmed by $CALP^+$ cell quantification (Figure II-12A).

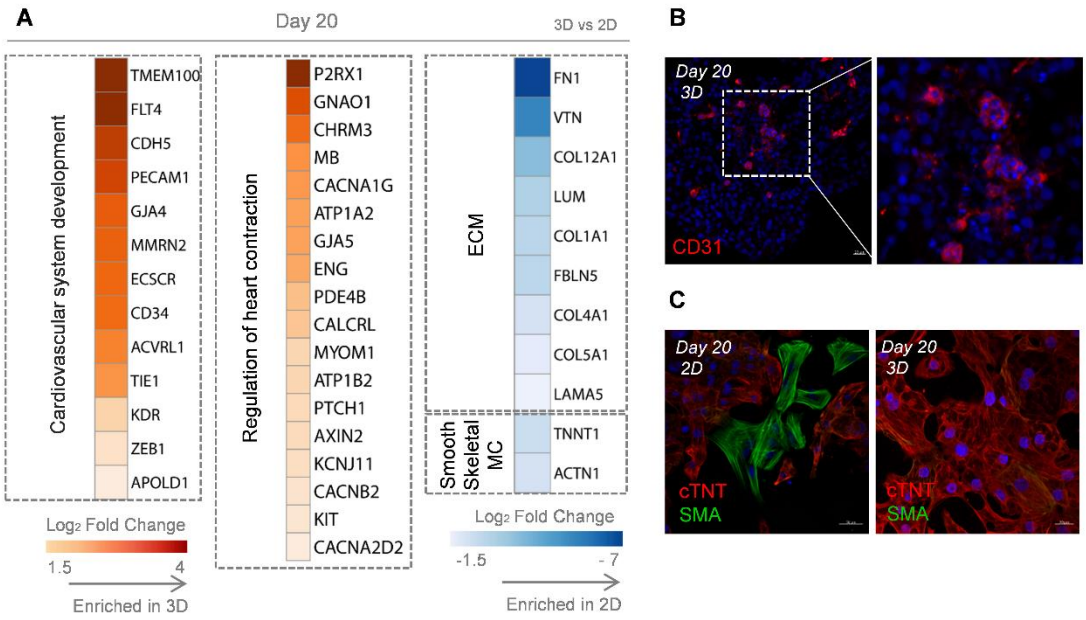

Figure II-10: Characterization of D20 hiPSC-derived cardiac population in both 2D and 3D conditions. (A) Heat map highlighting the differentially expressed genes (Log_2 FC < -1 and Log_2 FC > 1) and adjusted p-value < 0.05) related with the most significant GO terms for 3D-D20 vs 2D-D20 differential expression analysis. See Table S3 for full DE gene list. (B) Representative section of 3D aggregates on day 20 of differentiation, highlighting the presence of $CD31^+$ cells. Scale bars, 20 µm. (C) Replated CMs from dissociated 3D aggregates and 2D cardiac tissue at day 20 of differentiation, highlighting the prevalence of SMA^+ cells in the 2D culture when compared to 3D conditions. Scale bars, 50 µm and 20 µm in 2D and 3D conditions, respectively.

II.4.4 3D cardiac differentiation impacts the cellular composition of cardiac aggregates and the maturity of cardiomyocytes

Taking into consideration the results obtained from the RNA-seq data regarding the transcriptional effect of 3D culture of hiPSC prior to cardiac differentiation, it was tested the effect of increasing the pre-differentiation period from 2 to 3 days, while maintaining the optimized D0

aggregate size (Figure II-11A). This increment resulted in a significant increase of CM differentiation efficiency from ± 70% to > 90% cTNT⁺ (92 ± 1%) cells after 15 days of differentiation (Figure II-11B), without compromising the expression of pluripotency markers OCT4, SSEA4 and TRA-1-60, at D0 (Figure II-11C). Also, increasing the pre-differentiation period improved the reproducibility among biological runs, which is still a common bottleneck in different reported studies of 2D cardiac differentiation, mainly the ones based on the Wnt signaling modulation (Laco et al., 2018).

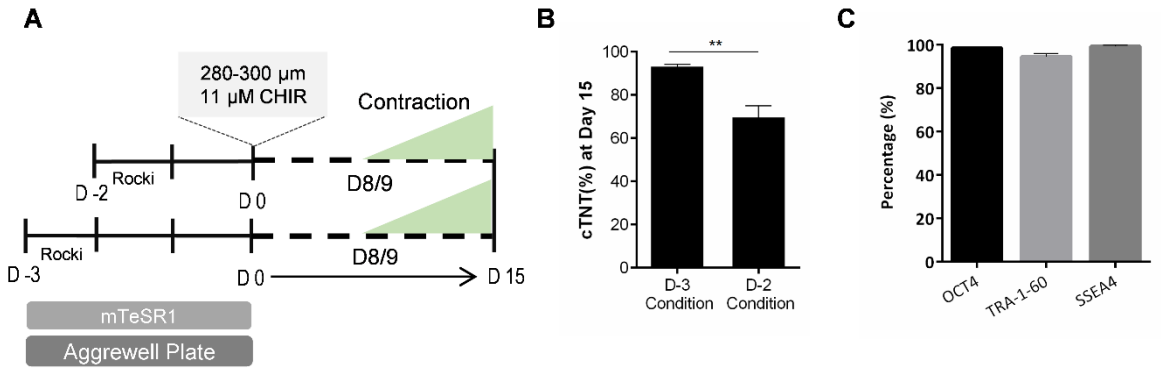

Figure II-11: Optimization of pre-differentiation period improves 3D CM differentiation efficiency. (A) Schematic representation highlighting the optimized 3D cardiac differentiation platform, in which hiPSC aggregates remain for 3 days in pluripotency maintenance medium before starting the differentiation process. The aggregate diameter at D0 was the same obtained with the previous version of the 3D platform (pre-differentiation period of 2 days) since the initial cell seeding density was decreased. (B) Cardiomyocyte differentiation efficiency in terms of cTNT⁺ cells after 15 days of differentiation in both conditions, pre-differentiation period of 2 days (D-2) or 3 days (D-3). Data are represented as mean ± SEM, n=6 independent experiments. (C) Flow cytometry analysis of hiPSCs 3D aggregates at D0 of differentiation, after 3 days in pluripotency maintenance media, for the pluripotent transcription factor OCT4, and surface markers TRA-1-60 and SSEA4. Data are represented as mean ± SEM, n=3 independent experiments.

The 3D cardiac spheroids obtained with this improved 3D cardiac differentiation platform were then further characterized in terms of cell composition and compared to 2D monolayer. In 3D aggregates, apart from CMs, a small population of non-cardimyocyte cells were detected at D15, comprising mainly CD90⁺ stromal cells (3.3 ± 0.1 % CD90⁺ cells) (Figure II-12A). Additionally, immunostaining of different sections of cardiac aggregates shows the presence of different areas staining positively for the endothelial marker CD31 (Figure II-12B), demonstrating the existence of few endothelial cells inside the aggregates. At day 30, 3D aggregates show a decreased percentage of cTNT⁺ cells, which can be attributed to the increased number of proliferative cells, particularly CD90⁺ fibroblast-like cells, which percentage increased to ± 6% at D30 (Figure II-12A). However, it can also be attributed to the observed decrease in total cell number (±20% of cell loss) from D15 to D30 of differentiation, which potentially results from aggregate agglomeration. After 4 weeks in culture, CMs from 3D cardiac aggregates show positive staining for connexin 43 between neighbor CMs, which is an important gap junction present in the working myocardium (Figure II-12C).

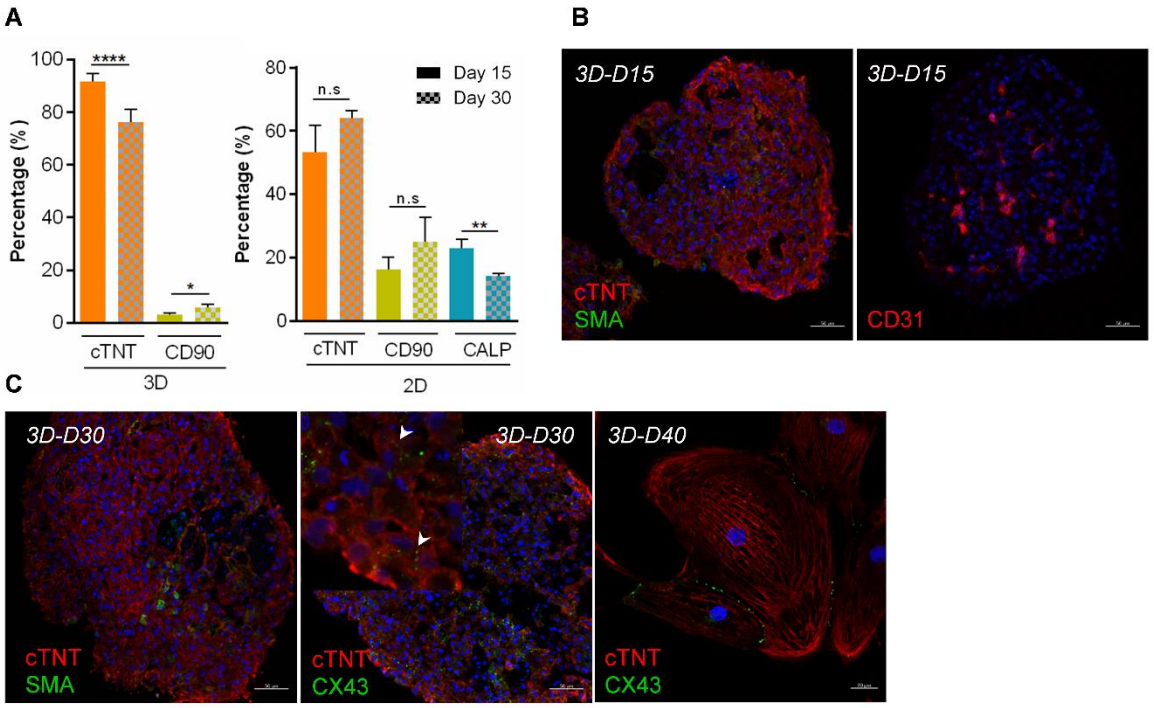

Figure II-12: Assessment of 3D CM aggregate and 2D CM monolayer composition at D15 and D30 of differentiation. (A) Quantification of the percentage of different cardiac cell types present in 2D monolayer and 3D aggregates at D15 and D30 of differentiation (cTNT$^+$ - CMs; CD90$^+$ - Fibroblast-like cells; CALP$^+$ - Smooth Muscle cells). Data are represented as mean ± SEM, at least n=3 independent experiments. Student´s t-test (two-tailed) statistics, ** p<0.005, **** p<0.00005, n.s., no statistically significant (p-value > 0.05). (B) Sections of 3D aggregates on day 15 of differentiation. Scale bars, 50 µm. (C) Sections of 3D aggregates on D30 of differentiation and D40 replated CMs. Scale bars, 50 µm, for sections, and 20 µm in replated CMs.

When compared with the 3D culture format, the efficiency of 2D cardiac differentiation was lower (55±5% cTNT$^+$ cells) at D15 and a higher variability between biological runs was observed (Figure II-12A). In agreement with what was detected in RNA-seq data, a higher prevalence of fibroblast-like cells (16±2% CD90$^+$ cells) and smooth muscle cells (23±2% CALP$^+$ cells) was also observed in the 2D cardiac differentiation platform. Additionally, 2D cardiac monolayer differentiation led to the detachment of contracting areas from the surface of culture matrix after approximately 20 days of culture, resulting in a considerable cell loss (± 50%) and consequently a reduced cell yield and increased variability between biological runs.

In order to further characterize the 3D protocol of differentiation in comparison with the 2D monolayer, we made a double staining using cTNT to specifically label CMs and Ki67 as a marker of cell proliferation. We demonstrated the decrease in proliferating CMs-KI67$^+$ cells in both culture formats from D15 to D30. However, 3D aggregates show a significantly lower percentage of CMs staining positively for Ki67 at both analyzed time points, decreasing from 11.9 ± 0.6% at D15 to 2.9 ± 0.7% at D30, whereas in 2D it decreases from 19.7 ± 1.2% at D15 to 10.0 ± 1% at D30 (Figure II-

13A). This progressive exit from the cell cycle during maturation in 3D conditions suggests a more mature phenotype compared to the one obtained in the 2D monolayer. Importantly, the expression of TNN13, which represents the more mature isoform of cardiac troponin TNNI (Bedada et al., 2014), is higher in 3D aggregates compared to 2D monolayer at D15 of differentiation (Figure II-14B), reinforcing the idea of a higher degree of CM maturation in 3D cardiac aggregates at this time point.

Additionally, CMs replated from D30 aggregates show an average area of ±1,456 μm^2 and a roundness of ± 0.45, with 20.6±1.6% of binucleated CMs (Figure II-13C-E), which is in agreement with previous reports of CM in 3D culture (Correia et al., 2017; Ronaldson-Bouchard et al., 2018b). Finally, using the patch clamp technique, it was also possible to demonstrate the electrophysiological activity of CMs dissociated from aggregates at day 30 of differentiation (Figure II-13F). According to previously described criteria (Burridge et al., 2014b), we detected the presence of three different subtypes of CMs, including ventricular-like (APD_{90}/APD_{50} = 1.2 ± 0.1), atrial-like (APD_{90}/APD_{50} = 2.2 ± 0.2) and nodal-like (APD_{90}/APD_{50} = 1.6 ± 0.1) CMs (Fig. 4K). The electrophysiology study is in line with the RNA-seq data since it was identified the presence of ventricular, atrial and nodal like CMs, with ventricular-like CMs showing a APD_{90}/APD_{50} ratio of around 1.2, which is similar to the values observed for mature ventricular CMs (Foo et al., 2018).

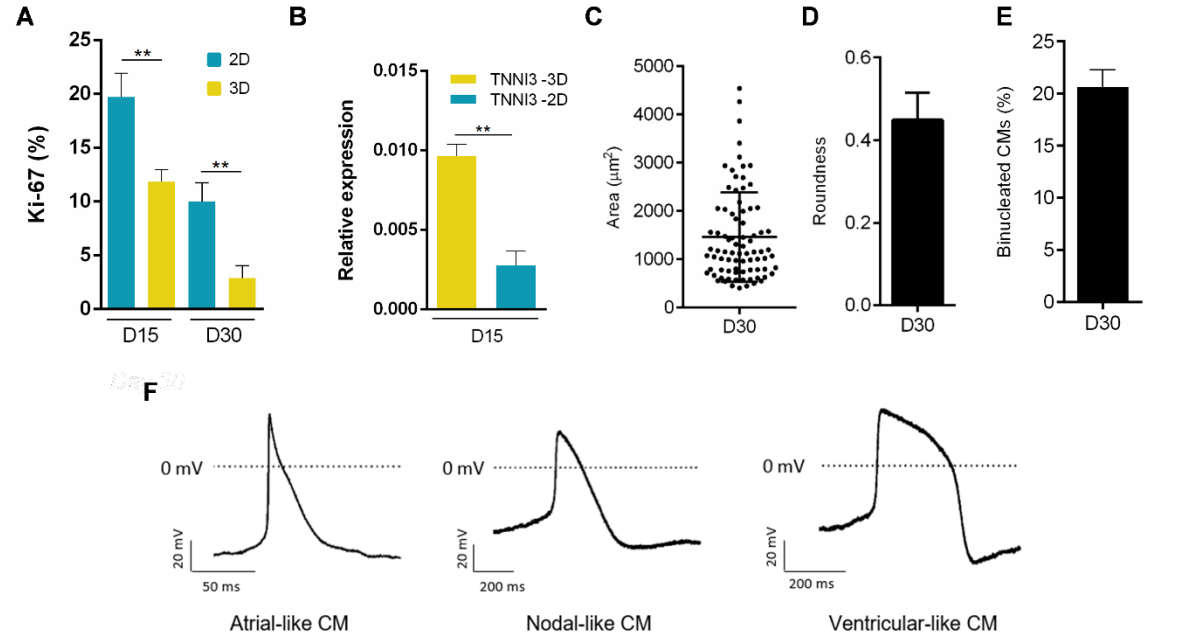

Figure II-13: Structural and functional characterization of CMs obtained from 3D culture system. (A) Percentage of CMs-ki67$^+$ cells in 3D aggregates and 2D monolayer at D15 and D30 of differentiation. Data are represented as mean ± SEM, n=3 independent experiments. Student´s t-test (two-tailed) statistics, ** p<0.005. (B) Relative gene expression of cardiac troponin TNNI3 at D15 of differentiation in both culture conditions (2D and 3D). Values are normalized to *GAPDH* and *TNNT2*. Data are represented as mean ± SEM, n=3 independent experiments. Student´s t-test (two-tailed) statistics, ** p<0.005. (C-E) Characterization of D30 replated CMs in terms of CMs area (C) and roundness (D) (data are represented as mean, n=3 (82 cells) independent

experiments), and binucleation (E) (data are represented as mean, n=3 (317 cells) independent experiments). (K) Representative traces of action potential (AP) recordings of three different cardiomyocyte subtypes present in day 30-35 of replated 3D aggregates of CMs, using whole cell patch clamp. CMs subtypes were categorized as atrial-, nodal-, or ventricular-like according to (Burridge et al., 2014b). n=3 independent experiments.

Since for different applications it may be important to maintain the developed hPSC-CMs for long periods of time in culture, in order to avoid the phenomenon of aggregate agglomeration, two different modifications to the initial method were evaluated including i) single-cell dissociation of the 3D aggregates at D10 of differentiation followed by re-aggregation in 96 well plates or ii) direct transfer of the 3D aggregates to 96-well plates (Figure II-14A). Both approaches allowed the maintenance of 3D aggregates with high viability until D30 of cardiac differentiation (Figure II-14B and C).

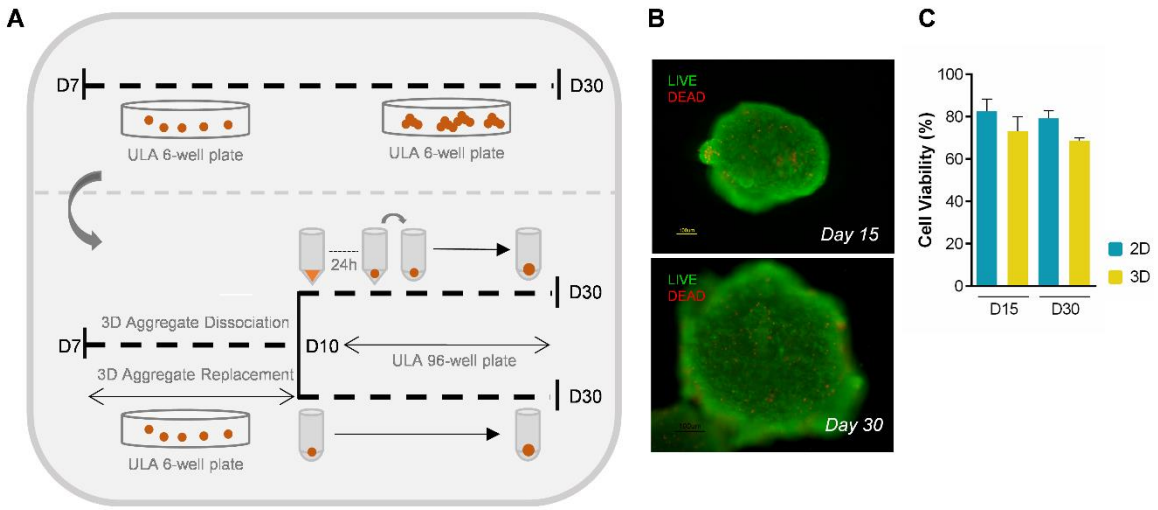

Figure II-14 Improvement of the 3D CM differentiation platform to allow longer periods of culture. (A) Schematic representation of alternative methodologies for the long term maintenance in culture of 3D cardiac aggregates using 96-well plates. (B) live/dead staining of aggregates at D15 (top) and D30 (bottom) of differentiation, showing high cell viability. (C) Flow cytometry quantification of cell viability at D15 and D30 of differentiation for both culture conditions (2D and 3D). Data are represented as mean ± SEM, n=3 independent experiments.

II.5 DISCUSSION

When compared to 2D culture systems, 3D differentiation of hPSCs has proved to better mimic the process of embryogenesis *in vivo*, by recreating important spatial gradients of different signals that are essential for normal embryonic development, particularly for cardiogenesis (Mohr et al., 2010). Previous studies in the literature have mainly explored the implication of the 3D environment in cardiac tissue maturation, starting with a population of cardiac progenitor cells (Correia et al., 2018)

or CMs previously differentiated in 2D monolayer culture systems (Mills et al., 2017b; Ronaldson-Bouchard et al., 2018b; Shadrin et al., 2017). In a complementary approach to these studies, here it was revealed important implications involved in transitioning the Wnt signaling-based 2D culture system to a novel integrated 3D culture platform, starting with forced and size-controlled aggregation of hiPSCs followed by their expansion, cardiac differentiation and maturation, in a 3D environment.

Oxygen gradients have been described as a fundamental physiological cue during organogenesis in the developing embryo (Al-Mehdi et al., 2012). In fact, due to oxygen diffusional limitations and also due to a non-established circulatory system, the development of the embryo in the early stages of embryogenesis occurs in a relatively oxygen-poor environment (Mohyeldin et al., 2010). In the 3D culture platform herein developed, aggregates at day 0 of differentiation have already around 300 µm of diameter, which can result in oxygen gradients since oxygen diffusion distance is estimated to be approximately 150 µm (Gatenby and Gillies, 2004).

In this work it was demonstrated that 3D culture of hiPSC before cardiac differentiation induced important regulatory changes that influenced the efficiency and robustness of cardiac differentiation. It was attributed the 3D culture format itself and the consequent hypoxic response generated inside the aggregates as the major triggers for the transcriptional changes that were observed, namely (1) the stabilization of TGF-β/ Nodal pathway, (2) the upregulation of MAPK/ JNK/ ERK pathway and (3) the increase in glycolysis energy metabolism, which culminates in a balance between pluripotency maintenance and hiPSCs priming towards mesendoderm lineage differentiation. In fact, in the literature there are already evidences that suggest the priming of hPSCs towards mesoderm when these cells are cultured as 3D aggregates (Azarin et al., 2012; Hsiao et al., 2014). Also, *HIF1α* has been described to indirectly induce *NODAL* transcription via Notch signal stabilization (Gustafsson et al., 2005; Quail et al., 2011), which can explain TGF-β/Nodal pathway stabilization in our 3D hiPSC aggregates. The induction of mesoderm, during heart development, begins with high concentrations of *NODAL* in the proximal epiblast on mouse embryos (Burridge et al., 2012). Additionally, *in vitro* studies revealed that canonical Wnt and TGF-β/Nodal signaling work together in the regulation of PS formation and suppression of *NODAL* prevents β-catenin mediated PS induction by CHIR addition (Funa et al., 2015b), reinforcing the importance of the Nodal signaling during the early stages of cardiac differentiation. Here it was demonstrated that the initial stage of hiPSC culture as 3D hiPSC aggregates, before cardiac induction, influences the progression of differentiation, culminating in a faster and more efficient commitment of hPSC towards cardiac mesoderm and consequently towards CMs. We attribute this faster progression of cardiac differentiation in 3D aggregates, compared with 2D monolayer, not only to the differences in the initial cell population but also to the continuous hypoxic stimuli that may still be present throughout the differentiation process and the 3D structure itself, with increased cell-to-cell interactions.

Kinney and colleagues (Kinney et al., 2013) referred in their work that forced aggregation allows a more homogeneous control of intercellular adhesion dynamics which may impact the differentiation capacity of ESCs. Particularly, they explored the relationship between E-cadherin, linked to cell-cell

interaction, and β-catenin, involved in canonical Wnt signaling, which may be responsible for an enhanced cardiogenic differentiation capacity in 3D-EB-like aggregates. This fact can explain our RNA-seq data suggesting a higher degree of Wnt signaling activation in 3D aggregates at early stages of cardiac differentiation and also the upregulation of important targets of the Wnt/β-catenin pathway, such as *MESP1* and *MEF2C*. Additionally, previous studies suggest that hypoxia enhances the expression of mesodermal genes, acting as a mesoderm-inductive signal (Niebruegge et al., 2009), and also promote the activation of Wnt/β-catenin signaling pathway (Mazumdar et al., 2010). Additionally, hypoxia, through HIF1α stabilization, has been suggested to have, as direct targets, important cardiac transcriptional factors, such as *MEF2C* (Krishnan et al., 2008), which was upregulated in our 3D aggregates, and be also involved in the process of myofibrillogenesis (Krishnan et al., 2008). In fact, different genes involved in CMs structural and contraction apparatus, and also cardiac communication, including different gap junctions and ion channels genes, were upregulated at early stages of differentiation in 3D aggregates. This can potentially explain the earlier beginning of contraction in the 3D culture system when compared with 2D monolayer.

Zhang and colleagues(Zhang et al., 2015), which also studied in parallel 2D and 3D hiPSC cardiac differentiation systems, concluded that no major differences in the kinetics of cardiac differentiation became apparent between the 2D and 3D formats, suggesting a synchronized differentiation of the cells in both conditions. In that particularly study, aggregates were induced at the same day that differentiation starts, contrarily to what happens in the present platform, where a pre-differentiation period is integrated with the differentiation platform and, as discussed before, has significant impact on the progression of differentiation. Also, Kerscher and colleagues (Kerscher et al., 2016), which compared the differentiation into CMs from hPSCs encapsulated in a 3D hydrogel structure with a 2D monolayer culture system, reported that CM yield and gene expression level of cardiac markers were analogous to the ones observed in 2D monolayer for the same analyzed time points. This reinforces the relevance and novelty of the integrated 3D cardiac differentiation platform herein developed.

Interestingly, some of the upregulated genes during the progression of differentiation and in the final 3D cardiac spheroids, compared with the 2D culture system, are involved in cardiac cell communication, and some of them are described to be preferentially expressed in atrial, nodal and conduction system CMs. This suggests that different and/or more functional CMs of different subtypes might be present in the 3D aggregates compared with the 2D monolayer. Since different subtypes of CMs are described to be originated from different subtypes of cardiac progenitor populations (Lee et al., 2017c), it was suggested that the 3D environment is more prone to the development of a heterogeneous cardiac differentiation environment as a result of spatial gradients of molecules and oxygen inside the aggregates. In 2D monolayer culture systems cells are more homogenously exposed to the different stimuli, which can result in a more homogeneous differentiation towards a specific subtype of CMs. Taking into consideration the RNA-seq data, it cannot be claimed the existence of a different proportion or an enrichment in a specific CM subtype in each culture condition.

However, a recently identified surface marker for ventricular-like CM progenitor cells, *LIFR* (Foo et al., 2018), was upregulated (FC ± 2.7) in the 2D culture at day 7 of differentiation compared to 3D aggregates. In fact, the 2D differentiation protocol based solely on the temporal modulation of Wnt signaling, has already been described to bias the CMs differentiation towards ventricular-like CMs (Lian et al., 2012a). A single-cell RNA-seq approach could enable the identification and characterization of the different cardiac progenitor populations that are potentially developed at the early stages of differentiation and of the different subtypes of CMs present in the final 3D aggregates.

II.6 CONCLUSIONS

In conclusion, in this work it was developed a simple, highly efficient and robust 3D cardiac differentiation platform, using only the temporal modulation of Wnt signaling. This 3D integrated hiPSC expansion and differentiation platform contributes to a faster cardiac commitment of hiPSCs and to an earlier CM structural and functional maturation when compared with CMs obtained from monolayer culture. 2D differentiation of hiPSC into CMs using the Wnt signaling modulation, despite being a simple protocol, is a process that has a very high intrinsic variability (Laco et al., 2018) ending up to be a poorly reliable process when the aim is to obtain CMs in a consistent manner for further applications. CMs produced with the 3D platform can be easily used for the development of *in vitro* EHT models, which in the majority of the reported cases uses hPSC-CMs previously differentiated in 2D culture platforms. With the 3D differentiation platform, hiPSC-CMs can be obtained in a faster, more efficient and reproducible way, and additionally CMs show already a higher degree of maturation compared to the ones obtained from age-matched CMs in 2D culture. The 3D platform allows the achievement of 20-25 million CMs at D10-D15 of cardiac differentiation per Aggrewell plate, and overall, this number can be easily increased by scaling out the integrated process.

II.7 REFERENCES

Al-Mehdi, A.-B., Pastukh, V.M., Swiger, B.M., Reed, D.J., Patel, M.R., Bardwell, G.C., Pastukh, V. V, Alexeyev, M.F., and Gillespie, M.N. (2012). Perinuclear Mitochondrial Clustering Creates an Oxidant-Rich Nuclear Domain Required for Hypoxia-Induced Transcription. Sci. Signal. *5*, ra47–ra47.

Arthur, S.A., Blaydes, J.P., and Houghton, F.D. (2019). Glycolysis Regulates Human Embryonic Stem Cell Self-Renewal under Hypoxia through HIF-2α and the Glycolytic Sensors CTBPs. Stem Cell Reports *12*, 1–15.

Azarin, S.M., Lian, X., Larson, E.A., Popelka, H.M., de Pablo, J.J., and Palecek, S.P. (2012). Modulation of Wnt/β-catenin signaling in human embryonic stem cells using a 3-D microwell array. Biomaterials *33*, 2041–2049.

Barbosa, H.S.C., Fernandes, T.G., Dias, T.P., Diogo, M.M., and Cabral, J.M.S. (2012). New Insights into the Mechanisms of Embryonic Stem Cell Self-Renewal under Hypoxia: A Multifactorial Analysis Approach. PLoS One *7*, e38963.

Bedada, F.B., Chan, S.S.K., Metzger, S.K., Zhang, L., Zhang, J., Garry, D.J., Kamp, T.J., Kyba, M., and Metzger, J.M. (2014). Acquisition of a quantitative, stoichiometrically conserved ratiometric marker of maturation status in stem cell-derived cardiac myocytes. Stem Cell Reports *3*, 594–605.

Birket, M.J., Ribeiro, M.C., Verkerk, A.O., Ward, D., Leitoguinho, A.R., den Hartogh, S.C., Orlova, V. V, Devalla, H.D., Schwach, V., Bellin, M., et al. (2015). Expansion and patterning of cardiovascular progenitors derived from human pluripotent stem cells. Nat. Biotechnol. *33*, 970–979.

Burridge, P.W., Thompson, S., Millrod, M.A., Weinberg, S., Yuan, X., Peters, A., Mahairaki, V., Koliatsos, V.E., Tung, L., and Zambidis, E.T. (2011). A universal system for highly efficient cardiac differentiation of human induced pluripotent stem cells that eliminates interline variability. PLoS One *6*.

Burridge, P.W., Keller, G., Gold, J.D., and Wu, J.C. (2012). Production of De Novo Cardiomyocytes: Human Pluripotent Stem Cell Differentiation and Direct Reprogramming. Cell Stem Cell *10*, 16–28.

Burridge, P.W., Matsa, E., Shukla, P., Lin, Z.C., Churko, J.M., Ebert, A.D., Lan, F., Diecke, S., Huber, B., Mordwinkin, N.M., et al. (2014). Chemically defined generation of human cardiomyocytes. Nat. Methods *11*, 855–860.

Chen, B., Dodge, M.E., Tang, W., Lu, J., Ma, Z., Fan, C.-W., Wei, S., Hao, W., Kilgore, J., Williams, N.S., et al. (2009). Small molecule–mediated disruption of Wnt-dependent signaling in tissue regeneration and cancer. Nat. Chem. Biol. *5*, 100–107.

Chen, V.C., Ye, J., Shukla, P., Hua, G., Chen, D., Lin, Z., Liu, J., Chai, J., Gold, J., Wu, J., et al. (2015). Development of a scalable suspension culture for cardiac differentiation from human pluripotent stem cells. Stem Cell Res. *15*, 365–375.

Chiquet, M., and Flück, M. (2001). Chapter 8 Early responses to mechanical stress: From signals at the cell surface to altered gene expression. In Cell and Molecular Response to Stress, pp. 97–110.

Correia, C., Koshkin, A., Duarte, P., Hu, D., Teixeira, A., Domian, I., Serra, M., and Alves, P.M. (2017). Distinct carbon sources affect structural and functional maturation of cardiomyocytes derived from human pluripotent stem cells. Sci. Rep. *7*, 8590.

Correia, C., Koshkin, A., Duarte, P., Hu, D., Carido, M., Sebastião, M.J., Gomes-Alves, P., Elliott, D.A., Domian, I.J., Teixeira, A.P., et al. (2018). 3D aggregate culture improves metabolic maturation of human pluripotent stem cell derived cardiomyocytes. Biotechnol. Bioeng. *115*, 630–644.

Cyganek, L., Tiburcy, M., Sekeres, K., Gerstenberg, K., Bohnenberger, H., Lenz, C., Henze, S., Stauske, M., Salinas, G., Zimmermann, W.-H., et al. (2018). Deep phenotyping of human induced pluripotent stem cell–derived atrial and ventricular cardiomyocytes. JCI Insight *3*, e99941.

Dahlmann, J., Kensah, G., Kempf, H., Skvorc, D., Gawol, A., Elliott, D.A., Dräger, G., Zweigerdt, R., Martin, U., and Gruh, I. (2013). The use of agarose microwells for scalable embryoid body formation and cardiac differentiation of human and murine pluripotent stem cells. Biomaterials *34*, 2463–2471.

Desireddi, J.R., Farrow, K.N., Marks, J.D., Waypa, G.B., and Schumacker, P.T. (2010). Hypoxia Increases ROS Signaling and Cytosolic Ca 2+ in Pulmonary Artery Smooth Muscle Cells of Mouse Lungs Slices. Antioxid. Redox Signal. *12*, 595–602.

Dhanasekaran, D.N., and Reddy, E.P. (2008). JNK signaling in apoptosis. Oncogene *27*, 6245–6251.

Dias, T.P., Pinto, S.N., Santos, J.I., Fernandes, T.G., Fernandes, F., Diogo, M.M., Prieto, M., and Cabral, J.M.S. (2018). Biophysical study of human induced Pluripotent Stem Cell-Derived cardiomyocyte structural maturation during long-term culture. Biochem. Biophys. Res. Commun. *499*, 611–617.

Döring, Y., Pawig, L., Weber, C., and Noels, H. (2014). The CXCL12/CXCR4 chemokine ligand/receptor axis in cardiovascular disease. Front. Physiol. *5*, 212.

Fan, D., Takawale, A., Lee, J., and Kassiri, Z. (2012). Cardiac fibroblasts, fibrosis and extracellular matrix remodeling in heart disease. Fibrogenesis Tissue Repair *5*, 15.

Fonoudi, H., Ansari, H., Abbasalizadeh, S., Larijani, M.R., Kiani, S., Hashemizadeh, S., Zarchi, A.S., Bosman, A., Blue, G.M., Pahlavan, S., et al. (2015). A Universal and Robust Integrated Platform for the Scalable Production of Human Cardiomyocytes From Pluripotent Stem Cells. Stem Cells Transl. Med. *4*, 1482–1494.

Foo, K.S., Lehtinen, M.L., Leung, C.Y., Lian, X., Xu, J., Keung, W., Geng, L., Kolstad, T.R.S., Thams, S., Wong, A.O., et al. (2018). Human ISL1 + Ventricular Progenitors Self-Assemble into an In Vivo Functional Heart Patch and Preserve Cardiac Function Post Infarction. Mol. Ther. *26*, 1644–1659.

Funa, N.S., Schachter, K.A., Lerdrup, M., Ekberg, J., Hess, K., Dietrich, N., Honoré, C., Hansen, K., and Semb, H. (2015). β-Catenin Regulates Primitive Streak Induction through Collaborative Interactions with SMAD2/SMAD3 and OCT4. Cell Stem Cell *16*, 639–652.

Garg, P., Garg, V., Shrestha, R., Sanguinetti, M.C., Kamp, T.J., and Wu, J.C. (2018). Human Induced Pluripotent Stem Cell–Derived Cardiomyocytes as Models for Cardiac Channelopathies.

Circ. Res. *123*, 224–243.

Gatenby, R.A., and Gillies, R.J. (2004). Why do cancers have high aerobic glycolysis? Nat. Rev. Cancer *4*, 891–899.

Gustafsson, M. V, Zheng, X., Pereira, T., Gradin, K., Jin, S., Lundkvist, J., Ruas, J.L., Poellinger, L., Lendahl, U., and Bondesson, M. (2005). Hypoxia Requires Notch Signaling to Maintain the Undifferentiated Cell State. Dev. Cell *9*, 617–628.

Hsiao, C., Tomai, M., Glynn, J., and Palecek, S.P. (2014). Effects of 3-D microwell culture on initial fate specification in human embryonic stem cells. AIChE J. *60*, 1225–1235.

Husain, M., Zandstra, P.W., Niebruegge, S., Kumacheva, E., Peerani, R., Woodhouse, K.A., and Bauwens, C.L. (2008). Control of Human Embryonic Stem Cell Colony and Aggregate Size Heterogeneity Influences Differentiation Trajectories. Stem Cells *26*, 2300–2310.

Kattman, S.J., Witty, A.D., Gagliardi, M., Dubois, N.C., Niapour, M., Hotta, A., Ellis, J., and Keller, G. (2011a). Stage-Specific Optimization of Activin/Nodal and BMP Signaling Promotes Cardiac Differentiation of Mouse and Human Pluripotent Stem Cell Lines. Cell Stem Cell *8*, 228–240.

Kattman, S.J., Witty, A.D., Gagliardi, M., Dubois, N.C., Niapour, M., Hotta, A., Ellis, J., and Keller, G. (2011b). Stage-specific optimization of activin/nodal and BMP signaling promotes cardiac differentiation of mouse and human pluripotent stem cell lines. Cell Stem Cell *8*, 228–240.

Keith, B., and Simon, M.C. (2007). Hypoxia-Inducible Factors, Stem Cells, and Cancer. Cell *129*, 465–472.

Kempf, H., Olmer, R., Kropp, C., Rückert, M., Jara-Avaca, M., Robles-Diaz, D., Franke, A., Elliott, D.A., Wojciechowski, D., Fischer, M., et al. (2014). Controlling Expansion and Cardiomyogenic Differentiation of Human Pluripotent Stem Cells in Scalable Suspension Culture. Stem Cell Reports *3*, 1132–1146.

Kempf, H., Olmer, R., Haase, A., Franke, A., Bolesani, E., Schwanke, K., Robles-Diaz, D., Coffee, M., Göhring, G., Dräger, G., et al. (2016a). Bulk cell density and Wnt/TGFbeta signalling regulate mesendodermal patterning of human pluripotent stem cells. Nat. Commun. *7*, 13602.

Kempf, H., Olmer, R., Haase, A., Franke, A., Bolesani, E., Dra, G., Po, O., Joos, T., Schwanke, K., Coffee, M., et al. (2016b). Bulk cell density and Wnt/TGFbeta signalling regulate mesendodermal patterning of human pluripotent stem cells.

Kensah, G., Zenker, M., Lang, A., Haghighi, F., Piekorz, R.P., Nakhaei-Rad, S., Ahmadian, M.R., Kutschka, I., and Dahlmann, J. (2018). bFGF-mediated pluripotency maintenance in human induced pluripotent stem cells is associated with NRAS-MAPK signaling. Cell Commun. Signal. *16*, 1–14.

Kerscher, P., Turnbull, I.C., Hodge, A.J., Kim, J., Seliktar, D., Easley, C.J., Costa, K.D., and Lipke, E.A. (2016). Direct hydrogel encapsulation of pluripotent stem cells enables ontomimetic differentiation and growth of engineered human heart tissues. Biomaterials *83*, 383–395.

Kinney, M.A., Sargent, C.Y., and McDevitt, T.C. (2013). Temporal Modulation of β-Catenin Signaling by Multicellular Aggregation Kinetics Impacts Embryonic Stem Cell Cardiomyogenesis. Stem Cells Dev. *22*, 2665–2677.

Krishnan, J., Ahuja, P., Bodenmann, S., Knapik, D., Perriard, E., Krek, W., and Perriard, J.-C. (2008). Essential role of developmentally activated hypoxia-inducible factor 1alpha for cardiac morphogenesis and function. Circ. Res. *103*, 1139–1146.

Laco, F., Woo, T.L., Zhong, Q., Szmyd, R., Ting, S., Khan, F.J., Chai, C.L.L., Reuveny, S., Chen, A., and Oh, S. (2018). Unraveling the Inconsistencies of Cardiac Differentiation Efficiency Induced by the GSK3β Inhibitor CHIR99021 in Human Pluripotent Stem Cells. Stem Cell Reports *10*, 1851–1866.

Lee, J.H., Protze, S.I., Laksman, Z., Backx, P.H., and Keller, G.M. (2017). Human Pluripotent Stem Cell-Derived Atrial and Ventricular Cardiomyocytes Develop from Distinct Mesoderm Populations. Cell Stem Cell *21*, 179-194.e4.

Lian, X., Hsiao, C., Wilson, G., Zhu, K., Hazeltine, L.B., Azarin, S.M., Raval, K.K., Zhang, J., Kamp, T.J., and Palecek, S.P. (2012a). Robust cardiomyocyte differentiation from human pluripotent stem cells via temporal modulation of canonical Wnt signaling. Proc. Natl. Acad. Sci. U. S. A. *109*, E1848-57.

Lian, X., Hsiao, C., Wilson, G., Zhu, K., Hazeltine, L.B., Azarin, S.M., Raval, K.K., Zhang, J., Kamp, T.J., and Palecek, S.P. (2012b). Robust cardiomyocyte differentiation from human pluripotent stem cells via temporal modulation of canonical Wnt signaling. Proc. Natl. Acad. Sci. *109*, E1848–E1857.

Lian, X., Hsiao, C., Wilson, G., Zhu, K., Hazeltine, L.B., Azarin, S.M., Raval, K.K., Zhang, J., Kamp, T.J., and Palecek, S.P. (2012c). Robust cardiomyocyte differentiation from human pluripotent stem cells via temporal modulation of canonical Wnt signaling. Proc. Natl. Acad. Sci. U. S. A. *109*, E1848-57.

Lian, X., Zhang, J., Azarin, S.M., Zhu, K., Hazeltine, L.B., Bao, X., Hsiao, C., Kamp, T.J., and Palecek, S.P. (2013). Directed cardiomyocyte differentiation from human pluripotent stem cells by modulating Wnt/β-catenin signaling under fully defined conditions. Nat. Protoc. *8*, 162–175.

Liu, J., Laksman, Z., and Backx, P.H. (2016). The electrophysiological development of cardiomyocytes. Adv. Drug Deliv. Rev. *96*, 253–273.

Ma, Z., Wang, J., Loskill, P., Huebsch, N., Koo, S., Svedlund, F.L., Marks, N.C., Hua, E.W.,

Grigoropoulos, C.P., Conklin, B.R., et al. (2015). Self-organizing human cardiac microchambers mediated by geometric confinement. Nat. Commun. *6*, 7413.

Mazumdar, J., O'Brien, W.T., Johnson, R.S., LaManna, J.C., Chavez, J.C., Klein, P.S., and Simon, M.C. (2010). O2 regulates stem cells through Wnt/β-catenin signalling. Nat. Cell Biol. *12*, 1007–1013.

Metsalu, T., and Vilo, J. (2015). ClustVis: A web tool for visualizing clustering of multivariate data using Principal Component Analysis and heatmap. Nucleic Acids Res. *43*, W566–W570.

Mi, H., Muruganujan, A., Casagrande, J.T., and Thomas, P.D. (2013). Large-scale gene function analysis with the panther classification system. Nat. Protoc. *8*, 1551–1566.

Mills, R.J., Titmarsh, D.M., Koenig, X., Parker, B.L., Ryall, J.G., Quaife-Ryan, G.A., Voges, H.K., Hodson, M.P., Ferguson, C., Drowley, L., et al. (2017). Functional screening in human cardiac organoids reveals a metabolic mechanism for cardiomyocyte cell cycle arrest. Proc. Natl. Acad. Sci. U. S. A. *114*, E8372–E8381.

Mohr, J.C., Zhang, J., Azarin, S.M., Soerens, A.G., de Pablo, J.J., Thomson, J. a, Lyons, G.E., Palecek, S.P., and Kamp, T.J. (2010). The microwell control of embryoid body size in order to regulate cardiac differentiation of human embryonic stem cells. Biomaterials *31*, 1885–1893.

Mohyeldin, A., Garzón-Muvdi, T., and Quiñones-Hinojosa, A. (2010). Oxygen in stem cell biology: a critical component of the stem cell niche. Cell Stem Cell *7*, 150–161.

Moriyama, M., Moriyama, H., Uda, J., Kubo, H., Nakajima, Y., Goto, A., Morita, T., and Hayakawa, T. (2017). BNIP3 upregulation via stimulation of ERK and JNK activity is required for the protection of keratinocytes from UVB-induced apoptosis. Cell Death Dis. *8*, e2576.

Niebruegge, S., Bauwens, C.L., Peerani, R., Thavandiran, N., Masse, S., Sevaptisidis, E., Nanthakumar, K., Woodhouse, K., Husain, M., Kumacheva, E., et al. (2009). Generation of human embryonic stem cell-derived mesoderm and cardiac cells using size-specified aggregates in an oxygen-controlled bioreactor. Biotechnol. Bioeng. *102*, 493–507.

Pei, D., Xu, J., Zhuang, Q., Tse, H.-F., and Esteban, M.A. (2010). Induced pluripotent stem cell technology in regenerative medicine and biology. Adv. Biochem. Eng. Biotechnol. *123*, 127–141.

Quail, D.F., Taylor, M.J., Walsh, L.A., Dieters-Castator, D., Das, P., Jewer, M., Zhang, G., and Postovit, L. (2011). Low oxygen levels induce the expression of the embryonic morphogen Nodal. Mol. Biol. Cell *22*, 4809–4821.

Rao, J., Pfeiffer, M.J., Frank, S., Adachi, K., Piccini, I., Quaranta, R., Araúzo-Bravo, M., Schwarz, J., Schade, D., Leidel, S., et al. (2016). Stepwise Clearance of Repressive Roadblocks Drives Cardiac

Induction in Human ESCs. Cell Stem Cell *18*, 341–353.

Ronaldson-Bouchard, K., Ma, S.P., Yeager, K., Chen, T., Song, L., Sirabella, D., Morikawa, K., Teles, D., Yazawa, M., and Vunjak-Novakovic, G. (2018). Advanced maturation of human cardiac tissue grown from pluripotent stem cells. Nature *556*, 239–243.

Ruttkay-Nedecky, B., Nejdl, L., Gumulec, J., Zitka, O., Masarik, M., Eckschlager, T., Stiborova, M., Adam, V., and Kizek, R. (2013). The role of metallothionein in oxidative stress. Int. J. Mol. Sci. *14*, 6044–6066.

Schier, A.F. (2009). Nodal morphogens. Cold Spring Harb. Perspect. Biol. *1*, a003459.

Shadrin, I.Y., Allen, B.W., Qian, Y., Jackman, C.P., Carlson, A.L., Juhas, M.E., and Bursac, N. (2017). Cardiopatch platform enables maturation and scale-up of human pluripotent stem cell-derived engineered heart tissues. Nat. Commun. *8*.

Takahashi, K., Tanabe, K., Ohnuki, M., Narita, M., Ichisaka, T., Tomoda, K., and Yamanaka, S. (2007). Induction of pluripotent stem cells from adult human fibroblasts by defined factors. Cell *131*, 861–872.

Takeda, M., Miyagawa, S., Fukushima, S., Saito, A., Ito, E., Harada, A., Matsuura, R., Iseoka, H., Sougawa, N., Mochizuki-Oda, N., et al. (2018). Development of In Vitro Drug-Induced Cardiotoxicity Assay by Using Three-Dimensional Cardiac Tissues Derived from Human Induced Pluripotent Stem Cells. Tissue Eng. Part C Methods *24*, 56–67.

Varum, S., Momcilović, O., Castro, C., Ben-Yehudah, A., Ramalho-Santos, J., and Navara, C.S. (2010). Enhancement of human embryonic stem cell pluripotency through inhibition of the mitochondrial respiratory chain. Stem Cell Res. *3*, 142–156.

Warmflash, A., Sorre, B., Etoc, F., Siggia, E.D., and Brivanlou, A.H. (2014). A method to recapitulate early embryonic spatial patterning in human embryonic stem cells. Nat. Methods *11*, 847–854.

van Weerd, J.H., and Christoffels, V.M. (2016). The formation and function of the cardiac conduction system. Development *143*, 197–210.

Wolling, H., Konze, S.A., Höfer, A., Erdmann, J., Pich, A., Zweigerdt, R., and Buettner, F.F.R. (2018). Quantitative Secretomics Reveals Extrinsic Signals Involved in Human Pluripotent Stem Cell Cardiomyogenesis. Proteomics *18*, 1800102.

Yang, X., and Papoian, T. (2018). Moving beyond the comprehensive in vitro proarrhythmia assay: Use of human-induced pluripotent stem cell-derived cardiomyocytes to assess contractile effects associated with drug-induced structural cardiotoxicity. J. Appl. Toxicol. 1–11.

Zhang, M., Schulte, J.S., Heinick, A., Piccini, I., Rao, J., Quaranta, R., Zeuschner, D., Malan, D., Kim, K.-P., Röpke, A., et al. (2015). Universal cardiac induction of human pluripotent stem cells in two and three-dimensional formats: implications for in vitro maturation. Stem Cells *33*, 1456–1469.

III. UNRAVELING THE PATH FOR EPICARDIAL CELL SPECIFICATION FROM HUMAN PLURIPOTENT STEM CELLS IN 3D CONDITION

III.1 ABSTRACT

Knowing the relevance that epicardium has on normal embryonic human heart development, *in vitro* protocols to generate epicardial cells from hPSCs in 2D monolayer culture systems have been described in the literature. In this chapter, previously reported 2D hPSC-PECs differentiation protocols were transposed and adapted to a 3D environment by taking advantage of the initial steps of the 3D CMs differentiation platform previously developed in chapter II. Starting from a progenitor cell population that is common to the CM differentiation protocol, it was possible to develop for the first time a methodology to derive PECs from hPSCs in a 3D environment that allows the robust generation of ±80% $WT1^+$ cells after 11 days of differentiation, representing a yield of $4x10^6$ PECs per each initial hPSC. The generated hPSC-PECs present an epithelial-like structure after replating and have the capacity to undergo EMT and differentiate into CF and SMCs. Additionally, it was also demonstrated that D11 PEC aggregates include endodermal-derived gut-epithelial like structures, revealing that at early stages of the 3D CM differentiation platform, definite endoderm and lateral plate mesoderm progenitors are simultaneously generated. In an attempt to eliminate the gut-like structures in PEC aggregates, two strategies were explored, including (1) the modulation of the PEC induction period through BMP and Wnt signaling pathways manipulation, and (2) the manipulation of the Wnt signaling pathway during the first days of hPSCs differentiation, envisaging minimize the generation of endoderm progenitor cells. From these studies it was possible to retrieve important insights regarding the role of Wnt and BMP4 signals in PECs induction from mesoderm progenitors and also to highlight how slight differences in Wnt signaling manipulation during the first days of hPSC differentiation impact mesendoderm progenitor cells specification, namely into definitive endoderm, lateral plate mesoderm and paraxial mesoderm. Additional studies are now being performed to improve the 3D PECs differentiation process by controlling the generation of endoderm progenitor cells. Knowing the potential use of hPSC-PECs in the context of a cell therapy for regenerative medicine applications, the developed protocol can be easily improved towards the production of a pure population of PECs. Additionally, these cells can be further explored in more complex multicellular cardiac models to be used in *in vitro* applications, as it will be explored in the next chapter.

III.2 INTRODUCTION

The epicardium is the epithelial layer that covers the outer surface of the heart, playing an essential role in normal heart development. Contrarily to the myocardium and endocardium layers, the epicardium originates outside the primitive heart tube in a transient structure, known as PEO, which develops from the posterior SHF mesoderm progenitors. These cells are normally identified by the expression of *WT1, TBX18, TCF21, SEMA3D* and *SCX* markers (Cano et al., 2016; Katz et al., 2012; Lupu et al., 2020a). The full composition of PEO is still controversial. Some reports suggest the existence of different subclusters of cells within the PEO (Katz et al., 2012)(Cano et al., 2016), which are characterized by different sets of markers and have different differentiating fates. A more recent study, however, refutes that idea stating that all the cells present in PEO present the same phenotype and cell fate (Lupu et al., 2020a).

The role of epicardium during embryonic heart development is well described in the literature. After epicardium establishment, during early embryonic heart formation, part of the epicardial cells present in the epicardial layer give rise to coronary smooth muscle cells, critical for coronary vasculature development, and myocardial fibroblasts, that give the support and contribute to the formation of a functional connective tissue in the myocardium. Although the contribution of epicardial cells to coronary endothelium is still debatable, mainly due to contradictory results from lineage tracing studies in animal models, some reports support that idea (Katz et al., 2012)(Cano et al., 2016). Moreover, epicardium, apart from serving as a progenitor cell source of cardiac cells, it is also described to release paracrine signals that are essential to induce proliferation, compaction and maturation of the developing myocardium.

Knowing the relevance of those cells in cardiac development *in vivo*, different groups have tried to establish *in vitro* protocols to generate epicardial cells from hPSCs. These already reported protocols were well succeeded in developing hPSC-PECs in 2D systems, through BMP4, Wnt and RA signaling manipulation after the generation of lateral plate mesoderm (LPM) progenitor cells (Witty et al., 2014b)(Iyer et al., 2015)(Bao et al., 2016)(Zhao et al., 2017). The functionality of hPSC-PECs has been proved *in vitro* by assessing the capacity of those cells to undergo EMT and differentiate into fibroblasts and functional vascular smooth muscle cells. These hPSC-PECs are now starting to be explored in co-culture systems with hPSC-CMs to evaluate the impact on CM functional and structural maturation and also to develop more complex 3D cardiac models. Additionally, it has been also highlighted in the literature the potential of using hPSCs-derived epicardial cells resembling the fetal stage of embryonic epicardium, in regenerative medicine applications (Bargehr et al., 2019). In fact, contrarily to what is observed in other species, in which quiescent epicardium is activated and contributes for myocardial regeneration following injury, human heart displays inadequate epicardial activation and fails to regenerate myocardium post-injury. Thus, the development of *in vitro* platforms

that allow large scale generation of hPSC-PECs can be also considered a valuable tool for regenerative medicine applications.

In this work, the 3D CM differentiation protocol reported in chapter II was adapted and optimized to obtain $WT1^+$ PECs from hPSCs. The developed platform allows the generation of ±80% $WT1^+$ cells after 11 days of differentiation, which represents a yield of $4x10^6$ PECs per each initial hiPSC. The generated hPSC-PECs present an epithelial-like structure after replating and maintain the phenotype after several passages in culture. Additionally, the capacity of those cells to undergo EMT and differentiate into fibroblasts and vascular smooth muscle cells was demonstrated. Apart from $WT1^+$ PECs, it was also identified the presence of endodermal-derived $CDX2^+$ gut-like cells in D11 aggregates generated with this protocol. To explore the possibility of reducing this non epicardial cell population, additional adaptions to the developed hPSC-derived PECs differentiation platform were explored. The preliminary results obtained demonstrated that this reduction may be possible by decreasing the generation of the endoderm progenitor cell population, which is co-derived with the cardiac mesoderm progenitors in the 3D differentiation platform.

III.3 MATERIALS AND METHODS

III.3.1 Cell Maintenance

hiPSCs (cell line iPS-DF6-9-9T.B) were maintained in mTeSR™1 (StemCell Technologies) in six-well plates coated with Matrigel™ (Corning). Medium was changed daily. Cells were routinely passaged every three to four days using 0.5mM EDTA solution (Thermo Fisher Scientific).

III.3.2 Cardiomyocyte and Pro-Epicardial Cell Differentiation

hiPSCs were harvested with accutase (Sigma) for 7 min at 37ºC. After dissociation, cells were quickly re-aggregated using microwell plates (AggreWell™800, StemCell Technologies) according to the manufacturer's instructions. Cells were plated at a cell density of $1.2x10^6$ cells/well in mTeSR™1 supplemented with 10µM ROCKi. 24 hours later, the total volume of medium was replaced and cells were maintained in mTeSR™1 without ROCKi for an additional two days. For cardiac progenitor differentiation, an adapted GiWi protocol was used (Lian et al., 2013). RPMI 1640 medium (Thermo Fisher Scientific) was used as basal medium. From day 0 to day 5, cells were cultured in RPMI supplemented with 2%(v/v) B-27 minus insulin (Thermo Fisher Scientific). At day 0 of differentiation, the Wnt signaling pathway was activated using the GSK3 inhibitor CHIR99021 (Stemgent) at a final concentration of 11 µM. After 24 hours, medium was changed. At day 3, cells were cultured in basal medium supplemented with Wnt inhibitor IWP-4 (Stemgent) at a final concentration of 5 µM, for two days. At day 5, in the case of CMs differentiation, the medium was changed to basal medium (RPMI+B27-INS), and in the case of pro-epicardium differentiation, CHIR (0-5µM), BMP4 (0-100

ng/mL) and RA (4 µM) was added from D5-D7, using DMEM/F12+Glutamax+Ascorbic acid as basal medium. At day 7 (D7), aggregates were flushed from the AggreWell™800 plate and transferred to 6-Well Ultra-Low Attachment plates. Thereafter, medium was changed every 2 days until cell harvest. In VEGF epicardial differentiation protocol, VEGF at 100 ng/mL concentration was added between D7 and D9, and VEGF at a concentration of 50 ng/mL was added between D9 and D11. PECs were further differentiated in SMCs and CFs, and maintained as PECs. For that D11-PEC aggregates were dissociated are replated in gelatin-coated 12-well plates at a density of 7 x 10^4 cells/well, and cultured in DMEM/F12 Glutamax+Ascorbic acid with 10 ng/mL of FGF, 5 ng/mL of TGF-β1 and 0.5 µM A83, in the case of CFs and SMCs commitment or PECs maintenance, respectively.

III.3.3 Flow Cytometry Analysis

For flow cytometry analysis, 3D cell aggregates were washed with PBS and then singularized with 0.25% trypsin-EDTA or with TrypLE 1X, in the case of surface marker analysis, at 37ºC for 7 min. For enzymatic digestion neutralization, FBS-containing medium was added. After centrifugation and washing the cell pellet, cells were fixed with 2% PFA reagent for 20 minutes at RT or stored at 4ºC. For cell surface marker analysis, cells were washed twice with PBS and re-suspended in primary antibody (Table III-1) diluted in PBS+2% (v/v) BSA, at approximately 500,000 cells per condition, and incubated for 30 min at RT. Afterwards, cells were washed with PBS and re-suspended in secondary antibody diluted in FACS buffer for another 15 min, at RT, in the dark. In the case of the conjugated antibodies (Table III-1), a single incubation period of 30 minutes at RT in the dark was performed. Finally, cells were washed twice with PBS for a final volume of 300 µL/FACS tube. For intracellular marker analysis, cells were first incubated with 90% (v/v) cold methanol at 4ºC for 15 min. Cells were then washed 3 times with a solution constituted by 0.5% BSA solution in PBS. Cell pellet was resuspended and incubated with the primary antibody diluted in 0.1% Triton X-100 and 0.5% BSA in PBS, at RT for 1 h. After incubation, cells were washed twice and cell pellet was resuspended and incubated in the secondary antibody at RT for 30 min in the dark.

III.3.4 Immunostaining Analysis

Sample collection. 2D replated cardiac cells were fixed in 4% PFA for 20 min at RT. 3D aggregates were fixed in 4% PFA at 4ºC for 30 min in an agitation platform. After PFA removal, cells were stored in PBS at 4ºC for further analysis. 3D aggregates were incubated in 15% (m/v) sucrose in PBS, at 4ºC overnight and afterwards embedded in 7.5%/15% gelatin/sucrose and frozen in isopenthane at -80ºC. Aggregates with ten/twelve-µm sections were cut on a cryostat-microtome (Leica CM3050S, Leica Microsystems), collected on Superfrost™ Microscope Slides (Thermo Scientific) and stored at -20ºC. Sections were then de-gelatinized for 45 min in PBS at 37ºC.

Staining. 3D aggregate sections and replated cells in coverslips were incubated in 0.1 M Glycine (Millipore) for 10 min at RT, permeabilized with 0.1% Triton X-100 (Sigma), at RT for 10 min and blocked with 10% fetal goat serum (FGS, Gibco) in TBST (20 mM Tris-HCl pH 8.0, 150 mM NaCl and 0.05% Tween-20, Sigma), at RT for 30 min. Cells were then incubated with the primary antibody diluted in 10% FBS in TBST solution (Table III-1) at 4ºC overnight. Secondary antibodies were added for 30 min and nuclear counterstaining was performed using 4',6-diamidino-2-phenylindole (DAPI, 1.5µg/mL, Sigma), at room temperature for 5 min.

Table III-1: List of antibodies used in Flow Cytometry and Immunostaining analysis.

Antibody	Source	Reference	Isotype	Dilution
CD31	Dako	M0823	Mouse IgG	1:50 (FC/IS)
cTNT	Thermo Fisher	MA5-12960	Mouse IgG	1:800 (FC)
α-SMA	Sigma-Aldrish	161208D	Rabbit IgG	1:200 (IS/FC)
Calponin	Abcam	ab700	Mouse IgG1	1:200 (FC/IS)
CXCR4	Santa Cruz	Sc-12764	Mouse IgG2a	1:20 (FC)
KDR-PE	ReD Systems	FAB357P	Mouse IgG1	1:10 (FC)
C-KIT-PE	Biolegend	313204	Mouse IgG1	1:10 (FC)
CD140a-APC	BD Pharmingen	562777	Rat IgG2a	1:25 (FC)
ISL1	Abcam	Ab178400	Rabbit IgG	1:200 (FC)
WT1	Abcam	ab89901	Rabbit IgG	1:100 (IS/FC)
ALDH1A2	Abcam	ab96060	Rabbit IgG	1:100 (IS)
Collagen I	Abcam	ab34710	Rabbit IgG	1:300 (IS)
Collagen IV	Abcam	ab6311	Mouse IgG1	1:300 (IS)
Periostin	Abcam	ab14041	Rabbit IgG	1:100 (IS)
E-Cadherin	Cell Signaling Technology	24E10	Rabbit IgG	1:200 (IS)
CDX2	Abcam	ab76541	Rabbit IgG	1:200 (IS/FC)

III.3.5 Quantitative real time (qRT)-PCR

Total RNA from 3D cardiac aggregates was extracted using High Pure RNA Isolation Kit (Roche) according to manufacturer´s instructions, and converted into cDNA with High Capacity cDNA Reverse Transcription Kit (Thermo Fisher Scientific). PCR reactions were performed with Green Master Mix (nzytech) (Table III-2). Reactions were run in triplicate in ViiA7 Real-Time PCR Systems (Applied BioSystems). For each analyzed time point, gene expression was normalized against the expression of the housekeeping gene glyceraldehyde-3-phosohate dehydrogenase (*GAPDH*) and results analyzed with the QuantStudio™ RT-PCR Software.

Table III-2: List of primers used in qRT-PCR analysis.

SYBERGREEN	
Gene	PRIMER (5´>3´)
GAPDH	FW: GAGTCAACGGATTTGGTCGT RV: TTGATTTTGGAGGGATCTCG
ISL1	FW: GCGGAGTGTAATCAGTATTTGGA RV: GCATTTGATCCCGTACAACCT
NKX2.5	FW: CCAAGGACCCTAGAGCCGAA RV: GTCCGCCTCTGTCTTCTCCA
TBX5	FW: GAGGTGGGATAGTTGGAGAGC RV: GAATCGCAGGGCAGGTCTTT
TNNT2	FW: GTCCAAACCAAAGCCCAGGT RV: CCACTCTCTCTCCATCGGGG
WT1	FW: CAGCTTGAATGCATGACCTG RV: TATTCTGTATTGGGCTCCGC
TBX18	FW: CCCAGGACTCCCTCCTATGT RV: TAGGAACCCTGATGGGTCTG
ALDH1A2	FW: TCGCATCTTCGTGGAGGAGT RV: TGCTCAGTGGTGGGGTCAAA
SEMA3D	FW: GGAAAGTGCAGACCATCGTT RV: CATCACAGAGTGCCGCTTTA
TCF21	FW: ACCCTCTTCCTCGCTTTCTC RV: TGCTCTCGTTGGAAGTCACA
PDGFRA	FW: ATCGGAGGAGAAGTTTCCCAGAG RV: GGTACTGCCAGCTCACTTCA
ACTA2	FW: CACTGTCAGGAATCCTGTGA RV: CAAAGCCGGCCTTACAGA
CNN1	FW: GTCCACCCTCCTGGCTTT RV: AAACTTGTTGGTGCCCATCT
CD31	FW: GCTGACCCTTCTGCTCTGTT RV: TGAGAGGTGGTGCTGACATC
MYH11	FW: GGTCACGGTTGGGAAAGATGA RV: GGGCAGGTGTTTATAGGGGTT
CDX2	FW: GGGCTCTCTGAGAGGCAGGT RV: CCTTTGCTCTGCGGTTCTG
SOX17	FW: CTCCGGTGTGAATCTCCCC RV: CACGTCAGGATAGTTGCAGTAAT
GATA4	FW: CTGAAGCTCTCCCCACAAGG RV: GCTGTTCCAAGAGTCCTGCT

III.3.6 RNA *In situ* hybridization

The first step of this protocol comprised the preparation of the probes used for in situ hybridization. For that, a cDNA template for SEMA3D gene was amplified by PCR. Afterwards, the *in situ* probes were synthesized using that cDNA template and the following primers, *SEM3D-Fw* – ATTCACTCGATCCCTTGGGC and *SEMA3D-RV(+T7)* – TAATACGACTCACTATAGGGACGATGGTCTGCACTTTCCT. The PCR products were gel- purified using the NZYGelpure kit (NZYTech) and used for reverse transcription with T7 polymerase (Agilent Technologies), DIG-dNTPs (Sigma), and RNase inhibitor. The RNA was precipitated with EtOH and NaOAC3 at 20°C overnight, centrifuged 30min at 13.000g, and then washed with 70% EtOH, dried, and resuspended in nuclease-free H_2O with 10mM of EDTA situ (stored at 20°C until use).

Aggregates were fixed in 4% PFA during 30 min at RT. Fresh sections (12µm) were incubated with the probes, overnight, at 65ºC in hybridization buffer, containing 1x salts, 10% dextran sulphate, 1 mg/mL rRNA, 1x Denhardt`s and 50% of deionized formamide (Sigma). After hybridization, the slices were washed twice, for 30 min at 65 °C, using a washing buffer (50% formamide (Sigma) and 50% 0.3 M NaCl/0.03 M Sodium Citrate dihydrate solution) and then washed twice at RT with TBST (NaCl 150 mM, KCl 10 mM, Tris pH 7.5 50 mM, Tween-20 0.1% in H_2O. The slices were then blocked using TBST with 2% blocking reagent (Roche) and 20% heat inactivated sheep serum (Sigma) for 1h at RT. For staining step, the slices were incubated with antibody anti-DIG (Abcam) diluted into TBST, 2% blocking reagent, 1% sheep serum and left overnight, at 4ºC. After incubation, slices were washed four times with TBST. Afterwards, slices were incubated twice during 10min in 0.4M NaCl, Tris 0.1M (pH 8). For staining revelation, the slices were finally incubated with Fast-red tablets substrate (Sigma) diluted in 0.4M NaCl, Tris 0.1M (pH8) for 1-3h in the dark until the staining became visible. When that occurred reaction was stopped with PTW (PBS+0.1%Tween-20). Immunofluorescence staining was then performed after. The cell images were acquired using Zeiss LSM 710 Confocal Laser Point-Scanning Microscopes and were processed in ZEN 2.3 blue edition software (Zeiss).

III.4 RESULTS

III.4.1 Establishment of a novel 3D platform to generate PECs from hPSCs

Since, *in vivo*, PECs develop from LPM progenitor cells, we adapted the previously described 3D CM differentiation protocol (Chapter II) to specify PECs from hPSCs. Briefly, hPSCs were firstly differentiated to LPM cells through the temporal modulation of Wnt signalling, using CHIR from day 0 (D0) to D1 of differentiation and IWP4 from D3 until D5 (Figure III-1A). The generation of a LPM progenitor cell population was confirmed at D5 of differentiation by the expression of the mesoderm markers PDGFRA (CD140a) (±80% positive cells) and KDR (CD309) (±72% positive cells) (Figure III-1B). Additionally, the percentage of cells expressing the SHF cardiac progenitor marker ISL1, at

this time point of differentiation, was also determined to be ±68%. These three markers have been used in previously described PEC differentiation protocols to confirm the identity of the desired mesoderm progenitor cell population before PECs induction (Witty et al., 2014a) (Iyer et al., 2015) (Bao et al., 2017).

To direct LPM progenitors to an epicardial lineage, different 2D differentiation protocols have been reported in the literature. According to those studies, BMP signaling is required for PEC specification and, although the endogenous Wnt signaling has been demonstrated to be sufficient to allow for PEC derivation, further activation of this pathway improves epicardial cell specification (Iyer et al., 2015) (Witty et al., 2014a). Additionally, the activation of RA signalling pathway has also been reported to be critical to generate epicardial cells *in vitro* (Iyer et al., 2015)(Zhao et al., 2017). At the opposite side, Bao and co-workers demonstrated that the activation alone of Wnt signaling, in low density replated cardiac progenitor cells, was enough to generate PECs from cardiac progenitors (Bao et al., 2017). Therefore, two different protocols were tested in this work, Protocol A, in which only Wnt signalling was activated, and Protocol B, in which a combination of Wnt, BMP4 and RA signals modulation was used to induce PECs (Figure III-1A). In Protocol A, the small molecule CHIR was used for Wnt signalling activation at a concentration of 3 µM (Bao et al., 2017), and in protocol B, CHIR (3µM), BMP4 at 50 ng/mL and RA at 4µM were used as described by Iyer and colleagues (Iyer et al., 2015). The percentage of $WT1^+$ cells after 11 days of differentiation was used as the main readout to compare both protocols, having as control the 3D CM differentiation protocol (Control). PECs induction with Protocol B showed the best results in terms of efficiency and reproducibility, with ± 80% $WT1^+$ cells being obtained at D11 of culture, reason why this was the condition selected for further studies (Figure III-1C). We additionally tested Protocol A with two other CHIR concentrations, specifically 6µM and 11µM, which resulted in less efficient outcomes, and tested the PECs induction period starting at D6 or D7, resulting also in a lower percentage of $WT1^+$ cells at the end of differentiation period. Importantly, in the CM differentiation protocol, no $WT1^+$ cells were detected by flow cytometry analysis after 11 days of differentiation (Figure III-1C).

The dynamic changes in gene expression of important markers involved in CM and PECs specification in both CM and PEC differentiation protocols, was analysed (Figure III-1D). The results showed a reduction of the CM progenitor markers *NKX2.5* and *ISL1* expression right after PECs induction, and a clear upregulation of the PECs markers *WT1*, *TBX18, ALDH1A2* and *TCF21*. *TBX5*, although being a known transcription factor essential for proper cardiogenic lineage specification, has been also reported to have an important role in PECs development (Hatcher et al., 2004). In fact, the expression of this marker showed a significant increase after the PECs induction period, maintaining the level of expression until D11. *GATA4* has been also described to be expressed in LPM at the earliest stages of cardiac differentiation and subsequently maintained in cardiac lineage throughout development (Watt et al., 2004).

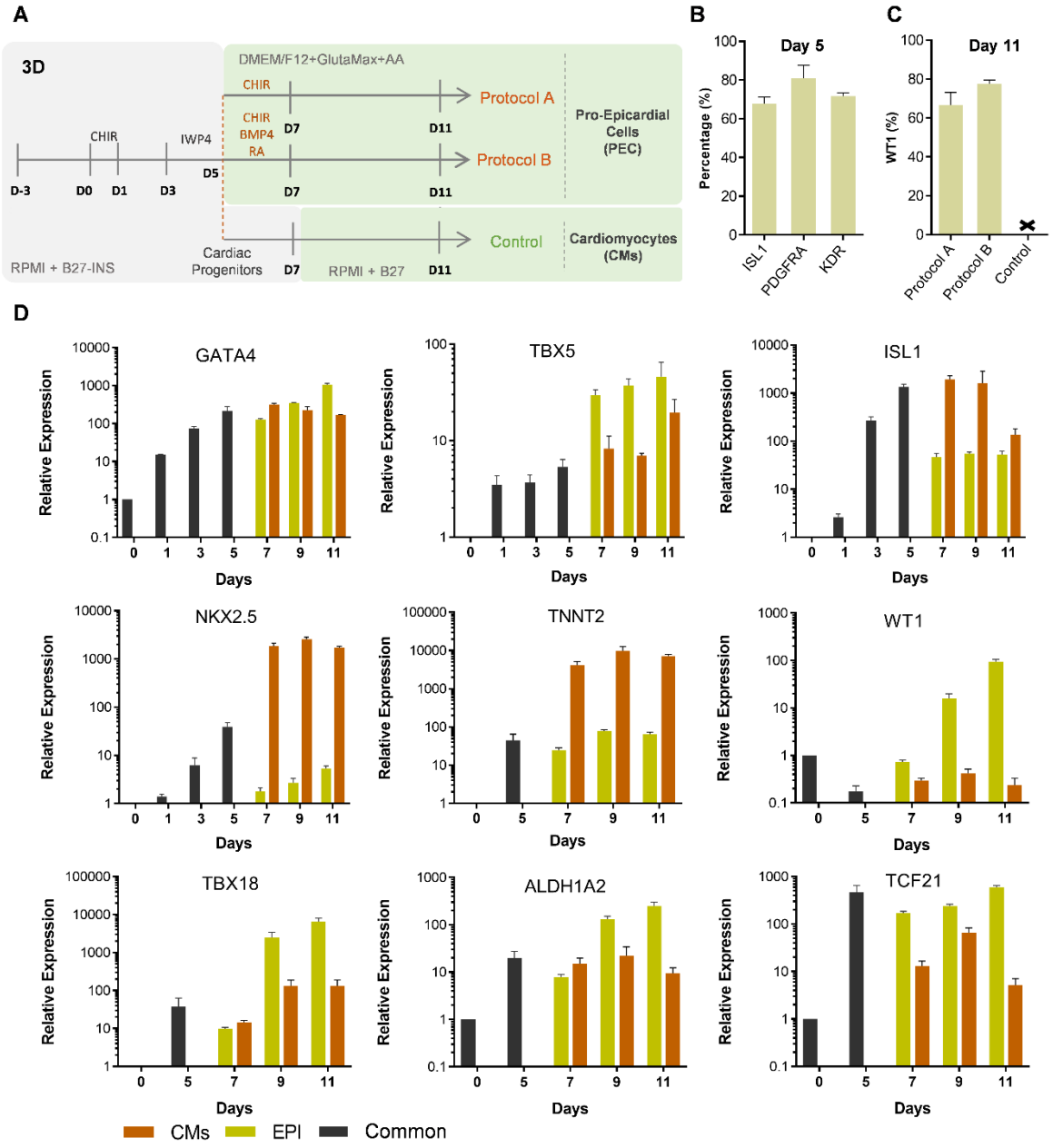

Figure III-1 Establishment of the protocol to generate PECs from hPSCs in a 3D environment. (A) Schematic representation of PECs differentiation from hPSC in a 3D culture system. Two different protocols were tested (Protocol A and B) for PECs generation. 3D CMs differentiation platform was used as control. (B) Average percentage of ISL1, CD309 (KDR) and CD140a (PDGFRA) positive cells at D5 of differentiation. Data are represented as mean ± SEM, n=4 independent experiments for ISL1 and CD309, and n=2 independent experiment for CD140a. (C) Percentage of WT1 positive cells after 11 days of PECs differentiation for the two tested protocols (Protocol A and B) and for the CM differentiation protocol. Data are represented as mean ± SEM, n=3 independent experiments. (D) Expression profile of *ISL1, NKX2.5, TBX5, GATA4, TNNT2, WT1, TCF21, ALDH1A2 and TBX18* genes from D0 up to D11 of differentiation for Protocol B and Control conditions.

CMs, orange bars, represent the Control differentiation protocol; EPI, green bars, represent the Protocol B differentiation; Common, blacks bars, represent the first days of hPSC differentiation which are common to both protocols. Values are normalized to *GAPDH* and to D0 of differentiation. Data are represented as mean ± SEM, of at least n=3 independent experiments.

Also, it has been described to be expressed and involved in PECs establishment (Watt et al., 2004). In agreement with this knowledge, the expression of *GATA4* in our model increased during the first days of differentiation, maintained the expression level in the case of CM differentiation process, and in the case of PECs differentiation, increased until D11. Regarding the CM marker *TNNT2*, no significant changes in the expression of these gene were observed after PECs induction, when compared to a considerable expected increase in expression in the control condition.

In conclusion, it was successfully established a 3D differentiation protocol that allows the generation of ± 80% $WT1^+$ cells after 11 days of differentiation, which represents a yield of ±5 PECs/hPSC, using, as a starting point, a progenitor cell population that is common to the previously established CM differentiation platform.

III.4.2 3D differentiated hPSC-PECs undergo EMT

An important feature of PECs is the capacity to undergo EMT and differentiate into SMCs and CFs. To test the capacity of the generated PECs to differentiate into those cells, we selected two different protocols based on the supplementation of largely reported regulators of EMT. The selected regulators, which were applied at D11 PECs and were maintained over 8 days of treatment, were (i) TGFβ1 for SMCs differentiation; and (ii) FGF2 for CFs generation (Bao et al., 2017)(Witty et al., 2014b). As control, it was used a culture condition where PECs were replated and maintained with the TGFβ signaling inhibitor A83 to prevent EMT (Bao et al., 2017). At the end of the differentiation period, samples from the different three protocols were collected and analyzed by qRT-PCR and immunostaining. Comparing the three conditions at D19 of differentiation, the A83-treated PECs showed a significantly higher expression of the epicardial markers, *WT1, TBX18*, *ALDH1A2 and TCF21* (Figure III-2A). It is interesting to highlight that, although at a lower expression level, *TCF21* and *TBX18* are also expressed in PECs-derived CFs and SMCs, respectively, as previously reported in the literature (Lupu et al., 2020a). Dissociation and replating of PECs, at low cell density, revealed that these cells adopted a cobblestone-like organization, typical of cultured primary epicardium, and expressed the pan-cadherin marker (Guadix et al., 2017), confirming the epithelial nature of these cells (Figure III-2B). Additionally, it was confirmed by immunostaining that epicardial cells were also $ALDH1A2^+$. This is a marker for aldehyde dehydrogenase enzyme, responsible for the conversation of retinol in RA, being an indicative of epicardial cells activity. On the other hand, when using the SMCs protocol, it was possible to observe an increased expression of the SMCs markers *MYH11*, *CNN1* and *ACTA2* compared with the two other tested protocols (Figure III-2A) and at D19 of differentiation, by immunostaining, the expression of α-SMA and CNN1 was confirmed in PECs-

derived SMCs (Figure III-2B). The expression of the fibroblast marker *PDGFRA* was enriched in the CF protocol (Figure III-2A) and at D19 of differentiation, high-density cultures of fibroblasts positively stained for ECM proteins fibronectin and collagen I, which were evenly distributed throughout the monolayer cultured cells, and for the fibroblast cytoskeletal protein vimentin (VIM) (Figure III-2B).

All together, these results indicate that hPSC-PECs generated in the 3D environment were capable of undergoing EMT and to differentiate into SMCs and CFs.

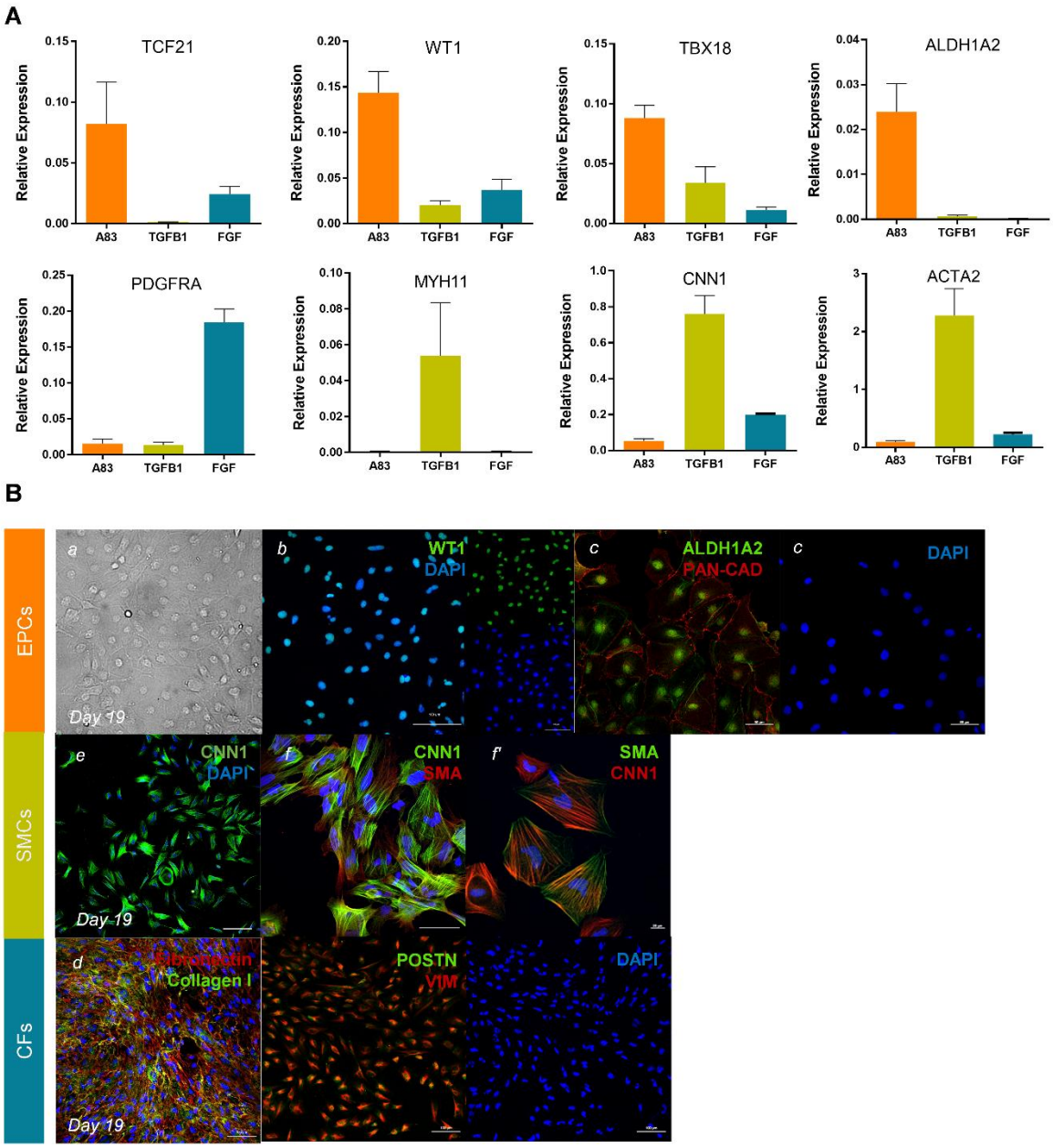

Figure III-2: PECs obtained from hiPSCs with the established 3D differentiation platform undergo EMT and differentiate into SMCs and CFs. (A) Expression profile of the epicardial cell markers *WT1, TCF21,*

ALDH1A2 and TBX18, SMCs markers *MYH11, ACTA2* and *CNN1,* and CFs marker *PDGFRA*, after 8 days of EMT differentiation protocols. A83 column represents the protocol used to maintain undifferentiated PECs in culture; TGFB1 column represents the protocol used to differentiate PECs into SMCs; and FGF column represents the protocol used to differentiate PECs into CFs. Values are normalized to *GAPDH*. Data are represented as mean ± SEM, of n=3 independent experiments, for A83 and TGFB1 protocols, and n=2 for FGF protocol. (B) Immunofluorescence analysis of replated D19 PECs, SMCs and CFs. Scale bars, 100 µm.

III.4.3 PEC aggregates show vascularization and co-emergent gut-like structures

In order to understand in more detail the cellular composition and the presence of any structural organization inside the D11 PEC aggregates, sections of the aggregates were analyzed by immunostaining. Two different regions were clearly distinguished including (1) an epithelial-like structure that stained positive for E-cadherin but was WT1 negative, surrounded by organized CD31^{+} endothelial-like cells (Figure III-3A *a, b* and *c*), and (2) a surrounding area that comprises the WT1^{+} cell population. It was confirmed by qRT-PCR that CD31 expression increases overtime in PECs differentiation protocol and, at D11, the expression of this endothelial marker is statistically significantly higher in D11 PEC aggregates compared with age matched CM aggregates (Figure III-3B). Additionally, it was also possible to confirm the positive staining for ALDH1A2 (Figure III-3A *d*) and for ECM proteins, specifically collagen IV, restricted to the area surrounding the epithelial structures, and collagen I, throughout the entire D11 PEC aggregate (Figure III-3A *e*).

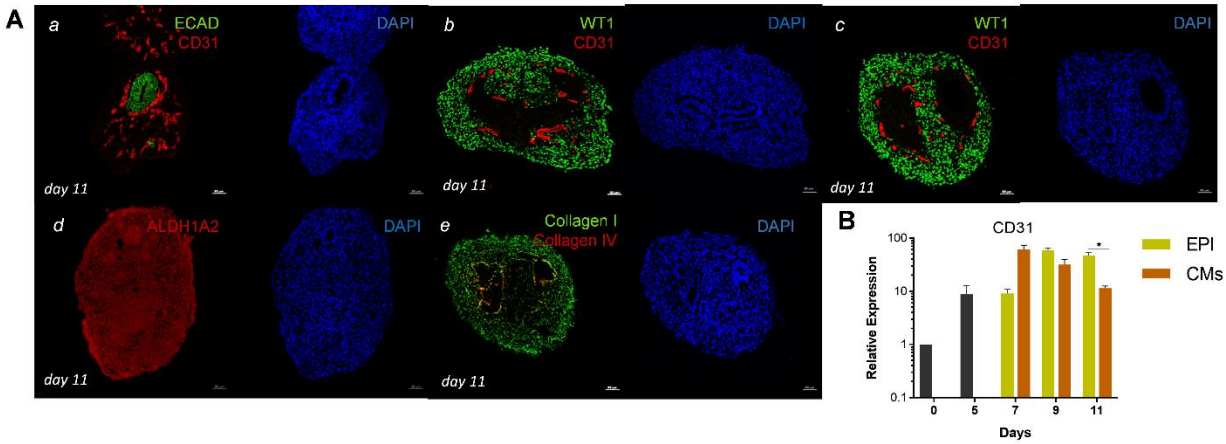

Figure III-3 Identification of different subpopulations of cells within PEC aggregates. (A) Immunofluorescence analysis of D11 PEC aggregate sections. Epithelial-like structures were identified with E-CAD expression, PECs were identified by expression of WT1, and endothelial-like cells were identified as CD31^{+}. Scale bars, 100 µm. (B) Expression profile of *CD31* gene from D0 up to D11 of differentiation in PECs and CMs differentiation conditions. Values are normalized to *GAPDH* and to D0 of differentiation. Data are represented as mean ± SEM, of at least n=3 independent experiments. Student´s t-test (two-tailed) statistics, * p<0.05.

In order to study the possibility of improving the vascularization and to disclose the identity of the epithelial structures present within the PEC aggregates, two additional set of experiments were performed.

III.4.3.1 VEGF signaling activation improves the vascularization within the PEC aggregates

To understand if D11 PEC aggregates could be enriched in the CD31 positive cell population, it was evaluated the addition of VEGF, a known growth factor involved in vascular cells specification and maintenance, from D7 until D11 of differentiation (Figure III-4A). The addition of this factor increased the expression level of CD31 throughout the differentiation process (Figure III-4B), which was reflected in an increment in the percentage of $CD31^+$ cells from 2 to 13% at D11 of differentiation (Figure III-4D), meaning that the progenitor cells present at D7 are still responsive to VEGF signaling. Addition of VEGF at D9 or even at D11 of PEC differentiation, had little or no effect, respectively, in the percentage of CD31 positive cells (data not shown). The incorporation of VEGF during the step of PECs induction (from D5 to D7) may also has an extra positive effect on the enrichment of endothelial-like cells, which will be further tested in future experiments. The increased expression of CD31 in PEC aggregates was also confirmed by immunostaining, in which an improved structural organization of $CD31^+$ cells was observed, with the establishment of micro vessels and lumens (Figure III-4E). Interestingly, the percentage of WT1 positive cells was not significantly affected by the addition of VEGF (Figure III-4C), suggesting that the progenitor population from where CD31 positive cells were derived is not the same as the one from where WT1 positive cells are generated. Interesting, Witty and colleagues, showed that the addition of VEGF had no impact on epicardial cell specification from hPSCs nor a contribution for CD31 positive cells generation in 2D monolayer culture (Witty et al., 2014c). However, it is important to take into consideration that the 3D environment of our model may favor the generation of different sub-populations of progenitor cells that can further contribute to the different cell populations observed inside the PEC aggregates.

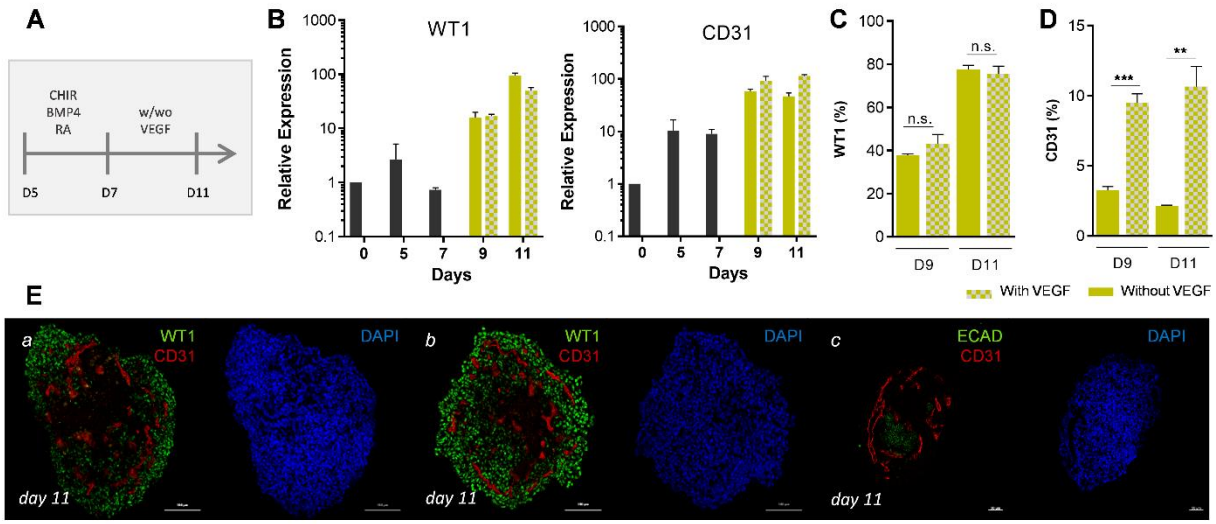

Figure III-4 VEGF treatment after the PECs induction period promotes enrichment of endothelial-like cells within the PEC aggregates. (A) Schematic representation of PECs differentiation protocol including the addition of VEGF from D7 to D11. w/wo VEGF means with or without VEGF addition. (B) Expression profile of the epicardial cell marker *WT1* and the endothelial cell marker CD31 throughout the differentiation into PECs and CMs. Values are normalized to GAPDH and to D0 of differentiation. Data are represented as mean ± SEM, of at least n=3 independent experiments. (C-D) Percentage of WT1 (C) and CD31 (D) positive cells after 9 and 11 days of PECs differentiation for the two tested protocols, with and without VEGF addition. Data are represented as mean ± SEM, n=3 independent experiments. Student´s t-test (two-tailed) statistics, ** p<0.005, *** p<0.0005, n.s., no statistically significant (p-value > 0.05). (E) Immunofluorescence analysis of replated D11 sections of PECs aggregates. Scale bar, 100 µm, in *a* and *b*; 50 µm, in *c*.

III.4.3.2 The epithelial structures present in D11 PEC aggregates represent gut-like tube structures

In order to identify the ECAD$^+$/WT1$^-$ cell population present in D11 PEC aggregates, two different hypotheses were tested including (1) the possibility that ECAD$^+$/WT1$^-$ cells represent a subpopulation of PECs inside the aggregates that may express other PEC markers, or (2) the possibility that the epithelial-like structure observed in D11 PEC aggregates has an endodermal origin.

Regarding the first hypothesis, some reports have described that PE is composed by different populations, one of them being identified by the expression of *SEMA3D* and *SCX* (Katz et al., 2012). Thus, it was decided to assess the expression of SEMA3D marker in PEC aggregates. Using *in situ* hybridization, it was possible to observe the staining of *SEMA3D* specifically in the epithelial structure (Figure III-5A), and by qRT-PCR it was confirmed a statistically significant higher expression of this marker in D11 PEC aggregates compared with D11 CM aggregates (Figure III-5B). Interestingly, SEMA3D positive cells have been described to influence the migration and organization of endothelial

cells in zebrafish (Hamm et al., 2016), which could justify the proximity between these two cell populations.

However, since there is no reported information regarding the existence of an epithelial-like structure within the PEO *in vivo*, it was assessed also the alternative hypothesis of an endodermal origin for the epithelial-like structure. To do so, the cell population at D5 of differentiation was further analyzed by flow cytometry. Using double staining for CXCR4, a mesendodermal marker, and C-KIT, which is expressed in endoderm and vascular progenitor cells but not in mesoderm progenitors, combined with additional expression analysis for the mesoderm markers KDR and PDGFRA, allowed the identification of different subpopulations in D5 aggregates. It was concluded that ±25% of the D5 cell population was $CXCR4^{+}/C\text{-}KIT^{+}/KDR^{-}/PDGFRA^{-}$ (Figure III-5C), meaning that, at this time point of differentiation, definitive endoderm progenitors are present in the aggregates (Zhang et al., 2018b)(Loh et al., 2014b)(Loh et al., 2016b). Additionally, ±5% of the analyzed cell population correspond to $CXCR4^{-}/C\text{-}KIT^{+}/KDR^{+high}/PDGFRA^{+}$ vascular progenitor cells (Yang et al., 2008)(Kattman et al., 2011c). The remaining cells, which were $CXCR4^{+}/C\text{-}KIT^{-}/KDR^{+low}/PDGFRA^{+}$, represent the mesoderm cell population (Bauwens et al., 2011) and account for ±62% of the total cell population. Taking into consideration the different types of cells that could be derived from endoderm progenitors, the expression of the kidney marker PAX2 and the gut progenitor cell marker CDX2 were analysed by immunostaining and qRT-PCR. By qRT-PCR analysis, it was possible to confirm that, specifically for the PEC differentiation protocol, there was a significantly higher expression of the endodermal marker *SOX17* at D7 of differentiation, right after the PEC induction period (Figure III-5D), and the expression of the gut progenitor marker *CDX2* started also to peak at D7 of PEC differentiation (Figure III-5E).

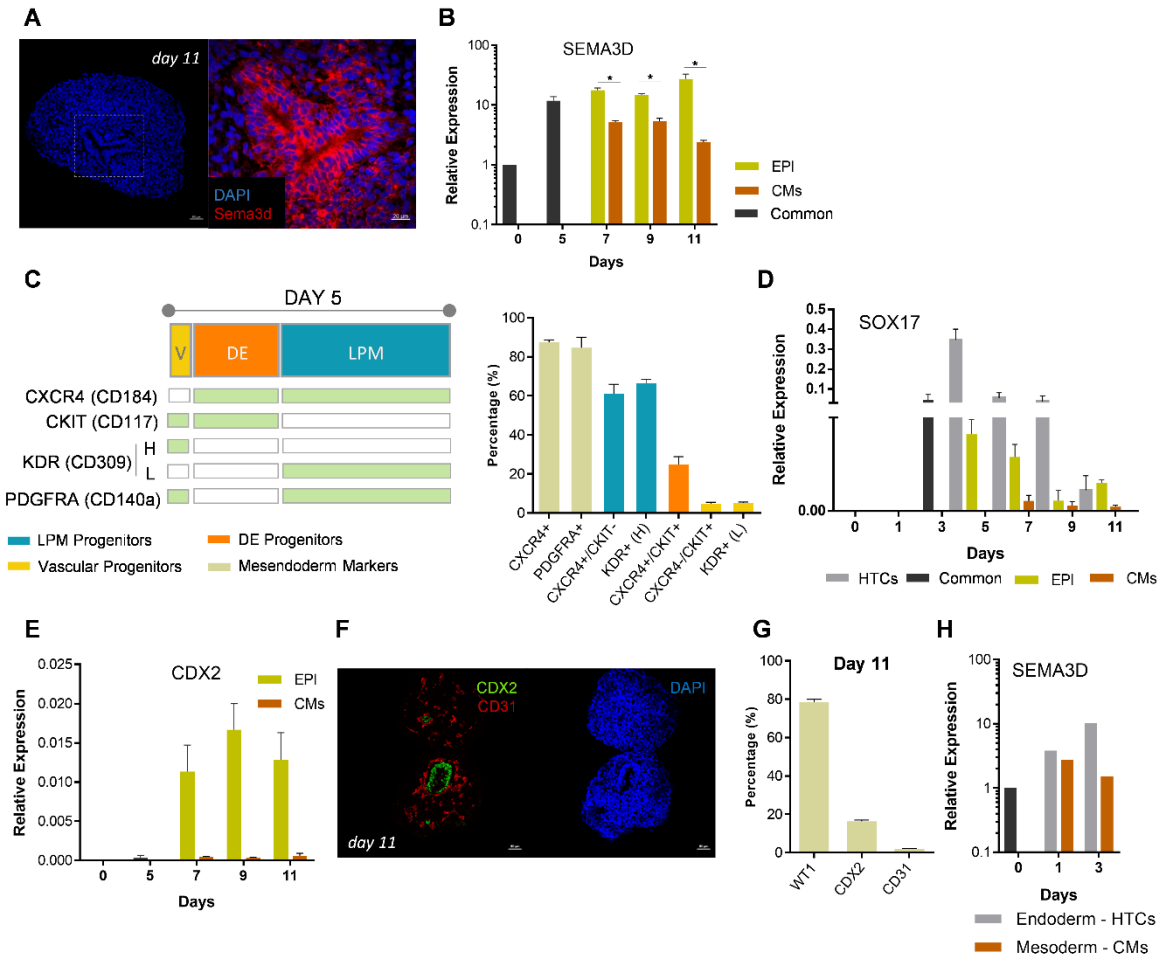

Figure III-5 PEC aggregates present CDX2⁺ gut-like structures. (A) Immunofluorescence / *in situ* hybridization analysis of D11 PE aggregates sections, highlighting the hybridization of Sema3d probe in the epithelial structure of PEC aggregates. Scale bars, 100 µm in DAPI staining and 20 µm in Sema3d/DAPI staining. (B) Expression profile of *SEMA3D* gene from D0 up to D11 of differentiation in PEC and CMs differentiation protocols. Values are normalized to *GAPDH* and to D0 of differentiation. CMs, orange bars, represent the CM differentiation protocol; EPI, green bars, represent the PEC differentiation protocol; Common, blacks bars, represent the first days of hPSC differentiation which are common to both protocols. Data are represented as mean ± SEM, of at least n=3 independent experiments. Student´s t-test (two-tailed) statistics, * p<0.05. (C-left) Schematic representation of the markers used to identify vascular (V), definitive endoderm (DE) and lateral plate mesoderm (LPM) progenitor cell populations. CXCR4^{+}/C-KIT^{+}/KDR^{-} population identifies DE; CXCR4^{-}/C-KIT^{+}/KDR^{+high} population identifies vascular progenitors, and CXCR4^{+}/C-KIT^{-}/KDR^{+low} population identifies mesoderm progenitors. DE progenitors are PDGFRA^{-} and V and LPM are PDGFRA^{+}. Green bars represent positive expression; white bars represent negative expression. (C-right) Percentage of CXCR4/C-KIT, KDR and PDGFRα populations at D5 of differentiation. Data from at least n=3 experiments. (D) Expression profile of *SOX17* from D0 up to D11 of differentiation in PEC (green bars) and CMs (orange bars) differentiation conditions. Data from hepatocyte differentiation protocol was used as positive control for endoderm differentiation (HTCs, grey bars) and obtained from the results of the PhD student João Cotovio. Common (black bars) refers to the first days of hPSC differentiation which are common to CM and PEC differentiation protocols. Values are

normalized to *GAPDH* and to D0 of differentiation. Data are represented as mean ± SEM, of at least n=3 independent experiments. (E) Expression profile of *CDX2* gene from D0 up to D11 of differentiation in PECs (green bars) and CMs (orange bars) differentiation conditions. Values are normalized to *GAPDH* and to D0 of differentiation. Data are represented as mean ± SEM, of at least n=3 independent experiments. (F) Immunofluorescence analysis of D11 PEC aggregate sections showing the staining of CDX2 in the epithelial structure. Scale bars, 50 µm. (G) Percentage of WT1, CD31 and CDX2 positive cells at D11 PEC aggregates. Data are represented as mean ± SEM, n=4 independent experiments for WT1 and CD31, and n=3 experiment for CDX2. (H) Expression profile of *SEMA3D* gene from D0 up to D3 of differentiation in the 3D cardiac differentiation protocol (CMs, orange bars) compared with 2D hepatocyte differentiation protocol (HTCs, grey bars). Values are normalized to *GAPDH* and to D0 of differentiation. Data are represented as mean ± SEM, of n=1 independent experiment.

By immunofluorescence it was also possible to confirm the CDX2 staining within the epithelial structure (Figure III-5F), and by flow cytometry the percentage of cells expressing CDX2 at D11 was determined to be ±16% (Figure III-5G). Interestingly, in a recent work from Rossi and co-workers it was observed the generation of very similar epithelial structures in mouse ES-derived gastruloids focused on cardiogenesis. The authors identified these structures as primitive gut tube-like structures (tube-shaped E-CAD positive epithelial tissue) and these were surrounded by a CD31-positive, putative endocardial-like layer, and were in proximity with the heart-like tube structure (Rossi et al., 2021). Although we did not analyse in detail the origin and characteristics of the ECs present in D11 PEC aggregates, it is possible that these cells represent also an endocardial-like population that generates from the vascular progenitor cells identified at D5 of differentiation.

Collectively, these results showed that, PEC aggregates contain $CDX2^+$ gut progenitor cells. Although it still needs further confirmation, one possible explanation to merge both hypothesis and justify also the expression of *SEMA3D* in the epithelial structure may be related with the involvement of this gene in endoderm specification as it has been indirectly suggested by Fisher and colleagues (Fisher et al., 2017). To test this hypothesis in our model, a preliminary experiment comparing the expression of *SEMA3D* in an endoderm differentiation protocol and in our 3D mesoderm differentiation model was performed, indicating a tendency for an overexpression of this gene in the endoderm protocol (Figure III-5H).

III.4.4 Towards the modulation of endoderm derived structures development in PEC aggregates

Aiming at mastering the modulation of the CDX2 positive population content present in PEC aggregates, two different strategies were analyzed including (1) the modulation of the PEC induction period through BMP and Wnt signaling pathways manipulation envisaging the elimination of the gut-like epithelial structure and (2) the manipulation of the Wnt signaling during the first days of hPSCs differentiation in order to try to minimize the generation of endoderm progenitor cells.

III.4.4.1 BMP and Wnt signaling manipulation during PEC induction phase influence PEC aggregate composition

In order to minimize the percentage of CDX2 positive cells within the PEC aggregates, it was first attempted the manipulation of the PEC induction step by testing different BMP4 and CHIR concentrations and combinations, as summarized in Figure III-6A. From the different tested conditions, it was possible to conclude that the reduction of CHIR concentration, for the same BMP4 dosage (50 ng/mL), potentiate the development of the $CDX2^+$ population and reduces the percentage of $WT1^+$ cells. Additionally, in the absence of Wnt signaling activation, increasing concentrations of BMP4 reduce also the $WT1^+$ cell population and potentiate the generation of $cTNT^+$ CMs, as it was also reported by Bao and colleagues (Bao et al., 2017). For the same concentration of CHIR, decreasing the BMP4 concentration from 50 ng/mL to 5 ng/mL doesn't seem to have impact on the $WT1^+$ cell population. Additionally, higher CHIR concentrations seem to reduce also de $WT1^+$ cell population. In conclusion, the protocol used in this study from the beginning, without further optimization, seems to be the one that maximizes the percentage of PECs present in the aggregates and that minimizes the $CDX2^+$ cell population. Additionally, it was possible to observe that the activation of the Wnt signaling at a specific concentration is the critical stimuli to induce PEC differentiation in the 3D platform.

Since some PECs differentiation protocols reported in the literature start the PEC induction with a mesoderm progenitor cell population that is not exposed to a Wnt signaling inhibition period (Iyer et al., 2015) (Witty et al., 2014a), it was decided also to test the induction of PECs differentiation at D3 instead of D5 of differentiation (Figure III-6B). Analysis of D3 progenitor cell population demonstrated also the existence of the three previously identified subpopulations, namely mesoderm (±58% $CXCR4^+/C\text{-}KIT^-$), endoderm (±36% $CXCR4^+/C\text{-}KIT^+$), and vascular progenitor cells (±3% $CXCR4^-/C\text{-}KIT^+$) (Figure III-6C). Interesting, starting the PECs induction at D3 allowed the generation of PEC aggregates with a percentage of ±78% of $WT1^+$ cells after 11 days of differentiation (Figure III-6D), which is similar to the value obtained at D11 for PECs induction at D5. However, with this new protocol, PEC aggregates still present the epithelial gut-like structure (Figure III-6E). From this result, it is possible to conclude that it is not mandatory to perform the step of Wnt signalling inhibition before PEC cells induction in our 3D PECs differentiation platform, opening the possibility of exploring this new protocol for further experiments.

In conclusion, these results demonstrate that it is not possible to completely eliminate the $CDX2^+$ cell population through manipulation of the PEC induction period nor by starting the PEC induction step earlier, at D3 of differentiation.

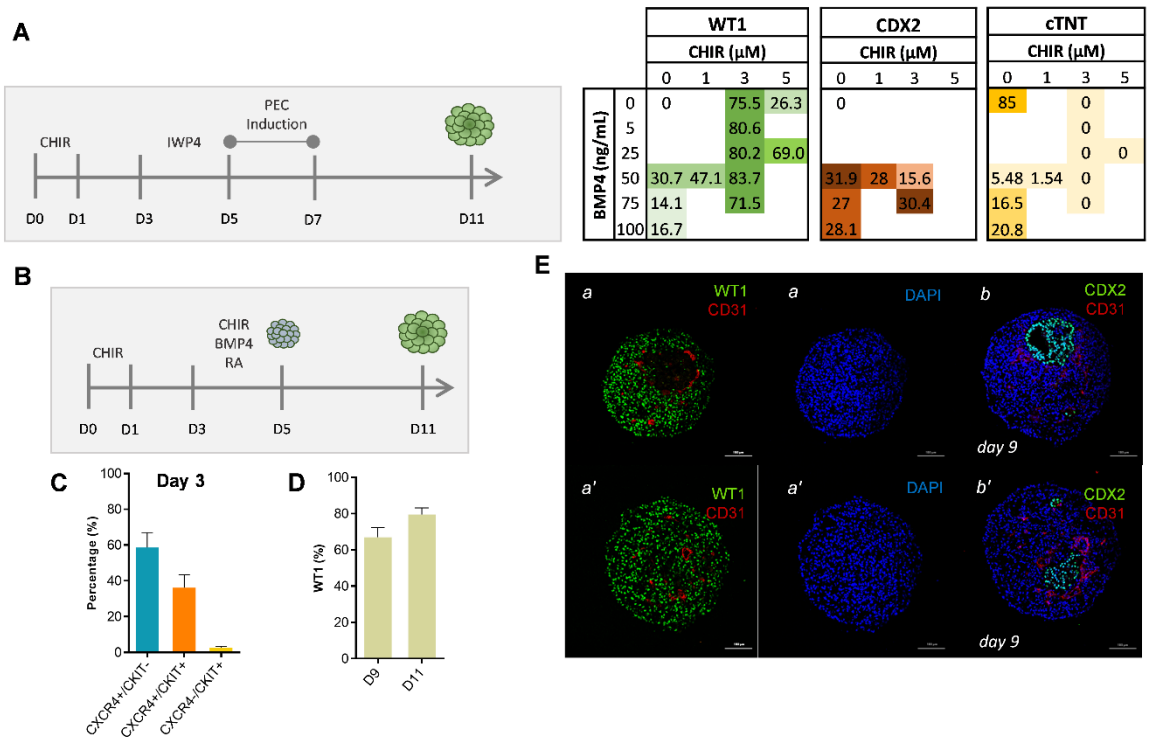

Figure III-6 Effect of BMP4 and Wnt signaling manipulation during the period of PECs induction on D11 PEC aggregate cell composition. (A) Effect of BMP concentration manipulation from 0 – 100 ng/mL and CHIR concentration from 0 – 5 µM on the percentage of WT1, CDX2 and cTNT positive cells at D11 of PEC aggregates, when starting the induction period at D5. The values correspond to percentages obtained by flow cytometry analysis from n=1 experiment for all the tested conditions, except for the one used as the starting point in this work (BMP4 50 ng/mL and CHIR 3µM), which represents the mean of n=11 independent experiments. RA concentration was fixed at 4µM for all the tested conditions. (B) Schematic representation of PECs differentiation protocol starting the PEC induction period at D3. (C) Percentage of CXCR4$^+$/C-KIT$^-$ (Mesoderm), CXCR4$^+$/C-KIT$^+$ (Endoderm), and CXCR4$^-$/C-KIT$^+$ (Vascular progenitors) cells in D3 population. Data are represented as mean ± SEM, n=4 independent experiments. (D) Percentage of WT1 positive cells at D9 and D11 in PEC aggregates, when starting PEC induction at D3. Data are represented as mean ± SEM, of n=3 and n=2 independent experiments in D9 and D11, respectively. (E) Immunofluorescence staining of D9 PEC aggregate sections when starting PEC induction at D3, highlighting the presence of epithelial CDX2$^+$-gut like structures. Scale bars, 100 µm.

III.4.4.2 Manipulation of Wnt signaling during the first stages of hPSC differentiation controls mesendoderm progenitor commitment

Continuing with the attempt to reduce the percentage of CDX2$^+$ cells in PEC aggregates, a different strategy was tested, based on the elimination of the endoderm progenitor population generated in the first days of hPSCs differentiation. In fact, it has been thoroughly described in the literature that the duration and timing of Wnt signalling activation and inhibition during the first days of hPSCs cardiac differentiation has a critical impact on hPSC fate determination (Kempf et al.,

2016a). Due to that, two different protocols, which reflect different Wnt signalling manipulation conditions, were tested (Figure III-7A and B). To evaluate the impact of the different tested protocols the percentage of (1) CXCR4, a mesendoderm marker, (2) PDGFRA, which is expressed in mesoderm progenitors, (3) KDR, which is expressed in LPM progenitor, and (3) C-KIT, which is expressed in endoderm progenitors, was assessed by flow cytometry. In both tested protocols, Wnt signalling inhibition had the duration of 2 days, equal to our 3D differentiation protocol. However, in the newly tested protocols this step was contiguous to the Wnt signalling activation period. The duration of Wnt signalling activation marked the difference between the two protocols, having been tested one day of activation (Figure III-7A) and two days of activation (Figure III-7B). Both protocols were effective on eliminating the C-KIT$^+$ endoderm progenitor population, however in the protocol with two days of Wnt signalling activation the percentage of cells expressing the mesoderm marker PDGFRA was also compromised (Figure III-7A). On the other hand, when applying only one day of Wnt signalling activation, this strategy allowed the generation of ±90% of mesoderm progenitor cells at D5 of differentiation. However, only ±30% of the cells present at D5 of differentiation were positive for the LPM marker KDR, which reflected on the low efficiency of PECs generation from this progenitor cell population (±40% WT1$^+$ cells) (Figure III-7C). The remaining mesodermal cells present at this time point of differentiation were identified as paraxial mesoderm progenitors, since the assessment of the expression profile of the paraxial mesoderm genes *TBX6* and *MSGN1* revealed an upregulation of these markers in the new developed protocol compared to the pre-established CM differentiation one (Figure III-7D).

In conclusion, further optimization of this early stage of hPSC differentiation is need to minimize the endoderm progenitor cells generation and maximize the LPM progenitor cell population.

III.5 DISCUSSION

In the past years, the optimization of protocols to obtain additional relevant cardiac cells apart from CMs have been reported in the literature. Epicardial cells have gain attention in the recent years and the generation of 2D-based PECs differentiation protocols from hPSCs have been recently described. The main objective of the present work was the adaptation of previously established 2D PEC differentiation protocols to a 3D format providing a more *in vivo* like environment that could bring functional advantages to the final obtained PECs, when compared to the ones obtained in 2D monolayer culture systems. Adding to that, since CMs and PECs developed from the same LPM progenitors, it was possible to take advantage of the previously described 3D CMs differentiation protocol by adapting it to generate PECs.

In this work, it was possible to obtain for the first time hPSC-derived PECs in a 3D environment in a robust way, starting from a progenitor cell population that is common to the CM differentiation protocol. The established platform generates ±80% of WT1$^+$ cells after 11 days of differentiation, representing a yield of 4x10^6 PECs/hPSC. The generated PECs show cobblestone-like organization,

typical of cultured primary epicardium, after replating, and undergo EMT and differentiate into CFs and SMCs. In spite of the high efficiency of PEC generation, ±16% of the cells present in the final PEC aggregates correspond to gut-like epithelial cells (CDX2^{+}). Through a deeper analysis of the first stages of differentiation, it was revealed that D5 aggregates comprise a mixed population of LPM, definitive endoderm and vascular progenitor cells, which was responsible for the generation of the endoderm-derived gut-like structures present in D11 PEC aggregates.

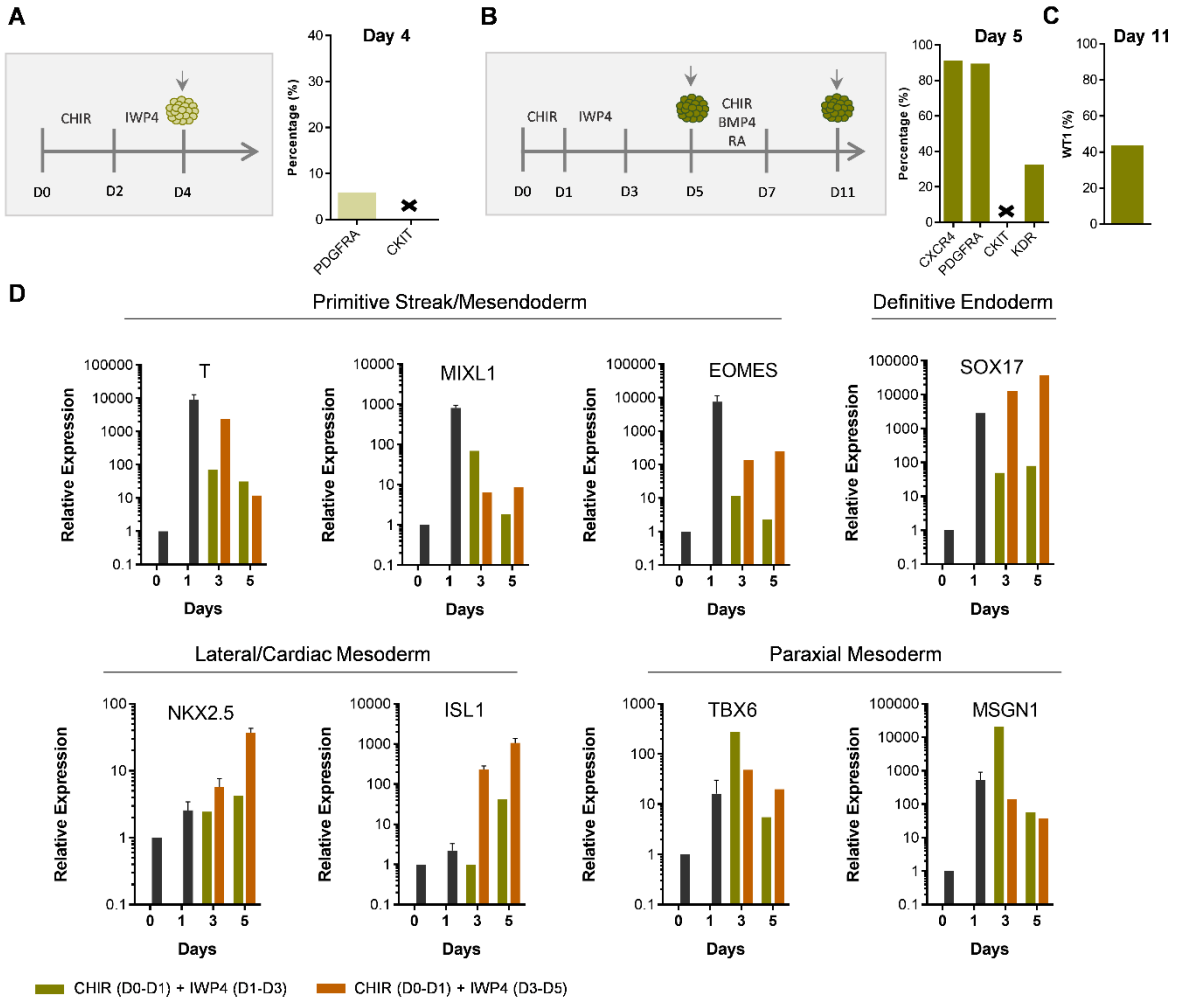

Figure III-7 Manipulation of Wnt signaling, during the first stages of hPSC differentiation, controls mesendoderm progenitor's commitment. (A) Percentage of CXCR4, PDGFRA and C-KIT positive cells at D4 of differentiation, using a period of Wnt signaling activation from D0 to D2 and Wnt signaling inhibition from D2 to D4. Data from n=1 independent experiment. (B-C) Percentage of CXCR4, PDGFRA, C-KIT and KDR positive cells at D5 of differentiation and WT1 positive cells at D11 of differentiation, using a period of Wnt signaling activation from D0 to D1 and Wnt signaling inhibition from D1 to D3. Data from n=1 independent experiment. Arrows in the scheme represent the collected time points for flow cytometry analysis. (D) Expression profile of *T, MIXL1, EOMES, SOX17, NKX2.5, ISL1, TBX6 and MSGN1* genes from D0 up to D5 of differentiation for two different protocols: orange bars present the protocol that uses Wnt signaling activation from D0 to D1 and Wnt signaling inhibition from D3 to D5, and green bars represent the protocol that uses Wnt signaling activation from

D0 to D1 and Wnt signaling inhibition from D1 to D3. Black bars, represent the first day of hPSC differentiation which is common to both protocols. Values are normalized to *GAPDH* and to D0 of differentiation. Data are represented as mean ± SEM, of at least n=1 independent experiment.

During embryonic development, precardiac mesoderm is in close proximity with the endoderm layer, which has been shown to play a crucial role in inducing embryonic cardiogenesis (Sugi and Lough, 1994)(Bauwens et al., 2011). Specifically, it is described that endodermal cells migrate along the outer surface of the LPM, ending up forming a bi-layered sheet of endoderm and mesoderm progenitors. The LPM further splits into an outer somatic mesoderm layer next to the ectoderm which gives rise to the limbs and body wall, and an inner splanchnic mesoderm layer, from where cardiac progenitors arise, which surrounds the epithelial gut tube (Han et al., 2020). It is clear that all of these events are tightly controlled by morphogenic events and spatial gradients of several signalling molecules. Since the present differentiation protocol occurs in a 3D environment, spatial gradients of molecules, oxygen and nutrients are naturally formed inside the aggregates, which are certainly involved in promoting the establishment of the different subpopulations of progenitor cells that were observed inside the 3D cardiac aggregates. In fact, the presence of three different subpopulations in D5 aggregates proves that the 3D environment potentiates a more *in vivo*-like environment that contributes for the co-emergence of endoderm and mesoderm populations, which, as described above, interact and are in close proximity *in vivo*. Although not assessed in this work, it will be now interesting to evaluate if these two populations have a specific spatial organization inside the aggregates, and how they evolve throughout the differentiation. The generation of co-emerged mesoderm and endoderm progenitor cell populations in a 3D cardiac differentiation protocol has been previously reported by Bauwens and colleagues (Bauwens et al., 2011). They proved that, even in the presence of a defined medium that contains factors that specify for cardiac commitment, aggregate size controlled cardiac differentiation efficiency. The effect of aggregate size on controlling CMs differentiation outcome was related with the development of an endoderm population in the 3D aggregates. Although in their model a different endoderm population was generated, they suggested that definitive endoderm progenitors could have also an impact on CM differentiation, specifically in SHF progenitor-like cells. In the present 3D cardiac differentiation protocol, where it was generated simultaneously LPM and definitive endoderm progenitor cells, the presence of this endoderm population at early stages of differentiation did not affect the final efficiency of CM production, as confirmed in the previous and also in the present chapter. In fact, the endoderm population may be involved in the faster and improved commitment of cardiac cells in the 3D model, compared with the 2D differentiation process, as observed in chapter II. This new data regarding our 3D CM differentiation platform motivates future studies to deeply understand the effect of endoderm-secreted factors on cardiogenesis.

The presence of endoderm progenitor cells before the PEC induction period potentiated the generation of gut-tube-like structures ($CDX2^+$). In an attempt to reduce the CDX2 population inside

the PEC aggregates, a series of different experiments were performed and two different strategies were tested including (1) the manipulation of Wnt and BMP signalling during the PEC induction period, to evaluate if the CDX2 population is affected, and (2) the manipulation of Wnt signaling, including duration and timing of Wnt signaling activation and inhibition, during the first stages of hPSCs differentiation to eliminate the endoderm progenitors at D5 population.

From the first tested hypothesis it was possible to take some interesting conclusions namely that (1) activation of Wnt signaling at a specific concentration is the critical stimuli to induce PEC cells differentiation in our 3D platform, (2) BMP4 signaling activation at low concentration (≤50 ng/mL) increases the efficiency of differentiation, although the elimination of the activation of this pathway also allows the generation of epicardial-like cells at high efficiencies (>70% $WT1^{+}$), (3) the elimination of Wnt activation during the PEC induction and increasing BMP concentration promote the generation of CMs, and (4) the step of Wnt signaling inhibition is not mandatory before PEC induction. However, none of the tested conditions allowed the reduction of the percentage of CDX2 positive cells in the final PEC aggregates. Interestingly, Wnt signaling has been described to play an important role in intestine specification from endoderm, specifically it has been described that Wnt signaling activates CDX2 expression in both mouse and human ES-derived anterior endoderm cells (Sherwood et al., 2011). The activation of Wnt signalling in DE progenitor cells in the presence of the inhibitor Notch signalling DAPT (Ogaki et al., 2015)(Takayama et al., 2019) or FGF4 (Spence et al., 2011) has been also described to induce the generation of $CDX2^{+}$ hindgut progenitor cells. Additionally, a recent protocol that generates intestinal organoids, uses a combination of Wnt, BMP and RA activation to induce the specification of endodermal cells into intestinal epithelial lineage (Mithal et al., 2020). Taking into consideration that the stimuli necessary to induce intestinal progenitor cells from DE and the ones that are needed to induce LPM cells to differentiate into PECs are similar, this may justify the fact that it is not possible to completely abolish the CDX2 positive cells present in PEC aggregates.

From the second tested hypothesis it was possible to conclude that the continuous manipulation of Wnt signalling at the first stages of hPSCs differentiation, meaning Wnt signalling activation from D0 to D1 and Wnt signalling inhibition from D1 to D3, resulted in the generation of a D5 progenitor cell population in which endoderm progenitor cells were not detected and, although it was possible to potentiate the mesoderm population, only 30% of that population represented LPM, being the remaining cells presumably paraxial mesoderm progenitors. These results confirmed the impact that slight differences in Wnt signalling have on mesendoderm commitment form hPSCs, as already deeply reported in the literature. A recent report showed that after Wnt signaling activation for one day, the continuous activation of this pathway, at a lower level, until the Wnt signaling inhibition step, potentiates mesoderm specification and limits the induction of endoderm progenitors (Zhao et al., 2019a). Additionally, it has been also described that BMP plays a crucial role in controlling the patterning of PS progenitors into paraxial or lateral mesoderm progenitors. Specifically, the exogenous activation of BMP signaling using BMP4 after one day of CHIR treatment has been described to potentiate the PDGFRA/KDR LPM population (Tan et al., 2013) (Loh et al., 2016b).

Based on this information, further experiments will be explored to find the condition that will allow the maximization of LPM progenitor specification in our 3D platform and consequently the elimination of gut-like progenitor cells in PEC aggregates.

Regarding the vascularization observed in PEC aggregates, although the origin of the ECs was not analysed in detail, it is possible that these cells represent an endocardial-like population that arises from the vascular progenitor cells identified at D5 of differentiation. Since in D11 CM aggregates the presence of CD31 positive cells was not as evident as in D11 PEC aggregates, and both protocols initiate from the same D5 progenitor population, it is possible that the PEC induction period favours the expansion of the vascular progenitor cell population identified. Alternatively, it could be also suggested that the CD31 positive cells originate from the $WT1^+$ cells. However, the addition of VEGF after the PEC induction period promoted the enrichment of CD31 positive cells on PEC aggregates without compromising the percentage of WT1 positive cells, which strengths the hypothesis of the ECs being originated from a mesoderm vascular progenitor cell population rather than from the epicardial cell population.

III.6 CONCLUSIONS

Overall, in this chapter it was developed an efficient platform to generate hPSC-PECs *in vitro* in a 3D environment which allowed to enrich the knowledge regarding the main signalling cues involved in PECs specification from hPSCs and how they can be manipulated to potentiate hPSC-PECs generation. It was also demonstrated that slight differences in Wnt signalling manipulation can deeply impact the trajectory of hPSCs commitment, as already deeply reported in the literature. This knowledge can now be used to improve the 3D PECs differentiation model by controlling the generation of endoderm progenitor cells. Knowing the potential use of hPSC-PECs in the context of a cell therapy for regenerative medicine applications, the developed protocol can be easily improved towards the production of a pure population of PECs. Finally, these cells can be added to more complex multicellular cardiac models to be used in *in vitro* applications, as it will be explored in the next chapter.

III.7 REFERENCES

Bao, X., Lian, X., Hacker, T.A., Schmuck, E.G., Qian, T., Bhute, V.J., Han, T., Shi, M., Drowley, L., Plowright, A.T., et al. (2017). Long-term self-renewing human epicardial cells generated from pluripotent stem cells under defined xeno-free conditions. Nat. Biomed. Eng. *1*, 1–12.

Bargehr, J., Ong, L.P., Colzani, M., Davaapil, H., Hofsteen, P., Bhandari, S., Gambardella, L., Novère, N. Le, Iyer, D., Sampaziotis, F., et al. (2019). regeneration. Nat. Biotechnol. *37*.

Bauwens, C.L., Song, H., Thavandiran, N., Ungrin, M., Massé, S., Nanthakumar, K., Seguin, C., and Zandstra, P.W. (2011). Geometric control of cardiomyogenic induction in human pluripotent stem cells. Tissue Eng. *17*, 1901–1909.

Cano, E., Carmona, R., Ruiz-Villalba, A., Rojas, A., Chau, Y.Y., Wagner, K.D., Wagner, N., Hastie, N.D., Muñoz-Chápuli, R., and Pérez-Pomares, J.M. (2016). Extracardiac septum transversum/proepicardial endothelial cells pattern embryonic coronary arterio-venous connections. Proc. Natl. Acad. Sci. U. S. A. *113*, 656–661.

Fisher, J.B., Pulakanti, K., Rao, S., and Duncan, S.A. (2017). GATA6 is essential for endoderm formation from human pluripotent stem cells. Biol. Open *6*, 1084–1095.

Guadix, J.A., Orlova, V. V., Giacomelli, E., Bellin, M., Ribeiro, M.C., Mummery, C.L., Pérez-Pomares, J.M., and Passier, R. (2017). Human Pluripotent Stem Cell Differentiation into Functional Epicardial Progenitor Cells. Stem Cell Reports *9*, 1754–1764.

Hamm, M.J., Kirchmaier, B.C., and Herzog, W. (2016). Sema3d controls collective endothelial cell migration by distinct mechanisms via nrp1 and plxnD1. J. Cell Biol. *215*, 415–430.

Han, L., Chaturvedi, P., Kishimoto, K., Koike, H., Nasr, T., Iwasawa, K., Giesbrecht, K., Witcher, P.C., Eicher, A., Haines, L., et al. (2020). Single cell transcriptomics identifies a signaling network coordinating endoderm and mesoderm diversification during foregut organogenesis. Nat. Commun. *11*.

Hatcher, C.J., Diman, N.Y.S.G., Kim, M.S., Pennisi, D., Song, Y., Goldstein, M.M., Mikawa, T., and Basson, C.T. (2004). A role for Tbx5 in proepicardial cell migration during cardiogenesis. Physiol. Genomics *18*, 129–140.

Iyer, D., Gambardella, L., Bernard, W.G., Serrano, F., Mascetti, V.L., Pedersen, R.A., Talasila, A., and Sinha, S. (2015). Robust derivation of epicardium and its differentiated smooth muscle cell progeny from human pluripotent stem cells. Development *142*, 1528–1541.

Kattman, S.J., Witty, A.D., Gagliardi, M., Dubois, N.C., Niapour, M., Hotta, A., Ellis, J., and Keller, G. (2011). Stage-specific optimization of activin/nodal and BMP signaling promotes cardiac differentiation of mouse and human pluripotent stem cell lines. Cell Stem Cell *8*, 228–240.

Katz, T.C., Singh, M.K., Degenhardt, K., Rivera-Feliciano, J., Johnson, R.L., Epstein, J.A., and Tabin, C.J. (2012). Distinct Compartments of the Proepicardial Organ Give Rise to Coronary Vascular Endothelial Cells. Dev. Cell *22*, 639–650.

Kempf, H., Olmer, R., Haase, A., Franke, A., Bolesani, E., Schwanke, K., Robles-Diaz, D., Coffee, M., Göhring, G., Dräger, G., et al. (2016). Bulk cell density and Wnt/TGFbeta signalling regulate mesendodermal patterning of human pluripotent stem cells. Nat. Commun. *7*, 13602.

Lian, X., Zhang, J., Azarin, S.M., Zhu, K., Hazeltine, L.B., Bao, X., Hsiao, C., Kamp, T.J., and Palecek, S.P. (2013). Directed cardiomyocyte differentiation from human pluripotent stem cells by modulating Wnt/β-catenin signaling under fully defined conditions. Nat. Protoc. *8*, 162–175.

Loh, K.M., Ang, L.T., Zhang, J., Kumar, V., Ang, J., Auyeong, J.Q., Lee, K.L., Choo, S.H., Lim, C.Y.Y., Nichane, M., et al. (2014). Efficient endoderm induction from human pluripotent stem cells by logically directing signals controlling lineage bifurcations. Cell Stem Cell *14*, 237–252.

Loh, K.M.M., Chen, A., Koh, P.W.W., Deng, T.Z.Z., Sinha, R., Tsai, J.M.M., Barkal, A.A.A., Shen, K.Y.Y., Jain, R., Morganti, R.M.M., et al. (2016). Mapping the Pairwise Choices Leading from Pluripotency to Human Bone, Heart, and Other Mesoderm Cell Types. Cell *166*, 451–467.

Lupu, I.-E., Redpath, A.N., and Smart, N. (2020). Spatiotemporal Analysis Reveals Overlap of Key Proepicardial Markers in the Developing Murine Heart. Stem Cell Reports *14*, 770–787.

Mithal, A., Capilla, A., Heinze, D., Berical, A., Villacorta-Martin, C., Vedaie, M., Jacob, A., Abo, K., Szymaniak, A., Peasley, M., et al. (2020). Generation of mesenchyme free intestinal organoids from human induced pluripotent stem cells. Nat. Commun. *11*.

Ogaki, S., Morooka, M., Otera, K., and Kume, S. (2015). A cost-effective system for differentiation of intestinal epithelium from human induced pluripotent stem cells. Sci. Rep. *5*, 1–11.

Rossi, G., Broguiere, N., Miyamoto, M., Kelly, R.G., Kwon, C., Lutolf, M.P., Rossi, G., Broguiere, N., Miyamoto, M., Boni, A., et al. (2021). Article Capturing Cardiogenesis in Gastruloids Article Capturing Cardiogenesis in Gastruloids. Stem Cell 1–11.

Sherwood, R.I., Maehr, R., Mazzoni, E.O., and Melton, D.A. (2011). Wnt signaling specifies and patterns intestinal endoderm. Mech. Dev. *128*, 387–400.

Spence, J.R., Mayhew, C.N., Rankin, S.A., Kuhar, M.F., Vallance, J.E., Tolle, K., Hoskins, E.E., Kalinichenko, V. V., Wells, S.I., Zorn, A.M., et al. (2011). Directed differentiation of human pluripotent stem cells into intestinal tissue in vitro. Nature *470*, 105–110.

Sugi, Y., and Lough, J. (1994). Anterior endoderm is a specific effector of terminal cardiac myocyte differentiation of cells from the embryonic heart forming region. Dev. Dyn. *200*, 155–162.

Takayama, K., Negoro, R., Yamashita, T., Kawai, K., Ichikawa, M., Mori, T., Nakatsu, N., Harada, K., Ito, S., Yamada, H., et al. (2019). Generation of Human iPSC–Derived Intestinal Epithelial Cell Monolayers by CDX2 Transduction. Cmgh *8*, 513–526.

Tan, J.Y., Sriram, G., Rufaihah, A.J., Neoh, K.G., and Cao, T. (2013). Efficient derivation of lateral plate and paraxial mesoderm subtypes from human embryonic stem cells through GSKi-mediated differentiation. Stem Cells Dev. *22*, 1893–1906.

Watt, A.J., Battle, M.A., Li, J., and Duncan, S.A. (2004). GATA4 is essential for formation of the proepicardium and regulates cardiogenesis. Proc. Natl. Acad. Sci. U. S. A. *101*, 12573–12578.

Witty, A.D., Mihic, A., Tam, R.Y., Fisher, S.A., Mikryukov, A., Shoichet, M.S., Li, R.K., Kattman, S.J., and Keller, G. (2014a). Generation of the epicardial lineage from human pluripotent stem cells. Nat. Biotechnol. *32*, 1026–1035.

Witty, A.D., Mihic, A., Tam, R.Y., Fisher, S.A., Mikryukov, A., Shoichet, M.S., Li, R.K., Kattman, S.J., and Keller, G. (2014b). Generation of the epicardial lineage from human pluripotent stem cells. Nat. Biotechnol. *32*, 1026–1035.

Witty, A.D., Mihic, A., Tam, R.Y., Fisher, S.A., Mikryukov, A., Shoichet, M.S., Li, R.K., Kattman, S.J., and Keller, G. (2014c). Generation of the epicardial lineage from human pluripotent stem cells. Nat. Biotechnol. *32*, 1026–1035.

Yang, L., Soonpaa, M.H., Adler, E.D., Roepke, T.K., Kattman, S.J., Kennedy, M., Henckaerts, E., Bonham, K., Abbott, G.W., Linden, R.M., et al. (2008). Human cardiovascular progenitor cells develop from a KDR+ embryonic-stem-cell-derived population. Nature *453*, 524–528.

Zhang, R.R., Koido, M., Tadokoro, T., Ouchi, R., Matsuno, T., Ueno, Y., Sekine, K., Takebe, T., and Taniguchi, H. (2018). Human iPSC-Derived Posterior Gut Progenitors Are Expandable and Capable of Forming Gut and Liver Organoids. Stem Cell Reports *10*, 780–793.

Zhao, J., Cao, H., Tian, L., Huo, W., Zhai, K., Wang, P., Ji, G., and Ma, Y. (2017). Efficient Differentiation of TBX18+/WT1+ Epicardial-Like Cells from Human Pluripotent Stem Cells Using Small Molecular Compounds. Stem Cells Dev. *26*, 528–540.

Zhao, M., Tang, Y., Zhou, Y., and Zhang, J. (2019). Deciphering Role of Wnt Signalling in Cardiac Mesoderm and Cardiomyocyte Differentiation from Human iPSCs: Four-dimensional control of Wnt pathway for hiPSC-CMs differentiation. Sci. Rep. *9*, 19389.

IV. INTEGRATION OF EPICARDIAL CELLS IN 3D CARDIAC ORGANOIDS IMPACTS CARDIOMYOCYTE STRUCTURAL AND FUNCTIONAL MATURATION

IV.1 ABSTRACT

The development of *in vitro* 3D cardiac models that better recapitulate the human heart in terms of cell diversity and structural complexity is being the focus of a great attention in the past years. In this chapter, hPSC-derived PECs were explored towards the development of a more complex 3D cardiac model. To do so, a 3D co-culture platform between hPSC-CMs and hPSC-PECs was developed allowing the successful recapitulation of important aspects of the early embryonic heart development and the generation of 3D cardiac organoids exhibiting multicellular composition, structural organization and functional maturation compared with age matched 3D CM aggregates. Particularly, these co-cultured aggregates were shown to present (1) a continuous $WT1^+$ epicardial-like layer surrounding a $cTNT^+$ CM core, (2) a CM core with two distinct areas; an outer layer, contiguous to the epicardial cells, more compact and containing more aligned and proliferative CMs, and an inner area where CMs present a loose organization, (3) an enriched staining for the gap junction Cx43 within the CM core, particularly enhanced near the epicardial layer, (4) an enrichment in fibroblast/ECM proteins surrounding the organoid and within the CM core, and (5) an improved network of vascular cells,. Although further improvements of the 3D cardiac model are still being addressed and CM functional assessment and further maturation are still being pursued, this platform constitutes the initial point towards the use of this 3D cardiac organoid model in different contexts, namely in disease modelling of cardiomyopathies, and in cardiotoxicity and drug screening settings.

IV.2 INTRODUCTION

The development of complex cardiac MTs *in vitro*, combining different cardiac cells in a 3D environment, has emerged as an interesting alternative to 2D monolayer culture models and even 3D CM aggregates, to better mimic the complexity and dynamic network of interactions and signals that are present in the human heart tissue (Ma et al., 2015; Warmflash et al., 2014), and consequently a more reliable cardiac model for different applications. In fact, cardiac models in which only CMs are present, do not recapitulate the *in vivo* environment of the heart, where CFs and vascular cells interact with and strongly impact CMs behaviour. CFs are critical for ECM production, allowing the maintenance of the 3D structure of the heart, and modulate and interfere with the electrical behaviour of CMs (Klesen et al., 2018). On the other hand, cardiac vascular cells play a critical role not only during the first stages of embryonic heart development but also in myocardium structural and functional maturation and survival.

Knowing the relevance that non-cardiomyocyte cardiac cells represent in the heart microenvironment and myocardium function, different studies have explored the effect of co-culturing hPSC-derived CMs with different cardiac cells, namely CFs, vascular cells, including ECs and mural cells, and epicardial cells, on CM structural and functional maturation in 2D and 3D models, including 3D spheroids and EHTs. To do so, the majority of these models are normally obtained through the combination of (1) terminally differentiated hPSC-derived CMs, (2) primary cultured ECs and fibroblasts, which in some cases do not have a cardiac origin, and (3) ECM proteins, at different proportions to recapitulate the composition of the human heart. Only recently it has been described a 3D multicellular spheroid that does not use primary ECs and CFs, and instead combines CMs/ECs/CFs derived from the same hPSC-derived mesoderm population (Giacomelli et al., 2020).

These 3D cardiac models present a degree of complexity and maturation greater than 2D-cultured CMs or even greater than 3D aggregates composed only of CMs, but they still lack structural organization and, in some cases, lack functional interaction between the different cardiac cells. A different strategy, still poorly explored in the literature, may consist in the generation of hPSC-derived organoids where cardiac cells emerge from the same initial hPSC culture and self-organize in a controlled, functional and 3D *in vivo*-like manner, mimicking aspects of the architecture, cellular composition, and function of the cardiac tissue. The 3D cardiac model that better complies with the definition of a cardiac organoid was recently described in the literature (Hofbauer et al., 2020). Through manipulation of different signaling pathways involved in cardiogenesis, the authors were able to control the self-organization and morphogenesis inside the 3D cardiac aggregates, having been possible to recreate chamber-like cavity structures and also myocardium and endocardium layers.

In this work, it was decided to explore the use of epicardial cells to develop a multicellular 3D cardiac model. Knowing the relevance of PECs in human heart development, as highlighted in

chapter III, the main objective herein was to combine the findings of chapter II and III and recreate the development of an epicardial layer in our previously described 3D CM aggregates. The main expected outcomes behind this strategy were (1) to promote the enrichment of the 3D cardiac model in fibroblasts and vascular cells, by taking advantage of the capacity that PEC cells have to undergo EMT, and also (2) to improve the cardiac MT function and structural maturation. To do so, PEC aggregates generated in the context of chapter III and CM aggregates described in chapter II were used to establish a co-culture system. With this model, it was possible to generate 3D cardiac organoids that self-organized in a complex and well-defined structure, which (1) present a continuous $WT1^+$ epicardial-like layer surrounding a CM core, (2) show a CM core with two distinct layers, an outer layer, contiguous to the epicardial layer, which is more compact and contains more aligned and proliferative CMs, and an inner area where CMs present a loose organization, (3) show an enriched staining for the gap junction Cx43 within the CM core, particularly enhanced near the epicardial layer, (4) show an enrichment in fibroblast/ECM proteins surrounding the organoids and within the CM core, (5) show an improved network of vascular cells, and (6) present evidences of improved functional maturation in comparison with 3D CM aggregates.

IV.3 MATERIALS AND METHODS

IV.3.1 Establishment of a co-culture system between hPSC-CMs and hPSC-PECs

To establish the co-culture system, D11 CMs and D11 PECs aggregates were singularized using 0.25% Trypsin-EDTA for 7 min at 37ºC. After cell counting, both cell types were combined at a proportion of 85%CMs:15%PECs and re-aggregated using microwell plates (AggreWell™800, StemCell Technologies). Cells were plated at a cell density of $3.3x10^6$ cells/well in DMEM/F12+Glutamax+Ascorbic acid supplemented with 10µM ROCKi. For control, CMs aggregates alone were also re-aggregated using the same method. After 24 hours, the aggregates were removed from the aggrewell plate, seeded in 6-well ULA plates for 6 days, and the medium was supplemented with 5 ng/mL FGF2 and 50 ng/mL VEGF in the mentioned experiments. After that time, each 3D cardiac aggregate was transferred and maintained in a well of a 24-well ULA plate, for the remaining time of co-culture, without medium supplementation.

IV.3.2 Flow Cytometry Analysis

For flow cytometry analysis, 3D aggregates were washed with PBS and then singularized with 0.25% trypsin-EDTA or with TrypLE 1X, in the case of surface markers analysis, at 37ºC for 7 min. For enzymatic digestion neutralization, FBS-containing medium was added. After centrifugation and washing the cell pellet, cells were fixed with 2% PFA reagent for 20 minutes at RT or stored at 4ºC. For cell surface marker analysis, cells were washed twice with PBS and re-suspended in primary

antibody (Table IV-1) diluted in PBS + 2%(v/v) BSA, at approximately 500,000 cells per condition, and incubated for 30 min at RT. Afterwards, cells were washed with PBS and re-suspended in secondary antibody diluted in FACS buffer for another 15 min, at RT in the dark. In the case of conjugated antibodies, a single incubation period of 30 minutes at RT and in the dark was performed. Finally, cells were washed twice with PBS for a final volume of 300 µL/FACS tube. For intracellular marker analysis, cells were first incubated with 90% (v/v) cold methanol at 4ºC for 15 min. Cells were then washed 3 times with a solution constituted by 0.5% BSA solution in PBS. Cell pellet was resuspended and incubated with the primary antibody diluted in 0.1% Triton X-100 and 0.5% BSA in PBS, at RT for 1 h. After incubation, cells were washed twice and cell pellet was resuspended and incubated in the secondary antibody at RT for 30 min in the dark.

IV.3.3 Immunostaining Analysis

Sample collection. 2D replated cardiac cells were fixed in 4% PFA for 20 min at RT. 3D aggregates were fixed in 4% PFA at 4ºC for 30 min in an agitation platform. After PFA removal, cells were stored in PBS at 4ºC for further analysis. 3D aggregates were incubated in 15% (m/v) sucrose in PBS, at 4ºC overnight and afterwards embedded in 7.5%/15% gelatin/sucrose and frozen in isopenthane at -80ºC. Aggregates with ten/twelve-µm sections were cut on a cryostat-microtome (Leica CM3050S, Leica Microsystems), collected on Superfrost™ Microscope Slides (Thermo Scientific) and stored at -20ºC. Sections were then de-gelatinized for 45 min in PBS at 37ºC.

Staining. 3D aggregate sections and replated cells in coverslips were incubated in 0.1 M Glycine (Millipore) for 10 min at RT, permeabilized with 0.1% Triton X-100 (Sigma), at RT for 10 min and blocked with 10% FGS in TBST (20 mM Tris-HCl pH 8.0, 150 mM NaCl and 0.05% Tween-20, Sigma), at RT for 30 min. Cells were then incubated with the primary antibody diluted in 10% FBS in TBST solution (Table IV-1) at 4ºC overnight. Secondary antibodies were added for 30 min and nuclear counterstaining was performed using 4',6-diamidino-2-phenylindole (DAPI, 1.5µg/mL, Sigma), at room temperature for 5 min.

Table IV-1: List of antibodies used in Flow Cytometry and Immunostaining

Antibody	Source	Reference	Isotype	Dilution
CD31	Dako	M0823	Mouse IgG	1:50 (FC/IS)
VCAM - PE	Biolegend	305806	Mouse IgG	1:10 (FC)
cTNT	Thermo Fisher	MA5-12960	Mouse IgG	1:200 (IS) 1:800 (FC)
CD90-PE	Biolegend	328110	Mouse IgG	1:10 (FC)
CX43	Sigma-Aldrish	C6219	Rabbit IgG	1:400 (IS)
MLC2A	Synaptic Systems	311011	Mouse IgG	1:200 (IS)
MLC2V	Proteintech	10906-1-AP	Rabbit IgG	1:200 (IS)
Vimentin	Sigma	V6630	Mouse IgG1	1:300 (IS)

WT1	Abcam	ab89901	Rabbit IgG	1:100 (IS/FC)
Collagen I	Abcam	ab34710	Rabbit IgG	1:300 (IS)
Fibronectin	Abcam	ab253288	Mouse IgG1	1:300 (IS)
cTNI	Abcam	ab47003	Rabbit IgG	1:200 (IS)
CDX2	Abcam	ab76541	Rabbit IgG	1:200 (IS/FC)
Ki-67	Abcam	ab833	Rabbit IgG	1:50 (IS)

IV.3.4 Quantitative real time (qRT)-PCR

Total RNA from 3D cardiac aggregates was extracted using High Pure RNA Isolation Kit (Roche) according to manufacturer´s instructions, and converted into cDNA with High Capacity cDNA Reverse Transcription Kit (Thermo Fisher Scientific). PCR reactions were performed with Taqman™ Gene Expression Assays (Thermo Fisher Scientific) or SYBR Green Master Mix (nzytech) (Table IV-2). Reactions were run in triplicate in ViiA7 Real-Time PCR Systems (Applied BioSystems). For each analyzed time point, gene expression was normalized against the expression of the housekeeping gene glyceraldehyde-3-phosohate dehydrogenase (*GAPDH*) and results analyzed with QuantStudio™ RT-PCR Software.

Table IV-2: List of primers used in qRT-PCR analysis

TAQMAN	
Gene	**Assay ID**
TNNT2	Hs00165960_m1
TNNI3	Hs00165957_m1
MYL2	Hs00166405_m1
MYL7	Hs01085598_g1
MYH6	Hs00411887_m1
MYH7	Hs01110632_m1
GAPDH	Hs02786624_g1
SYBERGREEN	
Gene	**PRIMER (5´>3´)**
GAPDH	FW: GAGTCAACGGATTTGGTCGT RV: TTGATTTTGGAGGGATCTCG
WT1	FW: CAGCTTGAATGCATGACCTG RV: TATTCTGTATTGGGCTCCGC
ALDH1A2	FW: TCGCATCTTCGTGGAGGAGT RV: TGCTCAGTGGTGGGGTCAAA

ITGA4	FW: GTATGGTACACAATGCCAATGCC RV: GCTCTGTTGGGAATGCTGTGT
POSTN	FW: GACACACCCGTGAGGAAGTT RV: TTGTGCTGATGTTTCAGTTCCTG
DDR2	FW: TTCTTTTTGGGTTGGGGAAACG RV: TGGGTCCTGGGAGGCATATCA
CD31	FW: GCTGACCCTTCTGCTCTGTT RV: TGAGAGGTGGTGCTGACATC
VIM	FW: ACTACGTCCACCCGCACCTA RV: AGCGAGAAGTCCACCGAGTC

IV.3.5 Calcium Transients Analysis

To perform calcium transient analysis, 3D co-cultured aggregates and 3D CM aggregates were collected and seeded individually in each well of a µ-slide 8-well ibidi chamber. Then, the culture medium was removed and Fluo-4 solution (2 µM) was added to each well and incubated for 30 minutes at 37ºC. After that time, Fluo-4 solution was removed, the aggregates were washed 2 times with PBS and incubated again in culture medium. The aggregates were left at 37ºC for an additional 30 minutes before confocal imaging acquisition. Fluo-4 excitation was performed using a 488 nm line with an Argon ion laser and fluorescence emission collected (500-650 nm) using a Leica HyD hybrid detector. The images were acquired with a dry objective, 10.0x magnification (numerical aperture of 0.40), at a frame interval of 97 mili-seconds and at a resolution of 128 x 128 pixels, with a scan speed of 700 Hz.

Image acquisition was performed for a period of 30 seconds. Calcium transients for both 3D co-cultured aggregates and aged matched 3D CM aggregates, were taken before and after 45 minutes of incubation with four different drugs, Verapamil, E-4031, Isoproterenol and Carbachol. The concentrations of each drug used in this study were 100 and 150 nM for isoproterenol, 10 µM for carbachol, 50 and 100 nM for E-4031, and 25, 50 and 100 nM for verapamil.

To obtain the calcium transient profiles, the confocal microscope manufacturer software was used to select three/four regions of interest on the aggregate being analysed. From that, the raw data that describes the variation in fluorescence intensity on those areas was extracted and a calcium transient profile generated. This profile was then used to obtain the functional parameters beats per minute, decay time and time between peaks.

IV.4 RESULTS

IV.4.1 Establishment of a co-culture platform between CMs and PECs

With the aim of develop a more complex and *in vivo*-like cardiac model than 3D aggregates of CM alone (chapter II), a novel 3D cardiac MT model was established by combining PECs and CMs

(Figure IV-1A). Different parameters were optimized to establish the co-culture platform, specifically the optimal time of PECs and CMs differentiation stage and the most appropriate ratio of each cell population to be combined.

Regarding the time point for co-culture, genetic studies performed in mouse suggested the importance of cell adhesion molecules in the process of PEC attachment to the myocardium. This interaction has been described to be controlled by the α4-integrin (ITGA4) in epicardial cells that binds to VCAM-1 ligand present in myocardium (Sengbusch et al., 2002)(Kwee et al., 1995). Additionally, it is described in the literature that PECs migrate towards the developing myocardium when this cell layer is already contracting (Plavicki et al., 2014). Taking into consideration this information from the literature, the expression level of *ITGA4* was assessed throughout the differentiation process. The higher expression level for this marker was registered at D11 of PECs differentiation and thus this time point was selected as the optimal one to initiate the co-culture (Figure IV-1B). Regarding CMs, since at D11 of differentiation, 3D aggregates are already beating and expressing the surface marker VCAM-1, this time point was also the selected one to establish the co-culture model, suggesting compatibility in terms of differentiation timing for both cell types. D11 CM aggregates have more than 85% of $cTNT^+$ cells, being more that 60% of the cells positive for VCAM-1. Moreover, this population is deprived form $WT1^+$ cells, and includes a small percentage of $CD31^+$ cells (±2%) and $CD90^+$ cells (±10%) (Figure IV-1C). To generate the 3D cardiac co-culture aggregates (CCA), it was envisioned to explore the intrinsic self-organization of both cell types, and to do so, D11 PECs and CMs aggregates were dissociated and combined at a specific ratio inside an Aggrewell plate. Regarding the proportion of both cell types, a recent report demonstrated that epicardial and epicardium-derived cells correspond to 12%, in terms of cells number, of the total number of cells that compose the heart (Lupu et al., 2020b). Additional, studies reported in the literature that performed co-culture between hPSC-CMs and hPSC-PECs used a percentage of the last mentioned cell type of approximately 7% (Bargehr et al., 2019) and 9% (Thavandiran et al., 2019). Taking that into consideration, it was decided to fix the optimal CMs:PECs ratio in 85%:15%, respectively. 24 hours after seeding the cells in the Aggrewell plates, (1) CCA were transferred to a 6-well ultra-low attachment plate, were CCA are maintained in a confluent environment (approx. 150 CCA/well), or (2) each CCA was directly transferred to 1 well of a 24-well ultra-low attachment plate. Although at D1 of co-culture both cell types were indistinguishable within the CCA (Figure IV-2D *a*), in both conditions, at D3, it was possible to observe that PECs and CMs segregate from each other and PECs tend to accumulate in one side of the aggregate, proving that they are able to self-organize (Figure IV-2D *b* and *c*).

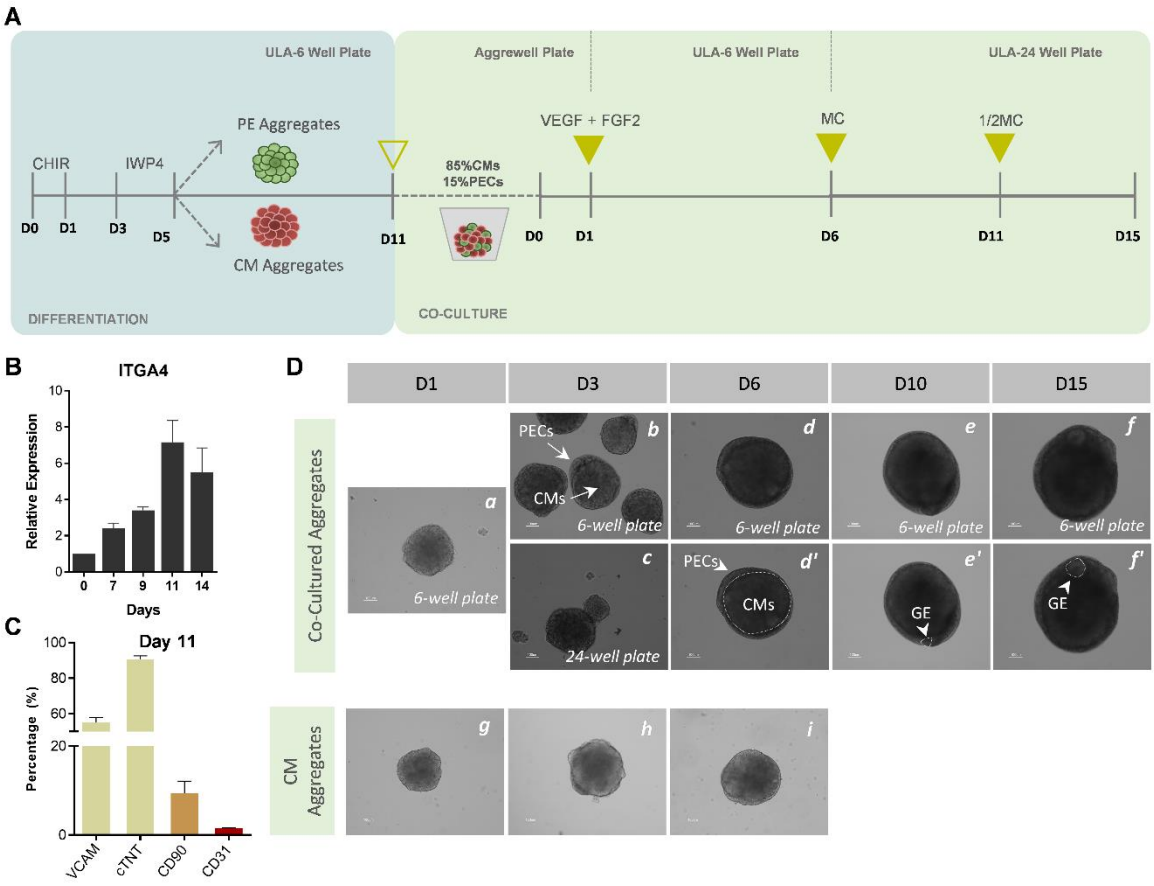

Figure IV-1 Establishment of a 3D cardiac model by co-culturing PECs and CMs. (A) Schematic representation of the established co-culture platform of PECs and CMs. D11 PECs and D11 CMs aggregates were dissociated into single cells and combined at a ratio of 85% CM:15% PEC in Aggrewell plates. After 24 hours, co-cultured aggregates were transferred to ultra-low attachment 6-well plate and after 6 days, each cardiac aggregate was transferred to one well of a ULA 24-well plate. MC, Medium Change, 1/2MC, Half Medium Change. (B) Expression profile of *ITGA4* gene from D0 up to D14 of PEC differentiation. Values are normalized to *GAPDH* and to D0 of differentiation. Data are represented as mean ± SEM, of at least n=3 independent experiments. (C) Percentage of VCAM, cTNT, CD90 and CD31 positive cells in D11 CM aggregates. Data are represented as mean ± SEM from at least n=3 independent experiments. (D) Bright field images of co-cultured aggregates over 15 days of culture (*a-f*) and age matched aggregates composed only by CMs (*g-i*). GE, Gut Epithelium.

To asses if the endogenous expression of important signalling factors is sufficient to stimulate the interaction between PECs and CMs, no soluble factors were added to the basal culture medium. Although in the conditions where CCA were maintained in a confluent environment in the 6-well plate (Figure IV-1D *b, d* and *d'*) it was possible to observe migration and arrangement of the PECs around the CMs over time, on the opposite side, CCA cultured individually since the early stage of co-culture showed compromised PECs migration and interaction with CMs (Figure IV-1D *c*). This seems to

indicate that the accumulation of endogenous factors secreted by the CCA potentiate migration of PECs. Due to that observation, it was established that during the first 6 days of co-culture, CCA were maintained in 6-well ULA plates. From D6 onward, CCA were transferred, each one for 1 well of a 24-well ULA plate. In fact, at this time point the process of PECs migration and arrangement surrounding the CMs core is completed (Figure IV-1D *d* and *d'*) and the CCA tend to merge in the 6-well plate due to static culture conditions that were used. Although we have shown that, without medium supplementation with additional signaling modulators, the migration and establishment of a PEC layer surrounding the CMs was achieved, the addition of VEGF and FGF2 during the first 6 days of co-culture period has been also observed to favor the development of a more complex vascularization inside the cardiac organoid and potentiate the migration and the arrangement of the PECs surrounding the CMs, respectively, as it will be showed later in this chapter. Contrarily to age matched CMs aggregates (the control condition) (Figure IV-1D *g-i*), CCA showed a considerable increase in size over time in culture, which can result from increased CMs proliferation and/or CFs growth within the CCA, which will be further confirmed and quantified in future experiments. Also, in the epicardial layer that surrounds the contracting area of the CCA, it was possible to observe the appearance of epithelial-like structures (Figure IV-1D *e'* and *f'*), which were presumably generated from the $CDX2^+$ population of cells present in D11 PEC aggregates used for the establishment of the co-culture system (Chapter III).

In conclusion, it was possible to successfully establish a culture platform for the generation of a 3D cardiac microtissue that is able to self-organize, forming a continuous epithelial-layer covering a CM core.

IV.4.2 The 3D co-cultured MTs emulate aspects of embryonic heart development and show a superior strucutral organization than 3D CM aggregates

To analyze in more detail the composition and structural organization inside the developed 3D cardiac MT, immunofluorescence staining of CCA slices and qRT-PCR analysis were performed after 15 days of co-culture, using as control age-matched 3D CMs aggregates. Immunostaining results reveled that CCA show the presence of a layer of $WT1^+$ epicardial-like cells surrounding a $cTNT^+$ CM core (Figure IV-2A a, a' and a''), which was not possible to observe in CM aggregates (Figure IV-4 *a* and *b*). The epicardial cells that surround each CCA, depending on the area, were arranged as a single (Figure IV-2A a', *1) or multi (Figure IV-2A a', *1) cell layers. Although most of the reported studies describe the epicardium as an uniform single layer of epithelium covering the myocardium, a recent study that characterized the human epicardium during embryonic heart development (Risebro et al., 2015) found differences between atrial and ventricular epicardium and showed that the ventricular epicardium contains regions of multiple cell layers, near blood vessels. However, it is also important to take into consideration that the CCA were analyzed after only 15 days of co-culture, and thus it will be interesting to evaluate if the organization of the epicardial layer after longer periods of

time suffers changes. It could be also interesting to test the effect of decreasing the percentage of PECs used to establish the co-culture model to 5/10% to evaluate how that alteration impacts the formation of the epicardial layer.

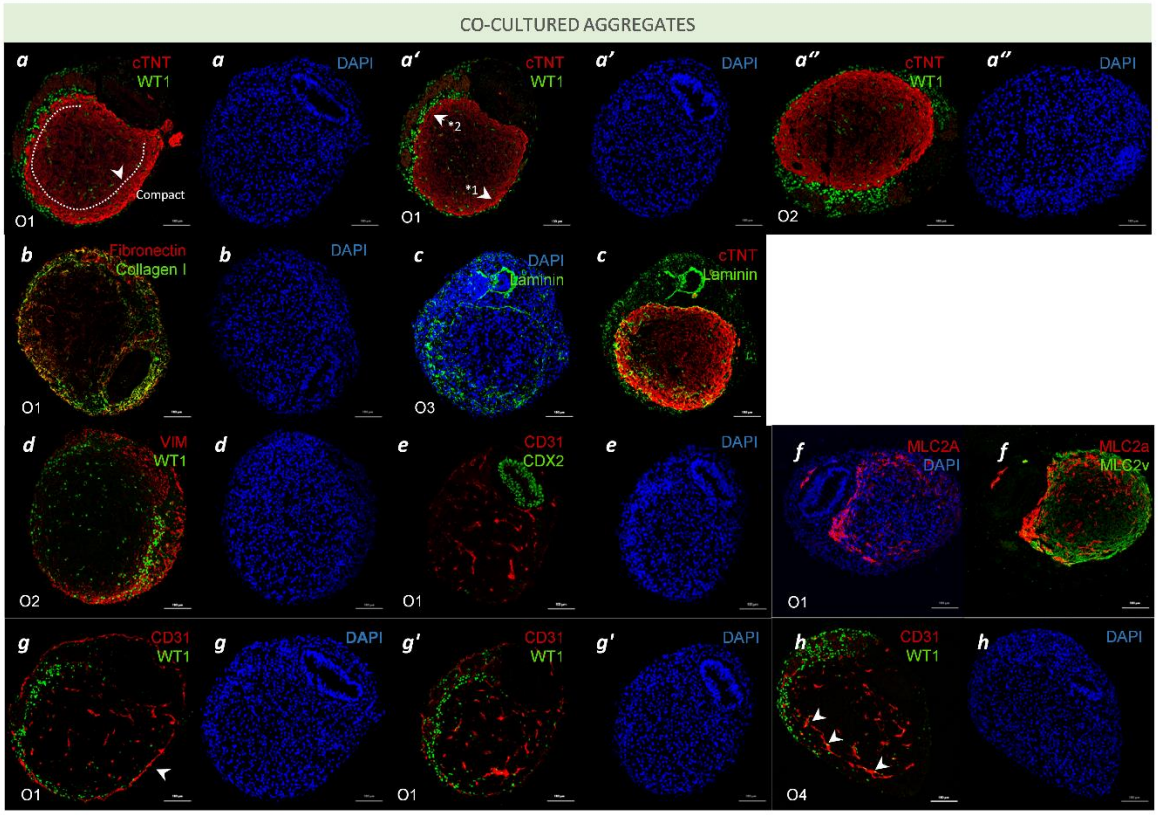

Figure IV-2: Co-cultured cardiac MT aggregates show structural organization and improved vascularization. (A) Immunofluorescence analysis of D15 co-cultured aggregates with VEGF and FGF addition between D1 and D6 of co-culture, except in 2A *g*, where no growth factors were added. (*a*) Dashed lines delineate the compact zone in CM core. (*a'*) *1 and *2 in white arrows highlight the presence of both single and multi-cell epicardial layer in the same organoid, respectively. (*g*) White arrow identifies the layer of $CD31^+$ cells that surrounds the cardiac organoids in the condition were VEGF was used during the first 6 days of co-culture (*h*) White arrows highlight the presence of $WT1^+/CD31^+$ ECs. Scale bars, 100 µm. Ox identifies the organoid.

Specifically regarding CMs, although still not quantified in this work, it was possible to observe that the $cTNT^+$ core in the cardiac MT was more compact and aligned, following the curvature of the CCA, near the epicardial layer, while CMs towards the center showed a more random and loose organization (Figure IV-2A *a* and *a'*). In fact, in the human heart, myocardium is divided into an outer, highly mitotic compact zone and an inner zone with lower mitotic activity known as trabecular zone, and epicardium has been described to play a crucial role in the development of the compact myocardium (Gittenberger-de Groot et al., 2000; Kastner et al., 1994; Kwee et al., 1995; Sucov et al., 1994; Yang et al., 1995), which may explain the mentioned observation in CCA. Interesting, using Ki-67 marker to identify proliferative CMs, it was possible to observed that the compact CM area

contiguous to the WT1^{+}-epicardial layer was enriched in proliferative CMs (cTNT^{+}/Ki-67^{+}), corroborating the observation that PECs in CCA induce a compact and mitotic CM layer (Figure IV-3A).

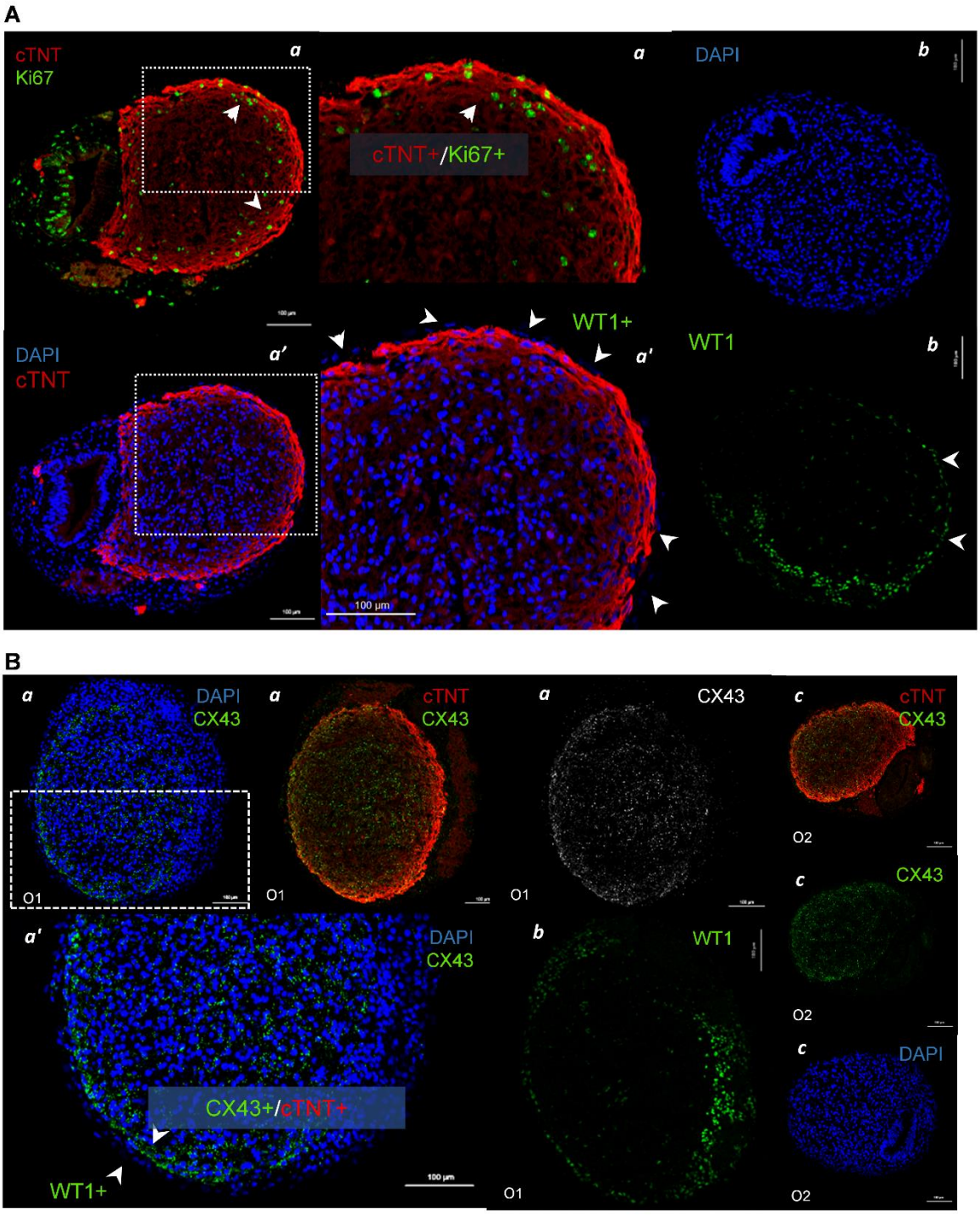

Figure IV-3 Epicardial cells promote CM proliferation and CX43 expression in co-cultured aggregates. (A) Immunofluorescence analysis of D15 co-cultured aggregates showing the staining of Ki-67 predominantly in cTNT^{+} cells near the epicardial layer. (*a*) White arrows identify cTNT^{+}/Ki-67^{+} CMs. (*a*' and *b*) White arrows identify

the $WT1^+$ cells. Staining *a* and *a'* correspond to the same slice and staining *b* corresponds to a different slice from the same CCA. (B) Immunofluorescence analysis of D15 co-cultured aggregates showing Cx43 staining in the CM core, which is enriched near the epicardial layer. (*a'*) White arrows identify an enriched area for $cTNT^+/Cx43^+$ staining near the $WT1^+$ layer. Staining *a* and *b* correspond to the same CCA but are from different sections. Staining c highlight the same results in a different CCA.

The developed 3D cardiac model showed also the presence of a layer of ECM deposition surrounding the CM core and co-localized with the epicardial cell layer, which stains for fibronectin, laminin, collagen I and VIM (Figure IV-2A *b, c* and *d*). Additionally, ECM deposition was also observed within the CM core, mainly fibronectin and laminin, which maybe related with the enrichment of fibroblasts derived from PECs in CCA. In CM aggregates, it was also possible to observe collagen I deposition, although almost no staining for fibronectin was observed (Figure IV-4 *e*). Other interesting observation, although this needs further confirmation, is related with the fact that the epicardial cells seem to induce ventricular maturation of CMs, with $cTNT^+$ cells near the epicardial layer staining for the ventricular marker MLC2V (Figure IV-2A *f*). Interestingly, it was also possible to observe the staining for the ventricular gap junction Cx43 throughout the CM core of CCA, although more pronounced in the contact area between CMs and the epicardial layer Figure IV-3B). This observation is in agreement with a recent study that highlighted the improved Cx43 expression in hPSC-CMs co-cultured with PECs (Bargehr et al., 2019). Moreover, the $CDX2^+$ epithelial structure (Figure IV-2A *e*), seems to benefit the maturation of CMs into the atrial subtype since it was possible to observe that CMs near the epithelial structure present a predominant staining for the atrial marker MLC2A (Figure IV-2A *e* and *f*). This observation is in agreement with another report recently described in the literature (Silva et al., 2020). In CM aggregates it was also possible to observe the presence of both MLC2A and MLC2V positive CMs, although without a specific organization/localization or proportion (Figure IV-4 *c*).

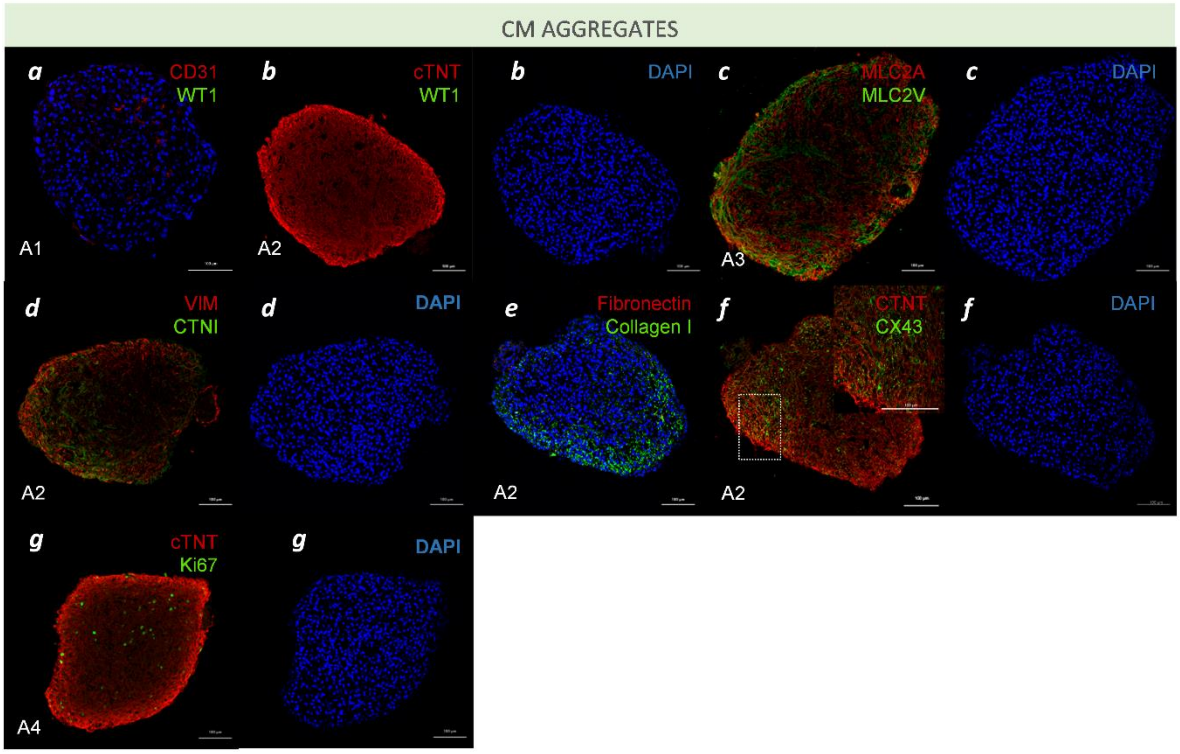

Figure IV-4 CM aggregates lack vascularization and structural organization. Immunofluorescence analysis of CM aggregates with the same time in culture of the day 15 CCA. Highlight for the lack of vascularization (CD31), low ECM deposition (collagen I and fibronectin), no structural organization (WT1), and prevalence of the atrial/immature CM marker MLC2A. Scale bars, 100 µm. Ax identifies the aggregate.

Interestingly, in contrast to the absence of vascular cells in CM aggregates (Figure IV-4 *a*), a vascular-like network of spindle-shaped cells that stained positive for the endothelial marker CD31 was observed within the CM core in CCA but it was also observed a layer of CD31 positive cells surrounding the entire MT (Figure IV-2A *g, g' and h*). In order to see if the improved vascularization, compared with age matched 3D CM aggregates, was dependent on the addition of VEGF during the first 6 days of co-culture, a parallel experiment without the addition of VEGF was performed. As it is possible to observe in Figure IV-2A *g*, the addition of VEGF promotes the development of the organized layer of CD31 positive cells surrounding the MTs, which is not visible in the culture condition without VEGF (Figure IV-2A *h*). However, in both conditions, improved vascularization within the CM nuclei is observed. It is important to highlight that D11 PEC aggregates have already a small percentage of endothelial-cells, which were hypothesised as not having an epicardial origin, and, since all the cells present in PECs aggregates are used to generate CCA, these cells are also added to the co-culture system. Adding to that, although the contribution of epicardial cells to the vasculature of the heart is currently debatable, interestingly, in CCA, it was possible to confirm the presence of $CD31^{+}$ endothelial cells that co-expressed $WT1^{+}$ (Figure IV-2A *h*), which may prove that at least part of the ECs presents in this novel cardiac model derived from the $WT1^{+}$ epicardial cells.

The improved cell diversity present in CCA compared with CM aggregates, namely regarding the presence of epicardial and epicardial-derived cells, ECs and CFs, was confirmed by qRT-PCR analysis for *WT1* and *ALDH1A2*, *CD31*, and *VIM*, *POSTN* and *DDRS*, respectively (Figure IV-5A). It is evident that, in the case of CM aggregates, there is also an increased expression, with time in culture, of fibroblast markers, which can be explained by the expansion of the $CD90^{+}$ cells present in CM aggregates used to establish the co-culture system.

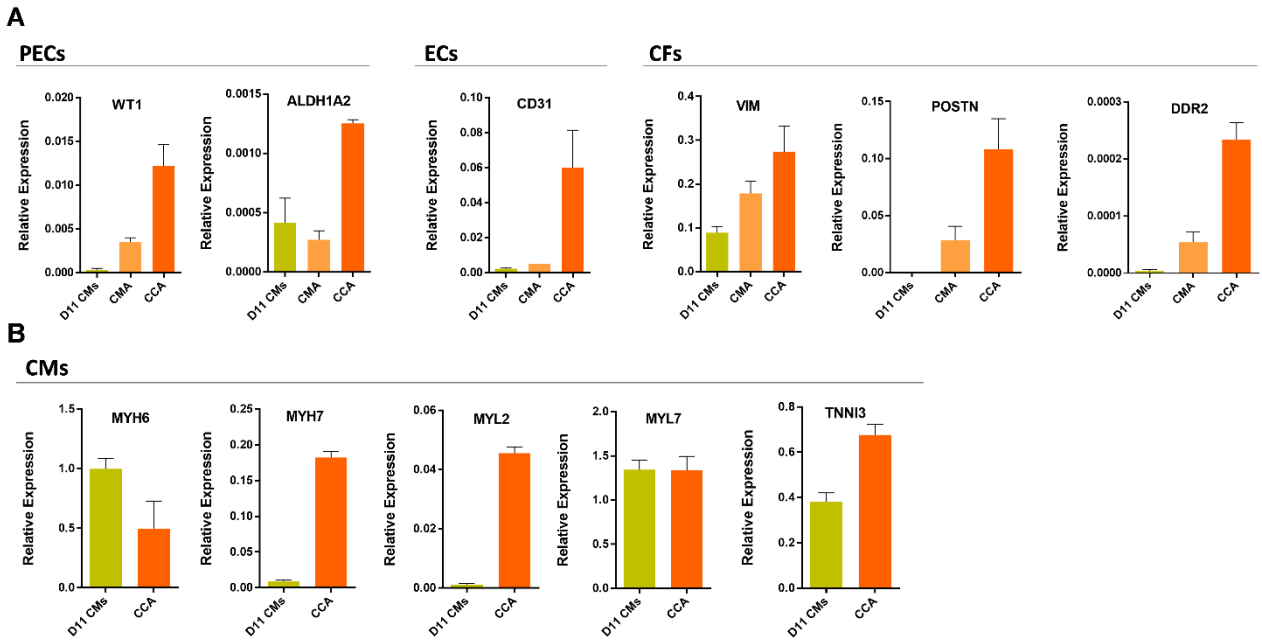

Figure IV-5 Evolution of the different cardiac cell populations within 3D CCA and assessment of CMs maturation. (A) Expression profile of epicardial markers *WT1* and *ALDH1A2;* endothelial marker *CD31;* and fibroblast markers *VIM, POSTN* and *DDR2* at D11 CM aggregates and at D15 of co-culture cardiac aggregates (CCA) and CM aggregates (CMA). Values are normalized to *GAPDH*. Data are represented as mean ± SEM, of n=3 independent experiments, for D11 CMs and n=2 for CMA and CCO conditions. (B) Expression profile of CM structural markers *MYH6, MYH7, MYL2, MYL7* and *TNNI3* at D11 CM aggregates and at D15 CCA. Values are normalized to *GAPDH* and *TNNT2*. Data are represented as mean ± SEM, of n=2 independent experiments.

Additionally, it was also possible to confirm by qRT-PCR analysis that the expression of the mature myosin isoform *MYH7* and the mature troponin isoform *TNNI3*, increased after 15 days of co-culture in CCA (Figure IV-5B). Interestingly, the expression level of the ventricular CM marker *MYL2* was also upregulated in CCA compared to the level observed in CMs used to establish the co-culture system. However, the expression level of the atrial marker *MYL7* remained unchanged. Both results seem to be in agreement with the immunostaining observations in which CMs present in CCA seem to have a ventricular-like phenotype (MLC2V expression) but the presence of gut-like epithelial structure favors also the presence of atrial CMs which may explain the levels of expression of *MYL7*. It will be now necessary to perform the same analysis in age matched CM aggregates to evaluate if

these improvements are due to increased time in culture or are directly related with the impact of the co-culture system.

In conclusion, it was possible to establish a 3D cardiac MT that shows structural organization accomplished by self-arrangement of the co-cultured CMs and PECs. The developed 3D cardiac model recapitulates important features of embryonic heart development and presents a well-defined continuous epicardial layer, improved vascularization and ECM deposition compared with 3D CM aggregates.

IV.4.3 Functional characterization of co-cultured cardiac MT aggregates

CMs function is deeply dependent on the presence and function of important ion channels and the resulting ion currents. As a first test to assess the CM functionally, the response of the 3D co-cultured aggregates to known drugs, using calcium transients as readout, was performed. Four different drugs were used to test the response of the 3D cardiac MTs, namely (1) isoproterenol, which is a selective β1-adrenergic agonist calcium channel activator, (2) carbachol, which is an agonist of muscarinic acetylcholine receptors and has been described to affect Ca^{2+} transient in CMs, (3) E-4031, which is a potassium hERG blocker and, as it has been described in the literature, is essential to demonstrate the sensitivity of the developed cardiac model to this drug (Gintant et al., 2020), and (4) Verapamil, which is L-type calcium channel blocker that also has an effect on hERG channel. Calcium transients for both CCA after 15 days of co-culture and age matched 3D CM aggregates, were taken before and after 45 minutes of incubation with the respective drug (Figure IV-6 and 7). Calcium transients were also taken in CCA after 65 days of co-culture (Figure IV-8). The tested concentrations for each drug used in this study were 100 and 150 nM for isoproterenol, 10 µM for carbachol, 50 and 100 nM for E-4031 and 25, 50 and 100 nM for verapamil. Additionally, it is important to refer that for all the tested conditions, the 3D models restored their basal calcium transient profile after a washout step.

E-4031, being a I_{kr} blocker, has been described to prolong the action potential duration, by slowing the phase 3 repolarization stage of the action potential profile, which translates into an increase in the Ca^{2+} peak interval and consequently decreasing the frequency of contraction (Takeda et al., 2018c)(Spencer et al., 2014)(Prajapati et al., 2018). Additionally, E-4031 has also been described to induce arrhythmic behavior in CMs, specifically, early after depolarizations (EADs) events (Spencer et al., 2014)(Prajapati et al., 2018). Regarding the observed effect of E-4031 on Ca^{2+} transients, for a concentration of 50 nM and in the case of CCA, it was detected an increment of around 20% in the time between peaks compared to the respective control without drug (Figure IV-6C). Contrarily to this observation, in CM aggregates and using the same concentration of drug, in some aggregates it was not detected any effect on Ca^{2+} transient profiles (Figure IV-6A) compared to the one observed before drug exposure, and in other CM aggregates it was observed an increased frequency of contraction (Figure IV-6B). By increasing the concentration of E-4031 up to 100 nM, it

was possible to observe an arrhythmic behavior in CM aggregates (Figure IV-6D), and an increased frequency of contraction in CCA with, although not so pronounced, arrhythmic events (Figure IV-6E). Since the expected effect at lower concentrations of E-4031 was not observed in CM aggregates, this may suggest that CMs lack or present a lower expression level of hERG channels, which may indicate a lower functional maturation compared with CCA. Additionally, since it was not observed EADs events for the tested concentrations of the drug, further experiments with higher concentrations of E-4031 will be performed.

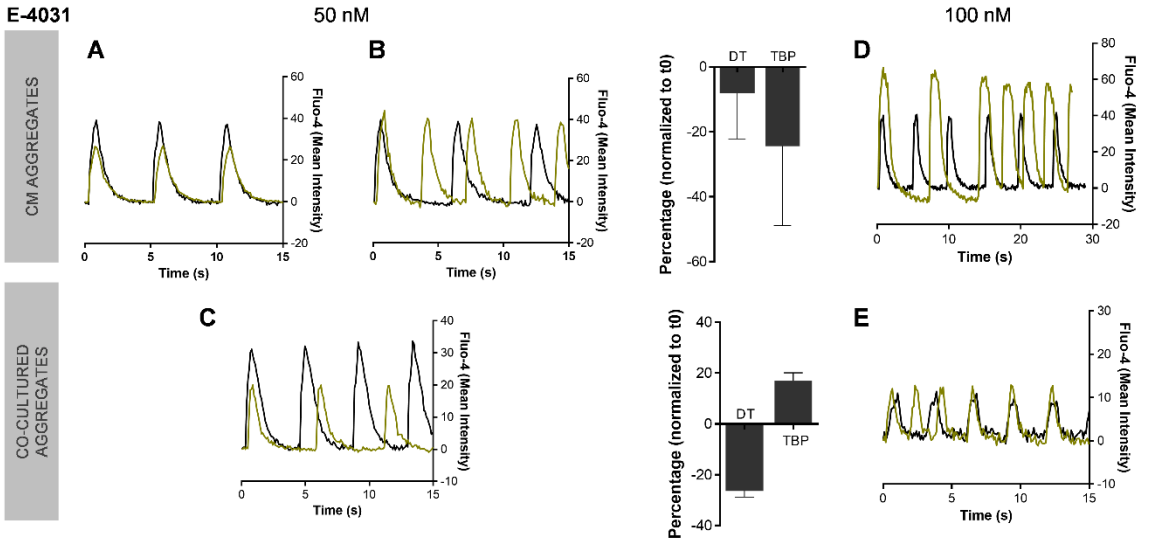

Figure IV-6 Effect of E-4031 drug on Ca^{2+} transient profile in CM aggregates and CCA after 15 days of co-culture. Ca^{2+} transient profiles after E-4031 drug exposure at a concentration of 50 nM in CM aggregates (A and B) and CCA (C). Ca^{2+} transient profiles after E-4031 drug exposure at a concentration of 100 nM in CM aggregates (D) and CCA (E), highlighting the arrhythmic events. The present Ca^{2+} transient profiles were obtained after 45 minutes of drug incubation. DT, Decay Time; TBP, Time Between Peaks; BPM, Beats Per Minute. Values were normalized to baseline Ca^{2+} profiles before drug exposure.

The majority of the studies reported in the literature using hPSC-derived CMs, shows that the addition of carbachol decreases the frequency of CM contraction (Hamad et al., 2019) (Sheng et al., 2012)(Navarrete et al., 2013). This is in agreement with the results herein obtained, showing an increased decay time and time between peaks interval for CM aggregates and day 15 CCA (Figure IV-7A). The same behavior was observed in day 65 CCA, which showed also lower frequency of contraction after carbachol exposure (Figure IV-8A). In the case of Isoproterenol, being a calcium channel activator, the obtained results in both models reflected that response by increasing the frequency of contraction in 34% in the case of CCA and 43% in the case of CM aggregates, which is in agreement with previously reported studies (Goldfracht et al., 2019)(Takeda et al., 2018b). This effect may be potentiated by increasing the isoproterenol concentration, as suggested in CCA after 65 of co-culture, where a small increase in isoproterenol concentration from 100 to 150 nM, induced

a slightly higher increment of the beat frequency (Figure IV-8B). Higher concentrations of this drug may potentiate the differences between the two models.

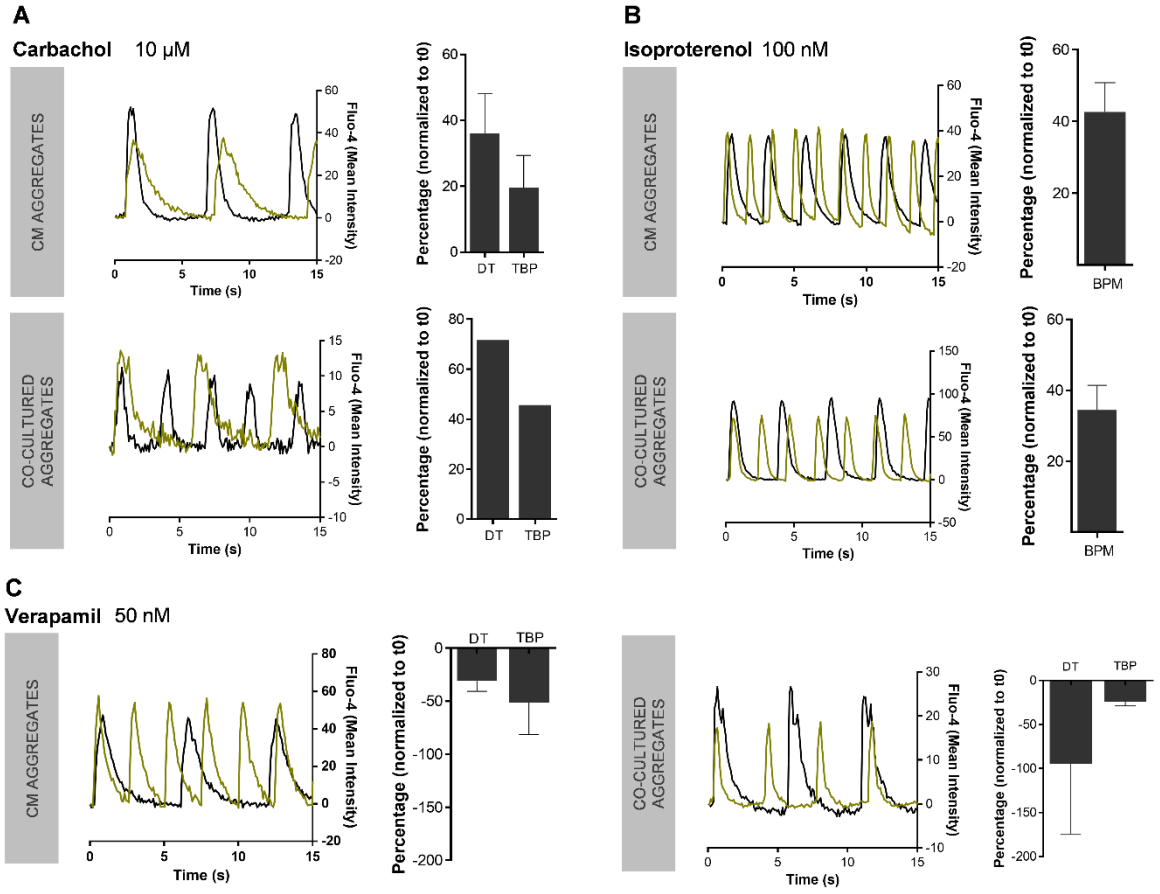

Figure IV-7 Effect of Carbachol, Isoproterenol and Verapamil drugs on Ca^{2+} transient profile in CM aggregates and CCA after 15 days of co-culture. Ca^{2+} transient profiles after Carbachol (10 µM) (A), Isoproterenol (100 nM) (B) and Verapamil (50 nM) (C) exposure in CM aggregates and CCA. The present Ca^{2+} transient profiles were obtained after 45 minutes of drug incubation. DT, Decay Time; TBP, Time Between Peaks; BPM, Beats Per Minute. Values were normalized to baseline Ca^{2+} profiles before drug exposure.

Contrarily to E-4031 drug, Verapamil, being a L-type calcium channel blocker, has been described to decrease the action potential duration by shortening the AP plateau phase, which translates in a less prolonged Ca^{2+} transient profile, and an increasing concentration of this drug culminates in CM ceasing contraction. The results that we obtained when exposing both models to this drug were dependent on the concentration of verapamil. For a concentration of 100 nM, CMs from both 3D models cease beating but this is recovered after a washout step, meaning that the viability of the cells was not affected. With concentrations of 25 and 50 nM, it was possible to observe a decrease in the decay time of Ca^{2+} transients in both models as expected (Maddah et al., 2015), but this effect was much more evident in the case of CCA from both day 15 and day 65 co-culture

conditions (Figure IV-7C and 8C), which may indicate a higher expression level of calcium channels in CCA, being in this way responsible for the more pronounced effect observed in the 3D co-culture model.

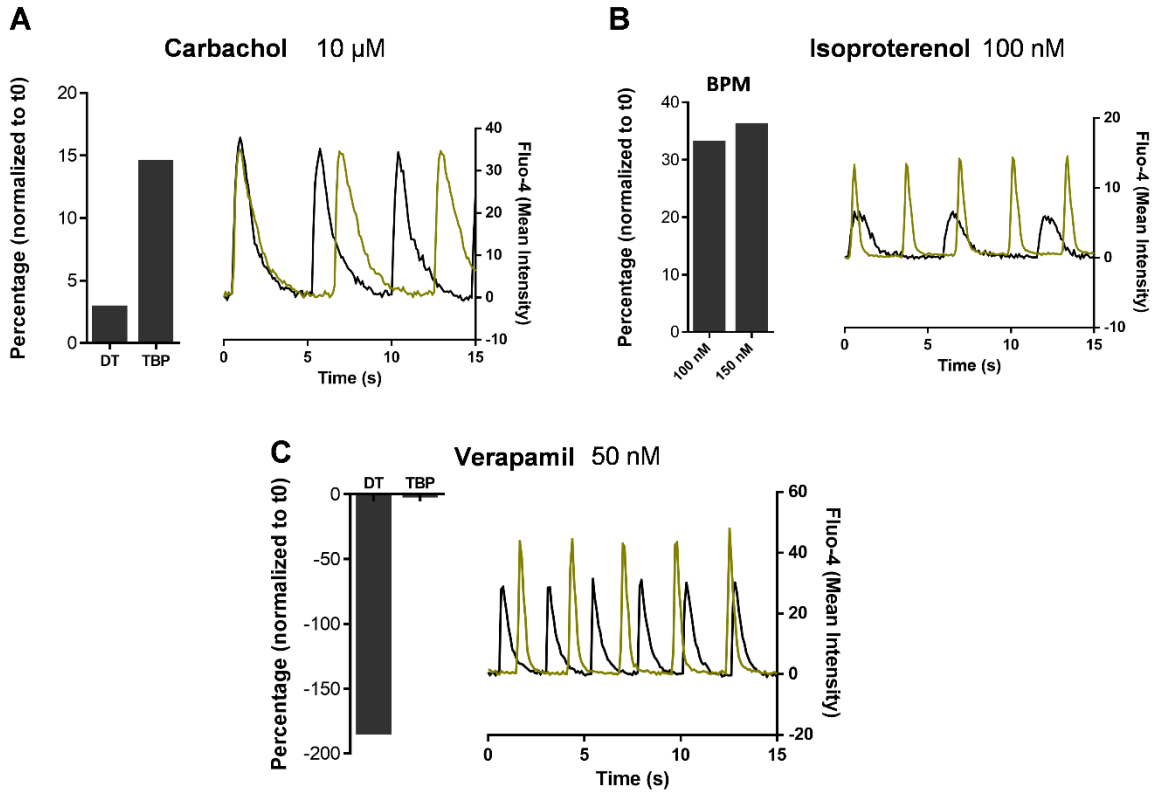

Figure IV-8 Effect of Carbachol, Isoproterenol and Verapamil drugs on Ca^{2+} transient profile in CM aggregates and CCA after 65 days of co-culture. Ca^{2+} transient profiles after Carbachol (10 µM) (A), Isoproterenol (100 nM) (B) and Verapamil (50 nM) (C) exposure in CM aggregates and CCA. The present Ca^{2+} transient profiles were obtained after 45 minutes of drug incubation. DT, Decay Time; TBP, Time Between Peaks; BPM, Beats Per Minute. Values were normalized to baseline Ca^{2+} profiles before drug exposure.

In conclusion, although further experiments are needed to confirm these results, the preliminary outcomes obtained from this study allowed already to highlight interesting differences between CM aggregates and CCA, which may indicate differences in CM functional maturation. These results also revealed important information regarding the effects of the tested drug concentrations and how this can be explored in the future to potentiate the assessment of the level of functional maturation in the developed cardiac model.

IV.5 DISCUSSION

The development of cardiac microtissues *in vitro* that reflect the structural and multicellular complexity observed in human heart has been described in the literature in the past few years. The

relevance of combining CMs with other cardiac cells present in the human heart in a 3D environment has been deeply explored and the effect on CMs and cardiac tissue functional and structural maturation have been highlighted. However, the majority of the recently developed 3D cardiac models combine already differentiated hPSC-derived or primary cardiac cells apart from CMs, including fibroblasts and ECs, at ratios that envision to mimic the proportions observed in the human heart. The main objective of the work described in this chapter was the establish a multicellular 3D cardiac model using a more *in vivo*-like strategy. Since the primary source of fibroblasts in the human heart is the epicardium, and since contribution of epicardium to endothelial cells, although debatable, has been described, it was envisioned to promote structural and multicellular improvement of the 3D CM aggregates developed in chapter II through the incorporation of PECs in the cardiac model. Through the establishment of a co-culture system between PECs and CMs, it was possible to generate 3D cardiac organoids that (1) present a continuous $WT1^+$ epicardial-like layer surrounding a CM core, (2) show a CM core with two distinct layers; an outer layer, contiguous to the epicardial layer, which is more compact and that contains more aligned and proliferative CMs, and an inner area where CMs present a loose organization, (3) show an enriched staining for the gap junction Cx43 within the CM core, particularly enhanced near the epicardial layer, (4) show an enrichment in fibroblast/ECM proteins surrounding the organoids and within the CM core, (5) show an improved network of vascular cells, and (6) present evidences of improved functional maturation.

The co-culture of CMs with hPSC-epicardial cells *in vitro* has been recently addressed in a few studies. However, those reports are mainly focused on understanding the effect of co-culture on CM maturation rather than exploring epicardial cells to the development of a self-organized and structural complex 3D cardiac model. The benefits of co-culturing hPSC-CMs and hPSC-EPCs in a 3D-EHT model have been described, highlighting the higher degree of sarcomere organization and length, myofibril alignment, higher degree of Cx43 expression, increased ratios of adult/fetal isoforms of contractile proteins (MYH7/MYH6), (MYL2/MYL7), (TNNI3/TNNI1) (Bargehr et al., 2019), and higher contraction force (Thavandiran et al., 2019). Only a recent work focused the efforts of using hPSC-PECs to improve the complexity of a 3D cardiac model (Hofbauer et al., 2020). In that study, 2D derived hPSC-PECs, were allowed to form small spheroids that where then co-cultured with the already developed 3D cardioids. They observed that the spheroids attached to the surface of the 3D cardioids, some epicardial cells start to spread and migrate on top of the CM layer and some differentiated into SMCs and CFs. Although being an interesting approach to generate 3D cardiac organoids with an epicardial layer, the methodology that they described did not allow the formation of a continuous layer of epicardial cells surrounding the CM core, being possible to observe only few clusters of hPSC-PECs on the surface of the cardioids, with impaired migration. Additionally, they also observed that the addition of exogenous stimuli was not necessary to observe the interaction of epicardial cells onto CM aggregate surface, which is in agreement to what was observed in the presently described model. In addition to that, it was also observed that the endogenous factors that are being released by the CCA and the concentration of those factors are crucial during the first days

of co-culture and improve the interaction, migration and structural organization of both CMs and PECs. To further explore this observation, it could be interesting to analyze the secretome of the CCA during the first days of co-culture, which may add valuable information regarding the stimuli involved in the establishment of epicardium during the *in vivo* heart development.

Due to the presence of $CDX2^+$ cells in the PEC aggregates used to establish the co-cultured model, it was possible to observe the development of epithelial-gut-like structures. Although the presence of these structures may be seen as an undesired outcome, a recent study that performed mouse gastruloids to recap specifically the process of cardiogenesis, found that the cTNT positive cardiac domain observed in 168-h gastruloids was exclusively located next to a gut-like tube-shaped E-cadherin-positive epithelial tissue (Rossi et al., 2021). This may suggest that our 3D cardiac organoid may recapitulate important *in vivo* stimuli that arises from the gut structure. In fact, although further experiments are needed to confirm this result, the presence of these endodermal-derived cells in cardiac organoids allowed the observation that those cells may be responsible for atrial CM specification, whereas epicardial cells induce ventricular CMs maturation. A recent study had also reported the generation of 3D cardiac-gut organoids and they also suggested that the presence of gut-like structure within the cardiac model induced atrial CM specification (Silva et al., 2020). In fact, they observed that the majority of the CM present in the 3D cardiac-gut organoids showed an atrial phenotype. Although in that cardiac model, some structural organization was observed, with the presence of an epicardial-like layer surrounding the 3D structure, the method used to generate the described organoids is barely reproducible. The authors start the multilineage differentiation process with a population of cells that is generated using a 2D protocol based on the Wnt signaling temporal modulation, which presents considerable variability between biological runs, reflecting in this way the possibility of ending with a cardiac, a gut or a mixed model without well-defined proportion between both cell types. Contrarily to that model, ours represents a tightly controlled and reproducible system to obtain 3D cardiac organoids, which is a crucial factor independently of the application of the developed model.

To further explore the impact that the gut-like structure has in the 3D cardiac model, it will be now interesting to develop alternative co-culture systems in which CDX2 positive cells are not present. As discussed in the previous chapter, alternative models of PEC aggregates are presently being explored which may overcame the presence of endoderm-derived cells and so be a viable alternative to establish the co-culture model. Additionally, it could be also explored the use of 2D differentiated hPSC-PECs, in which the generation of this $CDX2^+$ cell population has not been described in the literature. Furthermore, upon production of 2D differentiated PECs, it could be also interesting to evaluate if these cells will behave in the same way as 3D derived PECs, in terms of CM-PEC interaction and structural organization in the 3D organoids.

A proper coronary vasculature development is essential for late-embryonic and adult cardiac tissue performance. In our 3D cardiac MTs an extended vascular network of $CD31^+$ ECs was observed. Although the contribution of epicardium to coronary endothelium is controversial, in our

model we observed the generation of $WT1^+/CD31^+$ cells, which may support the idea that some PECs contribute to the vasculature observed in the cardiac organoids. In fact, evaluation of WT1 expression, in mouse and human fetal and adult hearts, revealed that WT1 is expressed in endothelial cells of both arteries and veins at early stages of development, becoming less expressed or absent in arteries in later stages but the expression in veins and capillaries remains present (Duim et al., 2015, 2016). Additionally, a lineage tracing study of ST/PECs performed in mouse identified $WT1^+/CD31^+$ cells in the developing coronary vasculature of the heart (Cano et al., 2016). These evidences may corroborate our findings. As discussed in the results section and in chapter III, in addition to $WT1^+/CD31^+$ coronary-like ECs, endocardial-like ECs may also be present. A deeper characterization of the vascular cell population present in 3D cardiac MTs should be performed to confirm the diversity of ECs. In addition to ECs, mural cells are critical for the establishment of a functional vasculature. Interestingly, staining for SMCs markers (α-SMA^- and $CNN1^-$) was not detected in CCA, which cannot be attributed to the impaired capacity of the developed PECs to differentiate in those cells, as it was proved in chapter III. It will be important to assess if longer periods of co-culture potentiate the development of more complex and functional vasculature, with the presence of SMCs. Alternatively, it could be also explored the addition of exogenous factors such as PDGF and TGFβ growth factors, which are known to induce SMC-EMT in PECs (Smith et al., 2011)(Bax et al., 2011). Additionally, and since the vascular system is constantly under hydrodynamic stress, it could be also interesting to explore dynamic systems, using for example microfluidic devices, to recapitulate this biophysical stimulus.

Although the focus of the work reported in this chapter was the establishment of a 3D cardiac organoid, it was already possible to perform preliminary functional assessment of the CCA in comparison with CM aggregates. We were able to observe preliminary differences regarding the response to known drugs that affect CMs function that indicate an improved functional maturation in the cardiac MTs. To observe more evident and critical maturation features, longer periods of co-culture should be considered, and further structural and functional tests should be performed in both models to assess differences. The use of single-cell transcriptomic analysis will be also a valuable tool to deeply understand and reveal the different subpopulations that are present inside the 3D cardiac model and also to allow the disclosure of further cues regarding the impact of co-culture on CM maturation. Additionally, since the basal medium that is being used to maintain the cardiac MTs is rich in glucose, and knowing that during embryonic heart development CMs switch from a glycolytic metabolism to a predominant fatty acid-oxidative metabolism, it could be also interesting to explore the gradual transition to a fatty acid enrichment medium to evaluate if it is possible to observe further cardiac maturation, without compromising the function and viability of the other cells present in the microtissue.

IV.6 CONCLUSIONS

In conclusion, in this chapter it was possible to establish a novel and reproducible 3D cardiac MT through CM and PECs co-culture, which shows important structural organization and multicellular features that resemble human heart. Overall, after performing a detailed molecular and structural characterization it was found that this novel cardiac MT presents a number of features complying with the definition of an organoid. Although further improvements of the 3D cardiac model are still being addressed and further functional maturation analysis are still needed, this platform can be further applied in different contexts, which we expect to explore in the near future, namely, the application of these cardiac organoids for disease modelling of cardiomyopathies, as well as in cardiotoxicity and drug screening settings.

IV.7 REFERENCES

Bargehr, J., Ong, L.P., Colzani, M., Davaapil, H., Hofsteen, P., Bhandari, S., Gambardella, L., Novère, N. Le, Iyer, D., Sampaziotis, F., et al. (2019). regeneration. Nat. Biotechnol. *37*.

Bax, N.A.M., Van Oorschot, A.A.M., Maas, S., Braun, J., Van Tuyn, J., De Vries, A.A.F., Gittenberger-De Groot, A.C., and Goumans, M.J. (2011). In vitro epithelial-to-mesenchymal transformation in human adult epicardial cells is regulated by TGFβ-signaling and WT1. Basic Res. Cardiol. *106*, 829–847.

Cano, E., Carmona, R., Ruiz-Villalba, A., Rojas, A., Chau, Y.Y., Wagner, K.D., Wagner, N., Hastie, N.D., Muñoz-Chápuli, R., and Pérez-Pomares, J.M. (2016). Extracardiac septum transversum/proepicardial endothelial cells pattern embryonic coronary arterio-venous connections. Proc. Natl. Acad. Sci. U. S. A. *113*, 656–661.

Duim, S.N., Kurakula, K., Goumans, M.J., and Kruithof, B.P.T. (2015). Cardiac endothelial cells express Wilms' tumor-1. Wt1 expression in the developing, adult and infarcted heart. J. Mol. Cell. Cardiol. *81*, 127–135.

Duim, S.N., Smits, A.M., Kruithof, B.P.T., and Goumans, M.J. (2016). The roadmap of WT1 protein expression in the human fetal heart. J. Mol. Cell. Cardiol. *90*, 139–145.

Giacomelli, E., Meraviglia, V., Campostrini, G., Cochrane, A., Cao, X., van Helden, R.W.J., Krotenberg Garcia, A., Mircea, M., Kostidis, S., Davis, R.P., et al. (2020). Human-iPSC-Derived Cardiac Stromal Cells Enhance Maturation in 3D Cardiac Microtissues and Reveal Non-cardiomyocyte Contributions to Heart Disease. Cell Stem Cell *26*, 862-879.e11.

Gintant, G., Kaushik, E.P., Feaster, T., Stoelzle-Feix, S., Kanda, Y., Osada, T., Smith, G., Czysz,

K., Kettenhofen, R., Lu, H.R., et al. (2020). Repolarization studies using human stem cell-derived cardiomyocytes: Validation studies and best practice recommendations. Regul. Toxicol. Pharmacol. *117*, 104756.

Gittenberger-de Groot, A.C., Vrancken Peeters, M.-P.F.M., Bergwerff, M., Mentink, M.M.T., and Poelmann, R.E. (2000). Epicardial Outgrowth Inhibition Leads to Compensatory Mesothelial Outflow Tract Collar and Abnormal Cardiac Septation and Coronary Formation. Circ. Res. *87*, 969–971.

Goldfracht, I., Efraim, Y., Shinnawi, R., Kovalev, E., Huber, I., Gepstein, A., Arbel, G., Shaheen, N., Tiburcy, M., Zimmermann, W.H., et al. (2019). Engineered heart tissue models from hiPSC-derived cardiomyocytes and cardiac ECM for disease modeling and drug testing applications. Acta Biomater. *92*, 145–159.

Hamad, S., Derichsweiler, D., Papadopoulos, S., Nguemo, F., Šarić, T., Sachinidis, A., Brockmeier, K., Hescheler, J., Boukens, B.J., and Pfannkuche, K. (2019). Generation of human induced pluripotent stem cell-derived cardiomyocytes in 2D monolayer and scalable 3D suspension bioreactor cultures with reduced batch-to-batch variations. Theranostics *9*, 7222–7238.

Hofbauer, P., Jahnel, S., Papai, N., Giesshammer, M., Tavernini, K., Grdseloff, N., Penc, M., Meledeth, C., Deyett, A., Schmidt, C., et al. (2020). Cardioids reveal self-organizing principles of human cardiogenesis.

Kastner, P., Grondona, J.M., Mark, M., Gansmuller, A., LeMeur, M., Decimo, D., Vonesch, J.L., Dollé, P., and Chambon, P. (1994). Genetic analysis of RXRα developmental function: Convergence of RXR and RAR signaling pathways in heart and eye morphogenesis. Cell *78*, 987–1003.

Klesen, A., Jakob, D., Emig, R., Kohl, P., Ravens, U., and Peyronnet, R. (2018). Cardiac fibroblasts. Herzschrittmachertherapie + Elektrophysiologie *29*, 62–69.

Kwee, L., Baldwin, H.S., Shen, H.M., Stewart, C.L., Buck, C., Buck, C.A., and Labow, M.A. (1995). Defective development of the embryonic and extraembryonic circulatory systems in vascular cell adhesion molecule (VCAM-1) deficient mice. Development *121*, 489–503.

Lupu, I.-E., Redpath, A.N., and Smart, N. (2020). Spatiotemporal Analysis Reveals Overlap of Key Proepicardial Markers in the Developing Murine Heart. Stem Cell Reports *14*, 770–787.

Ma, Z., Wang, J., Loskill, P., Huebsch, N., Koo, S., Svedlund, F.L., Marks, N.C., Hua, E.W., Grigoropoulos, C.P., Conklin, B.R., et al. (2015). Self-organizing human cardiac microchambers mediated by geometric confinement. Nat. Commun. *6*, 7413.

Maddah, M., Heidmann, J.D., Mandegar, M.A., Walker, C.D., Bolouki, S., Conklin, B.R., and Loewke, K.E. (2015). A non-invasive platform for functional characterization of stem-cell-derived cardiomyocytes with applications in cardiotoxicity testing. Stem Cell Reports *4*, 621–631.

Navarrete, E.G., Liang, P., Lan, F., Sanchez-Freire, V., Simmons, C., Gong, T., Sharma, A., Burridge, P.W., Patlolla, B., Lee, A.S., et al. (2013). Screening drug-induced arrhythmia events using human induced pluripotent stem cell-derived cardiomyocytes and low-impedance microelectrode arrays. Circulation *128*, 3–13.

Plavicki, J.S., Hofsteen, P., Yue, M.S., Lanham, K.A., Peterson, R.E., and Heideman, W. (2014). Multiple modes of proepicardial cell migration require heartbeat. BMC Dev. Biol. *14*.

Prajapati, C., Pölönen, R.P., and Aalto-Setälä, K. (2018). Simultaneous recordings of action potentials and calcium transients from human induced pluripotent stem cell derived cardiomyocytes. Biol. Open *7*.

Risebro, C.A., Vieira, J.M., Klotz, L., and Riley, P.R. (2015). Characterisation of the human embryonic and foetal epicardium during heart development. Dev. *142*, 3630–3636.

Rossi, G., Broguiere, N., Miyamoto, M., Kelly, R.G., Kwon, C., Lutolf, M.P., Rossi, G., Broguiere, N., Miyamoto, M., Boni, A., et al. (2021). Article Capturing Cardiogenesis in Gastruloids Article Capturing Cardiogenesis in Gastruloids. Stem Cell 1–11.

Sengbusch, J.K., He, W., Pinco, K.A., and Yang, J.T. (2002). Dual functions of α4β1 integrin in epicardial development: Initial migration and long-term attachment. J. Cell Biol. *157*, 873–882.

Sheng, X., Reppel, M., Nguemo, F., Mohammad, F.I., Kuzmenkin, A., Hescheler, J., and Pfannkuche, K. (2012). Human Pluripotent Stem Cell-Derived Cardiomyocytes: Response to TTX and Lidocain Reveals Strong Cell to Cell Variability. PLoS One *7*, 1–12.

Silva, A.C., Matthys, O.B., Joy, D.A., Kauss, M.A., Natarajan, V., Lai, M.H., Turaga, D., Alexanian, M., Bruneau, B.G., and McDevitt, T.C. (2020). Developmental co-emergence of cardiac and gut tissues modeled by human iPSC-derived organoids. BioRxiv 2020.04.30.071472.

Smith, C.L., Baek, S.T., Sung, C.Y., and Tallquist, M.D. (2011). Epicardial-derived cell epithelial-to-mesenchymal transition and fate specification require PDGF receptor signaling. Circ. Res. *108*.

Spencer, C.I., Baba, S., Nakamura, K., Hua, E.A., Sears, M.A.F., Fu, C.C., Zhang, J., Balijepalli, S., Tomoda, K., Hayashi, Y., et al. (2014). Calcium transients closely reflect prolonged action potentials in iPSC models of inherited cardiac arrhythmia. Stem Cell Reports *3*, 269–281.

Sucov, H.M., Dyson, E., Gumeringer, C.L., Price, J., Chien, K.R., and Evans, R.M. (1994). RXRα mutant mice establish a genetic basis for vitamin A signaling in heart morphogenesis. Genes Dev. *8*, 1007–1018.

Takeda, M., Miyagawa, S., Fukushima, S., Saito, A., Ito, E., Harada, A., Matsuura, R., Iseoka, H., Sougawa, N., Mochizuki-Oda, N., et al. (2018a). Development of in vitro drug-induced

cardiotoxicity assay by using three-dimensional cardiac tissues derived from human induced pluripotent stem cells. Tissue Eng. - Part C Methods *24*, 56–67.

Takeda, M., Miyagawa, S., Fukushima, S., Saito, A., Ito, E., Harada, A., Matsuura, R., Iseoka, H., Sougawa, N., Mochizuki-Oda, N., et al. (2018b). Development of In Vitro Drug-Induced Cardiotoxicity Assay by Using Three-Dimensional Cardiac Tissues Derived from Human Induced Pluripotent Stem Cells. Tissue Eng. Part C Methods *24*, 56–67.

Thavandiran, N., Hale, C., Blit, P., Sandberg, M.L., McElvain, M.E., Gagliardi, M., Sun, B., Witty, A., Graham, G., Mcintosh, M., et al. (2019). Functional arrays of human pluripotent stem cell-derived cardiac microtissues. BioRxiv 566059.

Warmflash, A., Sorre, B., Etoc, F., Siggia, E.D., and Brivanlou, A.H. (2014). A method to recapitulate early embryonic spatial patterning in human embryonic stem cells. Nat. Methods *11*, 847–854.

Yang, J.T., Rayburn, H., and Hynes, R.O. (1995). Cell adhesion events mediated by α4 integrins are essential in placental and cardiac development. Development *121*, 549–560.

V. CONCLUSIONS AND FUTURE TRENDS

In the past few years, major improvements have been made towards the *in vitro* independent generation of the different cell types that compose the human heart from hPSCs. This has opened the path to develop more complex, heterogeneous and thus physiologically relevant cardiac tissue models that have been already proven to standout in terms of their relevance for different applications such as disease modelling, drug screening and cardiotoxicity assays. The majority of the reported cardiac MTs are normally obtained through the combination of different terminally differentiated hPSC-derived cardiac cells, primary cultured cells, which in some cases do not have a cardiac origin, and ECM molecules at different proportions, trying to recapitulate the composition of the human heart. These 3D cardiac models present a degree of complexity and maturation greater than 2D cultured CMs or even greater than 3D aggregates composed only of CMs, but they still lack structural organization and, in some cases, lack functional interaction between the different cardiac cells. To overcome these limitations, 3D constructs coupled with mechanical load and/or electric stimulation (EHT tissues) have been shown to be a viable strategy to improve cardiac tissue maturation and have been already adapted for medium- to high- throughput screening formats. However, it is important to refer that the establishment and operation of these systems requires specialized and expensive equipment and expertise, which is not widely available and could be considered a complex solution to be applied for drug screening and cardiotoxicity test applications in industrial environments. Additionally, it is also important to understand if the improved hPSC-CM maturation observed in this type of systems is maintained when mechanical load or electric stimulation cease. Thus, as an alternative to EHT constructs, scaffold-free 3D multicellular MTs, obtained through self-assembly of terminally differentiated hPSC-derived cardiac cells and/or primary cells, represent a viable strategy to improve also hPSC-CM maturation, being cheaper and easier to produce when compared with EHT models.

Starting from this point (Figure V-1), this thesis aimed to develop a novel hPSC-derived 3D cardiac organoid model to be applied in different *in vitro* applications, namely disease modelling and toxicity assays. Contrarily to the mentioned above methods that have been used to generate 3D cardiac MTs, the idea behind this project was to emulate and take advantage of combined phenomena observed in embryonic human heart development to allow the self-organization and generation of more complex and *in-vivo*-like 3D cardiac models. This represents a promising strategy that, despite having started to be explored and reported in the literature (Hofbauer et al., 2020) (Silva et al., 2020), it is still very poorly developed.

To address this idea, in this work, we first established a simple and robust 3D CM differentiation platform, which was the basis for the development of more complex 3D cardiac MTs (Chapter II). Taking advantage of the knowledge gathered regarding *in vivo* embryonic heart development, we decided to further explore the combination of these 3D aggregates of CMs with PECs not only to recreate the development of an epicardial layer in our 3D cardiac model, but also as a progenitor cell population with potential to enrich these models with other important cells present in the human heart, namely CFs, SMCs and eventually ECs co-generated with CMs. In this way, we hoped to generate a

more *in vivo*-like model without mixing different terminally hPSC-differentiated or primary cardiac cells. By developing a 3D PEC differentiation platform (Chapter III), and by establishing a 3D co-culture model with CMs and PECs (Chapter IV), a complex 3D cardiac organoid was generated, that exhibits structural and morphological features observed in embryonic heart development as well as a similar heterogeneous cell composition. In fact, the developed 3D cardiac organoids present a well-defined epicardial layer surrounding a CM core. It was also possible to observe a dense vascularization and ECM deposition within the epicardial layer and also in the CM core. Moreover, epicardial cells seem to induce CM layer compaction and induce ventricular maturation. Increased time of co-culture and deeper characterization of the maturation status of the 3D model in terms of functional behaviour, will hopefully confirm the applicability of this new developed *in vitro* model in cardiotoxicity and disease modelling applications.

As important as the development of more complex and *in vivo*-like 3D cardiac models, is to assess if the developed model fits the purpose for the desired application. It is clear that the development of more complex hPSC-derived cardiac MTs can level up the applicability and the relevance of those models in cardiotoxicity screening assays, in testing new therapeutics for a specific cardiac disorder, or even to perform fundamental studies regarding human heart embryonic development process. However, and specifically for drug screening and cardiotoxicity assays, it is also important to take into consideration that with this increased complexity, important challenges arise namely the reproducibility between different batches of cardiac tissues. To define how far an *in vitro* model should go in terms of complexity, to be relevant for a specific application, it is important to define the main criteria in terms of hPSC-CMs maturation and cardiac tissue function that should be observed to be applied for a specific study. Additionally, having in mind the applicability of the developed 3D cardiac models in early pre-clinical settings, it is important also to standardize how these models should be tested and the readouts that should be analyzed to assess the functional performance of the developed models. Other important feature highlighted recently by Mannhardt and colleagues, which tested 10 different hPSC lines to generate CMs and perform drug screening in different EHT models using those hPSC-CMs, is related with the fact that biological variability between different hPSC-CMs was detected which impacted on the drug effect (Mannhardt et al., 2020). Due to that, in future applications of hPSC-derived cardiac models, it should be considered cardiac models generated from different hPSC lines to ensure more accurate results. Apart from confirming the applicability of the model, it is also important to balance other aspects including the cost of the cardiac tissue production, the compatibility with prolonged culture time to allow for long term studies and the possibility of adaptation to medium- to hight-throughput systems. Adding to that, as recently started to be explored in the literature (Lee et al., 2017a), the use of machine learning algorithms can also be a value tool to help on the automaticity of drug effect classification on the 3D cardiac models.

Other focus of interest in this area, which has gained attention in the past years and will continue to evolve in the following years, is the integration of hPSC-cardiac models in multi-organ-on-a-chip

devices, mainly in the context of drug screening applications (Huh et al., 2013; Miranda et al., 2018; Skardal et al., 2017) (Veldhuizen et al., 2020)(Yin et al., 2020). The relevance of these setups is linked to the importance of not only assessing the effect of a newly developed drug in a specific organ but the cumulative and synergetic effects at the multi-organ level. Although hPSC-derived cardiac MTs, alone or in combination with other organ MT models in microfluidic devices, could bring a valuable contribute to drug screening and cardiotoxicity assays, it is unlikely that animal models will be completely surpassed by these *in vitro* human-derived tissues in pre-clinical studies. However, these models can help on the replacement of the *ex vivo* experiments that have been used during the past years for cardiotoxicity assessment. These models can be also used for early detection of toxicity effects from a set of several possible new compounds and consequently reduce the necessity for extensive animal tests at an early stage of the drug development pipeline.

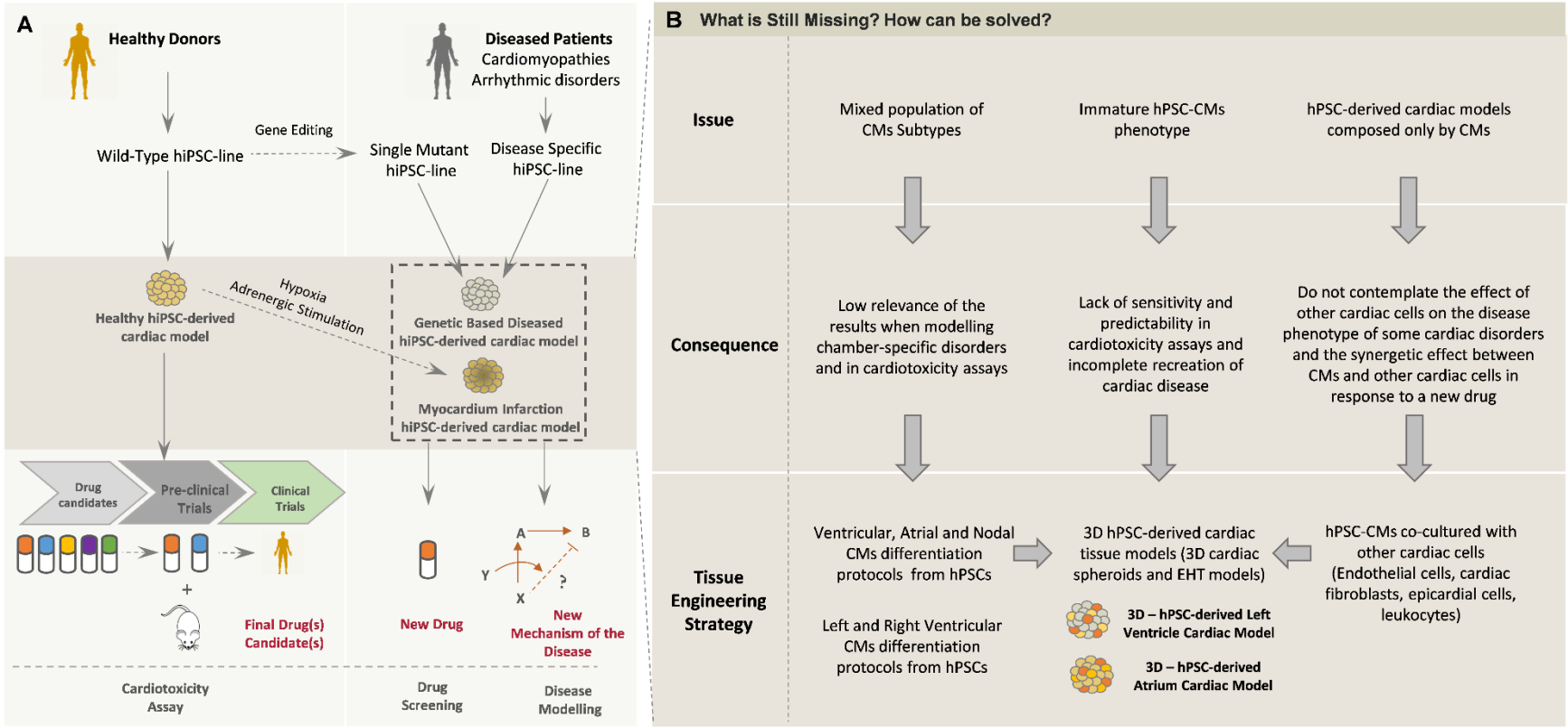

Figure V-1. hiPSC-derived 3D cardiac models: applications and challenges. (A) hPSCs, and specifically hiPSCs, is a powerful technology to generate wild-type and patient-specific cardiac models to be applied for drug screening, cardiotoxicity tests and disease modelling assays. (B) The most widely used cardiac models for *in vitro* applications still present some limitations that can be solved by using different tissue engineering strategies.